Calcium Channels in Cat Dorsal Root Ganglion Neurones

By

W.R. Taylor, BSc. (Hons)

Department of Physiology,
The John Curtin School of Medical Research,
Australian National University.

A thesis submitted for the degree of
Doctor of Philosophy at the
Australian National University in
December, 1986

I dedicate this work to the memory of my father,

George Anthony Morgan Taylor, G.C., MSc.,

who fired my curiosity of the natural world at an early age.

The work contained in this thesis is my own original work and none of it has previously been submitted for any other degree or examination.

Rowland Taylor

Acknowledgements

I would like to thank my supervisor, Professor P.W. Gage for all his advice and encouragement during the course of my PhD.

I am grateful to Professor A.R. Martin, Dr R.J. French, Dr A.J. Gibb, Dr M.E. Krouse and Dr J.E. Dawson for helpful discussions on some of the theoretical aspects of this thesis. I would also like to thank Dr S.J. Redman, Dr G.D. Lamb and Dr P. Sah for their valuable criticisms of the drafts. I enjoyed many stimulating discussions with my fellow PhD. students, Brian Robertson, Pankaj Sah, Mike Chua, Franscis Edwards, David McKinnon and Gavin Schnieder.

I am indebted to Dr R.E. Fyffe and Dr S. Ghosh for supplying the cat DRG used in this study, and to Professor R. Porter for the monkey ganglia.

Finally, it is a pleasure to thank my family for their assistance, interest and encouragement over the last four years, and N. Garnett for her unfailing support and patience during the preparation of this thesis.

ABSTRACT

The sustained calcium current was recorded in the soma of cat DRG neurones using two suction-electrode voltage clamp techniques. A detailed kinetic analysis of the calcium current revealed that the minimal sequential model that will describe the channel kinetics has three closed states preceding an open state. The proposed 4-state model was able to describe the voltage-sensitivity of the data quantitatively but did not adequately account for the temperature sensitivity of the calcium current. The number of gating charges per calcium channel depended on the model used to fit the data, and was $4.4e^+$ for the 3-state model and $5.6e^+$ for the 4-state model.

(±)Bay K8644 had only moderate effects on the calcium current at a concentration of 10μM. The drug decreased the slope of the steady-state activation curve, and reduced the threshold for activation of the calcium current. There were also complex changes in the activation and deactivation time constants.

The effects of replacing the external calcium ions with barium were largely due to changes in the surface charge. There was some evidence for a direct action on the calcium channel.

Calcium currents recorded from rabbit and monkey DRG appeared to be very similar to those recorded from the cat.

Preliminary data was obtained on the asymmetric capacitive currents in cat DRG neurones. The currents

satisfied a number of the criteria for gating currents associated with the activation of voltage dependent channels, and were tentatively identified as calcium gating currents.

The blocking effects of cadmium ions were investigated. The ion appeared to block the calcium channel at two distinct sites, one within the membrane electric field (K_d(0mV) = 16μM) and the other outside the electric field (K_d = 106μM). Cadmium block was relieved at hyperpolarized potentials as if the ion were able to pass through the channel. The voltage dependence of the relief of cadmium block was equivalent to a cadmium ion crossing 75% of the membrane electric field as it left the channel.

Reversal of the current flow through calcium channels was recorded with barium ions on both sides of the membrane. The instantaneous I-V rectified more sharply than expected from the difference in the ion concentrations across the membrane. The reason for this rectification was not clear.

Two sodium currents were recorded in cat DRG neurones, one blocked by TTX and the other resistant to TTX. There were marked differences in the kinetics and permeation properties of these channels.

CONTENTS

Chapter 1

INTRODUCTION

Preparation

The aim of this thesis was to investigate the properties of calcium channels in freshly isolated mammalian neurones. Two aspects of channel function were investigated, the voltage dependent gating process, and the permeation process. Some preliminary data were obtained on the charge movement associated with the activation of the calcium channels.

The cell bodies of cat dorsal root ganglion neurones were used. These neurones are specialized, in that the peripheral termination is an energy transducer, corresponding to one of the sensory modalities. The sensory information is relayed to the spinal cord, passing the cell bodies in the ganglia in transit. The cell soma is not part of the transmission pathway, and does not receive any synaptic input (Willis & Coggeshall 1978). Excitability of the soma is not required to transmit the information to the spinal cord, and the reason for action potentials in the cell body are unknown. A single axonal process leaves the soma and bifurcates, one branch projecting to the spinal cord and the other to the periphery. This morphology makes the soma ideal for voltage clamp studies, since the cell body can be electrically isolated, and excellent space clamp of the surface membrane achieved.

Interpretation of the data

The central theme of this thesis is the use of electrical recording techniques to assay the transitions between the various conformations of a membrane bound protein. The interpretation of the data relies on a number of basic assumptions.

1) The observed membrane current is proportional to the number of open channels. This requires that the single channel current be constant during the recording period. Previous single channel studies have indicated that the unit current amplitude is constant, independent of pulse duration (Lux & Brown, 1984). This result allows the current relaxations to be attributed to changes in the probability that the channel is open.

2) The observed current is produced by current flow through a homogeneous population of channels. This supposition is often easy to disprove, but very difficult to establish with certainty. The best that can be said is that the results are consistent with a single population of channels having particular properties. One can then say that the current is produced by a functionally homogeneous population. The underlying implication is that the channels are structurally homogeneous as well, which is not necessarily the case. This uncertainty underlies the basic problem in channel research; relating the architecture of the ion channels to the functional mechanisms.

3) The principle of microscopic reversibility (detailed balance) is assumed to hold. Each activation

reaction is reversible; the channels are not "used up" during the activation process.

4) Channel gating is assumed to involve a large conformational change in the protein molecule. The most direct evidence in support of this are volume changes which accompany channel activation (Conti et al. 1982, Zimmerberg & Parsegian 1986). In the case of voltage activated channels, it is generally assumed that the channel senses the changes in the membrane electric field through the dipole moment of the protein.

5) The channels act independently of each other. This assumes that the various reaction rate constants are not affected by the presence of another channel close by in the membrane. The density of many voltage activated channels is relatively low when compared to the density of channels at the neuromuscular junction where there are 9-15 x 10^3 acetylcholine activated channels per square micrometer (Fertuck & Salpeter 1974, Dreyer et al. 1978). Even at this high density the end-plate channels appear to act independently since end-plate currents follow approximately first order kinetics (Gage & Armstrong 1968, Magleby & Stevens 1973). A consequence of independence is that the rates of relaxation of the system after a perturbation will not depend on the initial conditions. The system response will depend only on its present condition and not on its past history. Independence allows the reaction kinetics to be formulated, in terms of probability theory, as a time-homogeneous Markov chain in which the conformational states are the random variables and the rate constants are the probabilities of exchange.

The application of stochastic theories to membrane channel reaction kinetics has been developed by a number of authors (Conti & Wanke 1975, Colquhoun & Hawkes 1977, Baumann & Easton 1981, Horn & Lange 1983).

Given the above conditions, if N exponentials are required to fit the macroscopic current relaxations (current due to the activation of a large number of channels), then there are at least N+1 conformations in the reaction scheme. Much of the data on the kinetic characteristics of membrane channels available at present gives an indication of the minimum number of channel states, and the possible pathways that link the states.

Perhaps it would be useful to clarify what is meant by channel "states" or "conformations". A particular state of a channel could be completely described if one knew the exact orientation and energy level of each atomic constituent of the protein at a particular instant. Viewed in this way the possible number of states for an average sized protein molecule would be extremely large. A slightly coarser approximation might be to look at the orientation of each constituent amino acid residue in the protein (Stein 1985). Even this will result in a very large number of channel states. The sodium channel from electroplax for example, has recently been sequenced and found to contain 1,820 amino acids (Noda et al. 1984). If it is assumed that each residue could adopt two orientations in the tertiary structure of the protein then the possible number of states is 2^{1820}. Much of the kinetic behaviour of the most widely studied channels can be

explained by invoking the existence of less than 7 channel conformations (eg. acetylcholine receptor; 4, Sine et al. 1986, Na channel; 4-6, Armstrong 1981, French & Horn 1983, Ca channel; 3-4, Hagiwara & Byerly 1983, K channel; 6, Gilly & Armstrong 1982) and in one case only two (K channel, Larbaca et al. 1980). This would lead one to believe that the vast majority of the conformational states of channels are functionally degenerate, in the sense that the energy fluctuations of single residues do not in general have immediate functional consequences.

Conformational states might be viewed as subsets of the total number of molecular orientations. These subsets would be linked by common members, the "transition complexes" of rate theory (Glasstone et al. 1941). The intersection of the conformational subsets would also be expected to contain a large number of elements as the constraints on the transition configuration must be reasonable if a significant proportion of the molecules are to adopt that configuration and pass through the reaction step. Thus a protein conformation might be viewed as a dynamic entity, consisting of a large number of different molecular configurations in rapid equilibrium.

In this thesis, "conformations" and "states" will be used interchangeably to refer to those subsets of orientations of the protein that can be resolved by electrophysiological techniques.

Channel structure and function

The probability of a large and complex molecule, with many degrees of freedom, adopting a transition configuration is greatly increased if an external energy source is present to drive the transition. In the case of voltage activated channels, the electric field across the membrane provides a force to physically move the components of the protein, producing the desired orientation of the various structures, and allowing the conformational change to take place. Although a great deal is known about the mode of activation of voltage activated channels, almost nothing is known about these underlying molecular changes.

Isolation of the genetic material coding for sodium and acetylcholine-receptor channels from eel electroplax has great potential for elucidating the molecular mechanisms of channel gating. The primary structure of these two channels has been established (Noda et al. 1983, Noda et al. 1984). The next problem is the elucidation of the secondary and tertiary structures. Detailed information at atomic resolution, on the structure of many proteins has been obtained using X-ray crystallography (Matthews & Bernhardt 1973). This technique is not readily applicable to membrane bound proteins, due to the difficulties in obtaining pure crystalline material (Eisenberg 1984). An alternative approach may prove to be very useful. The 3-dimensional structure of the protein is predetermined by the primary structure, and so it should be possible to accurately predict the secondary and

tertiary structures from the amino acid sequence (see Chou & Fasman 1978, Chothia 1984, Eisenberg 1984). On the basis of such calculations, Noda et al. (1983) proposed a secondary structure for the electroplax sodium channel having four α-helical membrane-spanning regions.

Even this preliminary structural data is highly suggestive, and seems compatable with the proposed number of channel states from electrophysiological data. For example, one might envisage that each trans-membrane region changed orientation sequentially to produce an open channel. Catterall (1986) has developed similar ideas, and more detailed predictions of the secondary structure have produced more detailed structural models (Greenblatt et al 1986, Guy & Seetharamulu 1986). Since there are four regions, this implies at least 4 closed states and one open state consistent with the electrophysiology (Armstrong 1981), assuming that the conformational changes during activation involve gross movements of the secondary structures (Zimmerberg & Parsegian 1986). It is also possible that some of the observed conformations could be due to movements of much smaller groups of residues or even single residues.

Covalent modification of membrane channels has been used previously in an effort to relate the structure of the channel to the functional characteristics (reviewed by Brodwick and Eaton 1982). One of the main problems with such experiments was that the position of the modified groups on the channel protein was unknown. The more detailed information now available on the structure of the

sodium channel should allow more accurate interpretation of such data, and may provide a means of testing the validity of proposed structural and functional models.

If, as Hille (1984) has suggested, the calcium channel is the evolutionary precursor to other voltage activated channels, then one might expect a certain amount of structural homology between it and the sodium channel. Certainly, the electrophysiological data suggest that the two channels probably have a similar number of closed conformations. It may turn out that electrophysiological data can accurately predict the number of structural components of membrane channels.

Permeation

The permeation properties of pores is another area where clear structural information will allow specific models to be advanced. Rate theory models have been used to describe the permeation characteristics of some biological channels. These models were developed as it became obvious that the widely used Goldman-Hodgkin-Katz (GHK) formalism (Goldman 1943, Hodgkin & Katz 1949), with its assumption of independence, was unable to account for the saturation and interaction of ions during permeation (Hodgkin & Keynes 1955, French & Adelman 1976, Hille & Schwarz 1978, Coronado, Rosenberg & Miller 1978, Begenisich & Cahalan 1980a,b). Application of rate theory to permeation can successfully account for saturation and ion interaction, without being specific about the

molecular mechanisms of the reactions. The main advantage/disadvantage of rate theory models is that there are generally a large number of free parameters. In some cases the number of free parameters can be reduced by making certain assumptions about the channel. For example the number of free parameters for the two site model for the calcium channel was halved by assuming the channel was symmetric.

Rate theory models are useful in that they are physically suggestive. Thus, it has been suggested that the energy wells or binding sites correspond to charged residues protruding from the walls of the channel (Kostyuk et al. 1982). For all the success of rate theory permeation models, they share the same status as the kinetic models; they are empirical approximations which are essentially independent of the actual molecular mechanism. Without precise structural information, it remains difficult to sort through the vast number of possibilities and produce a model that will successfully account for all the observations.

Even with an accurate picture of the structure of the pore, it may turn out that permeation cannot be approximated by rate theory with a static energy profile. Lauger and Apell (1982) have compared molecular dynamics simulations with rate theory and found that the two produce quantitatively different predictions. Molecular dynamics simulation models require very precise information about the physical structures of the reacting groups and the structure of the surrounding water. At

present the most detailed simulations have been applied to the gramicidin A channel, where the structure is well defined and the permeation properties have been studied extensively (Polymeropolous & Brickmann 1985). Additional information must be obtained before such models can be realistically applied to other more relevant biological channels.

This thesis examines the kinetic and permeation properties of the slowly inactivating calcium channels in cat dorsal root ganglion neurones, and relates the results to the rate theory models previously proposed for these processes.

Chapter 2

METHODS

2.1 Preparation

Dorsal root ganglia (L_5,L_6 & S_7) were removed from adult cats (1.2 - 2.5 kg) during the course other neurophysiological investigations carried out on the whole animal. The cats were anaesthetized with sodium pentobarbitone and a dorsal laminectomy performed. Ganglia were removed with 3 mm of the medial nerve trunk and 10mm of the peripheral nerve trunk attached, and transferred to cooled standard solution. The excess deura and connective tissue was dissected away using iridectomy scissors. The ganglia were pinned to the sylgard base of the recording chamber. More of the surface connective tissue covering the ganglia was stripped away using a fine pin, to expose the cell bodies. Trypsin (0.5% type IX, Sigma) and collagenase (0.5%, type IA, Sigma) were dissolved in standard solution and applied to the ganglia at 30^{o} C for one hour.

The enzyme treatment was essential for a number of reasons. The surface membrane of the cells was cleaned, allowing good sealing resistance between the suction electrodes and membrane to be formed. The removal of the connective tissue between the neurones dispersed the cells. It aided the breakdown of the aspirated piece of membrane when the suction electrode was applied, and so

facilitated internal perfusion. The enzyme treatment weakened the axons allowing the soma to be isolated.

It is difficult to assess the effects of the enzyme treatment on the properties of the neuronal membrane, since the suction electrode techniques could not be applied successfully to untreated cells. One might expect that integral membrane proteins, such as channels, would be relatively inaccessible to the active sites of proteases. The presence of numerous sugar residues on the external face of most membrane bound proteins might also hinder protyolytic attack. Certainly, the kinetic properties of the Ca and Na channels observed here are qualitatively similar to those observed previously in preparations which have not been exposed to proteases. Harper and Lawson (1985) found that collagenase treatment did not affect the properties of action potentials in rat sensory nerones. It should be borne in mind, however, that there may be some subtle differences between the results presented here and those that would be obtained from untreated membranes.

The best recordings were generally obtained within the first 2 hours after completion of the enzyme treatment (3 hours after removal from the animal), although in some exceptional cases good recordings were be obtained up to 4 hours later. Large calcium currents were only seen in healthy cells with resting potentials of more negative than -40 mV. The loss of calcium currents seemed to parallel the deterioration of the preparation.

The techniques described in this chapter were also

succesfully applied to ganglia obtained from rabbits and guinea pigs. The cell bodies of the neurones from these preparations were smaller than those obtained from the cat which made application of the two electrode voltage clamp less attractive. The results presented here were all obtained from cat ganglia.

The larger cells with diameters of 50 to 100 µm, were used as these cells were easier to work with. No attempt was made to correlate the size of the cells with the membrane properties. There were no obvious differences in the characteristics of the calcium currents from cell to cell.

2.2 Electrodes

The suction electrodes were fabricated from 1.5mm borosilicate haematocrit tubing. Two intracellular type electrodes were pulled on a vertical puller (Kopf, 500C). The heat setting was adjusted until the tips showed a pleasing taper. A short taper was advantageous for low resistance electrodes. The tip of the electrode was then scoured at an external diameter of 80 to 100 µm, and broken off. Scouring was done under a dissecting microscope at 80x magnification. The tip of the electrode was moved back and forth along the edge of a suitably positioned glass coverslip with the aid of a micromanipulator. After breaking, the end was generally flat normal to the shank of the electrode and the rim was perfectly smooth. The tip was then fire polished under a

microscope, on a microforge, to an internal diameter of 10-15µm. When filled with the internal solutions (see below), the resistance of the electrodes was 0.5-0.8 MΩ. The same electrodes could be used many times during the course of an experiment provided that the tips remained clean. Often debris could be cleaned from the tip by impaling the sylgard base of the bath.

The bath ground and bath voltage electrodes were simply lengths of 1mm electrode glass (Clark Electromedical), filled with 3 M KCl/agar.

2.3 Solutions

All concentrations are given in millimolar. The pH of all solutions was 7.4.

External solutions.

Standard external : 140 NaCl, 2 KCl, 5 $CaCl_2$, 10 N-2-hydroxyethylpiperazine-N-2-ethane-sulphonic acid (HEPES), 10 D-glucose.

Calcium currents : 115 choline-Cl, 25 tetraethylammonium bromide (TEA), 2 CsCl, 1 $MgCl_2$, 10 $CaCl_2$, 10 HEPES, and 10 D-glucose

Sodium currents : 115 NaCl, 25 TEA, 2 CsCl, 1 $MgCl_2$, 10 $CaCl_2$ & 1 $CdCl_2$ or 10 $CoCl_2$, 10 HEPES and 10 D-glucose.

Internal solutions.

Standard internal : 140 KCl, 20 NaCl, 10 ethyleneglycol-bis-(β-aminoethylether)-N,N-tetra-acetic acid (EGTA), 5 HEPES.

Calcium currents : 140 CsCl, 10 TEA, 10 EGTA, 5 HEPES.

Sodium currents : 120 CsCl, 20 NaCl, 10 TEA, 10 EGTA, 5 HEPES.

For many of the cadmium block experiments on the calcium current, 20mM of the internal CsCl was replaced with 20mM CsF. The internal flouride did not affect the calcium current, but did improve the stability of the recordings. This is an interesting observation, since internal flouride has been shown to block calcium currents in molluscan neurones (Kostyuk et al. 1975), but not in heart cells (Lee & Tsien 1984). It suggests a basic difference between mammalian and invertebrate calcium channels.

Bay K 8644 (a gift from Bayer) and nifedipine (Sigma) were dissolved in ethanol to a concentration of 10 mM and quantities of this stock added directly to the external solution. An equal amount of ethanol was added to the control solution. Solutions were made up freshly every two days and were kept refrigerated.

The bath temperature was maintained at 20°C by a peltier element. Solutions were perfused continuously at rates of 2-3 ml per minute, except when recording. The inflow tube ran through the peltier block before entering the bath. The pre-cooling was particularly important for the high perfusion rates used when exchanging the external solution. Solution flow was stopped while recording since the suction outflow produced a great deal of noise on the current trace. This was the major disadvantage of using a virtual-earth current monitor.

When the external solution was changed, 5-10 mls were perfused rapidly and records taken 1-2 minutes after commencement of perfusion. Care was taken to ensure that the temperature was steady before records were taken. The bath volume and dead space was about 0.25 ml and so the bathing solution was exchanged 10 to 20 times during the solution change over. The cell was moved well away from the ganglia so the solution around the cell was exchanged rapidly.

2.4 Voltage clamp

The voltage clamp used was of conventional design. The circuit diagram is shown in figure 2.1. The clamp consisted of 4 parts, the voltage recording headstage, the bath voltage headstage, the virtual earth current monitor and the rack-mounted clamp. These will be described in turn.

The voltage recording headstage consisted of a non-inverting voltage follower with 10x gain. The output could be fed back to the input through a capacitance via a second op amp with variable gain. This capacitance compensation was used only minimally. Input capacity was minimised by having the high impedance input of the voltage follower as close as possible to the recording electrode. The headstage amplifier was placed in a plastic 35mm film container (Kodak), and the assembly mounted onto the micromanipulator. The electrode socket was soldered directly to the non-inverting input of the

Figure 2.1 : Two Electrode Voltage Clamp.

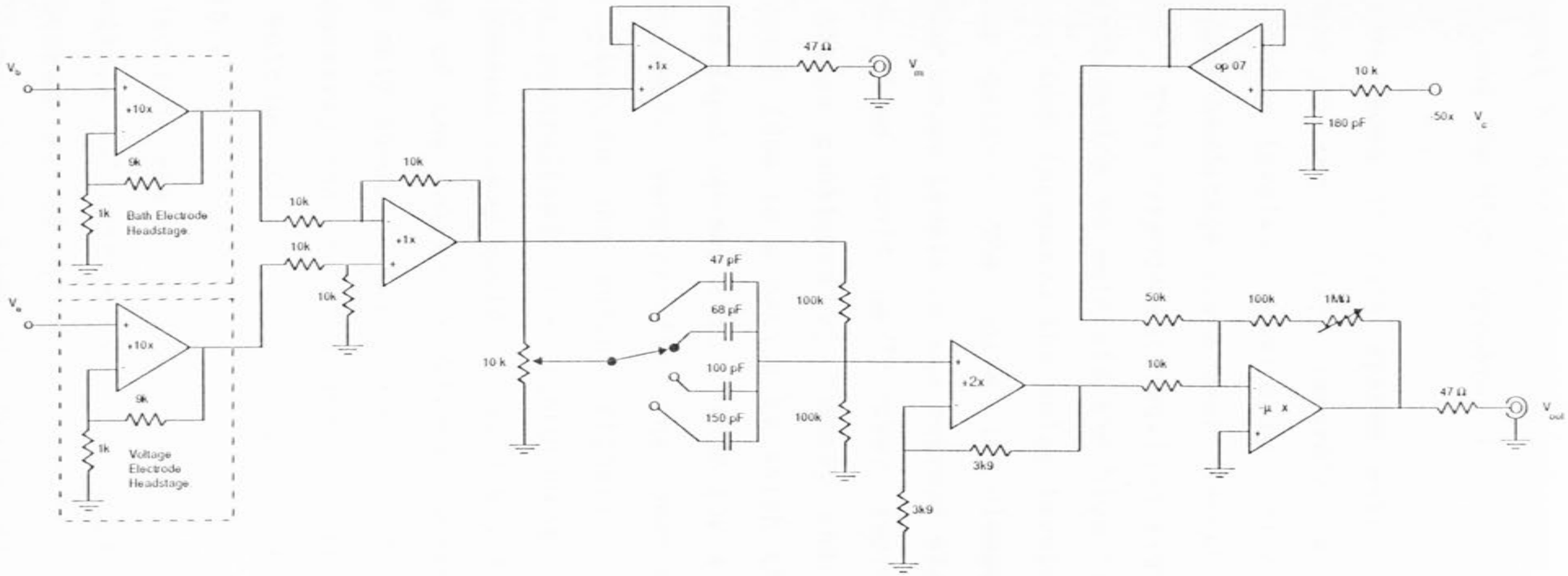

op-amp leaving about 7 cm of unshielded conductor between the electrode tip and the high impedance input of the op-amp.

The main advantages of this system were the high frequency response of the voltage recording electrode, coupled with low noise levels. Previously, the electrode was connected to the headstage via a short length (10 cm) of shielded cable. This arrangement required significant capacitance neutralization to maintain the high frequency response, which in turn increased the noise levels of the voltage recording path. The noise is clamped, and manifests as higher noise levels on the current signal.

The voltage clamp could be further improved by implementing a design published by Kootsey and Johnson (1973). The central idea is a method by which the input capacitance of the input op-amp (about 4 pF for a typical LF 356) is neutralized. Very briefly, the power rails of the op-amp are tied to the output signal. If this capacitance were neutralized, the improvement in performance of the present clamp would be marginal, since the RC time constant of the voltage electrode, op-amp input capacitance, was only about 2-3 μs. However, it would be beneficial to bootstrap the input op-amp, if one were to build a fast voltage clamp with higher resistance electrodes (>10MΩ).

The bath electrode was connected to the clamp via a non-inverting voltage follower with 10 fold gain. The signal was filtered at 16 kHz, to reduce the high frequency noise input to the summing junction which would

otherwise increase the noise levels or even destabilize the clamp causing oscillation. The bath electrode signal was subtracted from the voltage electrode signal by the differential amplifier on the input to the voltage clamp. Recording the membrane potential differentially obviated variations in the bath potential and any series resistance errors introduced by the finite resistance of the current monitor electrode.

The membrane current was measured by a virtual-earth current monitor. The bath was clamped at ground potential through a 1 MΩ feedback resistor. The current monitor was connected to the bath via a Ag/AgCl electrode and a KCl/agar bridge. The virtual earth method had the advantage that only currents flowing into the bath were measured. The other commonly used current monitoring technique is to measure the current flowing through a resistance in series with the current passing electrode. This method has two main disadvantages. 1) The resistance around the feedback path of the voltage clamp is increased, which compromises the performance of the voltage clamp. In the case of the voltage clamp system used here (using 0.5-0.7 MΩ current passing electrodes), a 1 MΩ resistor in series with the feedback path would increase the resistance of the current passing by almost three fold. 2) The current required to charge the electrode and cable capacitances is also recorded. Although this should be linear it adds to the noise of the system.

The rack mounted clamp contained three main elements.

The first stage was a unity gain differential amplifier which subtracted the bath potential from the voltage electrode signal. This signal fed into a phase compensation circuit and then to a summing juntion.

Phase compensation was implemented as described by Finkel (1985). Phase lead or lag could be added to the voltage signal at variable frequencies. Generally phase lead was used. The frequency was set to 150 kHz and the ten turn potentiometer set to 6-8. Phase compensation was incorporated to enable higher open loop gains to be used while maintaining the stability of the clamp during the voltage steps. Too little or too much phase lead would result in underdamped oscillation of the clamp after a voltage step. The phase compensation circuit was set to unity gain.

The compensated voltage signal was added to the command voltage at the summing junction of the output op-amp. The error signal from this variable gain inverting amplifier was applied to the current electrode. The clamp was usually run with the gain of this stage set at 40-60x, giving a total gain around the feedback path of 400-600 fold, more than adequate to obtain high DC fidelity and a very rapid step response (see Finkel & Gage 1985, equation 4). The low resistance of the current passing electrode ensured that the attenuation of the error signal by the current-electrode/membrane voltage divider was minimal. This attenuation factor tends to reduce the gain of the voltage clamp.

The inter-electrode coupling capacitance was

minimized by placing a grounded aluminium foil shield on the current electrode. The shield extended to within 1mm of the electrode tip. The clamp would invariably oscillate at low gains if the shield was not in place.

2.5 Series Resistance

Series resistance can be a major problem for voltage clamp systems as it causes distortions in the time course and the peak level of the currents recorded. It arises when there is a significant resistance to ground in series with the membrane resistance, and can occur for example, when the electrical access to the membrane is restricted due to very small interstitial space or membrane infolding. Series resistance due to membrane infolding is probably not significant in this preparation for the following reasons.

Many reports have indicated that there are numerous perikaryal projections from cells in sensory ganglia. Perikaryal projections are finger-like projections of the surface membrane ranging in length from 0.3 to 3.25 µm, and having a diameter of 0.2µm. The presence of these structures increases the surface area of the cell body by 43% in the cat thoracic DRG neurones (Pannese et al. 1983). The size and morphology of the perikaryal projections precludes them from contributing significantly to series resistance errors. Brown and co-workers (1983) estimated that the series resistance in helix neurones was less than 5kΩ, even with the extensive invaginations of

the membrane of the preparation. There does not appear to be the extensive invagination of the membrane in cat DRG neurones that is found in molluscan preparations and so one would expect the membrane series resistance in cat DRG neurones would be less than that measured in molluscan neurones.

A virtual earth circuit can also contribute to series resistance, if the membrane potential is not recorded differentially. The voltage clamp used measured membrane voltage differentially to eliminate series resistance errors added by the current monitor. Since many of the results reported here depend on accurate records of the large transient calcium tail currents the errors introduced by series resistance had to be assessed carefully.

Series resistance errors become significant when the series resistance is comparable to that of the clamped piece of membrane. The worst case for the present recording situation occured when recording a calcium tail current at -70 mV. The peak currents were as large as 400 nA. These values give a membrane resistivity of 200 kΩ. Therefore, series resistance would have to be 10 kΩ or less to give errors of less than 5% in the voltage signal. Attempts were made to measure the series resistance directly by applying 50 nA hyperpolarizing current pulses to the membrane and measuring the voltage reponses. A series resistance of 10 kΩ would result in an initial instantaneous jump of 0.5 mV followed by the slow charging of the membrane capacitance. The voltage response

appeared to rise directly from the base-line. At high gains it was difficult to decide whether an instantaneous jump in voltage had occured due to the very large voltage signal. Convincing evidence that series resistance did not introduce significant errors is shown in figure 5.1. Here the shape of the instantaneous I-V is independent of the amplitude of the tail currents.

2.6 Space clamp

For most of the experiments the soma was voltage clamped with up to 500µm of the axon attached. However in many cases the cells had less than 100µm of axon attached. There were no obvious differences in the calcium currents recorded in either case. This is probably because the calcium channels are restricted to the soma of the cells and are not found in the axons. Thus, when the sodium and potassium channels are blocked, the clamp current flowing into the poorly clamped distal regions of the axon should be linear over a large potential range and will be removed by the subtraction procedure.

The situation was less favourable when sodium currents were being recorded. Figure 2.2 shows a typical example of the problems encountered. The traces were obtained by stepping from -50mV to the potentials indicated. The broken lines show the currents recorded when there was about 5mm of the axon attached. The step to -20mV reveals a prominent "break through spike", presumably due to a regenerative response travelling away

Figure 2.2 Comparison of the sodium currents recorded in a cell before and after the soma is isolated from the axon. The broken lines show the current responses during 10ms voltage pulses to the potentails indicated next to each trace. The solid lines were obtained using identical voltage pulses, after the axon had been cut off close to the cell body. The poorly clamped regions in the axon tend to result in over estimation of the peak current, at potentials close to threshold. The magnitude of this error appears to become smaller at more positive potentials.

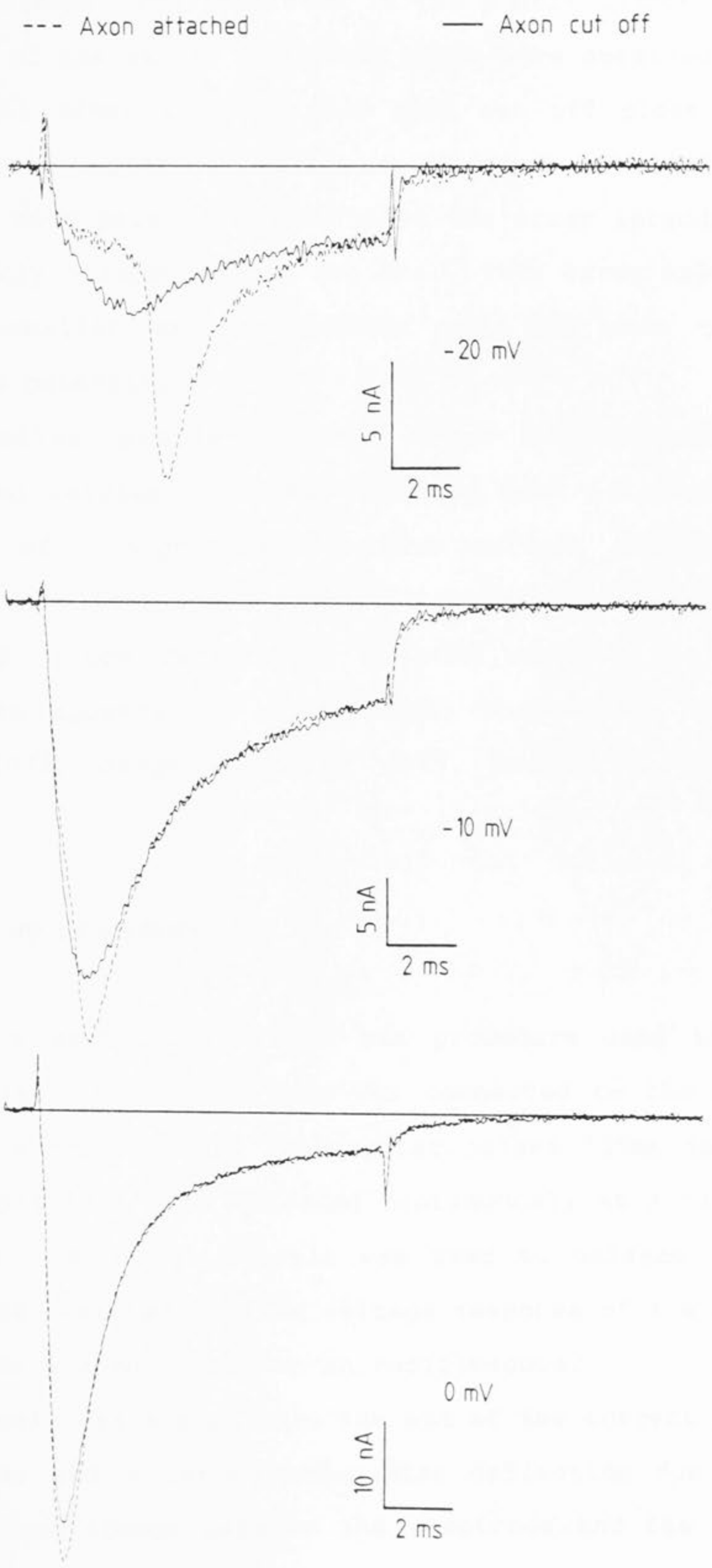
--- Axon attached
—— Axon cut off
-20 mV
5 nA
2 ms
-10 mV
5 nA
2 ms
0 mV
10 nA
2 ms

from the soma, and initiated in the poorly clamped distal regions of the axon. The solid lines were obtained in the same cell after the axon had been cut off close to the soma, using a pair of iridectomy scissors. The difference between each pair of traces shows the error introduced by the poorly clamped axonal regions. This error appears to become smaller as the voltage step is made to more positive potentials.

Similar problems were never encountered when recording calcium currents with the axon attached. The absence of a significant calcium current in the axon, allowed excellent space clamp of the calcium channel to be achieved. Low density of calcium channels in axonal membranes appears to be a common observation (Meves & Vogel 1973, Junge & Miller 1977, Dichter & Fischbach 1977).

2.7 Set up procedure

This section describes the procedure used to clamp the cells. A current pump was connected to the current passing electrode, and rectangular pulses (20ms duration, 10nA amplitude) were injected continuously at a frequency of 2 Hz. A bridge circuit was used to balance out the electrode resistance. The voltage response of the current electrode was monitored on an oscilloscope.

A cell was sucked onto the end of the current passing electrode and a large rectangular deflection due to the sealing resistance between the electrode and the surface

membrane was observed. Generally the aspirated piece of membrane would break down within seconds, and the voltage trace would round off, showing the charging curve characteristic of the cell membrane. If calcium currents were being recorded the cell was hyperpolarized by constant current injection before the voltage electrode was applied. Hyperpolarization was necessary to prevent calcium action potentials which would otherwise occur. The calcium action potentials (without potasssium currents) lasted for 0.5 to 5 seconds and presumeably produced a large transient increase in the internal calcium concentration close to the membrane. This would often lead to irreversible loss of the calcium current; the internal EGTA seemed unable to prevent this

Cells with an input resistance greater than 5 MΩ, and a resting potential more negative than -40 mV were examined further. The voltage electrode was brought up to the cell membrane until it was just touching the surface and suction was then applied. When the membrane within the electrode broke down the voltage trace was seen to drop and overlie the voltage trace of the current electrode. If there was no obvious deterioration of the input resistance or resting potential of the cell, after the voltage electrode was applied, the experiment was continued. An equilibration time of around two minutes was allowed before commencement of recording.

The voltage clamp was turned on and the membrane clamped at -50 mV. The clamp was tuned by applying 20 mV hyperpolarizing pulses to the membrane at 2 Hz. The step

response was observed at a high sweep speed (0.2 ms/division), and the clamp gain and phase compensation adjusted until an optimal response was obtained. Figure 2.3 shows typical voltage and current traces recorded for a 50 mV hyperpolarizing voltage step. The voltage trace is unfiltered. The current trace is filtered at 32 kHz. Both signals were recorded at 2 µs/point. The recorded voltage rose in 6µs, but oscillated for about 25µs. Although the current signal should show a similar settling time after a step change in potential, it is seen to oscillate for 60µs in this case. This apparent discrepency is due to the lower filter cut-off for the current signal.

The rapid settling time indicates that the potential across the membrane is established very quickly. In the data that will be presented, the first reliable point on subtracted current traces was 120µs after the potential step (marked by the vertical lines in figure 2.3). The response in figure 2.3 would suggest that the clamped membrane is isopotential at this time. The failure to realise the full dynamic response of the system was due in large part to timing errors during output of the command pulses, as described subsequently.

The peak of the capacitive transient in figure 2.3 is 2µA. The largest calcium tail currents were a fraction of this value which indicates that the clamp was capable of passing the current required to clamp these large transient currents.

A shaped wave form, generated by a "transient

Figure 2.3 The traces illustrate the dynamic response of the voltage clamp during a 50mV hyperpolarizing pulse from a holding potential of -50mV. The upper trace shows the recorded membrane potential, and the lower trace shows the membrane current recorded by the virtual earth current monitor. The vertical lines were drawn 120μs after the voltage step.

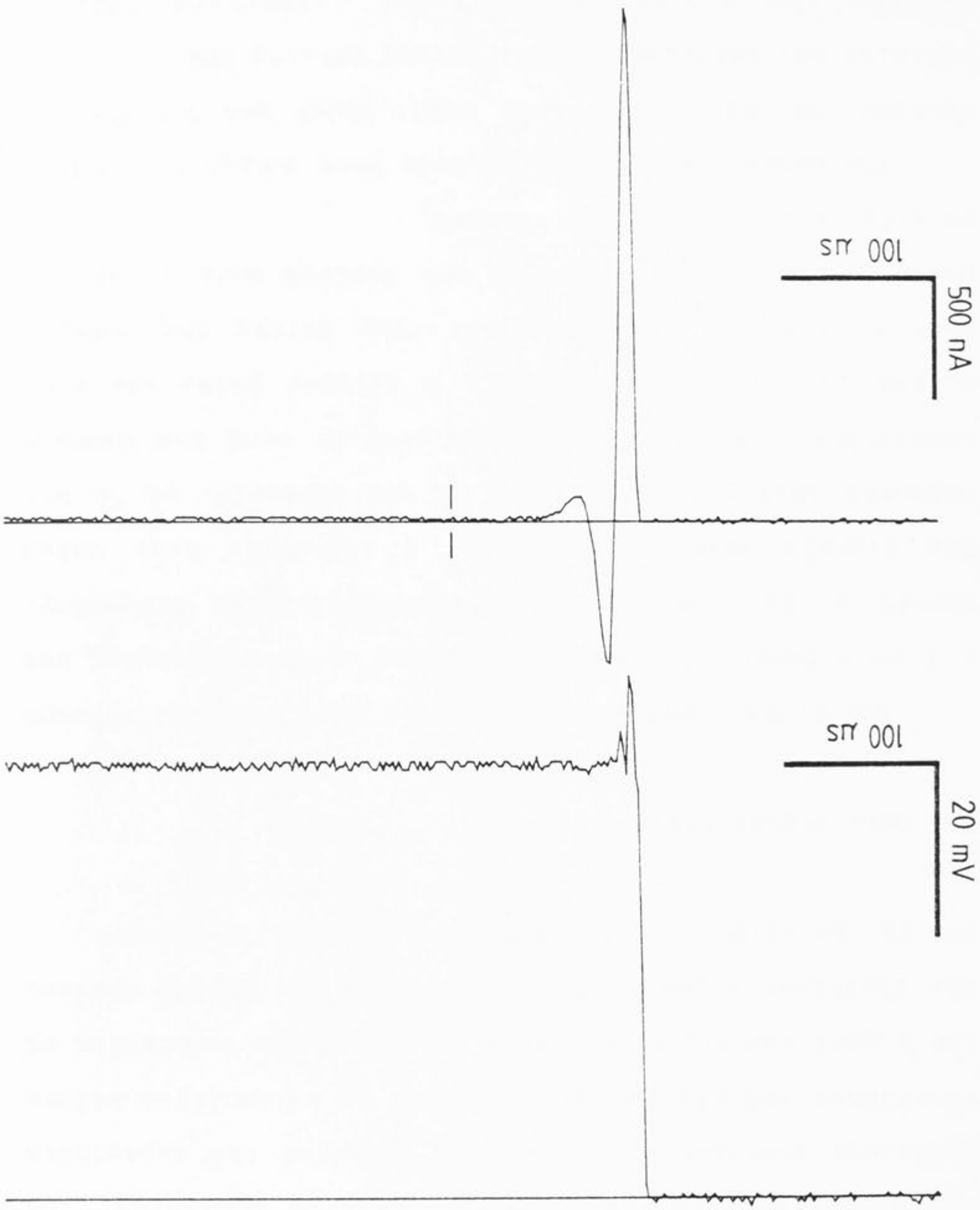
100 µs
500 nA
100 µs
20 mV

subtractor", was added to the current signal via a summing junction. The wave form mimmicked the capacitive transient, and had variable rise time and an exponential decay. After the clamp was tuned, the transient subtractor was turned on, and the wave form adjusted until the capacitive transient was as small as possible. The transient subtractor removed the peaks of the capacitive transients and allowed higher gains to be employed before the signal was digitized, thus improving the resolution of the digitized signal. The subtraction was seldom perfect due to the slight oscillation that was usually present.

2.8 Data acquisitition

The current and voltage signals were filtered through a 4 pole Bessel filter. The filter corner frequency was chosen to be lower than half the digitizing frequency. The signals were digitized by a tektronix cro, which captured 1016 points on each of two channels, at 10 bit resolution. A micro 11/23 was used to send the command pulses to the voltage clamp. A trigger pulse was also sent to the cro at a variable time during the command pulse profile, thus allowing the desired section of the profile to be captured by the cro.

The command and trigger pulses were output by a macro routine (written by Dr. A.J. Gibb) which was designed to minimize the instruction time during polling the clock and setting the digital to analogue converters (DACs). Without this precaution the variations between the actual

trigger times and step times could become significant compared to sampling rates of 10 to 20 µs. This jitter in the actual step time is effectively doubled when two traces are added. Unfortunately the problem could not be entirely alleviated and this mismatch contributed to the imperfect subtraction of the capacitive transients seen in most of the records illustrated. The mismatch is most evident in records of the fast sodium current recorded at 10 µs per point (see figure 6.3). Ideally a hardware device would be used to output the trigger and command pulses when sampling at rates less than 100 µs per point.

The digitized data was transferred from the cro to computor via a general purpose interface bus (GPIB) and subsequently stored on a hard disk. On completion of the experiment the data files were transferred to an 11/44 for analysis and archiving.

The leakage and capacitive currents were subtracted in all cases. Equal and opposite voltage pulses were applied to the membrane and the resulting currents added digitally prior to further analysis. This technique was refined in later experiments, and a series of small hyperpolarizing pulses (≤30mV) were added together on line, until the sum of the pulses was equal to the depolarizing test pulse. The second method was preferable as there was some indication that the leakage current was nonlinear for large steps away from the holding potential. This nonlinearity of the leak current is evident as a plateau current during the gating current experiments (see Chapter 4). It appeared to be time independent, and so did not

significantly distort the time course of the calcium currents. The reason for this nonlinearity is unknown, but it could have been due to asymmetry in the current flow across the sealing resistance.

2.9 Analysis

(i) Digital Filter

In many cases a digital filter was used to further reduce the noise level on the current traces before fitting the relaxations with exponential functions. A first order Butterworth filter was used (Beauchamp & Yuen 1979, pp 261) with a cut-off frequency set to the aquisition filter frequency. Generally the filter was passed forwards and backwards over the data which resulted in zero added phase shift for the filtered trace.

(ii) Curve Fitting

Theoretical curves could be fitted to the data using a modified Levenberg-Morrison-Marquardt (LMM) algorithm (Osborne, 1976), which minimizes the sum of the squared deviations between the observed and predicted values. The algorithm, with some modifications, was implemented in Fortran by A.J. Miller (1981). The LMM routine was used to fit single and double exponential functions to the current relaxations. Provided that good initial values of the parameters were selected, this algorithm converged

rapidly. Starting values for the various parameters were obtained by doing trial fits to the data by eye, with the aid of a graphics terminal. After some practice the starting values could be estimated by inspection. The final parameter estimates produced by LMM were also checked on the graphics terminal.

Much of the data presented depends on accurate measurement of the amplitude of the tail current relaxations. This represented a problem since the peak current at negative potentials was not resolved due to the very rapid decay rates. If the tail current measurements are to be compared, the measured amplitude must be independent of the time course of the tail current. Clearly, the peak tail current observed at -70 mV will be attenuated more than that observed at -40 mV, as the current decays more rapidly at -70 mV (see figure 5.1). Comparison of the observed peak currents in this case would be meaningless.

The attenuation can be corrected for if the peak tail current is measured by extrapolation. To do this, the tail relaxation is fitted by an exponential, or sum of exponentials (two in the case of calcium currents), and the fitted curve extrapolated back to the step time. In the example above , the extrapolation will be larger at -70 mV than at -40 mV, thereby correcting for the higher attenuation at -70 mV.

The major problem with the extrapolation technique is that small errors in fitting the fast decay can result in large errors in the amplitude. This is reflected in the

high correlation coefficients between the estimates of A_f and r_f produced by the LMM routine. The larger the extrapolation, the larger the potential for error. The magnitude of this error had to be estimated.

An initial estimate of the extrapolation error was obtained from measurements of the rundown of the calcium current. Figure 2.4 shows a comparison of the observed peak tail current, and the extrapolated tail current. The extrapolated tail current measurements were scaled down to overlie the observed peak current level. The scale factor was 0.53. The general shape of the two sets of data is very similar. Most errors are less than 10%, and appear to be random. This data indicates that the extrapolation technique produces consistent results although, as would be expected, the scatter is greater.

A more extensive assessment of the problem is shown in figure 2.5. The open squares show the observed peak current level. The crosses are the extrapolated peak tail currents measured in the same cells. Each point is an average of 11 cells. The extrapolated data has been scaled down to overlie the observed data. The scaling factor was 0.73. The excellent agreement between the two sets of data demonstrates that the error introduced by the extrapolation is not systematic, and should be smoothed out if the results from several cells are averaged. These comparisons demonstrate that the extrapolation procedure produces consistent results. This is an important result, since measurement of the instantaneous current-voltage relations presented in Chapter 5 rely on the accuracy of

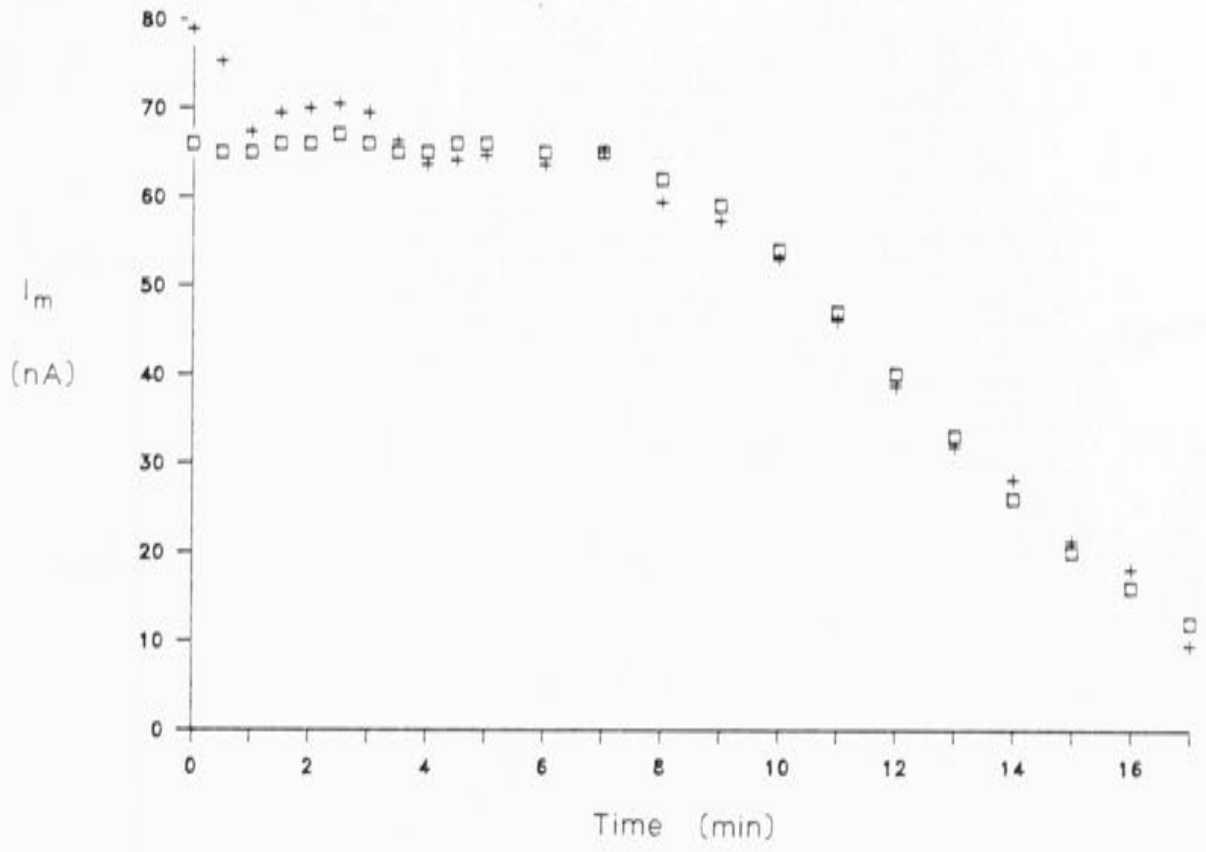

Figure 2.4 The open squares show the measured peak tail currents and the crosses show the extrapolated tail currents scaled down to overlie the open symbols. Tail currents were recorded at -50mV after a 10ms activating pulse to +20mV. The good agreement between the two sets of data indicates that measurement of the peak tail currents by extrapolation does not introduce large errors.

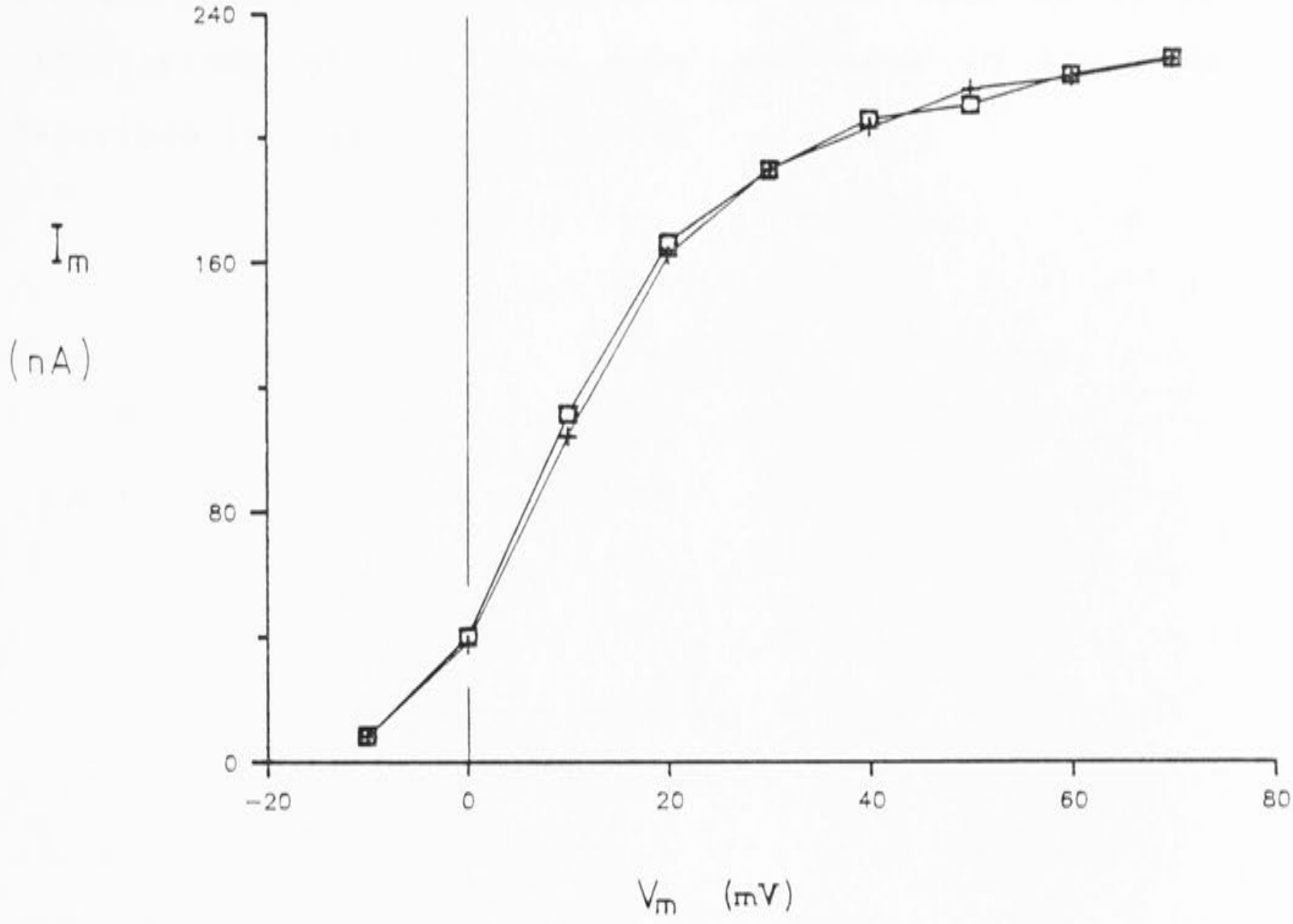

Figure 2.5 Comparison of the measured tail currents (squares) and the extrapolated tail currents (crosses) in 11 cells. The amplitude of the tail currents are plotted against the activation potential. The tail currents were measured at the holding potential of -50mV.

this technique.

Averaging and scaling of the data were performed using Lotus 123 software (Microsoft) running on a Fox 2000 microcomputer. This computer was also used to do the calculations of the four rate constants in the model described in Chapter 3.

Chapter 3

Calcium channel kinetics

Introduction

There have been a number of studies of the calcium current using conventional two intracellular microelectrode voltage clamp (Geduldig 1970, Standen 1974, Kostyuk et al. 1974, Adams & Gage 1979a, Connor 1979). These pioneering studies relied on external pharmacological agents to suppress the other ionic membrane currents. Consequently, they were limited by contamination of the current records, mainly by incompletely suppressed potassium currents. The development of internal perfusion techniques (Krishtal & Pidoplichko 1976, Lee et al. 1978, Hamill et al. 1981) largely solved this problem with the added advantage that the time resolution of the voltage clamp systems was greatly increased. There followed comprehensive studies of the kinetics of the sustained (slowly inactivating) calcium current in newborn rat DRG (Kostyuk et al. 1981c), clonal pituitary tumour cells (Hagiwara & Ohmori 1982), bovine chromaffin cells (Fenwick et al. 1982), and molluscan neurones (Brown et al. 1983, Byerly et al. 1984). In one case single channel recording and two electrode voltage clamp techniques were combined, to examine calcium currents in snail neurones (Lux & Brown 1984, Brown et al. 1984b).

There now appear to be at least three different types

of calcium channels, the well known sustained calcium channel and two more recently discovered transient calcium channels (Halliwell 1983, Carbone & Lux 1984, Nowycky et al. 1985a). A transient calcium current has now been observed in a number of tissues (pituitary cells; Armstrong & Matteson 1985, heart; Bean 1985, Nilius et al. 1985, sensory neurones; Bossu et al. 1985, Fedulova et al. 1985, skeletal muscle; Cognard et al. 1986). In the work that follows, "calcium channel" will refer to the sustained calcium channel. The work of Llinas and colleagues (1981), has indicated that the calcium channel involved with the release of transmitter at the squid synapse is probably the sustained calcium current. The release of transmitter in cultured neurones seems to be mediated by different calcium channel types, depending on the cell type (Perney et al. 1986). It seems important to gain an understanding of the functional properties of calcium channels, as this information will provide insights into the link between calcium channel function and the changes in the intracellular calcium concentration which are essential for the activation of many cellular processes.

Apart from the study by Kostyuk and co-workers (1981c), there is very little detailed data available on the kinetic characteristics of calcium channels in mammalian neurones. This study addresses the basic question; what is the minimal kinetic scheme that will account for calcium channel activity in sensory neurones ? The question has not been resolved for the calcium channel in any preparation. Previous workers have concentrated on sequential models and this approach will be used in this

study. It has been suggested that the kinetics of the calcium channel are not consistent with 3-state sequential activation schemes and a number of authors have proposed 4-state schemes (Hagiwara & Ohmori 1982, Brown et al. 1983, Byerly et al. 1984, Brown et al. 1984b). It has not been demonstrated that such schemes are able to account for the data quantitatively.

The dihydropyridine derivatives (DHPs) are potent modulators of calcium channels in cardiac and smooth muscle preparations (for reviews see Miller & Freedman, 1984, Reuter et al. 1985). Experiments using these compounds have suggested that there are marked differences between the calcium channels found in different tissues. For example the concentration for the half maximal effect of Bay K in ventricular cells is 30nM (Brown et al. 1984a, Hess et al. 1984b), whereas much higher concentrations (5-10μM) are required to produce an effect in neuronal preparations (Nowycky et al. 1985b). There does not appear to be any convincing evidence at present that the dihydropyridine calcium channel blockers are effective against nerve cell calcium channels (Miller & Freedman, 1984), whereas they block calcium currents in cardiac preparations at nanomolar concentrations (Bean 1984, Reuter et al. 1985). Some preliminary data were obtained on the effects of nifedipine in this preparation.

Single channel recording has shown that at low concentrations ($\sim 10^{-7}$M), the main effect of Bay K is to increase the number of openings of cardiac calcium channels during a depolarization (Brown et al. 1984a,

Brown et al. 1986). At higher concentrations, (~10μM), Bay K greatly prolongs the open time of calcium channels in heart (Hess et al. 1984b, Kokubun & Reuter 1984, Brown et al. 1984a, 1986) and neuronal cells (Nowycky et al. 1985b). Both these effects will cause an increase in the peak whole cell calcium current. The effect of Bay K may be quite different in smooth muscle, where it has been reported that Bay K increases the amplitude of the calcium current with no effects on the kinetics (Droogmans & Callewaert 1986).

The effects of Bay K 8644 on the calcium channel in cat DRG neurones are described in this thesis. Interpretation of the results is complicated by the recent finding that the two enantiomers of Bay K seem to have opposite effects on calcium channels in cardiac preparations (Franckowiak et al. 1985).

RESULTS

3.1 Evidence for a homogeneous calcium current

The calcium current was isolated by application of sodium and potassium channel blockers and by ion substitution. Sodium currents were eliminated by replacing the external sodium with choline. In some cases 0.3 μM TTX was applied externally, and this is indicated where applicable. Potassium currents were suppressed by perfusing internally with CsCl solution containing 10 mM TEA and by external application of 25 mM TEA.

In many cells, a slowly decaying inward tail current

was observed which persisted long after the calcium tail current had decayed completely. It was not a component of the calcium tail current as it was not present in every cell where calcium currents were recorded. This current was most probably a calcium activated chloride current (Miledi & Parker, 1984, Mayer, 1985), since it was not sensitive to potassium channel blockers and it could be recorded in solutions where the external sodium was replaced by choline. Figure 3.1 shows the calcium dependence of the current measured 5 ms after repolarization, when the calcium tail current had decayed to baseline. It can be seen that the amplitude of the slow inward tail current followed the integral of the calcium current very closely. The slow tail was blocked by calcium channel blockers (Co^{2+} and Cd^{2+}), consistent with it being a calcium activated current. The calcium activated current was not completely suppressed by the 5 mM internal EGTA, and cells displaying a slow inward tail current were rejected.

Three observations indicated that the contamination from other currents was minimal. Firstly, replacement of the external Ca^{2+} with Co^{2+} completely suppressed the Ca current (figure 3.2). A similar effect was observed when 1 mM $CdCl_2$ was added to the external solution. However, in this case, a residual tail current was invariably observed (Figure 3.2). The presence of tail currents in Cd solutions is consistent with the idea that the blockage of the calcium channel by Cd ions is relieved at hyper-polarized potentials (see Byerly et al. 1984). This

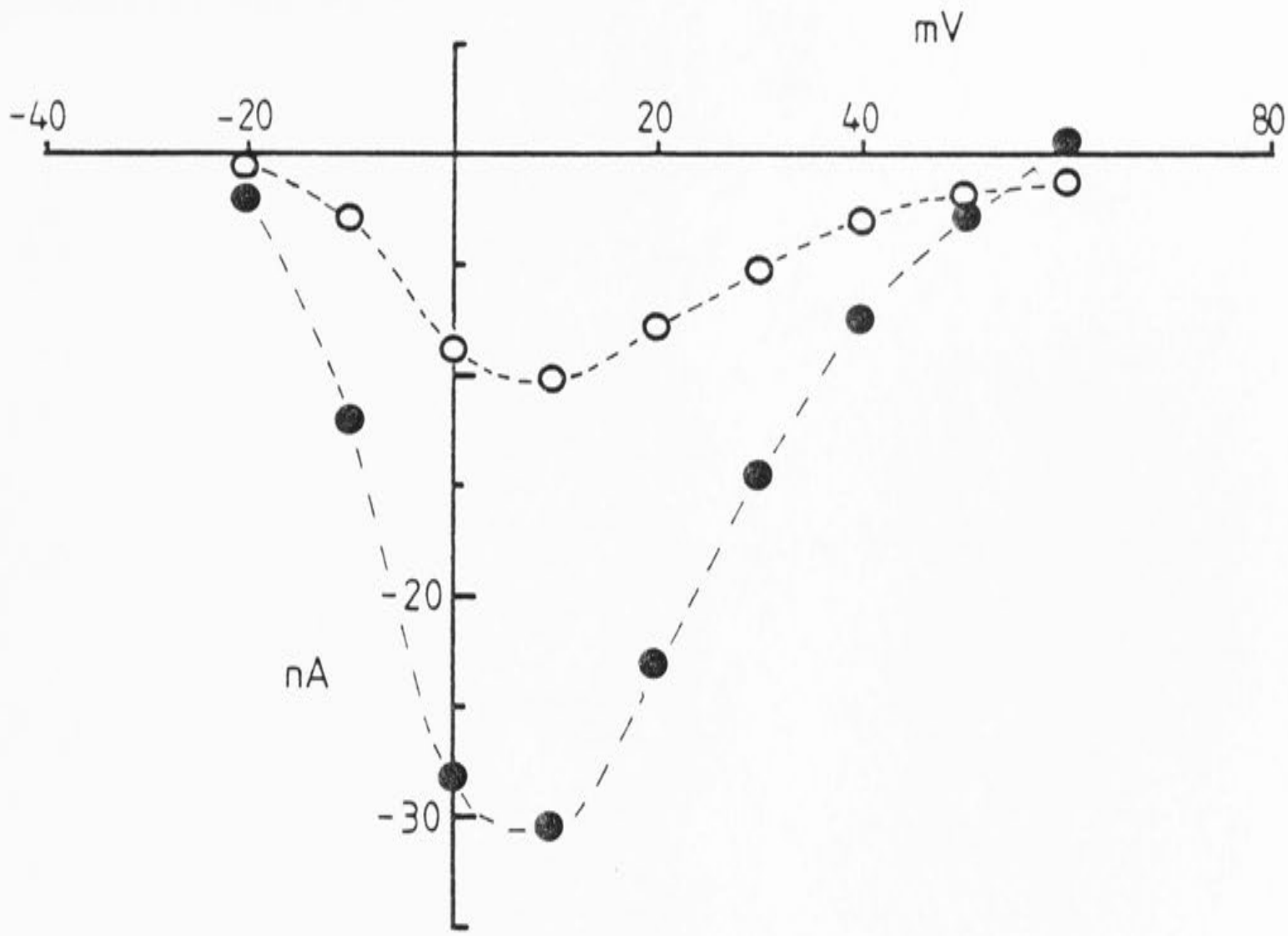

Figure 3.1 Comparison of the peak calcium current and the slow inward tail current. The solid symbols show the peak inward calcium current, and the open symbols show the tail amplitude recorded 5ms after repolarization. V_h = -50mV

Figure 3.2 The blocking effects of $CoCl_2$ and $CdCl_2$. The holding potential was -50mV. Inward current was measured at +10mV. The top figure shows the currents recorded before and after replacing the external calcium with cobalt. The bottom figure shows the blocking effect of 1mM $CdCl_2$ added to the control solution. The holding potential was -50mV.

Calcium currents :

Top trace, blocking effect of 10 mM Co .

Lower trace, blocking effect of 1 mM Cd .

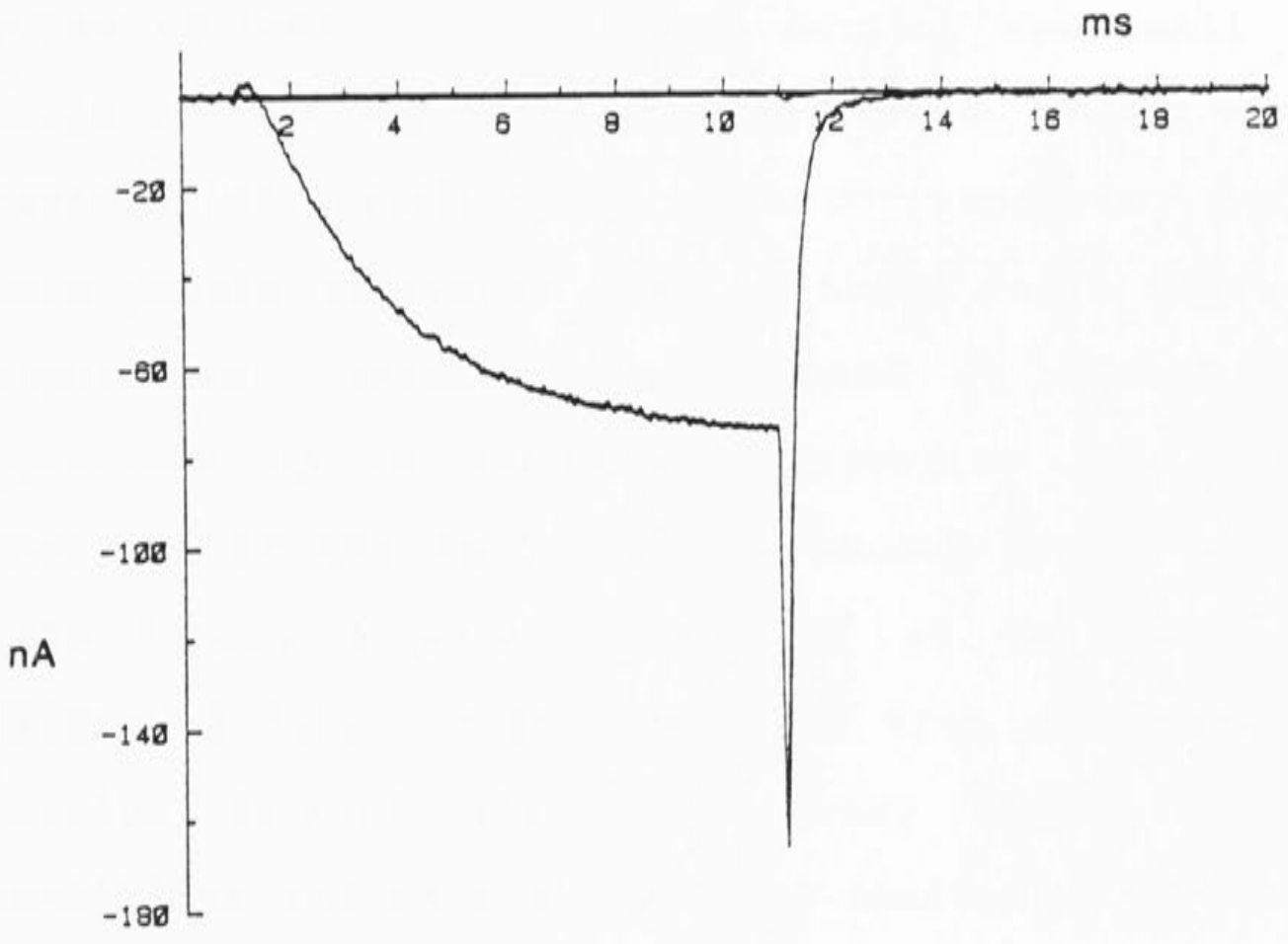

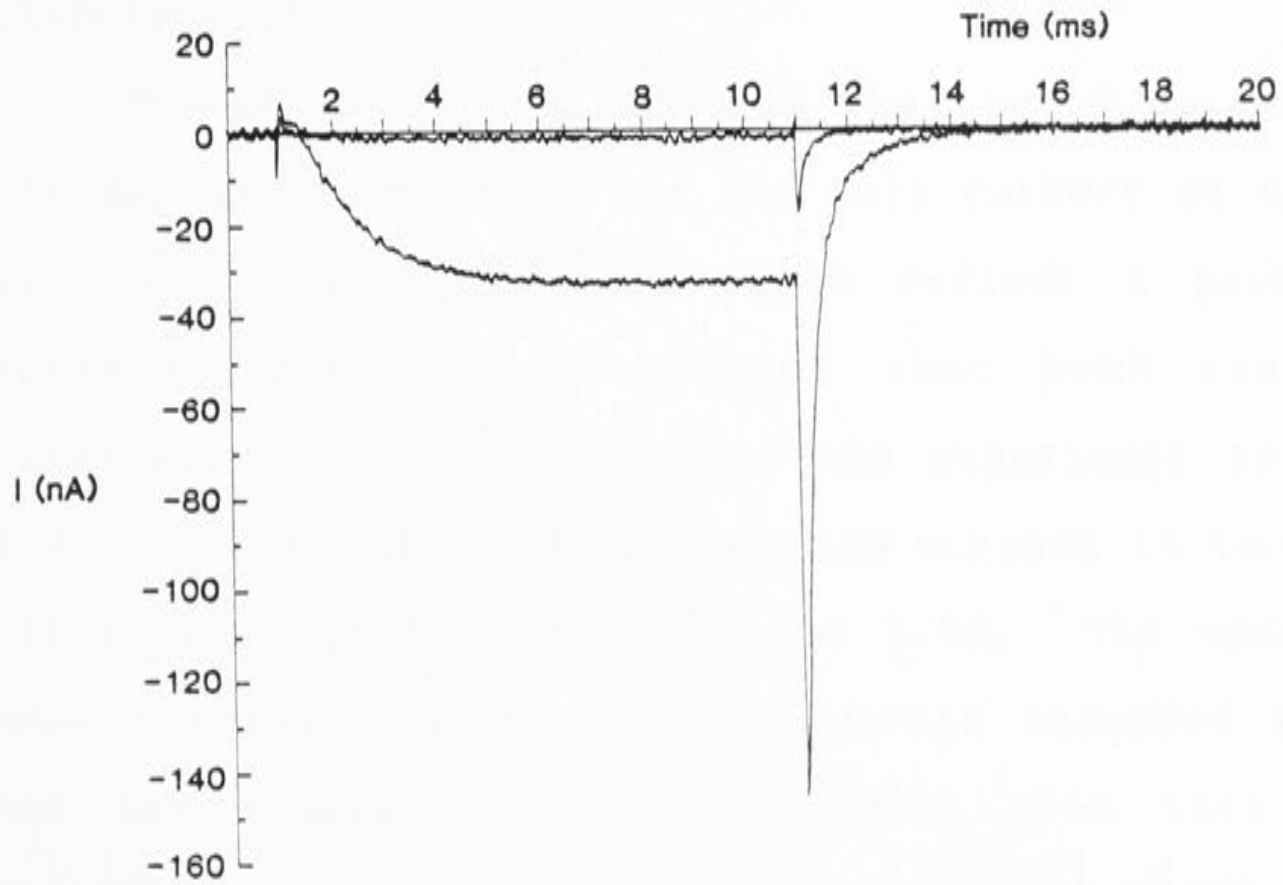

observation is explored more fully in a later section.

Secondly, pulses of varying duration were applied, and the inward current at the end of the pulse was compared with the peak tail current. Figure 3.3A shows the results of two such experiments. The open symbols show the tail current amplitude scaled down to overlie the pulse current. The calcium current was small in these cells so that any contaminating current should have become obvious immediately. The close correspondence between the data points indicates that in these cells there were no significant contaminating currents at +15 mV for pulse durations up to 500 ms. Supporting this conclusion, analysis of the tail currents showed that the two decay rate constants were independent of the pulse duration (figure 3.3B). It is also clear from this data that the calcium current inactivated very slowly under these conditions and this allowed the activation kinetics to be examined without complications from significant inactivation.

The third indication that the inward current during the depolarizing step, and the tail current at the return to the holding potential, both reflect a pure calcium current, was the observation that both ran-down in parallel during the course of the experiment (see figure 3.4). The run-down of the calcium current in two cells is illustrated in figures 3.5A and 3.5B. The open symbols show the peak inward calcium current recorded at +15 mV and the crosses show the measured peak tail currents scaled to overlie the open symbols. The close agreement

Figure 3.3 Currents were activated by stepping to +15mV. (A) The open symbols show the inward current recorded just prior to repolarization. The crosses show the amplitude of the tail current on repolarization, scaled down for comparison. (B) Rate constants recorded from the decay of the tail currents in two cells plotted against the depolarizing pulse duration. V_h = -50mV.

A

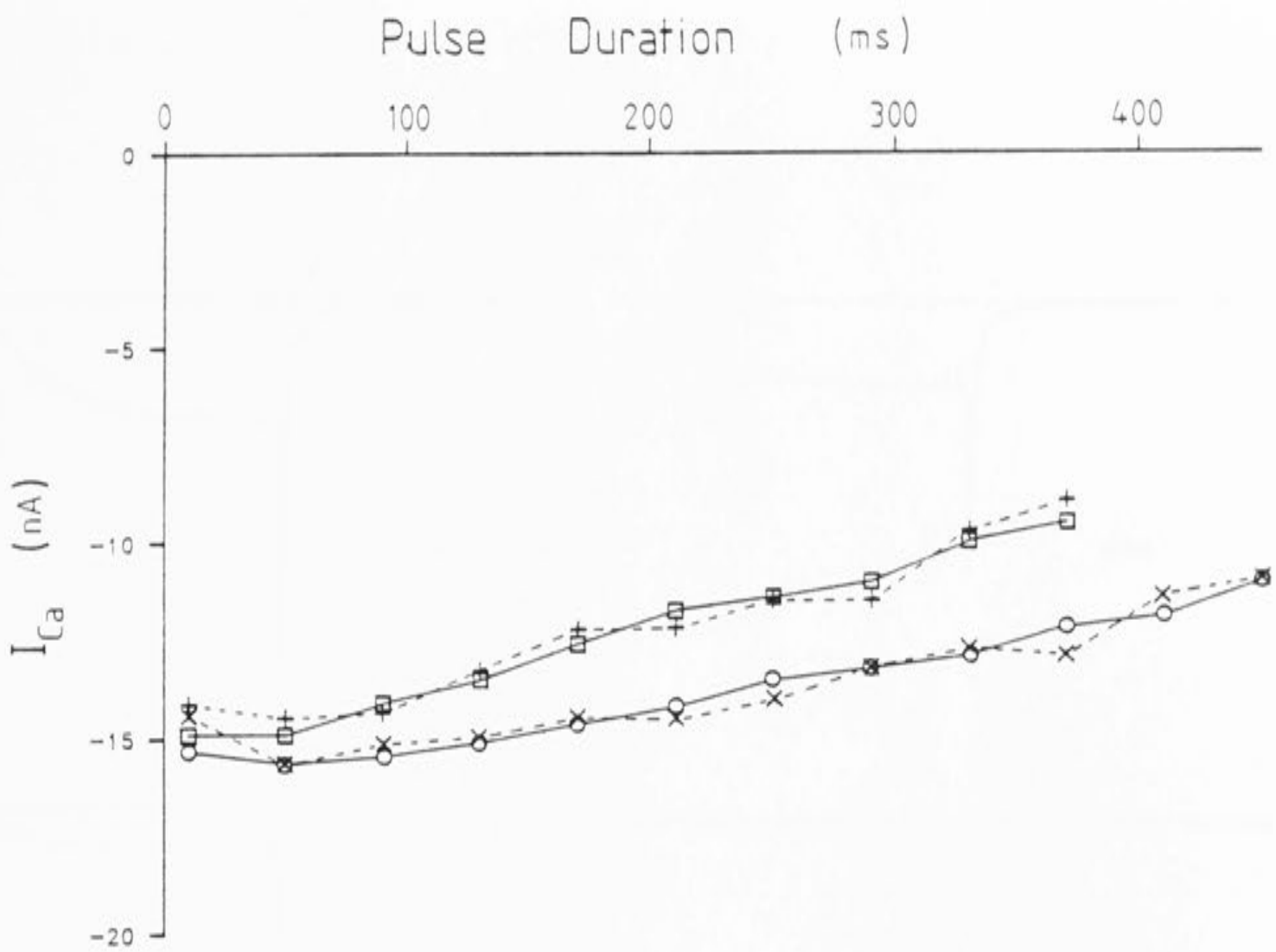
Pulse Duration (ms)
0
100
200
300
400
0
-5
-10
-15
-20
I_{Ca} (nA)

B

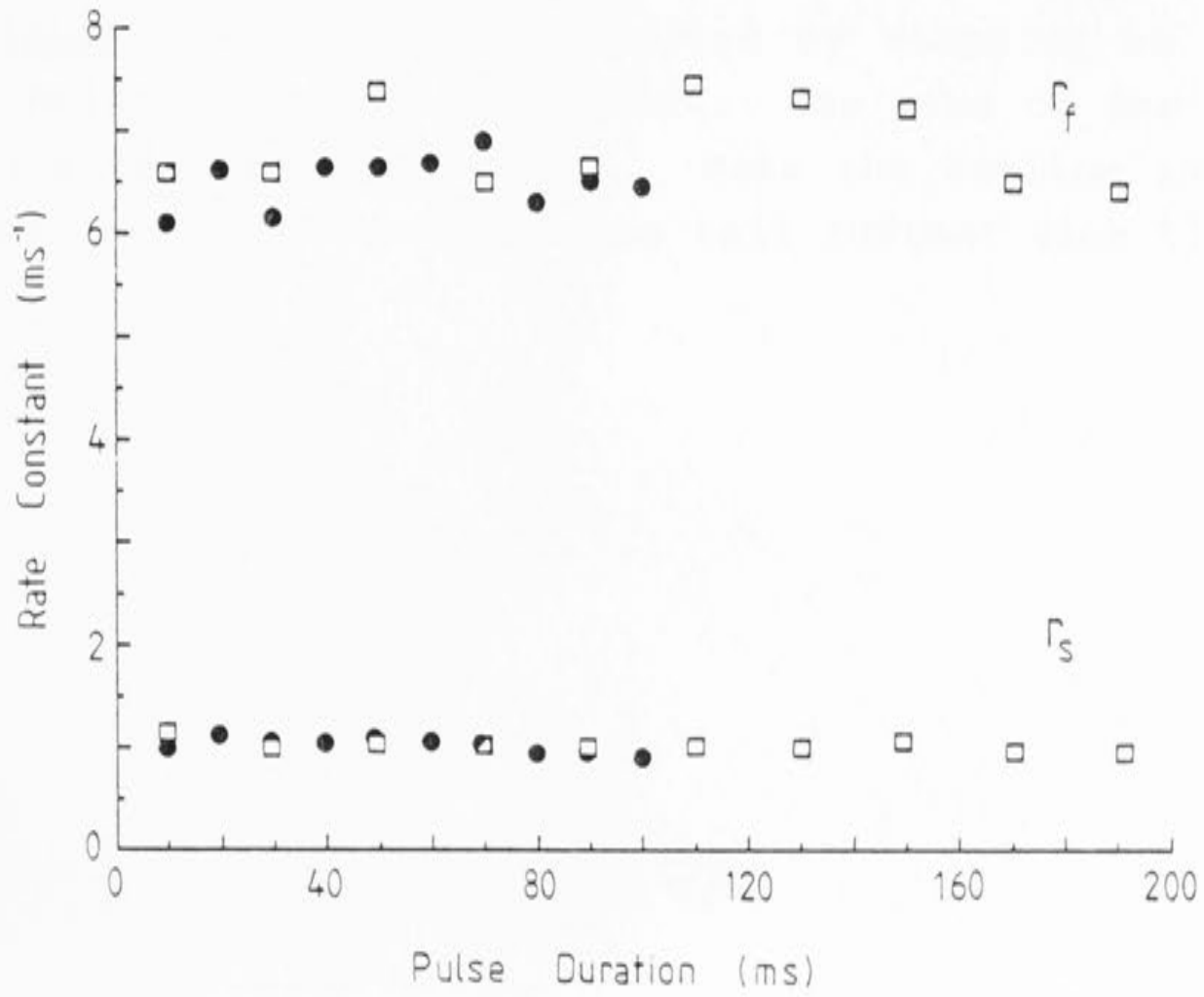
8
6
4
2
0
Rate Constant (ms^{-1})
Γ_f
Γ_s
0
40
80
120
160
200
Pulse Duration (ms)

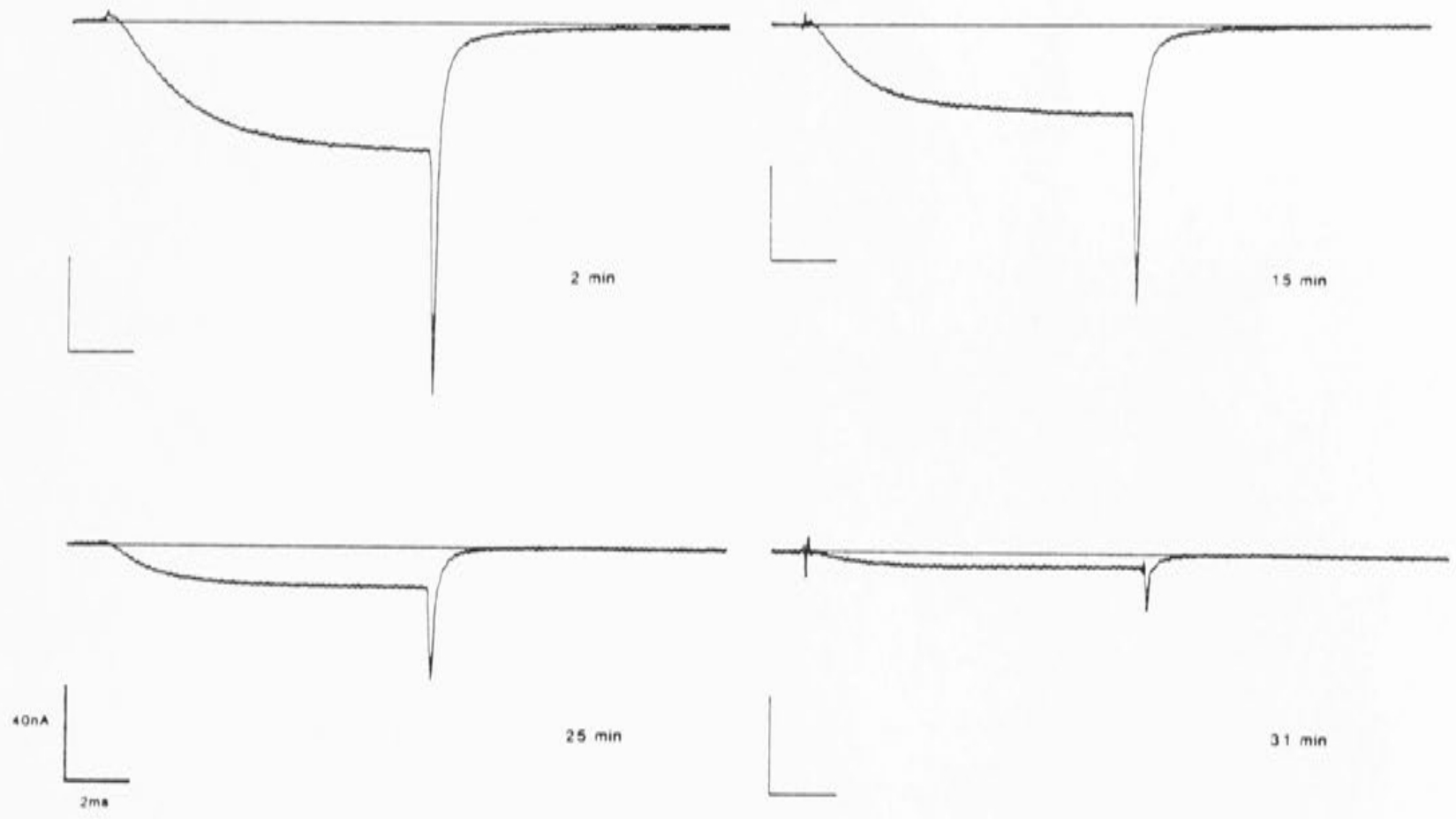

Figure 3.4 Currents elicited by stepping to +15mV from a holding potential of -50mV. The time of the pulse is indicated for each current. Note the decline in both the peak inward current, and the tail current with time.

Figure 3.5 Comparison of the peak inward current at +15mV (open squares) and the tail currents at -50mV (crosses). Both ran-down at the same rate during the recording period.

A

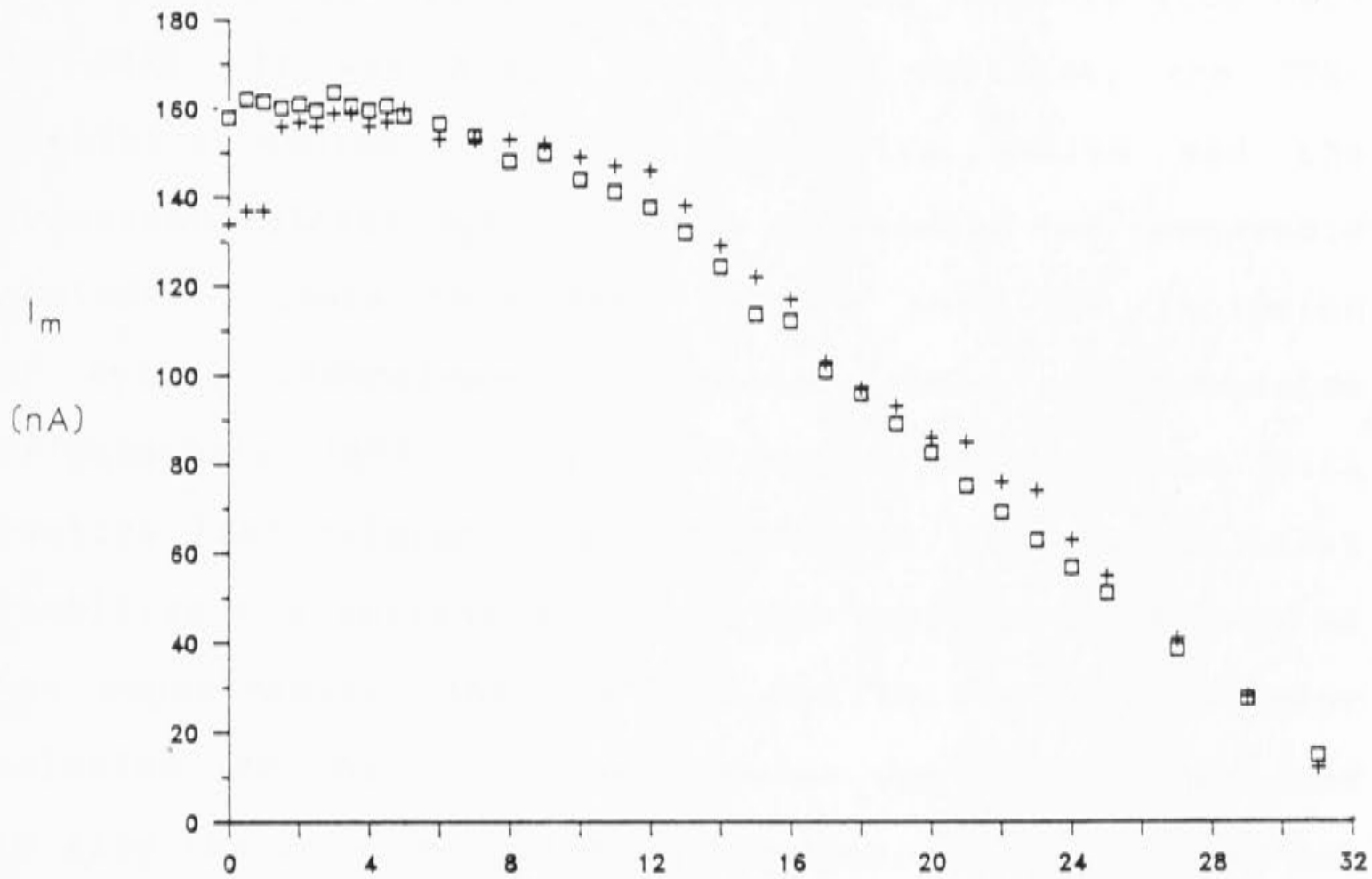
180
160
140
120
100
80
60
40
20
0
I_m
(nA)
0
4
8
12
16
20
24
28
32
Time (min)

B

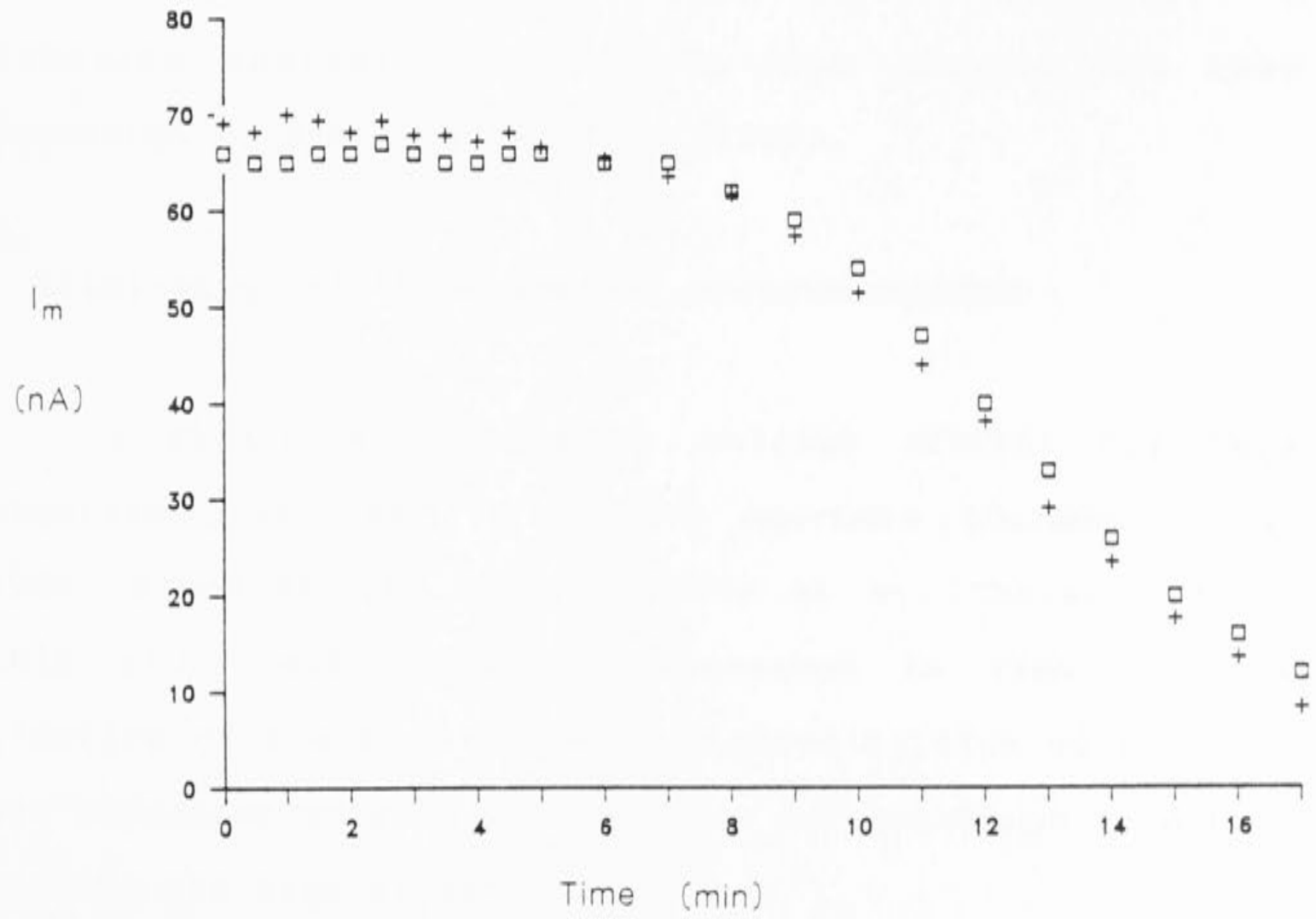
80
70
60
50
40
30
20
10
0
I_m
(nA)
0
2
4
6
8
10
12
14
16
Time (min)

between the two sets of data indicates that the contamination from other non-labile currents must be small.

The calcium current ran-down within 20 to 30 minutes, and although the rate of run-down was variable from cell to cell, it was always seen. In contrast, the TTX-sensitive sodium, the TTX-insensitive sodium and the transient calcium currents were all stable for comparable periods. There have been reports that the inclusion of cyclic adenosine-monophosphate (cAMP) and adenosine triphosphate (ATP) in the intracellular solutions will restore lost calcium currents (Kostyuk 1981) or at least stabilize the current and slow the run-down. In many of the experiments, cAMP was included in the intracellular solution and the overall impression was that it appeared to slow the run-down process. However, this point was not studied in any detail. The cAMP did not have any obvious effects on the kinetics of the calcium channels. A detailed analysis of the run-down process has been presented by Byerly & Yazejian (1986).

Elimination of the transient calcium current

A significant transient calcium current has been observed previously in sensory neurones (Carbone & Lux 1984, Bossu et al. 1985, Nowycky et al. 1985a). Since this study was primarily interested in examining the kinetics of the much larger sustained calcium current, it was important to ascertain whether contamination from this current was significant.

Figure 3.6A shows an example of the transient calcium

Figure 3.6 The effect of holding potential on the transient calcium current recorded in cat DRG neurones. (A) Top traces recorded during steps to -40 & -30mV from a holding potential of -50mV. Bottom traces were recorded during steps to -50, -40 & -30mV from -80mV. (B) Similar protocol to A, except a prepulse to -90mV for 1 second was used to remove inactivation. Note the prolonged inward tail current, which was not present in the cell shown in A. (C) Steady state inactivation of the transient calcium current in two other cells. The solid line was drawn using equation 3.5, with V_0 = -71mV and K_0 = 6.3mV.

A

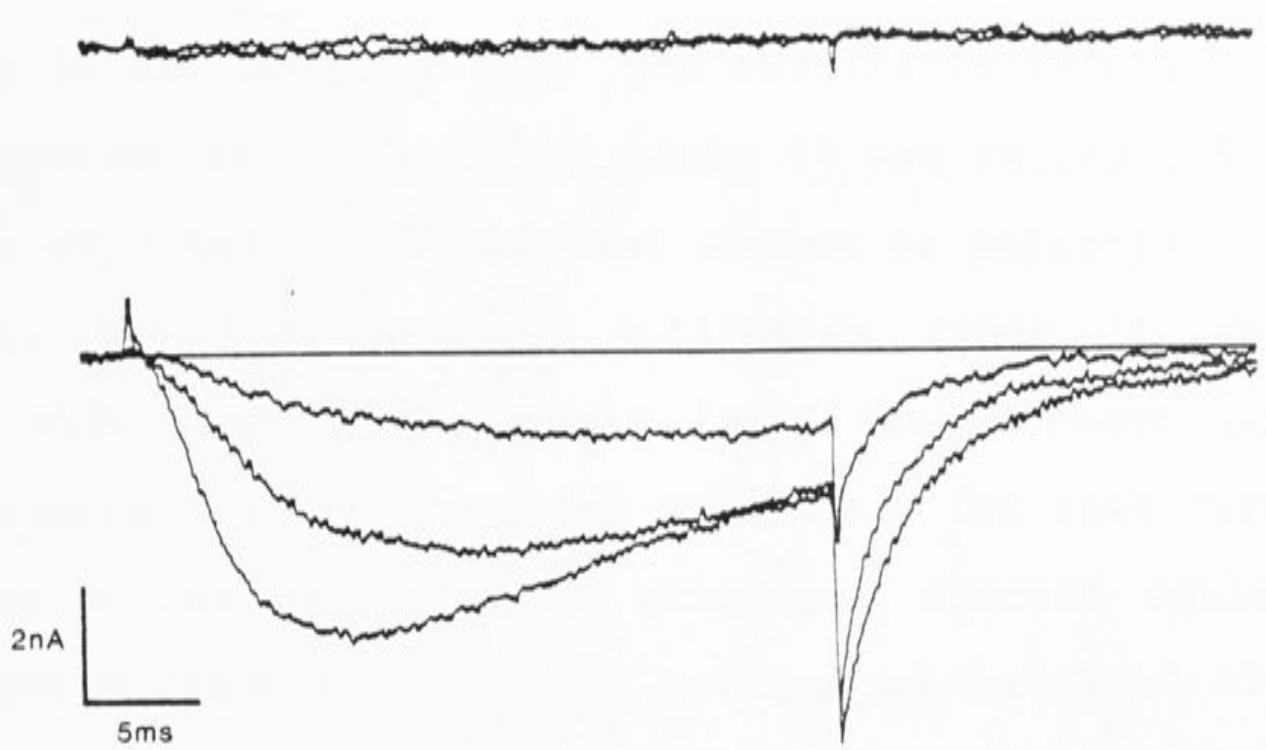
2nA
5ms

B

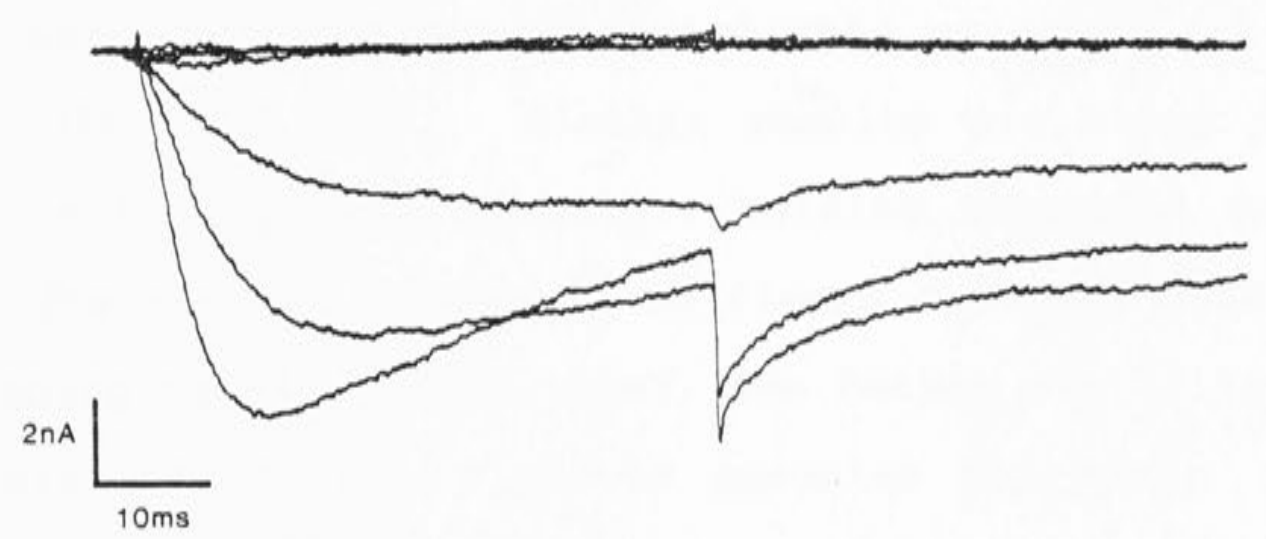
2nA
10ms

C

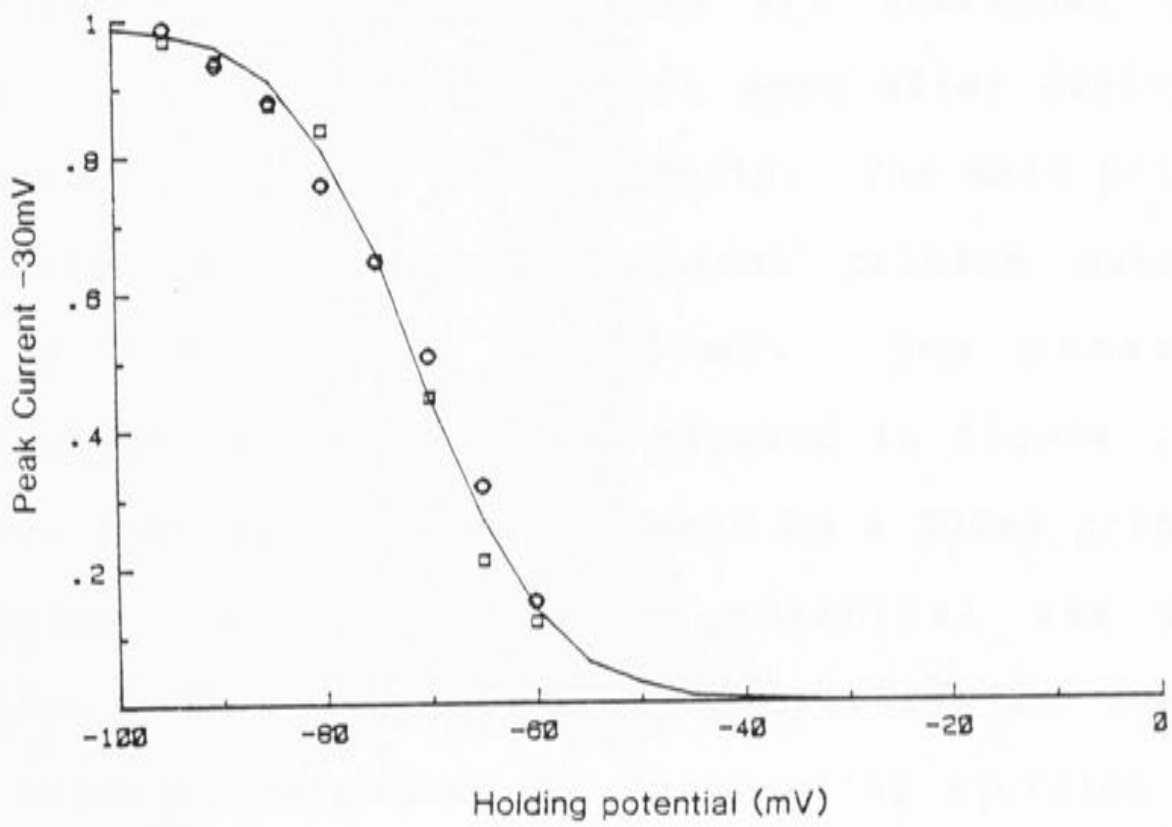
Peak Current -30mV
1
.8
.6
.4
.2
-100
-80
-60
-40
-20
0
Holding potential (mV)

current in cat DRG neurones. The current is identified as the transient calcium current since it was recorded in the absence of internal or external sodium or potassium ions. Further, the time course, activation range (threshold around -50mV) and steady-state inactivation range appear to be similar to that recorded previously for this current (Carbone & Lux 1984). The transient current could be selectively removed by using a holding potential of -50mV. The top traces in figure 3.6A show the current elicited upon stepping to -40 & -30mV from a holding potential of -50mV. When the holding potential was set at -80mV the second set of traces was recorded when stepping to -50, -40 & -30mV for 30ms. Similar results are shown in a second cell (figure 3.6B). The holding potential was -50mV. The top set of traces in figure 3.6B was obtained by stepping to -40, -35 & -30mV, the bottom set of traces were obtained after a 1 second prepulse to -90mV. This cell is illustrated because it displayed a prolonged inward tail current at the holding potential which may have been the calcium activated chloride current. The arguments for this supposition are analagous to those already given for the slow tail seen after activation of the sustained current in some cells. The main point to be made here is that the transient calcium current was largely inactivated at -50mV. The steady-state inactivation in two cells is plotted in figure 3.6C. In one case inactivation was produced by a 500ms prepulse, in the other cell the holding potential was adjusted manually. The results were essentially the same. The curve through the points was drawn using equtaion 3.5 with

V_0 = -71mV and K_0 = 6.3mV. The K_0 value is in reasonable agreement with previous estimates (Heart; Bean 1985, DRG; Fedulova et al. 1985, skeletal muscle; Cognard et al. 1986).

Cells with a significant inward current at potentials more negative than -20mV were not used for the analysis of the sustained calcium current. It is interesting to note that many cells did not have a significant transient calcium current, even when stepping from holding potentials of -80mV.

3.2 General properties of the sustained calcium current

The data presented indicated that it was possible to record a pure calcium current, and in the analysis that follows it was assumed that the current resulted from activation of a homogeneous population of calcium channels. The kinetic and steady-state properties of these channels were examined in some detail. The first point to emerge was that the time course of activation and deactivation could be fitted by the sum of a minimum of two exponential functions. This finding is illustrated in figure 3.7 which shows double exponential fits (broken lines) to calcium current relaxations.

During activation of the calcium current there is a clear delay before the current turns on (see figure 3.7). The delay is more obvious in currents recorded at low temperatures (see figure 3.19A), and becomes less pronounced as the potential is stepped to progressively more

Figure 3.7 Activation and deactivation of calcium currents. V_h -50mV. (A) Currents were activated by stepping the potentials indicated. A double exponential fit (equation 3.1) is superimposed on the data points. (B) The current was activated by stepping to +50mV for 5ms, and then returning to the holding potentials indicated. The broken lines are the double exponential fit to the data (equation 3.2) extrapolated back to the step time.

A : Activation

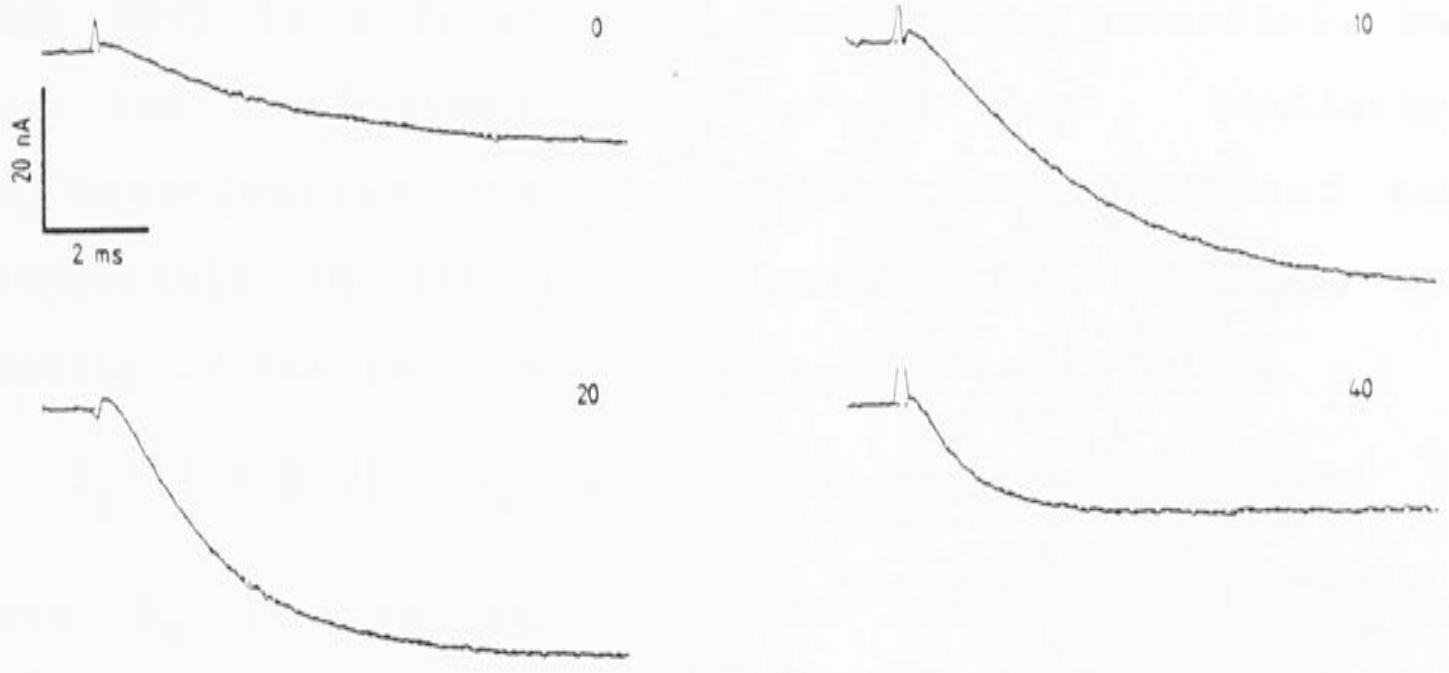

B : Deactivation

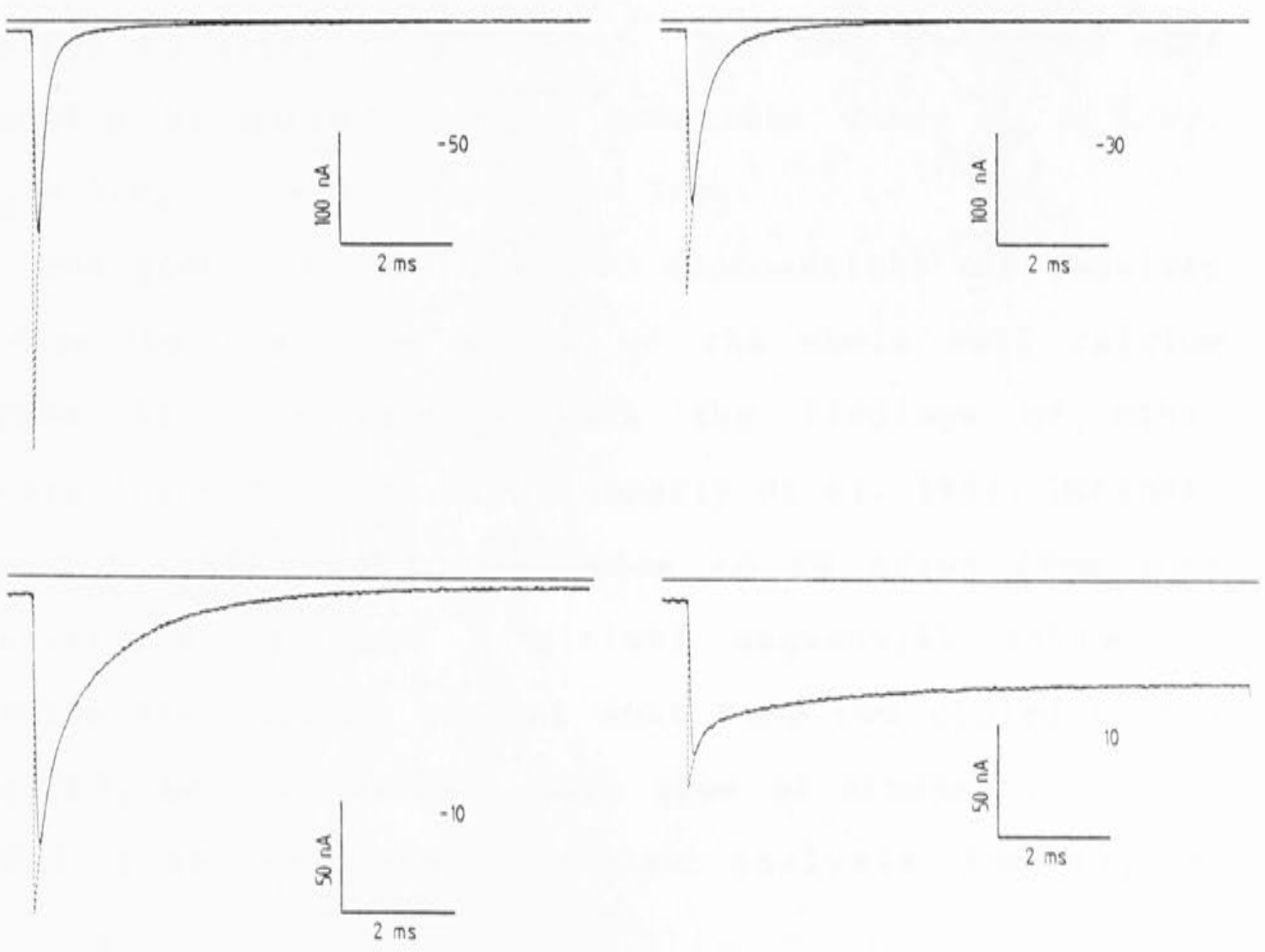

positive potentials. The activation of the currents was fitted by two exponential components of opposite polarity,

$$I_m(t) = B(V) + A_1.\exp(-r_1(V)t) - A_2.\exp(-r_2(V)t) \quad \ldots(3.1),$$

where B(V) is a function of the holding potential, and gives the final steady-state current level. Similarly, the deactivation (tail) currents also required two exponentials to fit them (figure 3.7B), although the polarity of the two components was the same,

$$I_m(t) = B(V) + A_s.\exp(-r_s(V)t) + A_f.\exp(-r_f(V)t) \quad \ldots(3.2),$$

where A_s is the amplitude of the slower decaying component and A_f is the amplitude of the faster component. These equations are presented at this point in order to define the various parameters which will be referred to later in the text. The rate constants will generally be quoted as time constants where $\tau_f = 1/r_f$, $\tau_s = 1/r_s$, $\tau_1 = 1/r_1$ and $\tau_2 = 1/r_2$.

The fact that at least two exponentials are required to describe the time course of the whole cell calcium current is in agreement with the findings of other workers (Fenwick et al. 1982, Byerly et al. 1984, Dubinsky & Oxford 1984). The conclusion to be drawn from such observations is that a minimal sequential scheme to describe the calcium current must have two closed states preceding an open state. This type of scheme provides a useful starting point for the analysis and may be

represented by,

$$C_1 \underset{k_2}{\overset{k_1}{\rightleftharpoons}} C_2 \underset{k_4}{\overset{k_3}{\rightleftharpoons}} O \qquad \ldots\ldots (3.3).$$

3.3 Steady-state activation

Membrane current due to a specific channel may be described by,

$$I_m(V,t) = N.i(V).P_o(V,t) \qquad \ldots\ldots (3.4),$$

where N is the total number of channels available, i(V) is the single channel current as a function of membrane potential and $P_o(V,t)$ is the probability that the channel is open as a function of membrane potential and time.

Figure 3.8 shows a plot of the steady-state inward current versus membrane potential. There is a sharp increase in the inward current at around -10 mV, with a peak at +10 to +20 mV, after which the peak inward current asymmtotes to the voltage axis at the most positive potentials. The line through the points was obtained by using equation 3.4, and values for $P_o(V)$ from the smooth curve in figure 3.11B, and i(V) from the fitted curve in figure 5.19.

In the steady-state $t \to \infty$ and $P_o(V,t) \to P_o(V)$, and this function was evaluated by measuring the amplitude of the tail currents at a holding potential of -50mV, after 10ms activating pulses. The use of 10 ms activating

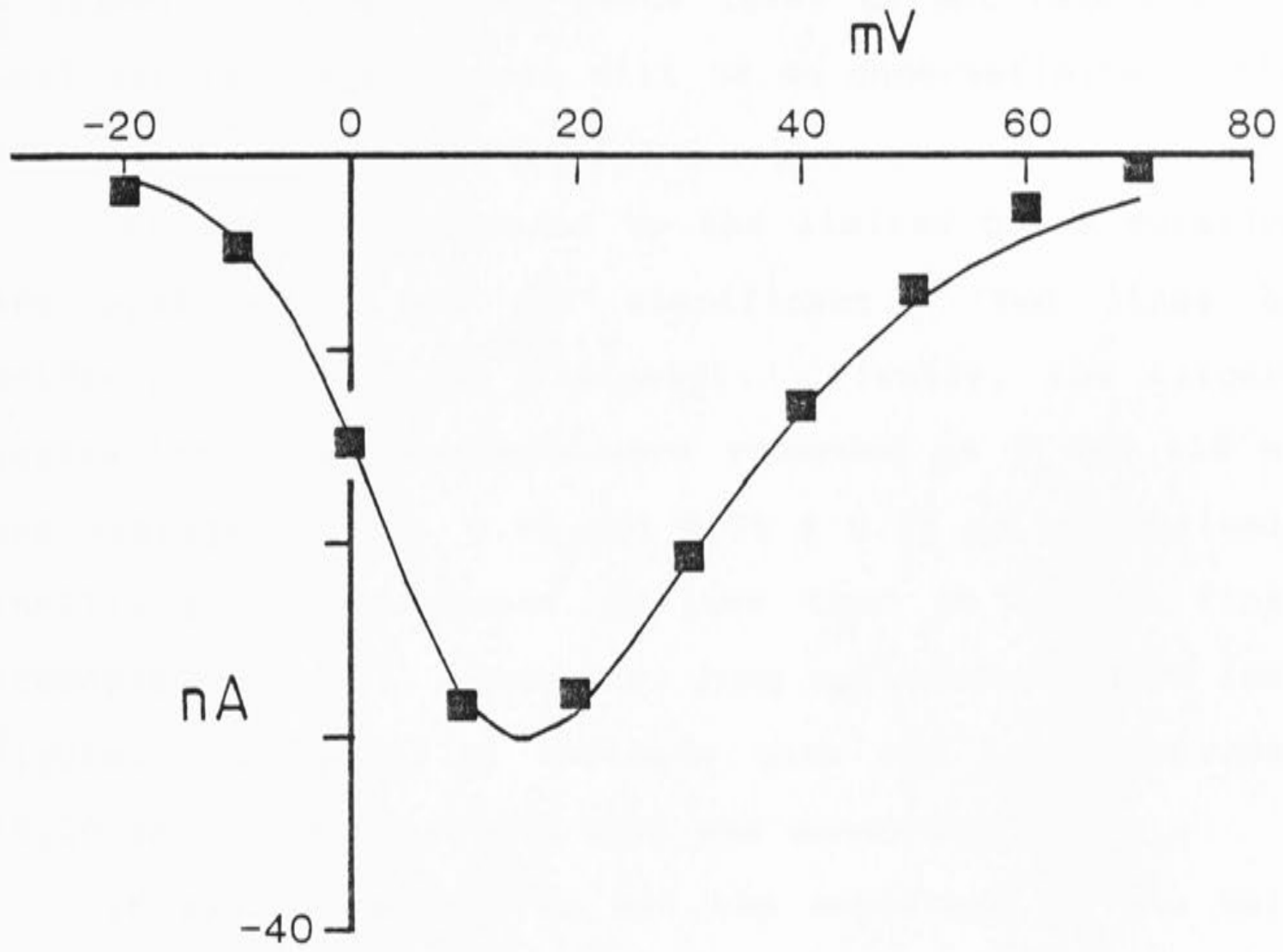

Figure 3.8 Peak inward current plotted against membrane potential. V_h = -50mV. The solid line through the points was drawn using equation 3.4 as described in the text.

pulses placed some restriction on the resolution of this technique. For example, a maximum error of 5% results if the exponential activation components have time constants < 3.3ms. If the steady-state level is not reached, the tail current measurements will be an underestimate of the true value.

The errors introduced by the limited pulse duration are systematic, but not significant. Two lines of evidence support this statement. Firstly, the largest activation time constants were recorded at 0 and +10 mV and averaged 2.72 ± 0.22 and 2.55 ± 0.20 ms respectively (n=11), producing errors of less than 3% in the final steady-state level. Secondly, long activation pulses (see figures 3.3A and 3.9) indicate that the inward current 10,20 and 30 ms after the step was constant.

It was convenient to use the amplitude of the tail currents as a measure of $P_o(V)$ as the function i(V) did not have to be evaluated. It does assume that i(-50) does not change due to ion accumulation or depletion during the activation pulse. This is not a problem since there is no indication that the inward current declines during a 10 or 30mS pulse. The term N.i(V) in equation 3.4 is a constant equal to the amplitude of the current at -50 mV when all activatable channels are open. The amplitudes of the tail currents were measured as described in the methods chapter (2.9). Some examples of the fits to the tail currents are shown in figure 3.10. The results from 11 cells are plotted in figures 3.11. The data for each cell were

Figure 3.9 Peak inward calcium current. The step potential for each trace is indicated. The pulse duration was 30ms and the holding potential -50mV. Note that there is no significant inward or outward current during the pulse to +70mV.

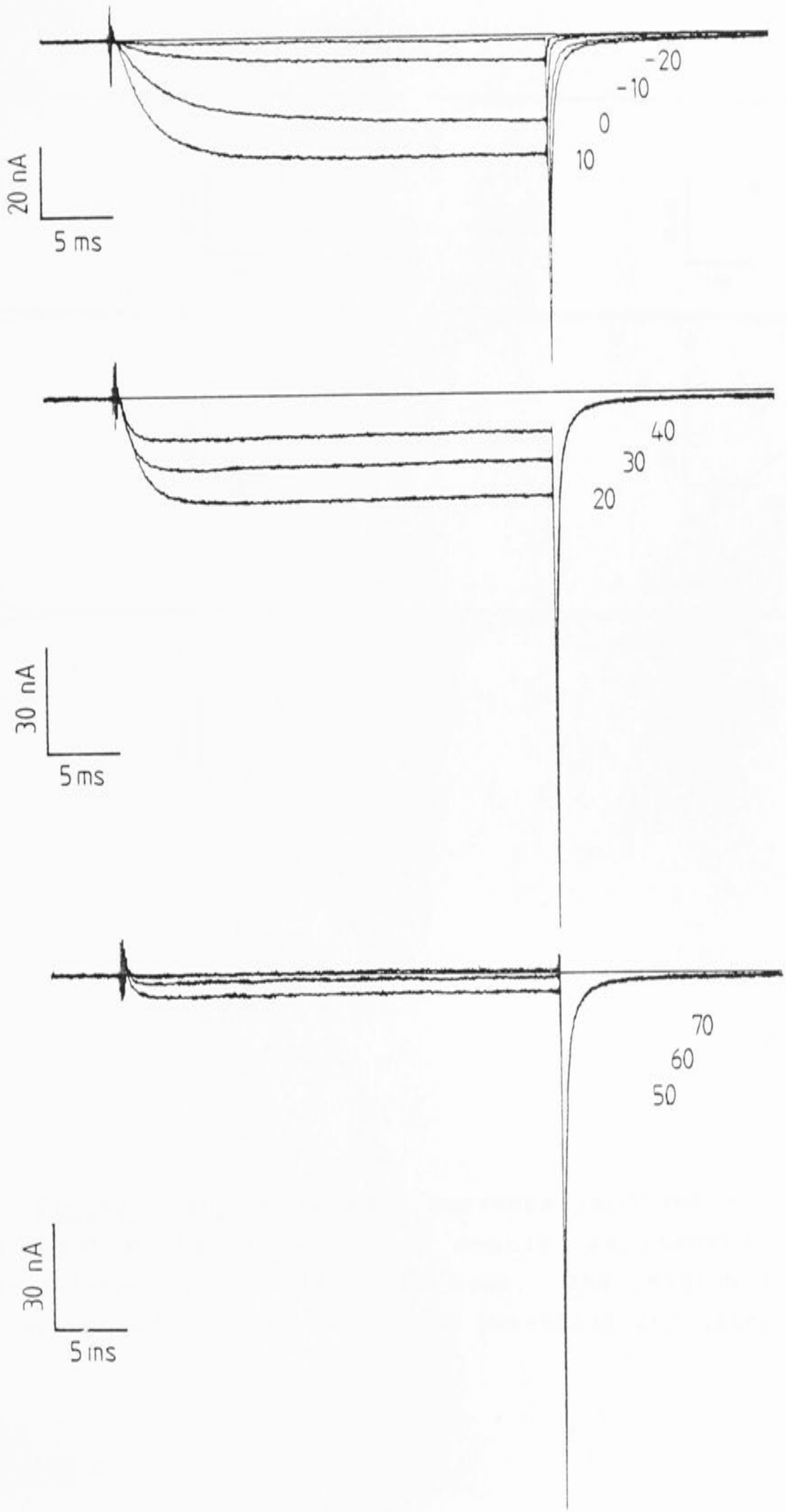
-20
-10
0
10
20 nA
5 ms
40
30
20
30 nA
5 ms
70
60
50
30 nA
5 ins

Peak Tail Current

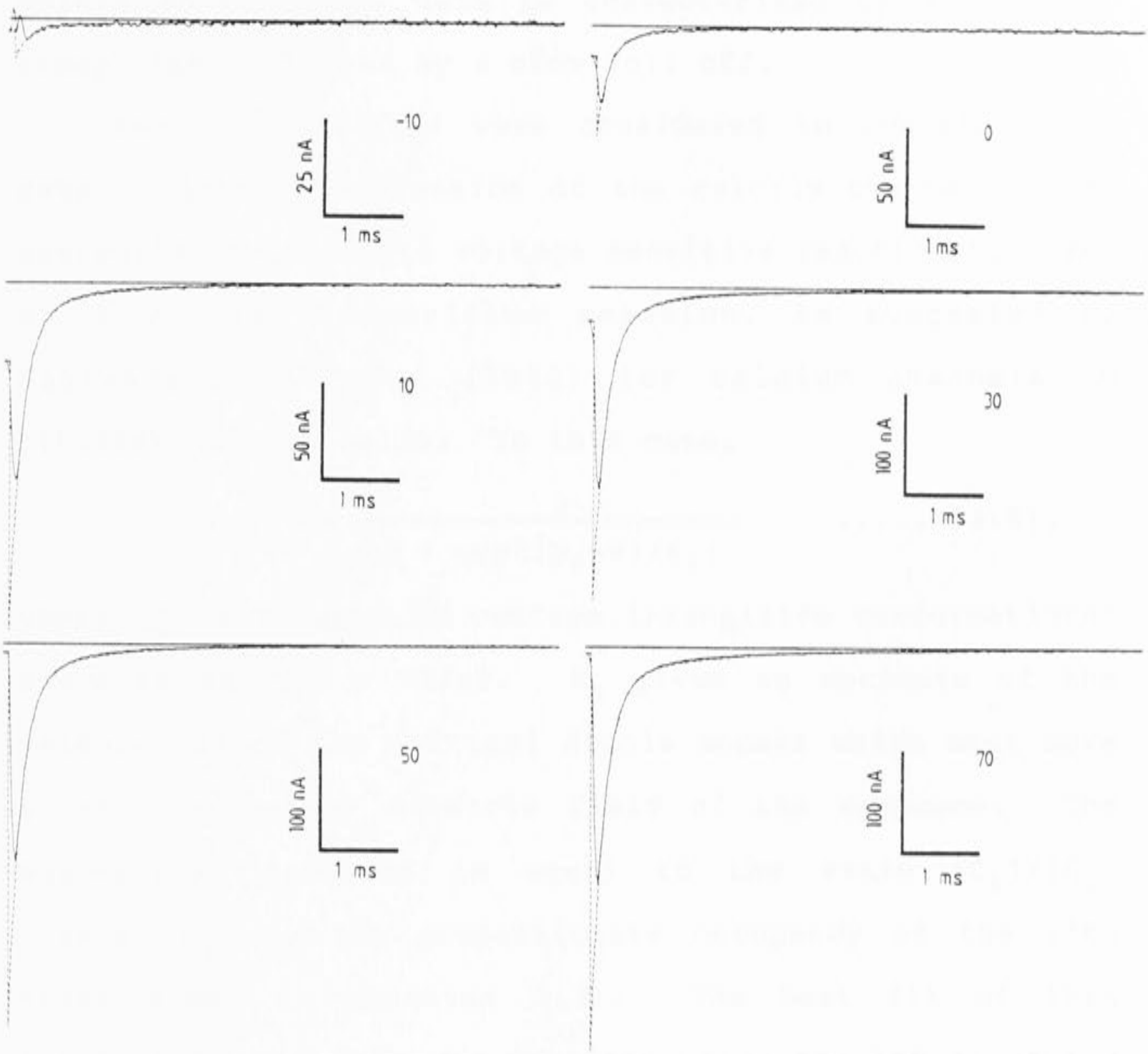

Figure 3.10 Peak tail currents recorded at -50mV. The broken lines are the double exponential fits extrapolated back to the step time. The calcium current was activated by stepping to the potential indicated.

normalized to the average value recorded at +50 mV and the normalized values were then averaged to obtain the data points shown. The data is characterized by an initial steep rise, followed by a slow roll off.

Two possibilities were considered to describe this data. Firstly, activation of the calcium channel may be controlled by a single voltage sensitive reaction followed by a voltage insensitive reaction, as suggested by Hagiwara and Ohmori (1982) for calcium channels in pituitary tumour cells. In this case,

$$P_o(V) = \frac{1}{1 + \exp((V_0 - V)/K_0)} \qquad \ldots\ldots (3.5),$$

where V_0 is related to voltage insensitive conformational energies and $K_0 = RT/zF$. K_0 gives an estimate of the valence (z) of the critical dipole moment which must move across the entire electric field of the membrane. The exponential function is equal to the ratio $[C_2]/[C_1]$ (where $[C_i]$ is the proportionate occupancy of the i'th state shown in equation 3.3). The best fit of this function to the data was obtained using the LMM algorithm and is shown in figure 3.11A. It was obtained with V_0 = 11.5 mV and K_0 = 8.1 mV, equivalent to a valence of 3.1 electronic charges (e^+).

A second way to model the data assumes that both reactions in equation 3.3 are voltage sensitive, and that the voltage sensitivities of the reactions are different. This is a more general model and,

$$P_o(V) = \frac{1}{1 + E_2 + E_1 \cdot E_2} \qquad \ldots\ldots (3.6),$$

Figure 3.11 The amplitude of the tail currents recorded at -50mV plotted against activation potential. Each point is the normalized average from 11 cells. The error bars are the standard errors. (A) The solid line shows the fit to equation 3.5. (B) Same data as A, the solid line shows the fit to equation 3.5. The probability that the channel is open is also plotted on the ordinate.

A

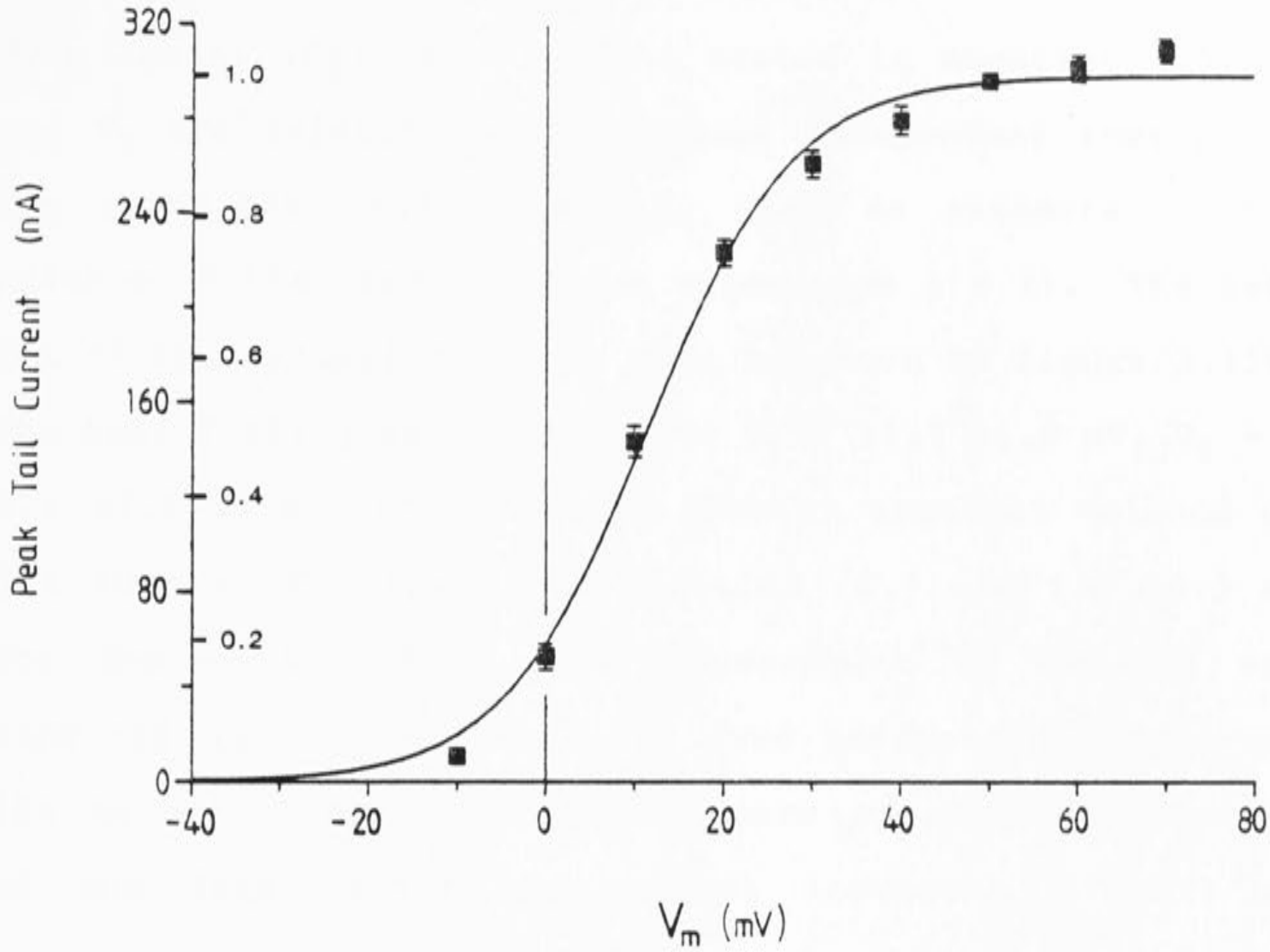
320
240
160
80
0
1.0
0.8
0.6
0.4
0.2
Peak Tail Current (nA)
-40
-20
0
20
40
60
80
V_m (mV)

B

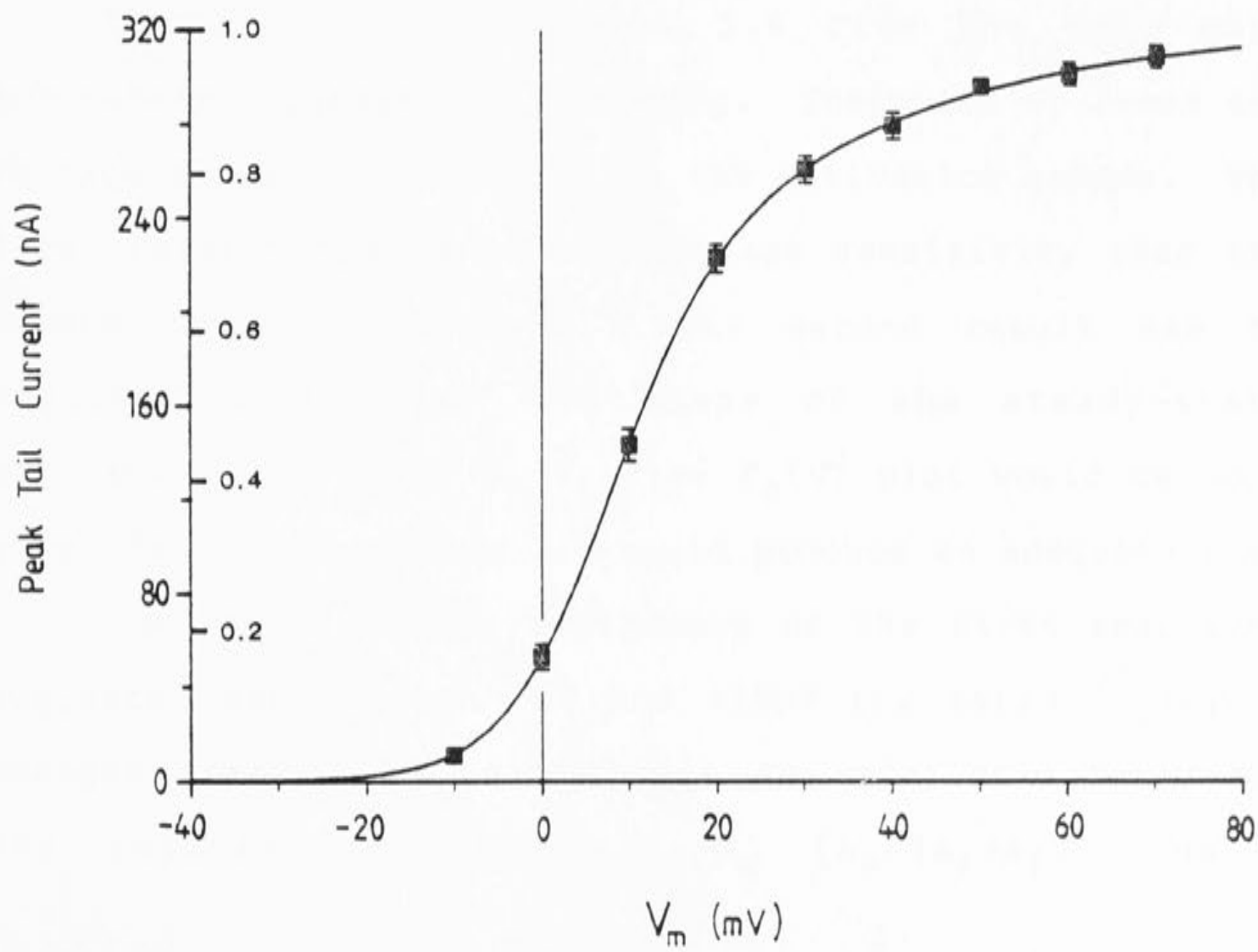
320
240
160
80
0
1.0
0.8
0.6
0.4
0.2
Peak Tail Current (nA)
-40
-20
0
20
40
60
80
V_m (mV)

where $E_1 = \exp((V_1-V)/K_1) = [C_1]/[C_2]$,

and $E_2 = \exp((V_2-V)/K_2) = [C_2]/[O]$.

Here again, $[C_i]$ refer to the states in equation 3.3, V_1 and V_2 are related to the voltage independent energy for the reactions, and K_1 and K_2 give an estimate of the valence of the reactions (see Appendices 1 & 2). The best fit of this equation to the data is shown in figure 3.11B. The best fitting parameters were V_1 = 13.7 ±1.8 mV, V_2 = -9.4 ±7.1 mV and the K values gave an apparent valence of 3.4 ±0.1 e^+ for the first reaction (K_1) and 1.0 ±0.2 e^+ for the second (K_2). The improvement in the fit was expected due to the two extra free parameters. However, the second equation provided a more accurate description of the data, since the gradual increase in $P_o(V)$ at positive potentials was seen in every cell where accurate records of the tail currents were obtained.

The fact that equation 3.6 fits the data more accurately suggests the following. There are at least two voltage sensitive reactions in the activation scheme. The first reaction has a higher voltage sensitivity than the second reaction ($K_1<K_2$). This second result can be deduced simply from the shape of the steady-state activation plot. If $K_2<K_1$, the $P_o(V)$ plot would be more sigmoidal, and equation 3.5 would produce an adequate fit.

The large voltage dependence of the first reaction, suggests that between -20 and +10mV the ratio $[C_1]/[C_2]$ changes steeply, after which it is relatively constant. The relative amplitude of A_s ($A_s/(A_s+A_f)$), as a

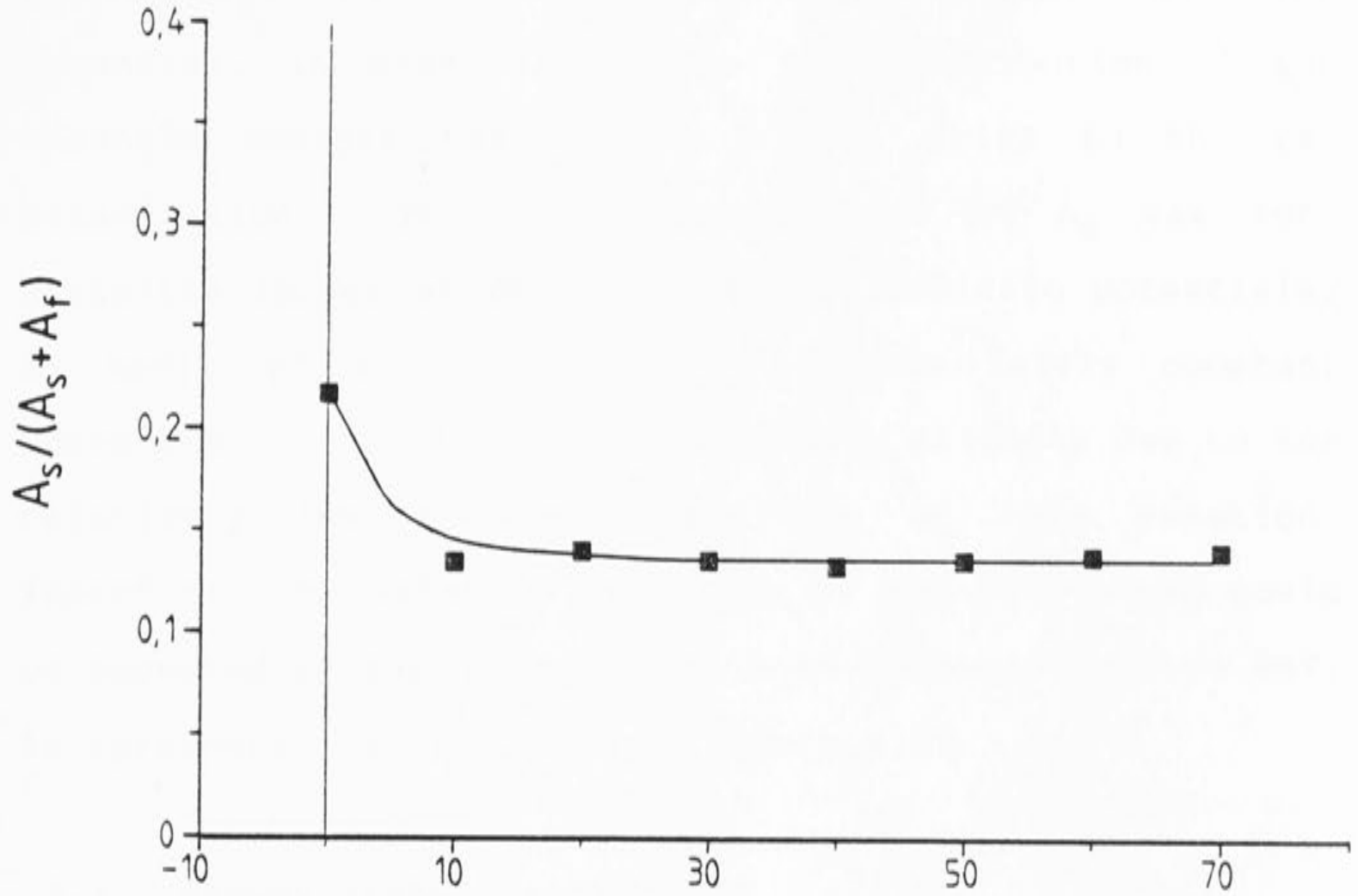

Figure 3.12 Relative amplitude of the slow phase plotted against activation potential. The slow exponential component represented a consistently larger proportion of the tail current amplitude at 0mV than at more positive potentials. The solid line was drawn through the points by eye.

function of membrane potential, is in qualitative agreement with this finding (see figure 3.12). Since $A_s/(A_s+A_f)$ is measured at a constant membrane potential, it depends only on the distribution of the channels amongst the various states prior to the repolarization. The relative amplitude of A_s was consistently larger at 0mV than at more positive potentials. As mentioned above, $[C_1]/[C_2]$ will be fairly constant above 0mV, and $[C_2]/[O]$ will vary only slightly due to the relatively low voltage sensitivity of this reaction. Therefore, the relative amplitude of the slow phase would be expected to change very little at potentials above 0mV, in agreement with the data in figure 3.12.

3.4 Steady-state inactivation

Steady-state inactivation of the calcium channel was measured using a two voltage pulse profile. A conditioning pulse lasting either 500 ms or 1 second was applied before a test pulse to +20mV. No differences were apparent between the two pulse durations. The trigger delay was set so that the final 20 ms of the voltage profile was captured.

The magnitude of the peak inward current during the test pulse is plotted against the conditioning potential in figure 3.13. The data indicates that there is negligible inactivation of the calcium channels between -90 and -30mV. There was a reduction in the peak current at -20 and -10 mV. Similar results were obtained by Bean

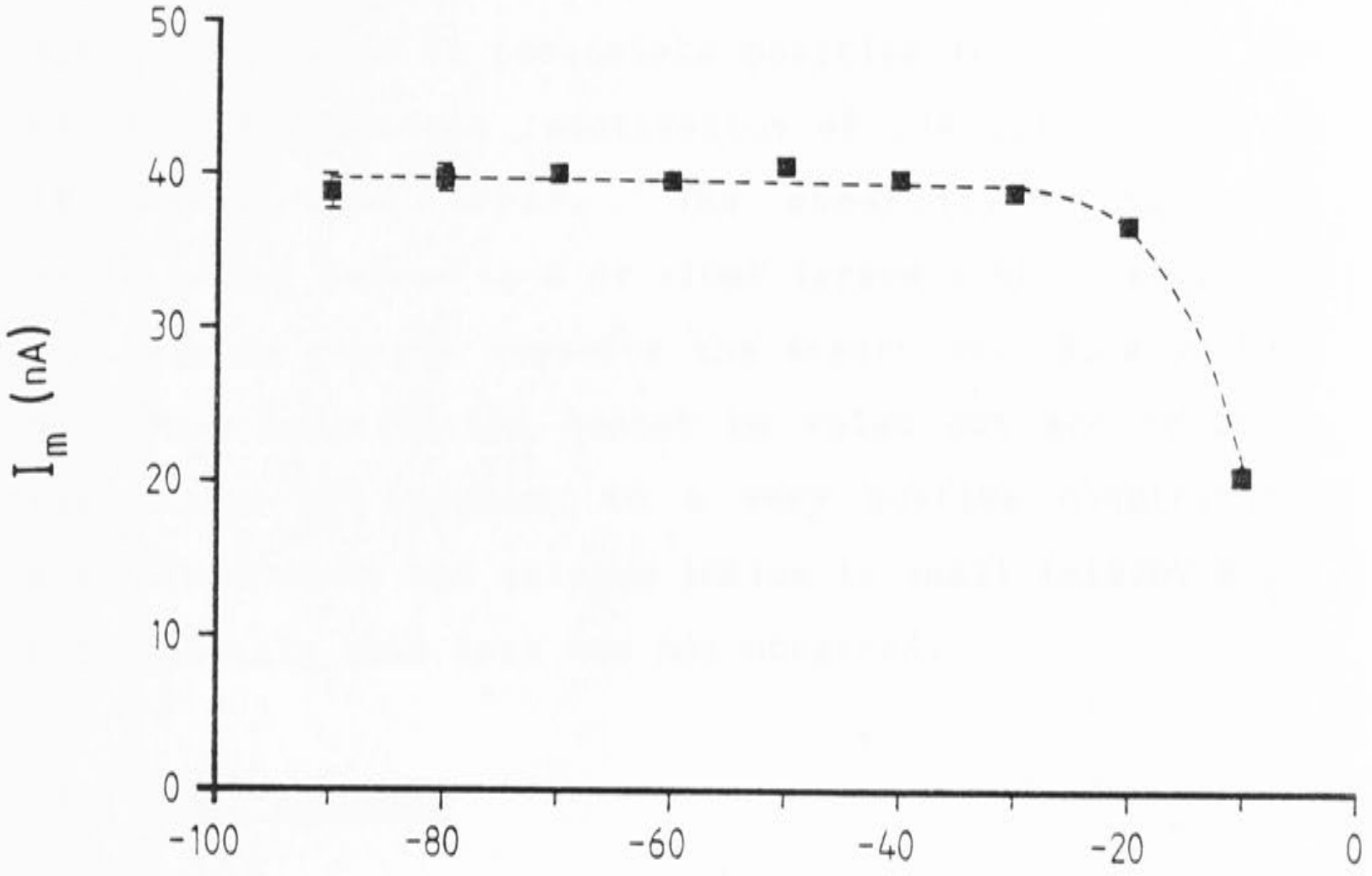

Figure 3.13 Steady state inactivation of the calcium channel. The points show the magnitude of the inward current at +20mV plotted against the initial holding potential. Each point is the normalized average from 5 cells.

(1985), in canine atrial cells. In 10 mM calcium the threshold of the calcium current is -20 mV (see figure 3.8). It it suggested that the reduction in the peak current observed at potentials positive to -20 mV is due to calcium dependent inactivation of the calcium channel (Eckert & Chad 1984). The observation that long conditioning pulses to 0 or +10mV irreversibly inactivated the calcium current supports the assertion. Some voltage dependent inactivation cannot be ruled out and could be tested for by stepping to a very postive conditioning potentials where the calcium influx is small (+100mV say). Unfortunately this data was not obtained.

3.5 Tail currents

Two voltage pulse protocols were used to examine the relaxation kinetics of the calcium channels over an extended potential range, from -70 to +50 mV. The protocol shown in figure 5.12 was used to look at the rate of deactivation of the channels after a step to +50 mV (at +50mV, P_o~0.9, see fig. 3.11B) and was useful for potentials up to +10 mV after which the tail current relaxations became too small to measure confidently. The test pulse duration was 10 ms which, again, places a limit on time resolution of the data as discussed earlier. Some examples of the currents measured are shown in figures 3.7B & 5.1. The solid squares in figures 3.14A and 3.14B show the voltage dependence of the two time constants obtained from the tail currents. Each point is the

Figure 3.14 Time constants measured from turn-on and tail current relaxations, plotted against the holding potential. (A) Average fast time constants. τ_f (squares, n=9) and τ_2 (circles, n=11) plotted against holding potential. (B) Average slow time constants. τ_s (squares, n=9) and τ_1 (circles, n=11) plotted against holding potential. The error bars are standard errors.

A

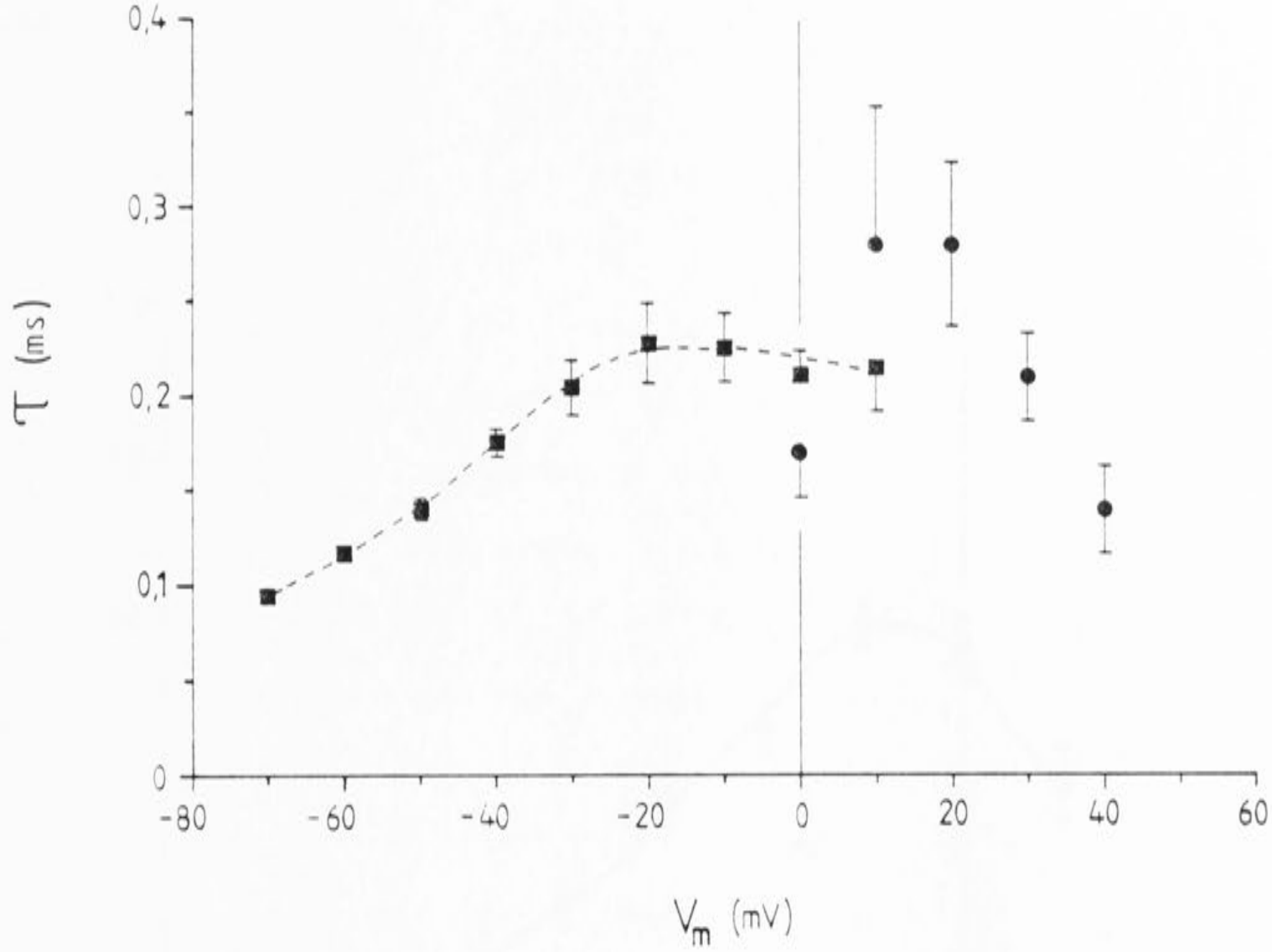
0,4
0,3
0,2
0,1
0
τ (ms)
-80
-60
-40
-20
0
20
40
60
V_m (mV)

B

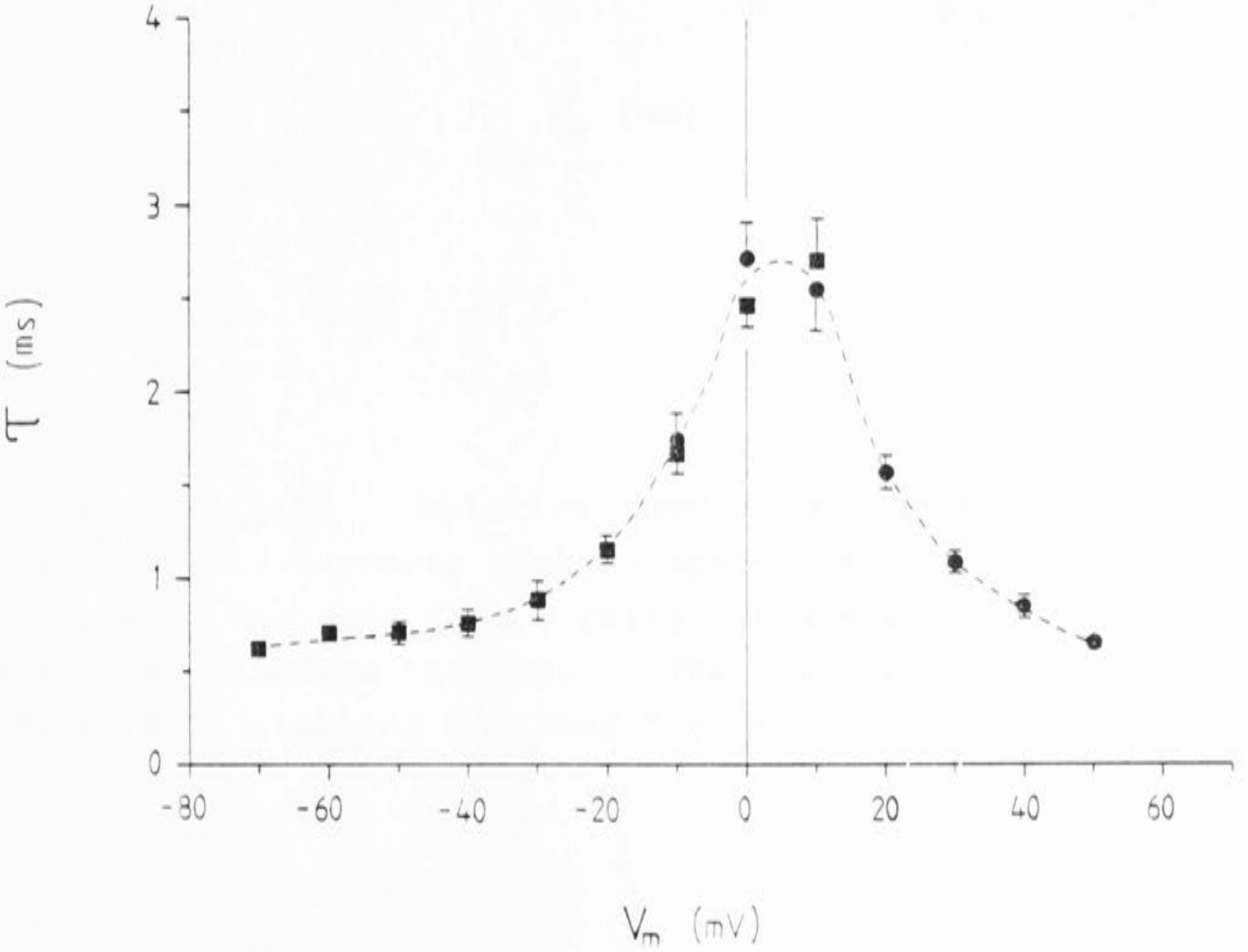
4
3
2
1
0
τ (ms)
-80
-60
-40
-20
0
20
40
60
V_m (mV)

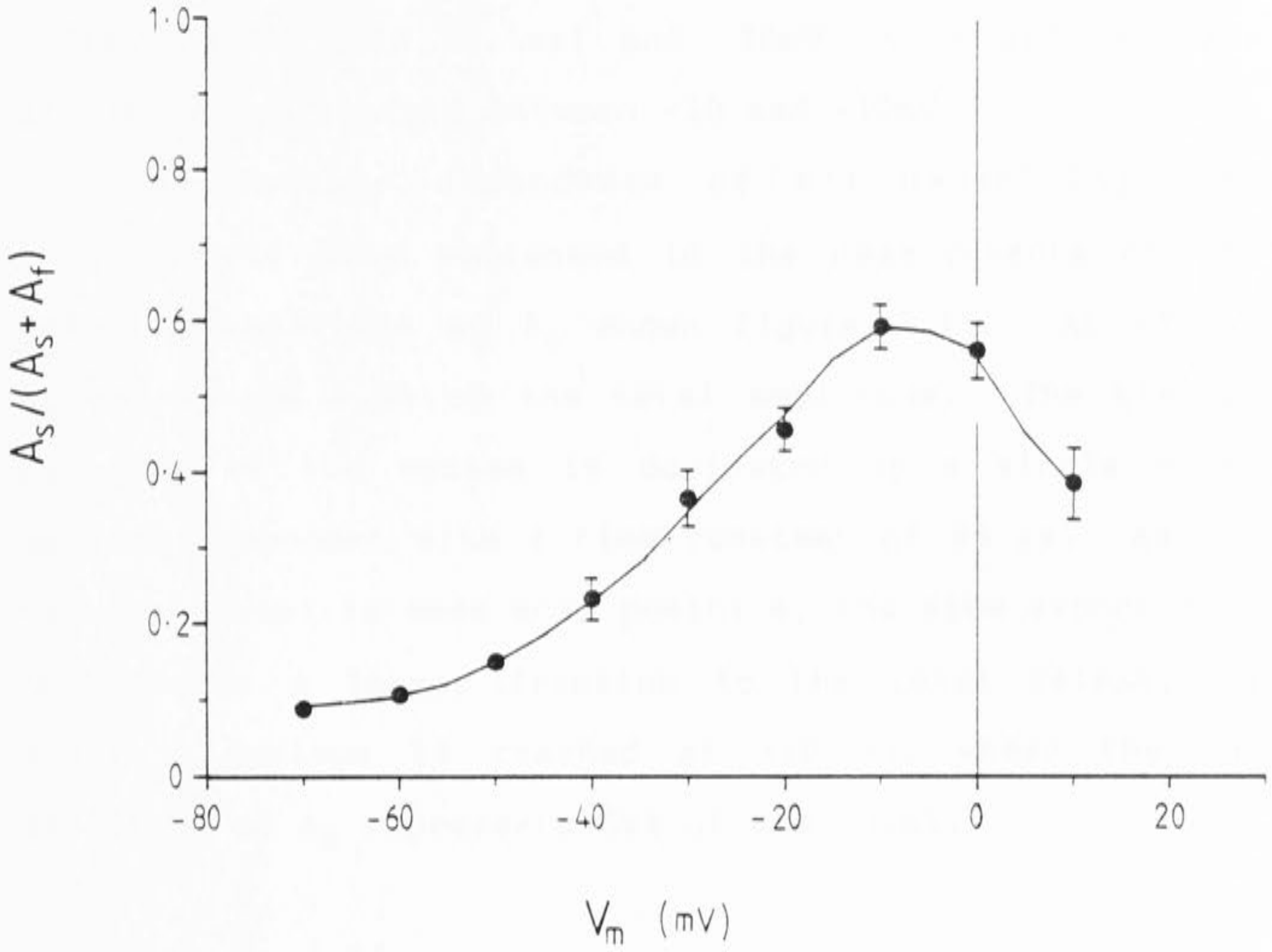

Figure 3.15 Relative amplitude of A_s (equation 3.2) from tail currents plotted against the repolarization potential. The data from 9 cells was averaged. The error bars are standard errors. The calcium current was activated by stepping to +50mV for 3ms.

average from 9 cells. The fast time constant (solid squares, figure 3.14A) increases steadily from 95 ±10μs at -70mV to 227 ±70μs at -20mV, and remains fairly constant from -20 to +10mV. In contrast, the slow time constant (solid squares, figure 3.14B), changes very little between -70mV (τ_s = 0.62 ±0.1ms) and -30mV (τ_s = 0.76 ±0.2ms) and increases sharply between -20 and +10mV.

The voltage dependence of the underlying rate constants is also reflected in the measurements of the relative amplitude of A_s shown figure 3.15. At -70mV, A_s represents 9.5% of the total amplitude. The kinetic response of the system is dominated by a single exponential component with a time constant of 95 μs. As the test potential is made more positive, the slow exponential contributes a larger fraction to the total relaxation, until a maximum is reached at -10 mV, where the the amplitude of A_s represents 59% of the total.

3.6 Activation time course

Two time constants (τ_1, τ_2) were also measured from the turn-on of the calcium current. Some examples are shown in figure 3.16, and the average values from 11 cells are shown by the solid circles in figures 3.14A and 3.14B. Nine of these cells were the same as those used for the tail current measurements. Two extra cells were included in which tail current runs were not recorded.

At -10 and in some cases 0mV, and at +50 and +60mV, the currents were too small to adequately resolve more

Figure 3.16 Activation of the calcium current on stepping to the potentials indicated. The broken lines through the data show the fits to equation 3.1. At positive potentials the current is initially outward. This is probably due to a time independent non-linearity in the leakage current which is evident when the calcium current is blocked using cobalt (section 4). Asymmetric capacitive currents may have made some contribution to the initial delay, however these currents are not large enough to fully account for the delay seen at +10 and +20mV.

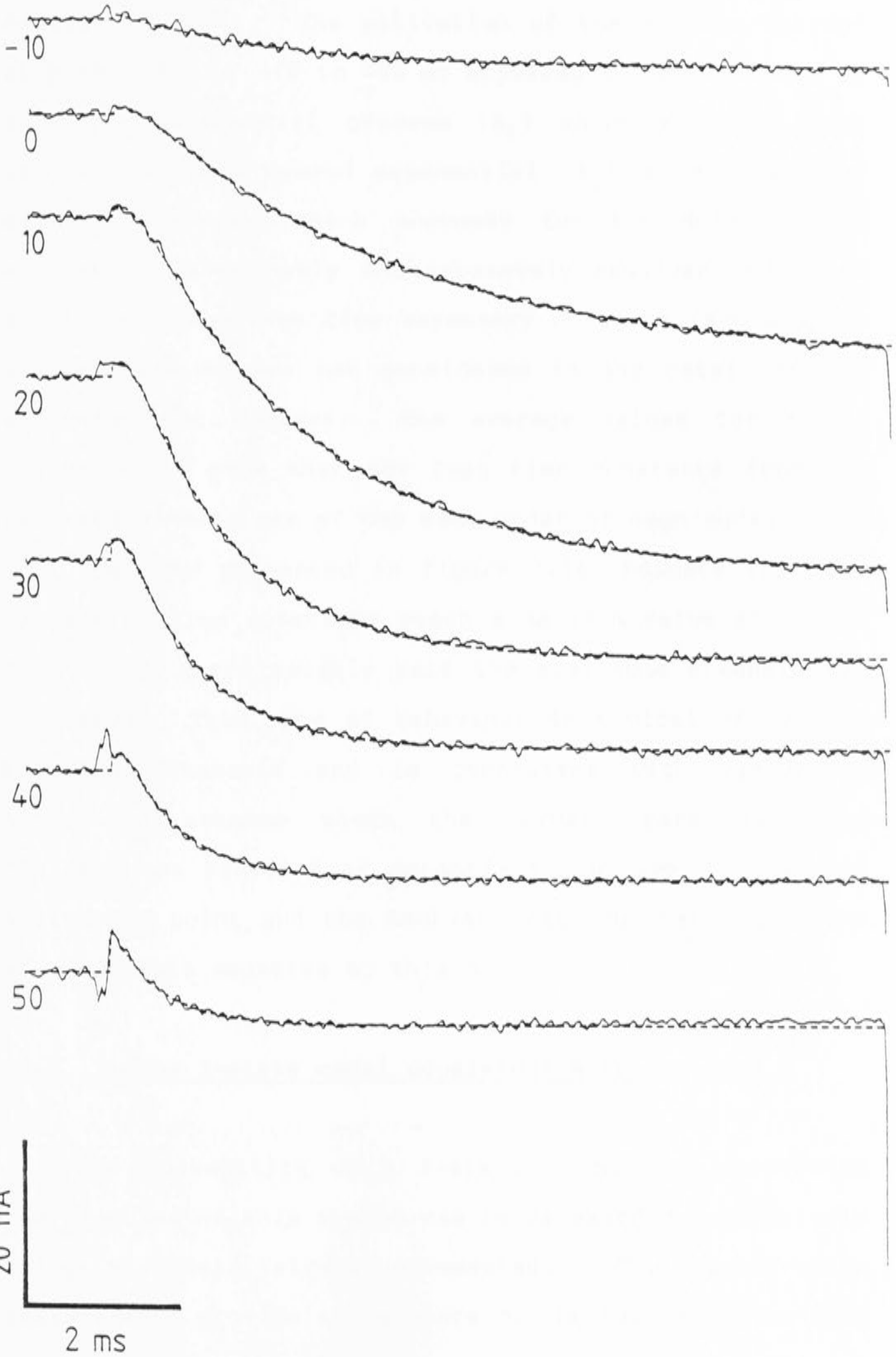
-10
0
10
20
30
40
50
20 nA
2 ms

than one exponential component during the activation. In these cases the currents were fitted by a single exponential function. The activation of the calcium current at potentials of +10 to +40 mV appeared to be dominated by a single exponential process (A_1) which was 8.4 times larger than the second exponential (A_2) at +10mV. The smaller component which accounts for the delay before activation is probably not accurately resolved and there may be contributions from asymmetry currents (see chapter 4). τ_2 and A_2 are not considered in any detail in the analysis that follows. The average values for τ_2 in figure 3.14A show that the fast time constants from the two sets of data are of the same order of magnitude.

The data presented in figure 3.14 indicate that the relaxation time constants reach a maximum value at around 0 to +10mV where roughly half the available channels are activated. This type of behaviour is typical of voltage activated channels and is consistent with sequential activation schemes where the forward rate constants dominate the kinetics at potentials positive to the half activation point and the backward rate constants dominate at potentials negative to this point.

3.7 Is the 3-state model consistent with the data ?

The suitability of a 3-state scheme for describing the kinetics of this system can be assessed quantitatively using the data already presented. The steady-state measurements provide an estimate of the ratios of the four

rate constants shown in equation 3.3. The equations are;

$$E_1 = \exp((V_1-V)/K_1) = \frac{k_2}{k_1} \quad \ldots. (3.7),$$

$$E_2 = \exp((V_2-V)/K_2) = \frac{k_4}{k_3} \quad \ldots. (3.8),$$

where E_1 and E_2 were evaluated from the fit of equation 3.6 to the steady-state activation data (figure 3.11B). Solution of the system of differential equations for the 3-state scheme gives two well known equations which relate the measured rate constants to the microscopic rate constants. The equations are,

$$r_1 + r_2 = k_1 + k_2 + k_3 + k_4 \quad \ldots. (3.9)$$
$$r_1 r_2 = k_1 k_3 + k_2 k_4 + k_1 k_4 \quad \ldots. (3.10).$$

Solving equations 3.7-3.10 for k_1 and k_3 gives these two rate constants as solutions to second order quadratics and therefore there are two sets of k values which satisfy the four equations 3.7-3.10. The two solutions differ in the assignment of the rapid transition. One solution has the $C_2 \leftrightarrow O$ transition being rapid, linked to a slower $C_1 \leftrightarrow C_2$ transition. The other solution is the inverse, with $C_2 \leftrightarrow O$ being the slower transition. Both solutions give identical predictions for the macroscopic rate constants.

The rate constants measured from the tail current relaxations were used for the calculations, since both rate constants were accurately resolved, whereas only a single rate constant was measured accurately from the turn-on of the currents. The major reservation about this type of analysis is that errors in E_1 and E_2 will be

magnified as these ratios are extrapolated to cover the potential range -70 to -20 mV. The estimates of V_1 and K_1 (see equation 3.6) are particularly worrying due to the large standard errors of the estimates. The results produced should be viewed with some caution.

If equation 3.3 provides an adequate description of the data then the four microscopic rate constants should depend exponentially on the membrane potential (equations similar to equation A1.1). The calculated rate constants are shown in figure 3.17. In each case the natural logarithm of the microscopic rate constant is plotted against membrane potential. The four rate constants seem to depend approximately exponentially on membrane potential as predicted.

To test the the data more quantitatively, a straight line was fitted to the points in figures 3.17. The slope (voltage sensitivity) and the intercept (barrier energy at 0 mV) of these four straight lines were used to recalculate the two macroscopic rate constants using equation A2.4. The result is plotted in figure 3.18 and illustrates clearly that the microscopic rate constants from the fits in figure 3.17 do not accurately predict the observed time constants at potentials greater than -20mV.

This analysis would tend to suggest that the $P_o(V)$ measurements are not consistent with the measured voltage dependence of the time constants when interpreted in terms of a 3-state sequential scheme. Assuming this result is correct, there must be other exponential components present in the relaxations which are not clearly resolved.

Figure 3.17 Natural logarithm of the microscopic rate constants in equation 3.3 calculated using equations 3.7-3.10 and the data in figure 3.11B and the τ_f and τ_s values in figure 3.14. The straight lines were obtained using least squares linear regression between -70 and -20mV in A, and -70 and +10mV in B. Note that the two lines in each figure intercept at V_1 (A) and V_2 (B) (equation 3.6).

A

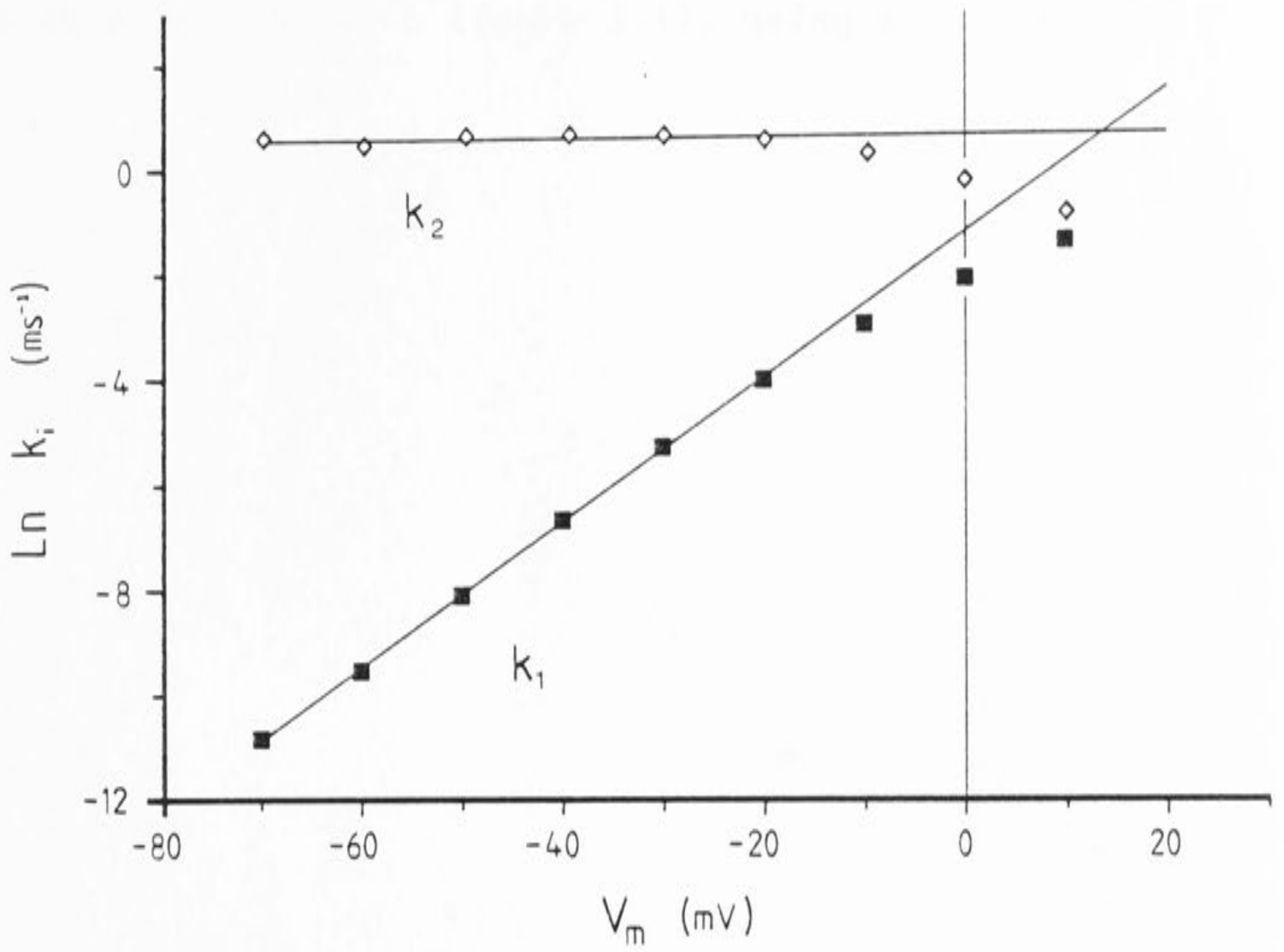
Ln k_i (ms^{-1})
0
-4
-8
-12
k_2
k_1
-80
-60
-40
-20
0
20
V_m (mV)

B

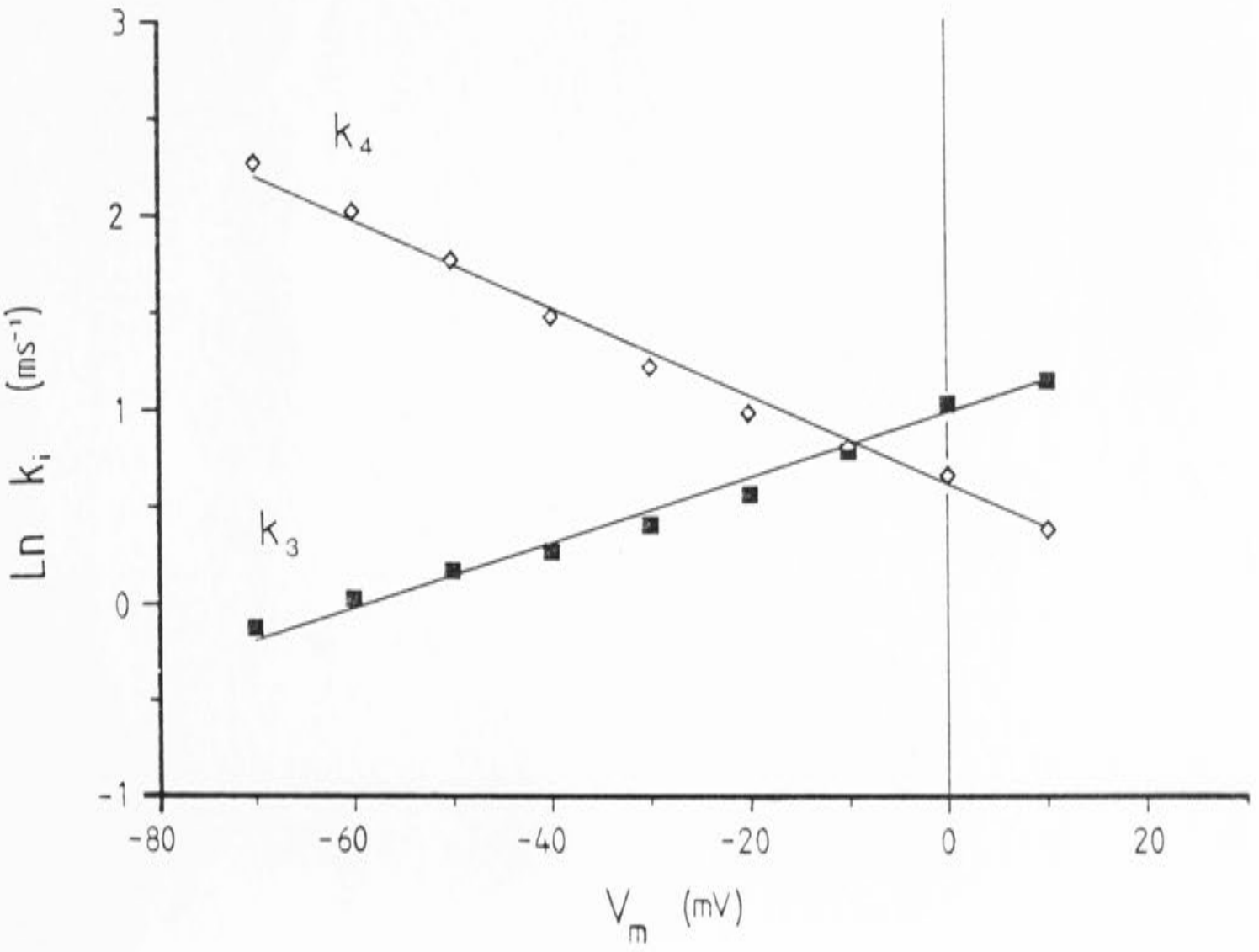
Ln k_i (ms^{-1})
3
2
1
0
-1
k_4
k_3
-80
-60
-40
-20
0
20
V_m (mV)

Figure 3.18 The points are the tail current time constants replotted from figure 3.11. The solid lines are the predicted values of the time constants calculated from the straight lines in figure 3.17, using equation A2.4.

A

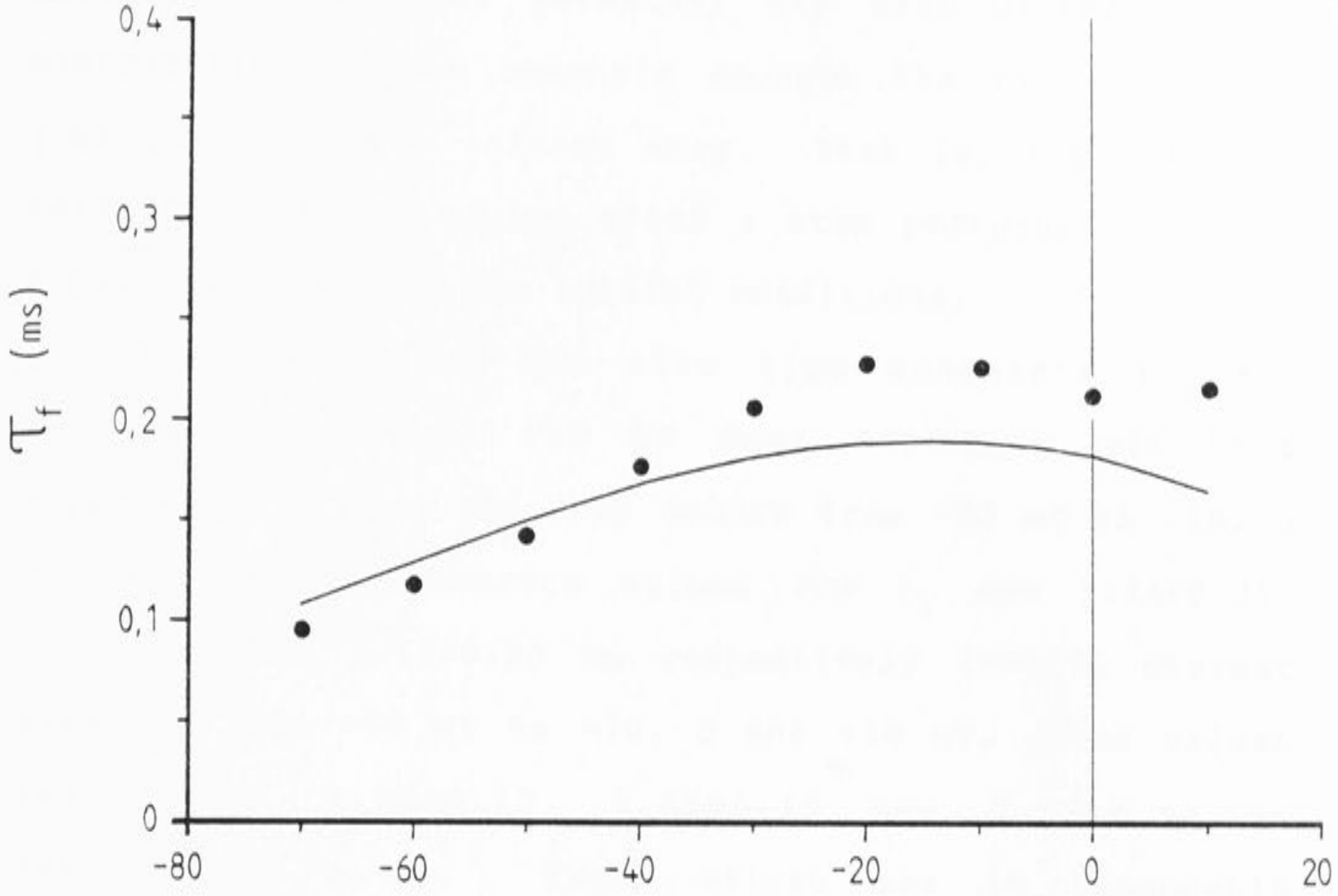
0,4
0,3
0,2
0,1
0
τ_f (ms)
-80
-60
-40
-20
0
20
V_m (mV)

B

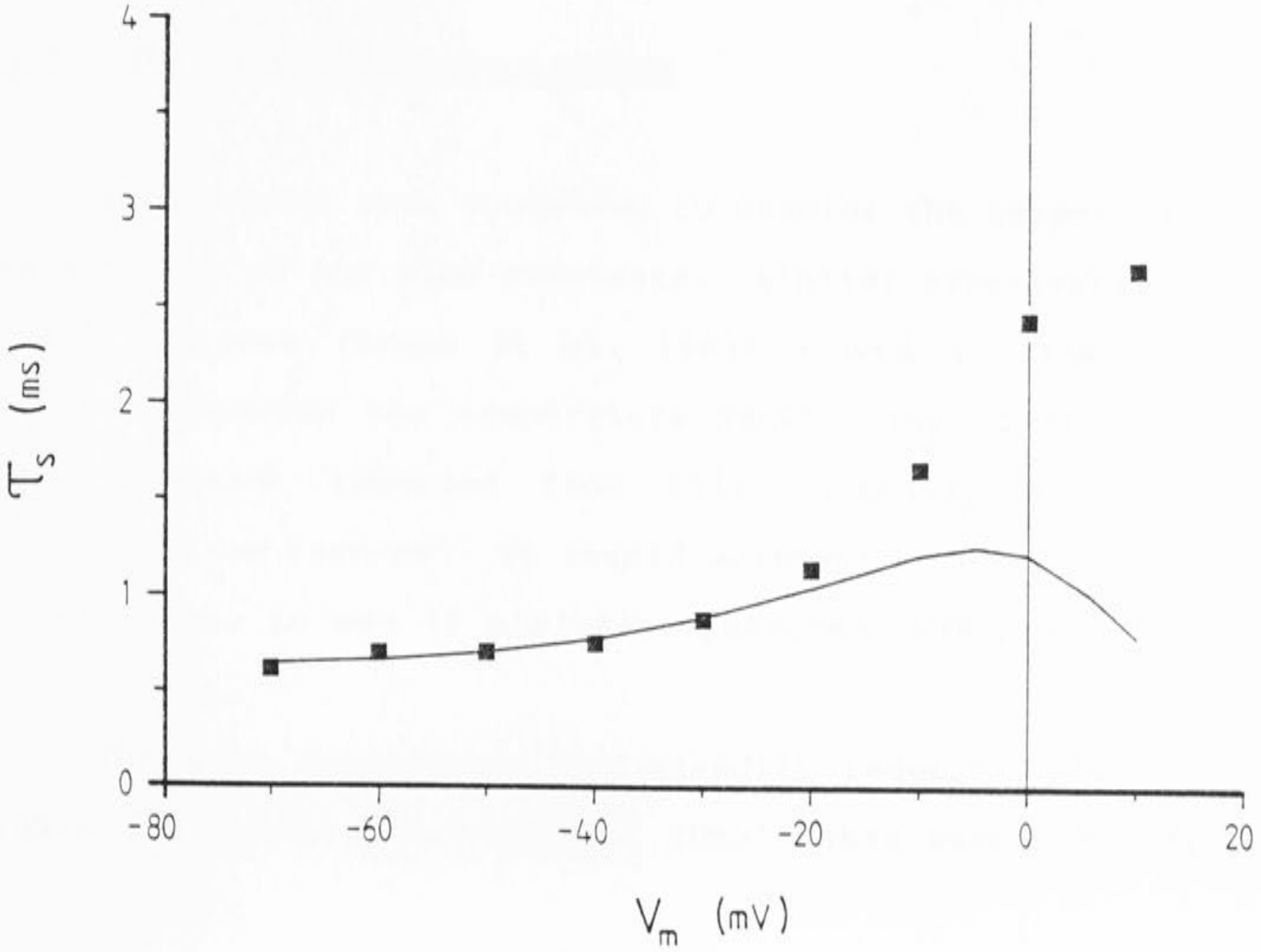
4
3
2
1
0
τ_s (ms)
-80
-60
-40
-20
0
20
V_m (mV)

If this were the case then the macroscopic rate constants measured at a given potential may well depend on the distribution of the channels amongst the various states just prior to the voltage step. That is, the rates of relaxation of the system after a step perturbation would appear to depend on the initial conditions.

Examination of the slow time constants (τ_s, τ_l) recorded at 0 and +10 mV does not bear out this expectation. When the step occurs from -50 mV to -10, 0 and +10 mV, the average values for τ_l are 1.74±0.21, 2.72±0.22 and 2.55±0.20 ms respectively (n=11), whereas stepping from +50 mV to -10, 0 and +10 mV, gives values for τ_s of 1.68±0.12, 2.46±0.12 and 2.70±0.24 ms respectively (n=9). These values are in reasonable agreement and would seem to suggest that the rate constants are independent of the initial conditions.

3.8 The effects of temperature

Experiments were conducted to examine the temperature sensitivity of the time constants. Similar experiments in snail neurones (Brown et al. 1983) showed a large discrepency between the temperature sensitivity of the slow time constant recorded from tail currents, and that recorded from turn-on. It seemed worthwhile to repeat the experiments, to see if a similar phenomena was present in these cells.

The bath temperature was steadily reduced (1^{o}C/min) and a test pulse (to +10mV for 10ms) taken each time the

Figure 3.19 The broken lines through the traces are the double exponentials fits obtained using the LMM routine. (A) Activation of the calcium current at +10mV at the temperatures indicated. There is a marked increase in the initial delay before activation as the temperature is reduced. (B) Tail currents from the same pulses shown in A. The time constant of the fast phase became significantly longer.

A

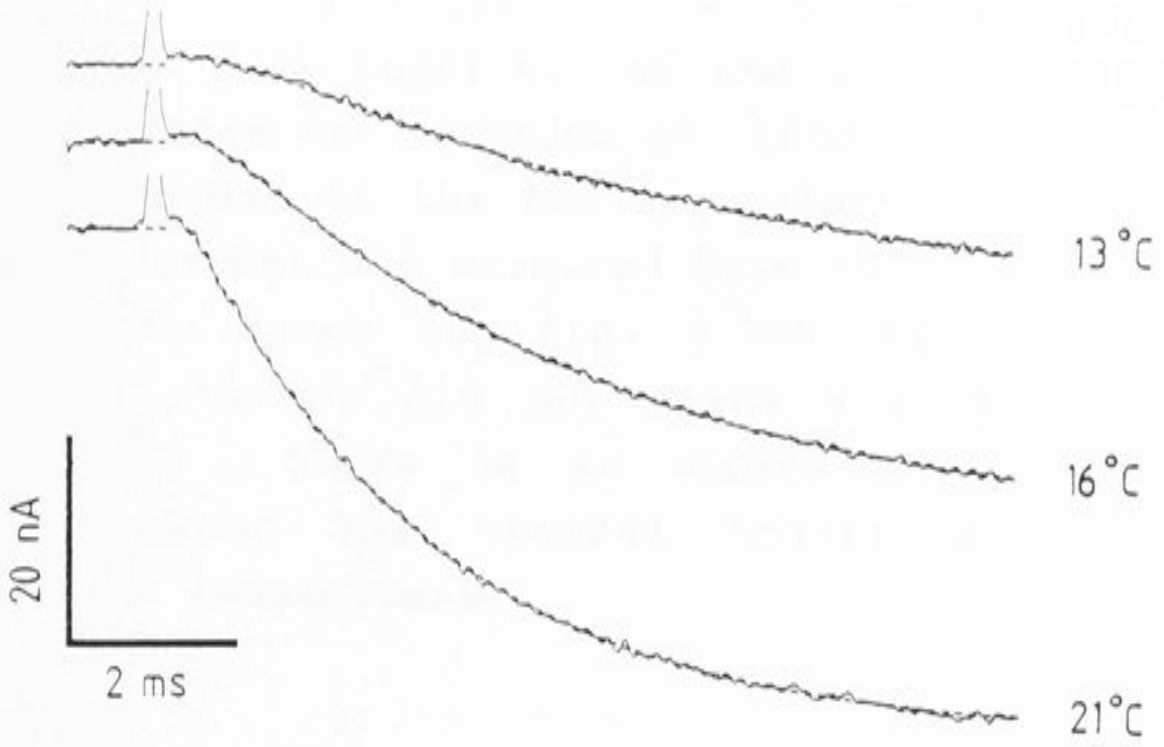

B

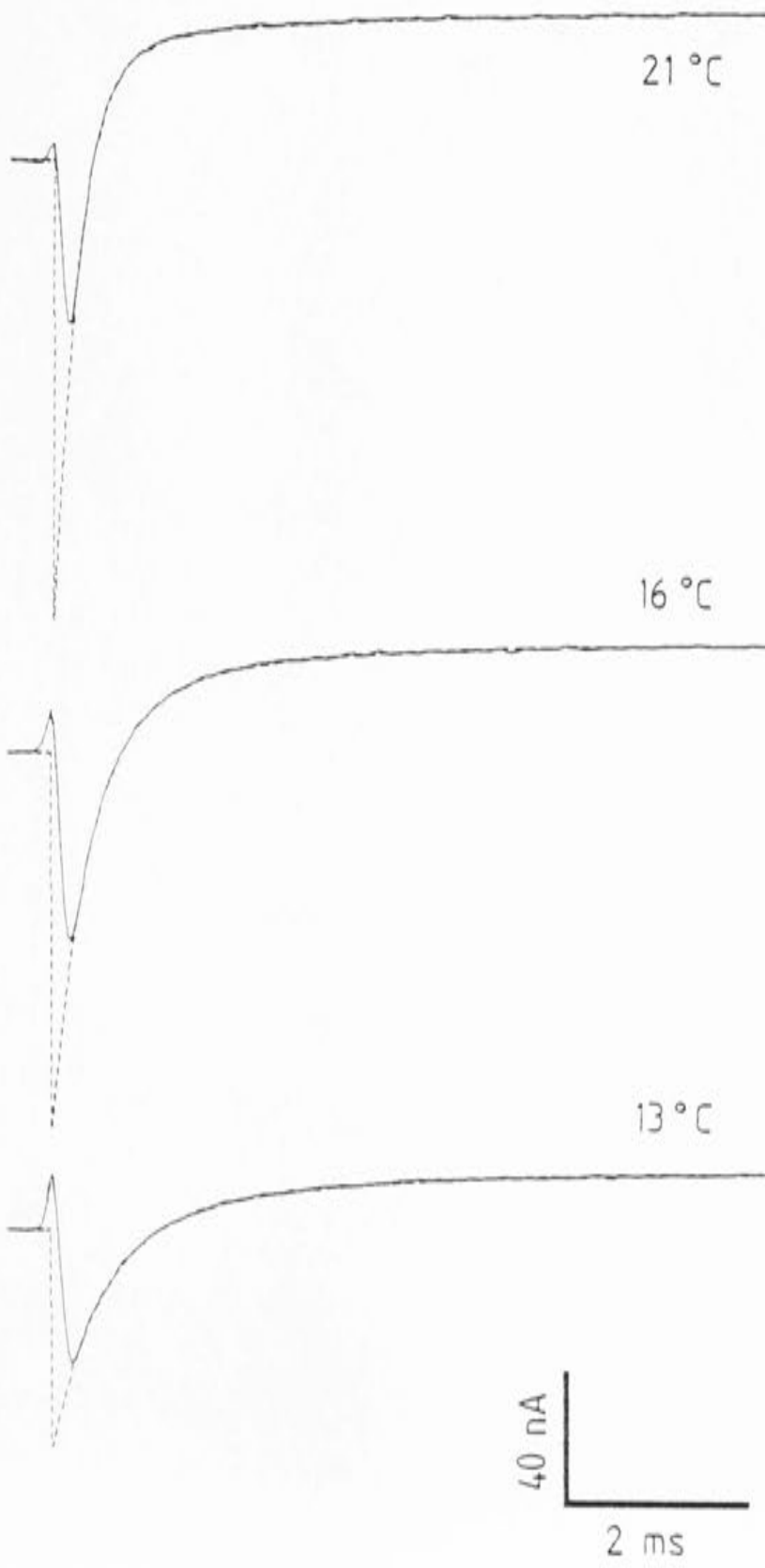

Figure 3.20 The figure shows the effects of temperature on the peak current, and the relaxation time constants. Activation was recorded at +10mV, and the tail currents were recorded at the holding potential (-50mV). The peak inward current was measured from the exponential fit to the current trace (eg fig. 3.19A) since at low temperatures the current did not reach a steady level during the pulse. There is an approximately linear relationship between the natural logarithm of the parameters and the temperature.

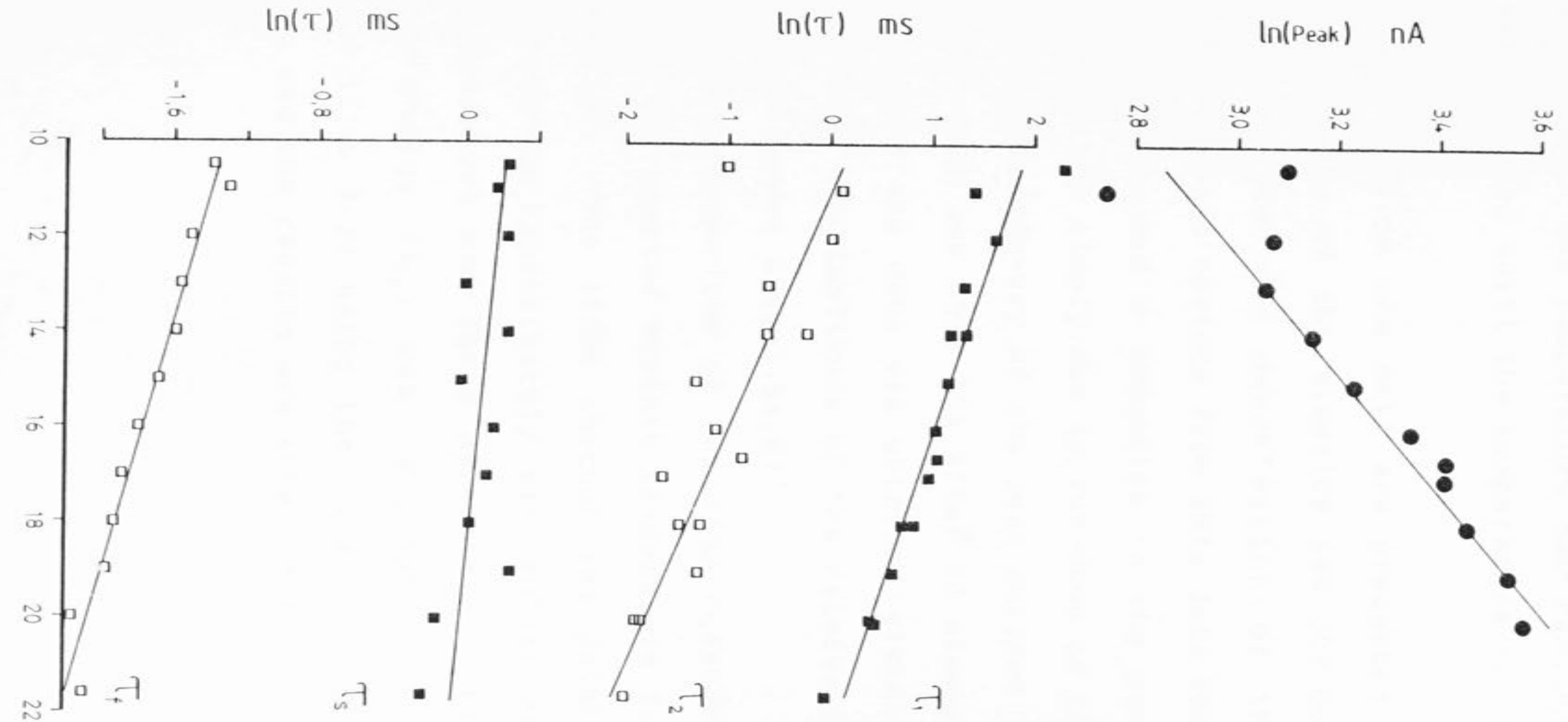
ln(Peak) nA
2,8
3,0
3,2
3,4
3,6
ln(τ) ms
-2
-1
0
1
2
T_1
T_2
ln(τ) ms
-1,6
-0,8
0
T_s
10
12
14
16
18
20
22
T_f
Temperature (°C)

temperature dropped by one degree. The temperature was monitored by a fine thermistor probe placed close to the preparation. When the temperature had reached 10°C, the process was reversed until the temperature had returned to 20°C.

The results from one cell are presented in figures 3.19. The slowing of the kinetics was obvious both for the activation and the deactivation of the calcium channel. It was also obvious from this data that reducing the temperature caused a reduction in the peak current. This effect was not simply due to run-down of the current, as there was good recovery of the peak current in one cell where the run-down was only 15% after 20 minutes. In the other two cells, the data was obtained within the first 10 minutes, when the amplitude of the calcium current was constant (see figures 2.4, 3.5A,B).

The natural logarithm of the time constants and the peak current are plotted against temperature for one cell in figure 3.20. The lines through the points indicate that there was an approximately exponential relationship between temperature and these parameters. The apparent activation energy (E_a) was calculated according to equations 3.11 & 3.12 using the data from this and two other cells and the results are shown in table 3.1.

Table 3.1 Temperature sensitivity of various parameters measured from calcium currents in 3 cells.

Parameter	(mV)	E_a (kJ/mol) ± s.e.	(Q_{10})
Peak current	(+10)	67 ± 9	(2.6)
τ_1 (slow)	(+10)	85 ± 4	(3.4)
τ_2 (fast)	(+10)	139 ± 15	(7.5)
τ_s	(-50)	29 ± 5	(1.5)
τ_f	(-50)	79 ± 6	(3.1)

The temperature sensitivity of the τ's appears to be lower at negative potentials. The interpretation of these results is left to the discussion.

3.9 Effects of (∓)Bay K 8644

The experiments described in this section investigated the effects of (∓)Bay K 8644 on the kinetics and $P_o(V)$ curve of the calcium channels. Initially, 5μM Bay K was applied, but the effect was marginal (figure 3.21). At 10μM, the effect was larger and more consistent (figure 3.21), and this concentration was used in the subsequent experiments. The effect of 10μM nifedipine was also tested on the calcium current in these cells. The result is shown in figure 3.22, and indicates that the calcium current is relatively insensitive to this compound. Nifedipine is light-sensitive, and the lighting levels were reduced during the experiment. The solution used was biologically active since solutions made from the same stock blocked part of the asymmetric charge movement in skeletal muscle fibers (Lamb 1985).

Bay K increased the steady-state inward current, in

Figure 3.21 The top two traces show the effects of 5μM Bay K on the calcium current. The step potential was +10mV. The more rapidly rising, slightly smaller current was recorded in the presence of Bay K. There was also a slight prolongation of the slow phase of the tail current. The decrease in the amplitude, is probably due to some run-down of the calcium current. The bottom traces show the effect of 10μM Bay K in another cell. In this case there was a marked increase in the amplitude of the current, and a prolongation of the tail current. The step potential was +20mV, and the holding potential -50mV.

Bay K 5 µM

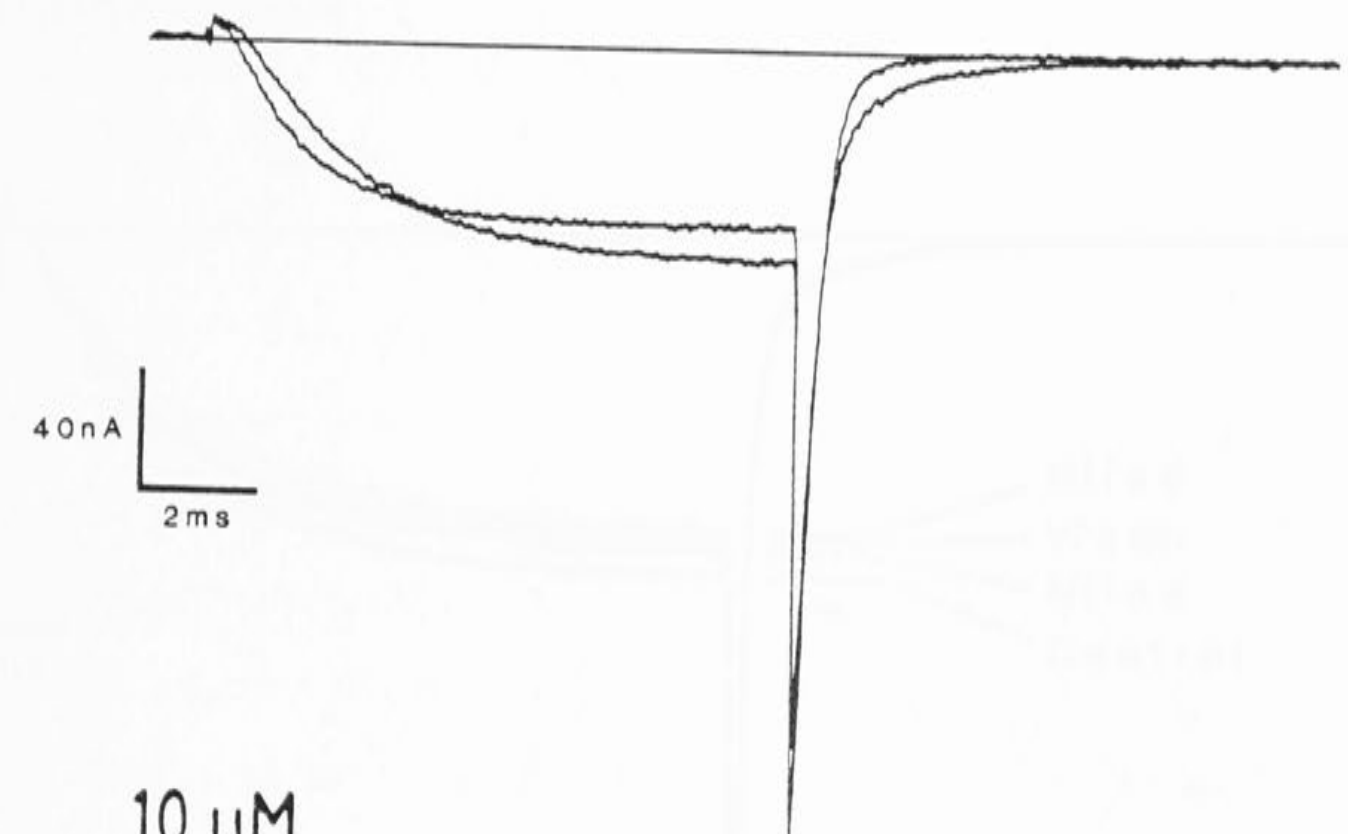

10 µM

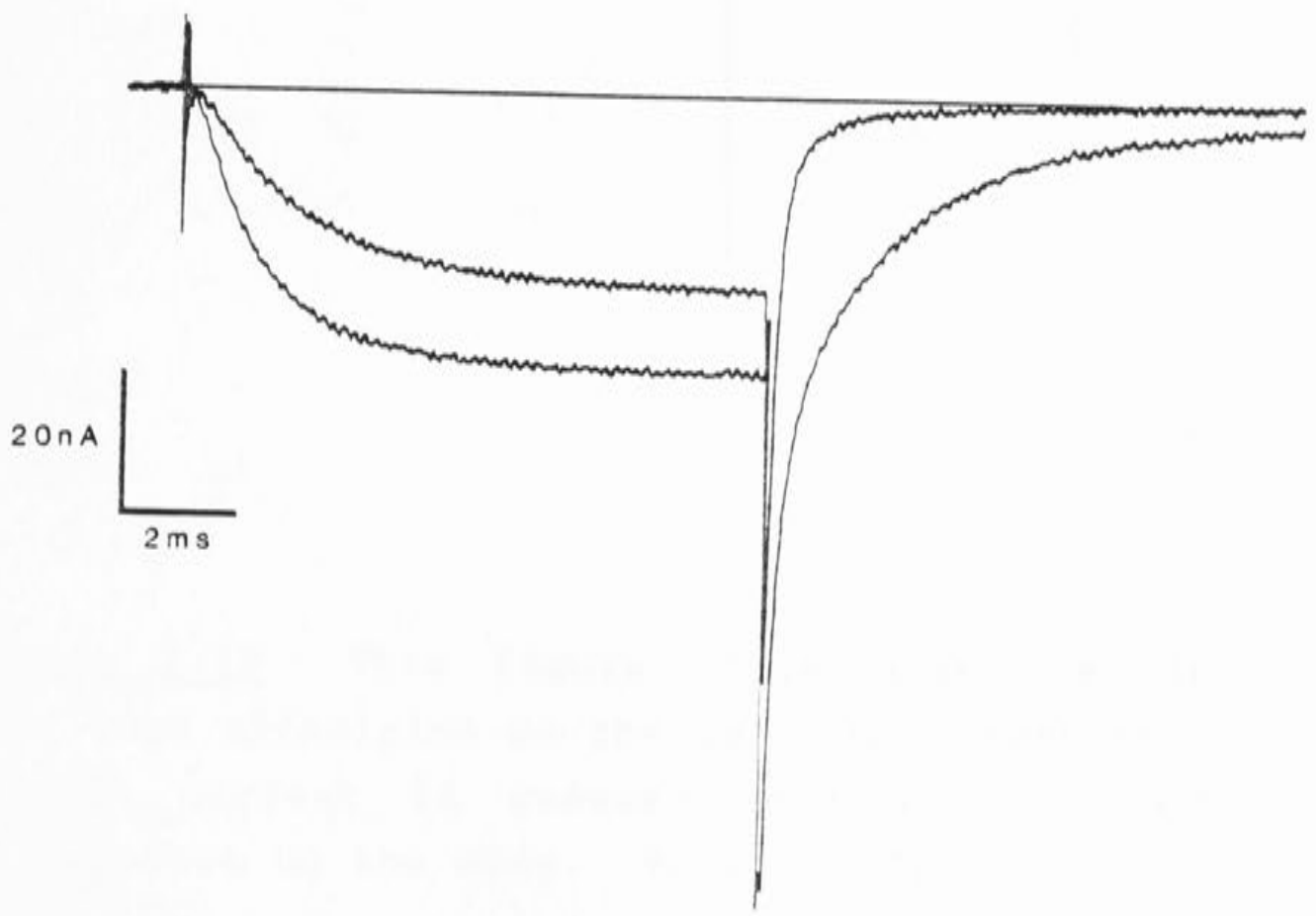

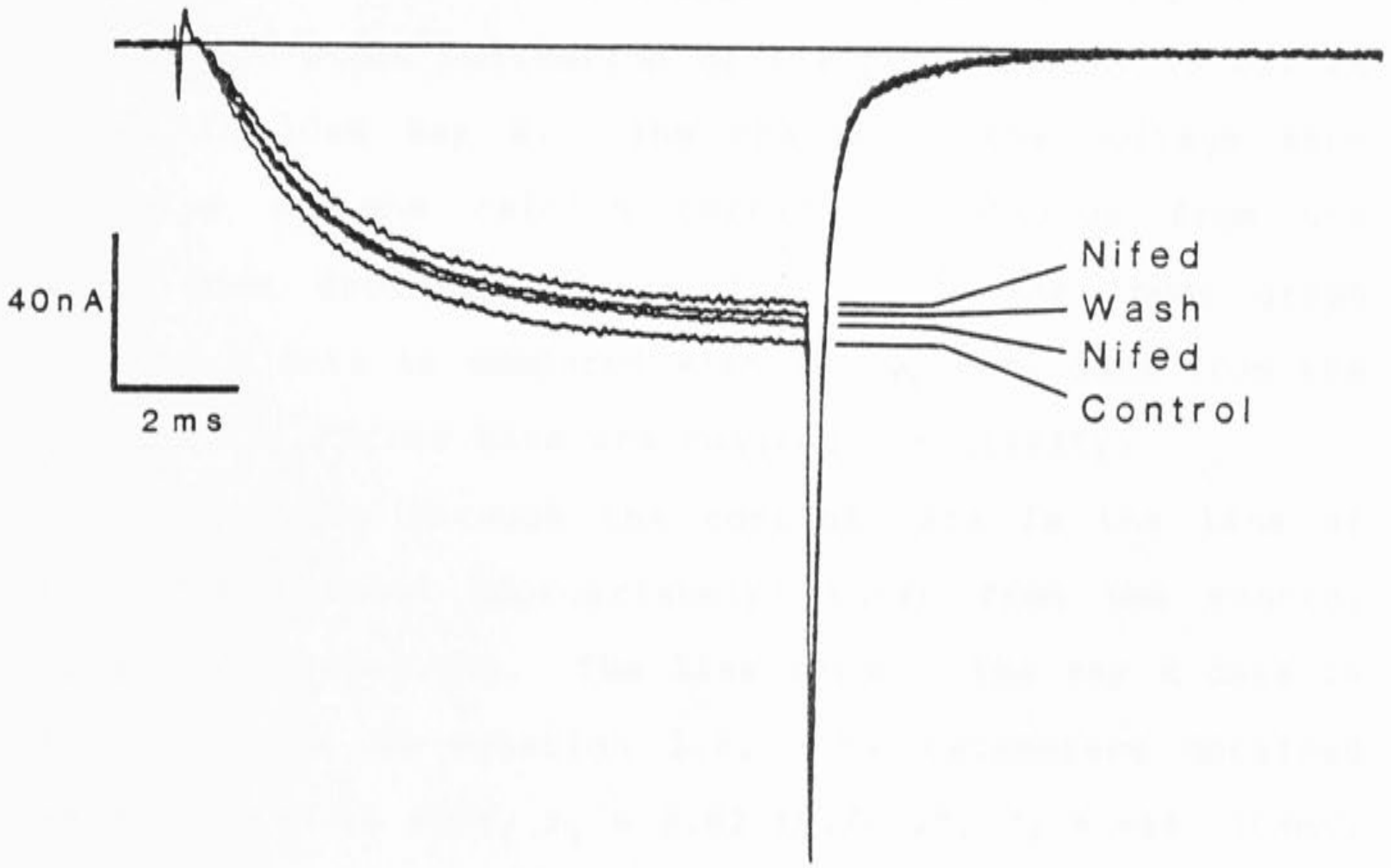

Figure 3.22 This figure illustrates the blocking effect of 10μM nifedipine on the calcium current at +10mV. The calcium current is reduced only slightly after 4 minutes exposure to the drug. V_h = -50mV.

cells in which the rundown was not too severe. This is shown in figure 3.21 which shows the effect of 10μM Bay K at +10mV. There is an increase in the peak inward current which is reached more rapidly, and prolongation of the tail current. Bay K shifted the activation of the calcium current to more negative potentials. This is shown in figure 3.23A which shows the normalized average results from 5 cells. It is also apparent from this figure that the steady-state activation of the peak current is not as steep in 10μM Bay K. The change in the voltage sensitivity of the calcium current is obvious from the $P_o(V)$ plot shown in figure 3.23B. In the lower graph the Bay K data is compared with the control data from the same cells. Error bars are omitted for clarity.

The curve through the control data is the line of best fit (scaled appropriately) taken from the control data in figure 3.11B. The line through the Bay K data is the best fit to equation 3.6. The parameters obtained were : V_1 = 15 ±8mV, z_1 = 2.82 ±0.69 e^+, V_2 = -69 ±104mV, z_2 = 0.37 ±0.97 e^+. The lower voltage sensitivity of the steady-state activation of the calcium channel is reflected in the smaller values for the dipole moment that are predicted from the fits to the data. The parameters produced by the fit suggest that Bay K could produce its effects by reducing the effective dipole moments of the activation reactions.

Given the change in the steady-state activation, one might expect significant changes in the relaxation time constants. A prolongation of the slow time constant of

Figure 3.23 Each point shows the normalized average (n=5) tail current recorded at -50mV plotted against the activation potential. The error bars are the standard errors. The line through the points is the fit to equation 3.6. A comparison of this and the control data recorded in the same cells is shown in the bottom graph. The line throught the control data is the fit from figure 3.11B.

A

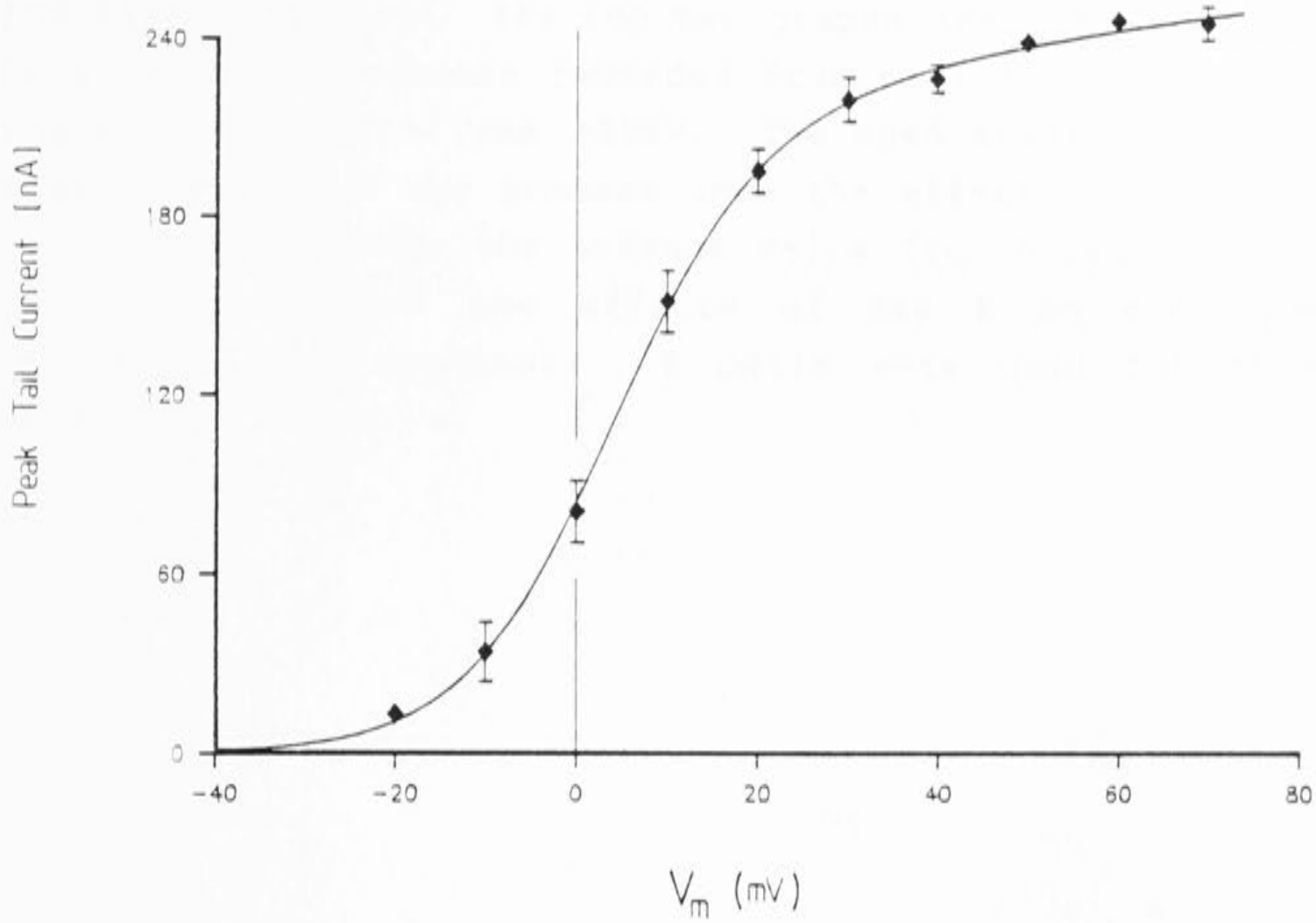
240
180
120
60
0
Peak Tail Current (nA)
-40
-20
0
20
40
60
80
V_m (mV)

B

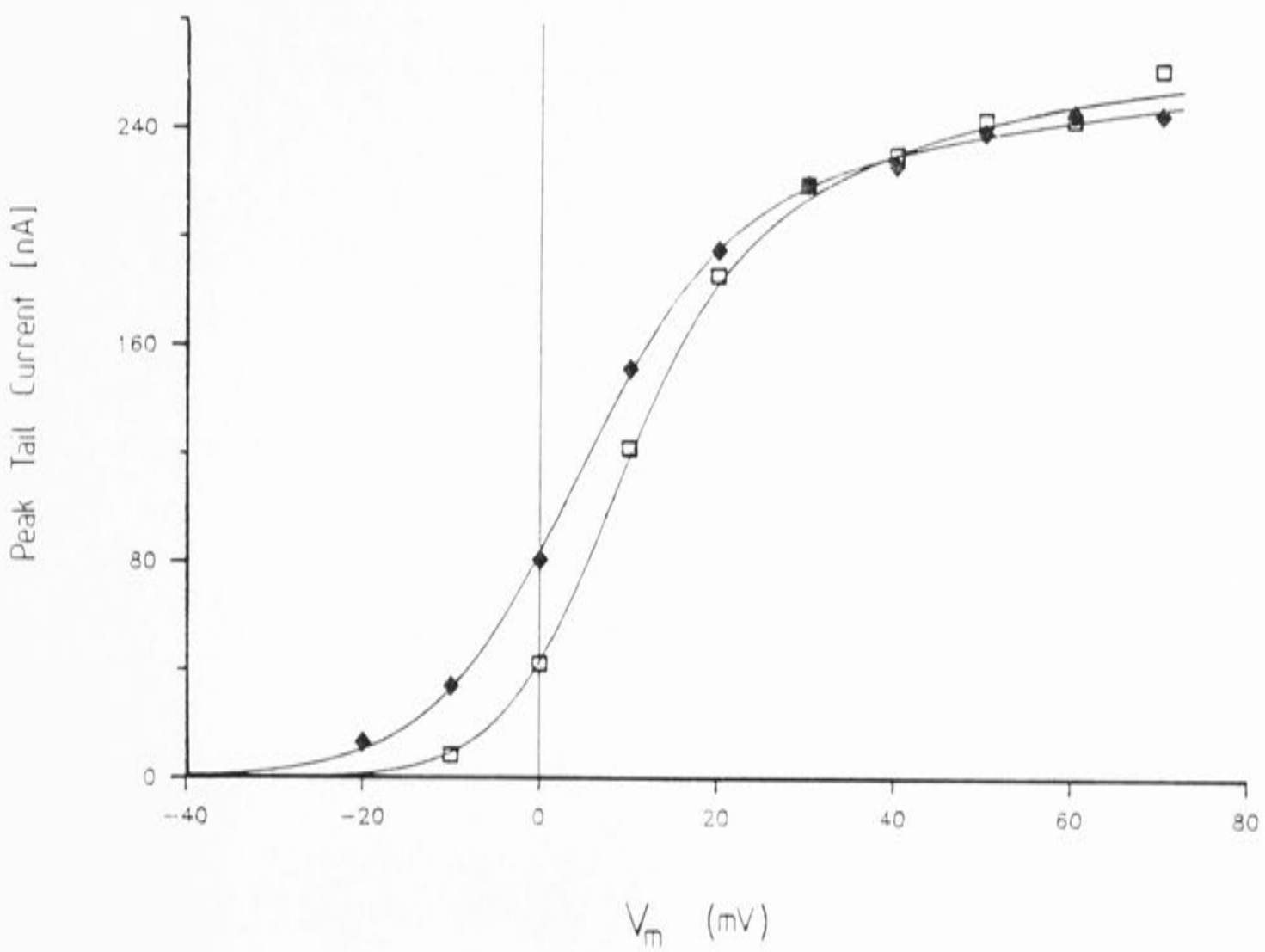
240
160
80
0
Peak Tail Current (nA)
-40
-20
0
20
40
60
80
V_m (mV)

Figure 3.24 Bay K produced marked effects on the slow time constants. The top two graphs show the fast and the slow time constants recorded from tail currents. The activation potential was +50mV. The open squares are the control data, and the crosses show the effect of 10μM Bay K. Each point shows the average value from 5 cells. The bottom figure show the effects of Bay K on the slow activation time constant. 5 cells were used for this average.

A

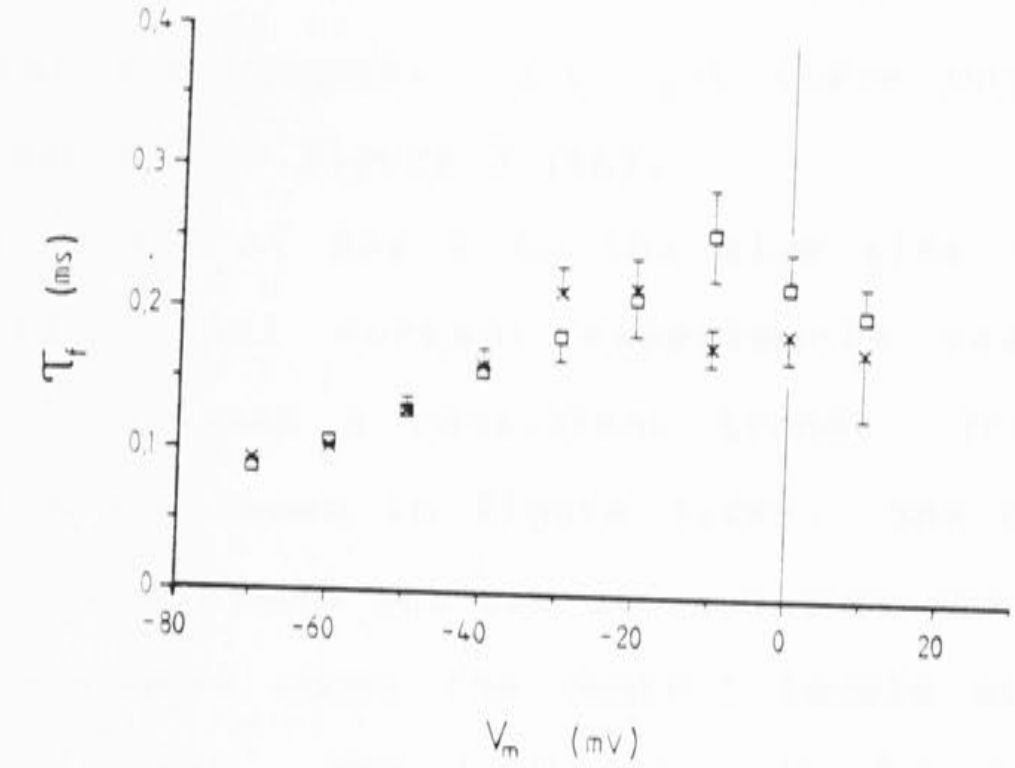
0.4
0.3
0.2
0.1
0
τ_f (ms)
-80
-60
-40
-20
0
20
V_m (mV)

B

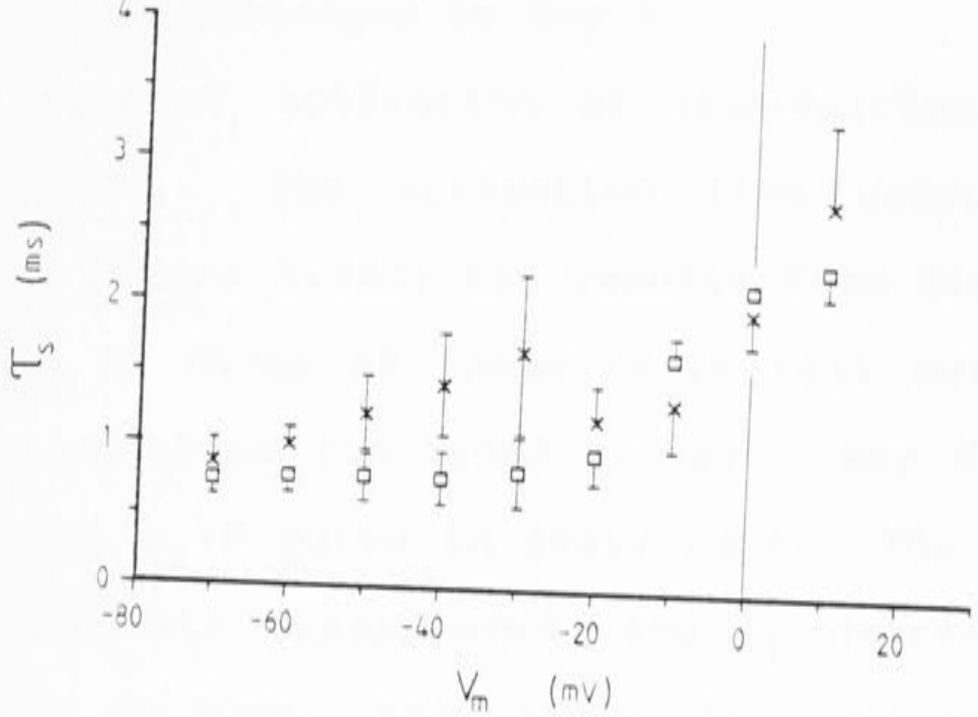
4
3
2
1
0
τ_s (ms)
-80
-60
-40
-20
0
20
V_m (mV)

C

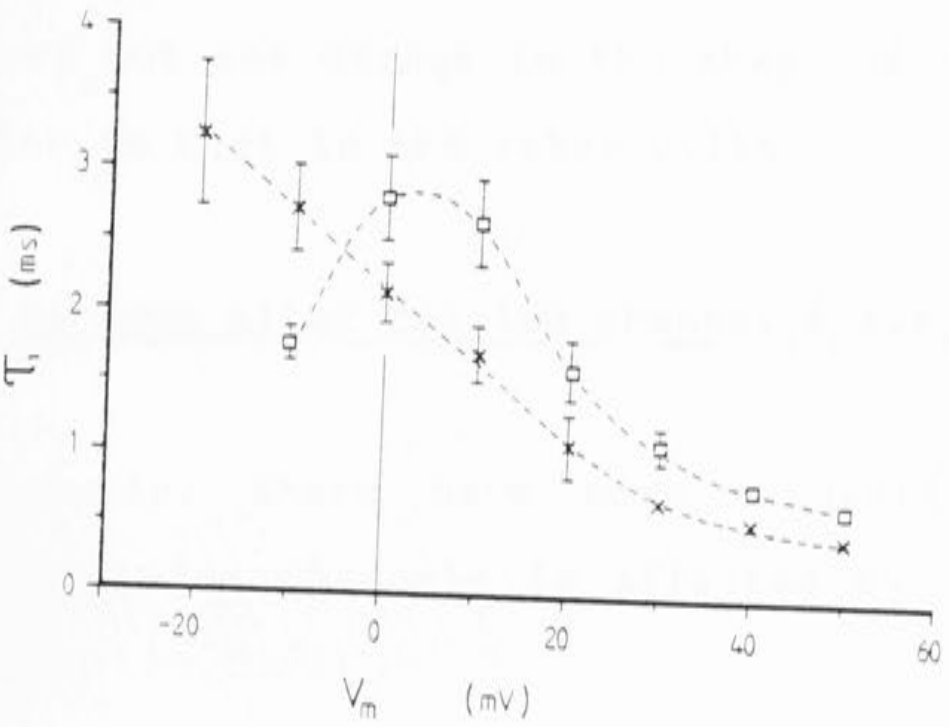
4
3
2
1
0
τ_i (ms)
-20
0
20
40
60
V_m (mV)

the tail currents at -50mV was the most obvious effect during the experiments. The τ_f-V curve was unaffected by 10μM Bay K (see figure 3.24A).

The effect of Bay K on the slow time constant recorded from tail current experiments was variable, although there was a consistent trend. The data from five cells are shown in figure 3.24B. The open squares show the control data and the crosses show the Bay K data. τ_s was increased above the control levels at potentials less than -20mV. The τ_s-V curve displayed a definite break around -20mV, and at more positive potentials, τ_s appeared to be unchanged by Bay K.

The rate of activation of the calcium current was also affected. The activation time constant (τ_1) is plotted in figure 3.24C; the results from five cells were averaged. In three of these cells tail current records were also obtained (included above). Bay K changed the shape of the τ_1-V curve in every case. The peak seen in the control data disappeared, and τ_1 decreased steadily between -20 to 50mV. The results for four cells showed a reduction in the average magnitude of τ_1 at potentials above 0mV. However in one cell the magnitude of τ_1 was not reduced but the change in the shape of the τ_1-V curve was similar to that in the other cells.

3.10 Do Ba ions alter calcium channel kinetics ?

Previously, there have been suggestions that the gating of calcium channels is affected by the nature of

the permeant ion (Saimi & Kung, 1982). Fenwick, Marty and Neher (1982), found that the gating of calcium channels in cultured bovine chromaffin cells was slowed when the 5 mM external Ca^{2+} was replaced by 5 mM Ba^{2+}. Such experiments are complicated by the fact that changing the concentration or type of external divalent cation often causes changes in the surface charge potential of the membrane.

The experiments described in this section compare the properties of the calcium channels when barium and calcium ions are the charge carriers. In the initial experiments the 10 mM external calcium was replaced by 20 mM barium. Under these conditions the peak current I-V was shifted to more negative potentials by 10mV. The shift is consistent with an increase in a negative (outside) surface charge potential.

Part of the shift could have been due to changes in the reversal potential of the current. The $P_o(V)$ curves shown in figure 3.25A demonstrate that this is not the case. The points are the extrapolated peak tail currents measured at -50 mV. A 10 mV negative shift is seen in this curve after the change to 20 mM barium.

If the changes observed in the gating of calcium channels are simply the result of changes in the surface potential, then the time constants of the current relaxations should be identical after correcting for the surface potential. The slow activation time constant is plotted in figure 3.25B Surface charge effects were corrected for, by shifting the values recorded in 20 mM

Figure 3.25 (A) The open symbols show the peak tail currents recorded in 10mM external calcium, plotted against activation potential. The solid symbols show the current recorded when the external calcium was replaced with 20mM barium. There is a ~10mV shift in the steady state activation curve to more negative potentials. (B) The open symbols are the control values, and the solid symbols were recorded in 20mM barium. The barium data was shifted 10mV to more negative potentials, to correct for the change in the external surface charge potential.

A

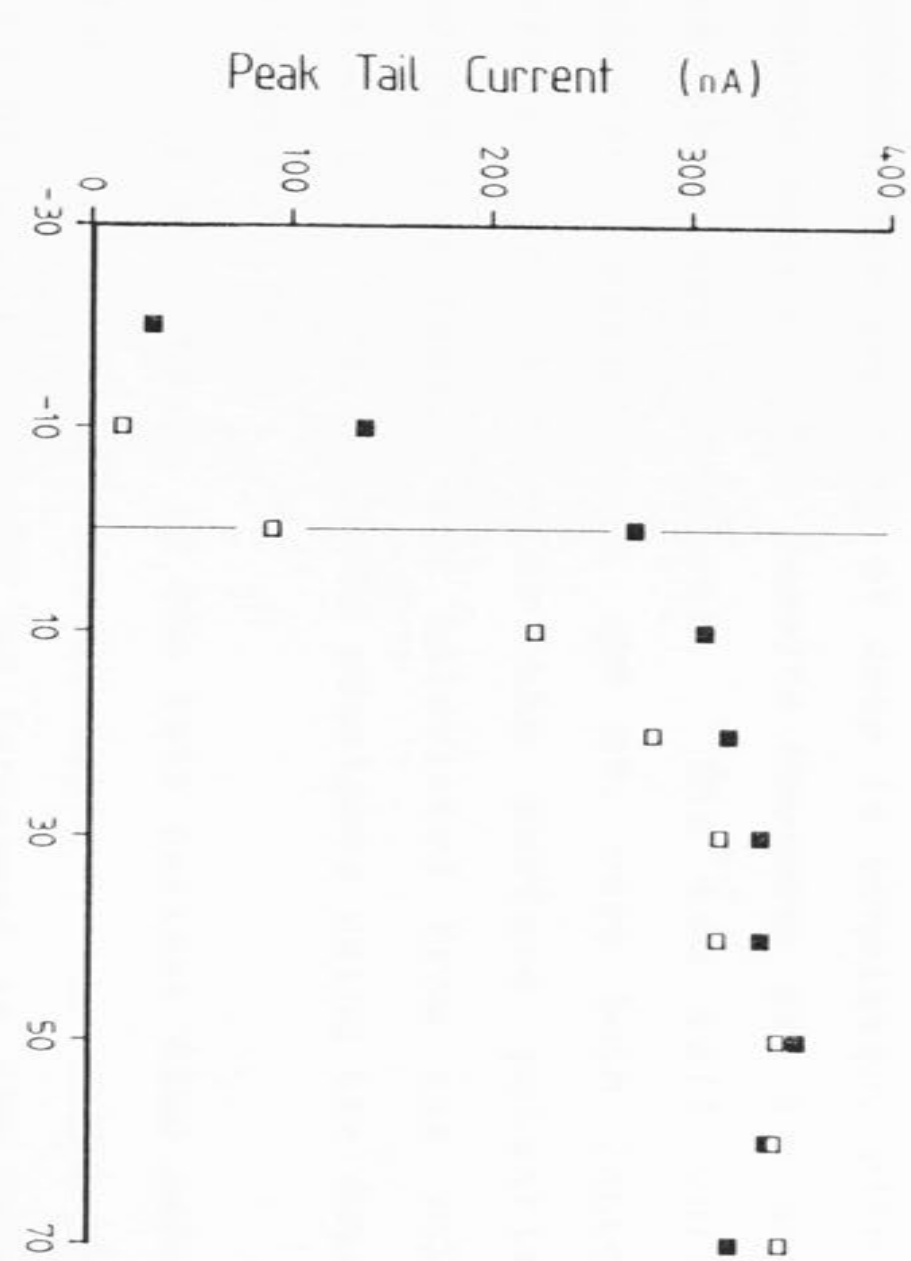
Peak Tail Current (nA)
0
100
200
300
400
-30
-10
10
30
50
70
V_m (mV)

B

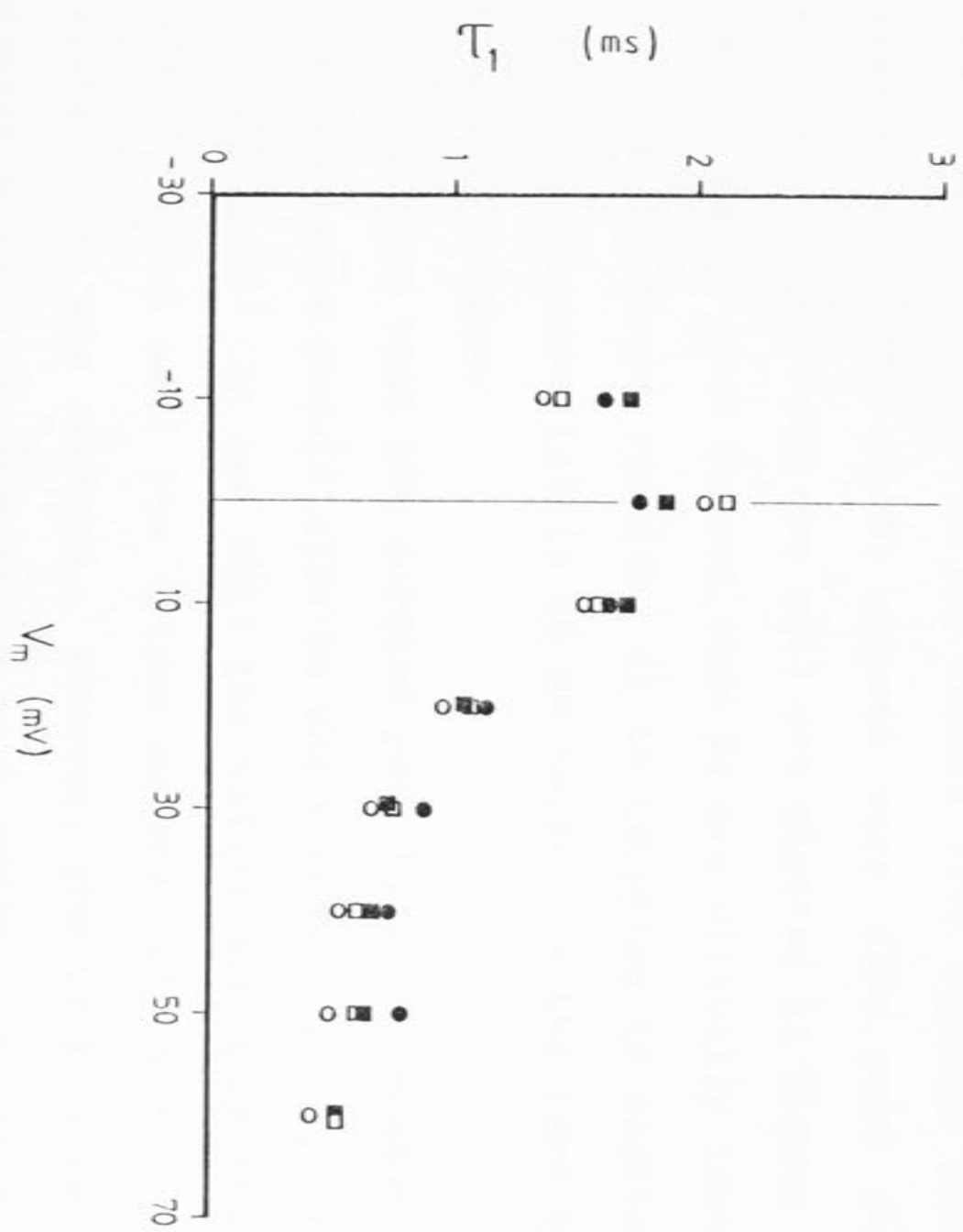
τ_1 (ms)
0
1
2
3
-30
-10
10
30
50
70
V_m (mV)

barium 10 mV more positive. The excellent agreement between the two sets of data is consistent with a surface charge action. The results however, are not as clear cut as this would suggest. The two tail current time constants measured at -50 mV, were both increased even after correcting for the surface potential. The correction factor was calculated from the voltage sensitivity of the two time constants using the data shown in figures 3.14A,B.

If the change in the tail current time constants was due to a direct effect of barium, one might expect that the prolongation would be increased as the concentration of barium was increased. If it were due to surface charge potential, then the effect should decrease at higher barium concentrations. The external barium concentration was increased to 40 mM. The peak current I-V curves in 10mM calcium and 40 mM Ba showed very similar potential dependence. The $P_o(V)$ curves were also very similar, and the results from one cell are plotted in figure 3.26A. The curves in 10mM Ca and 40mM Ba are virtually identical. In light of these results, it is tempting to suggest that the surface potential in 40 mM barium is the same as that in 10 mM calcium.

Assuming that the surface potential is unchanged, the time constants should also be unaltered. τ_1 is plotted in figure 3.26B. In one cell the values are much the same. In the second cell the values between -10 and 10 mV are greater than the control. However, the tail current time constants were increased in both cells. τ_f increased

Figure 3.26 (A) The protocol was the same as for the previous figure. The open symbols show the control data, and the solid symbols show the results obtained in 40mM external barium. The good agreement between the points suggests that the surface charge is approximately the same in 10mM Ca and 40mM Ba. (B) A comparison of the activation time constants for the two cells recorded in 10mM calcium (open symbols) and 40mM barium. In one cell the activation time constant was increased above the control levels.

A

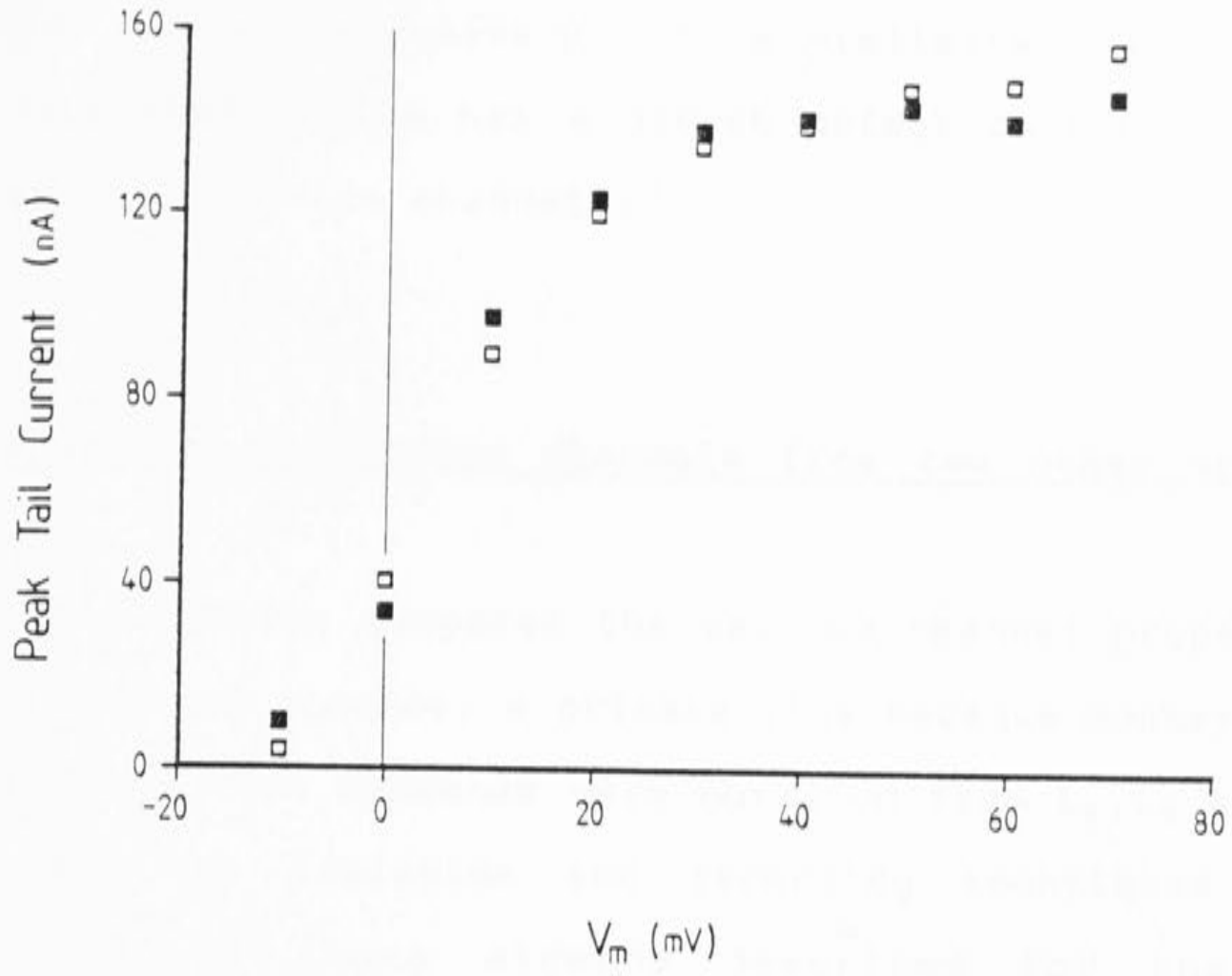
160
120
80
40
0
Peak Tail Current (nA)
-20
0
20
40
60
80
V_m (mV)

B

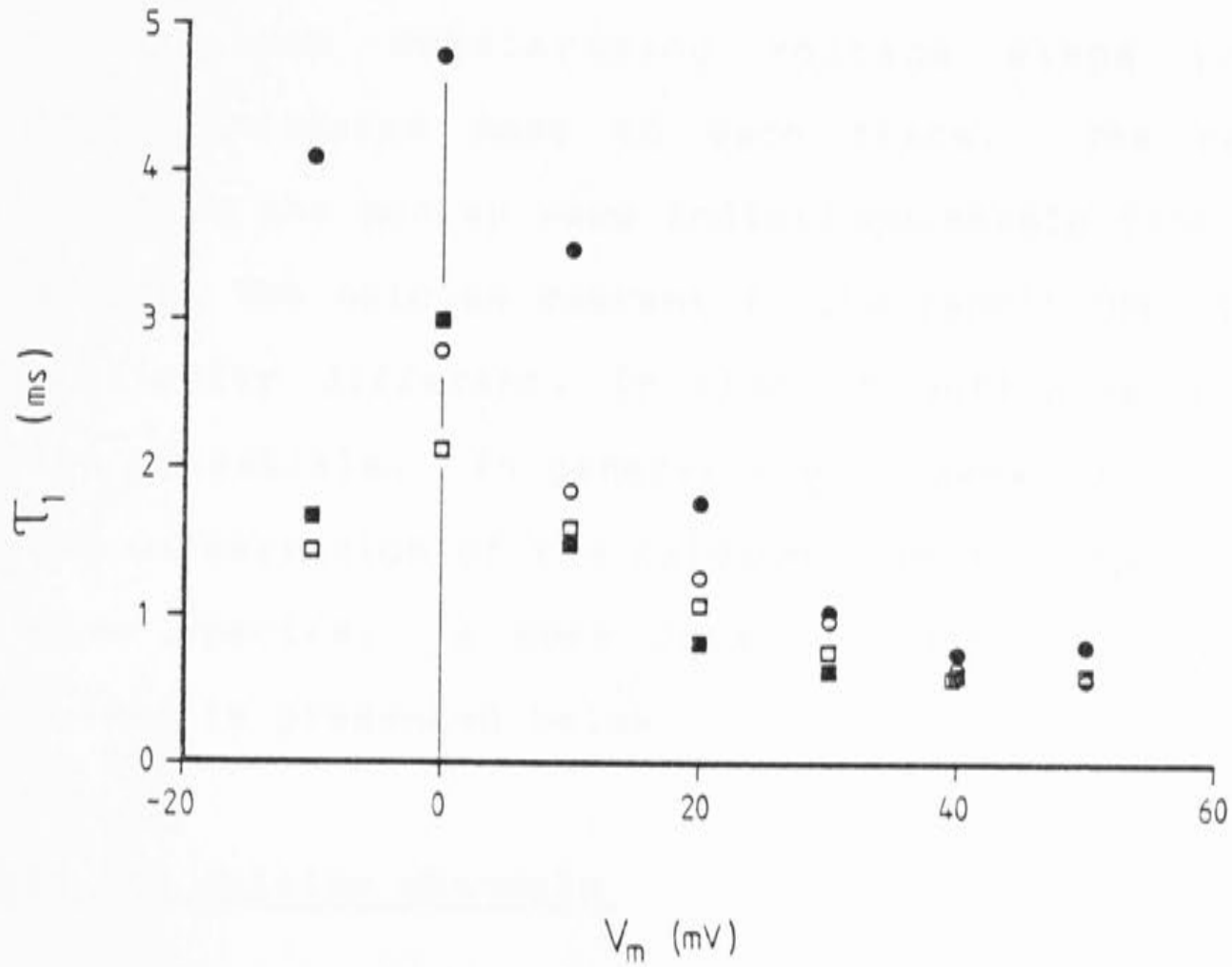
5
4
3
2
1
0
τ_1 (ms)
-20
0
20
40
60
V_m (mV)

1.5 and 1.6 fold, while τ_s increased 1.8 and 2.0 fold in the two cells respectively. This preliminary data would indicate that barium has a direct effect on the kinetics of neuronal calcium channels.

3.10

Comparison of calcium channels from two other species

This section compares the calcium channel properties from two other species, a primate (the macaque monkey) and the rabbit. The neurones were obtained from L_6, L_7 and S_1 DRG, and the isolation and recording techniques were identical to those already described for the cat experiments.

A general comparison of the calcium current from the three species is shown in figure 3.27. The currents were evoked by 10ms depolarizing voltage steps to the potentials indicated next to each trace. The results obtained from the monkey were indistinguishable from those of the cat. The calcium current in the rabbit DRG appears to be slighlty different, in that it activates at more negative potentials. In general there seems to be a high level of conservation of the calcium channel properties in the three species. A more detailed examination of the rabbit data is presented below.

Rabbit DRG calcium channels

Three rabbits were used for this section of the

Figure 3.27 Calcium currents recorded from a cat, rabbit and macaque DRG neurones in response to the voltage steps indicated. The holding potential was -50mV and the recording conditions essentially the same.

Cat DRG : I_{Ca}

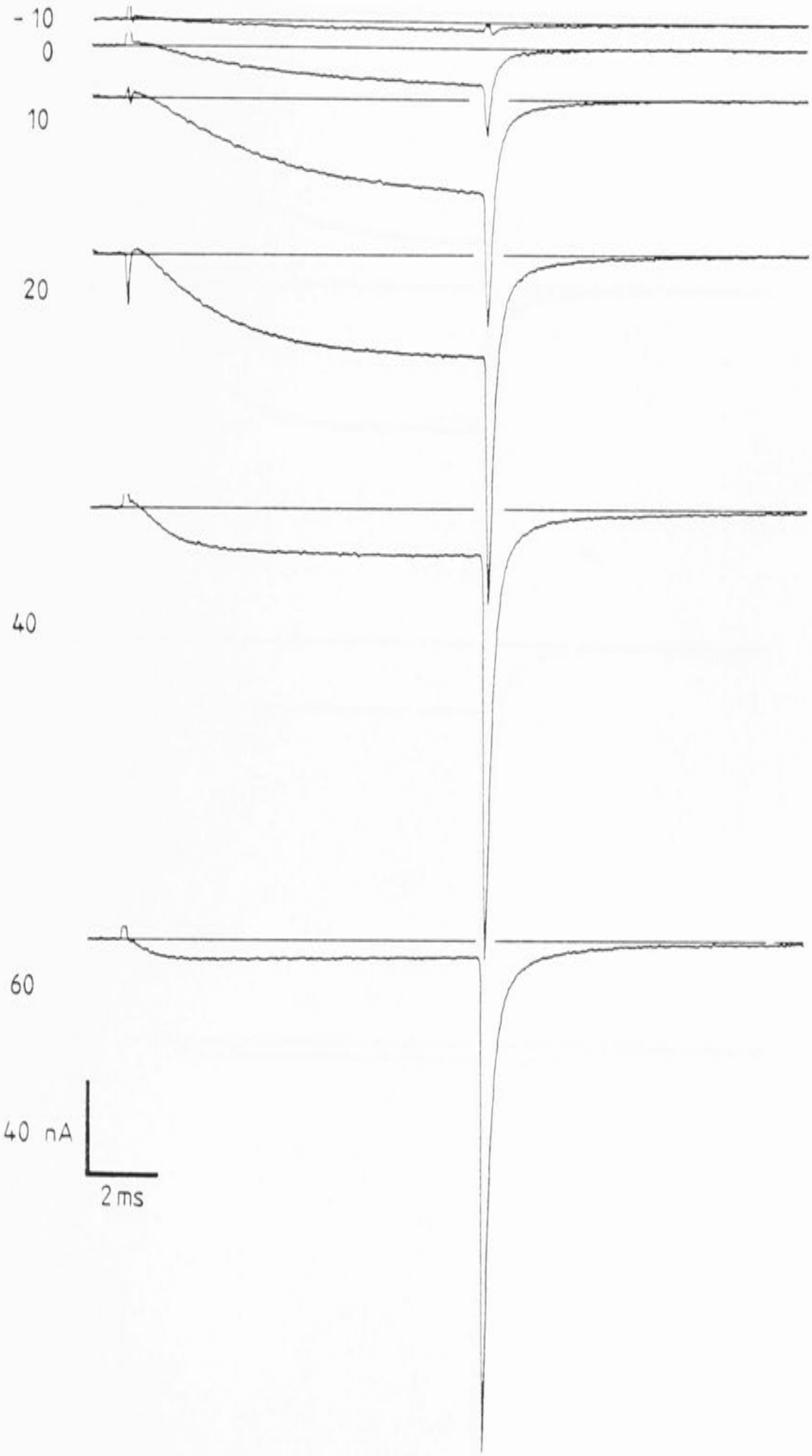

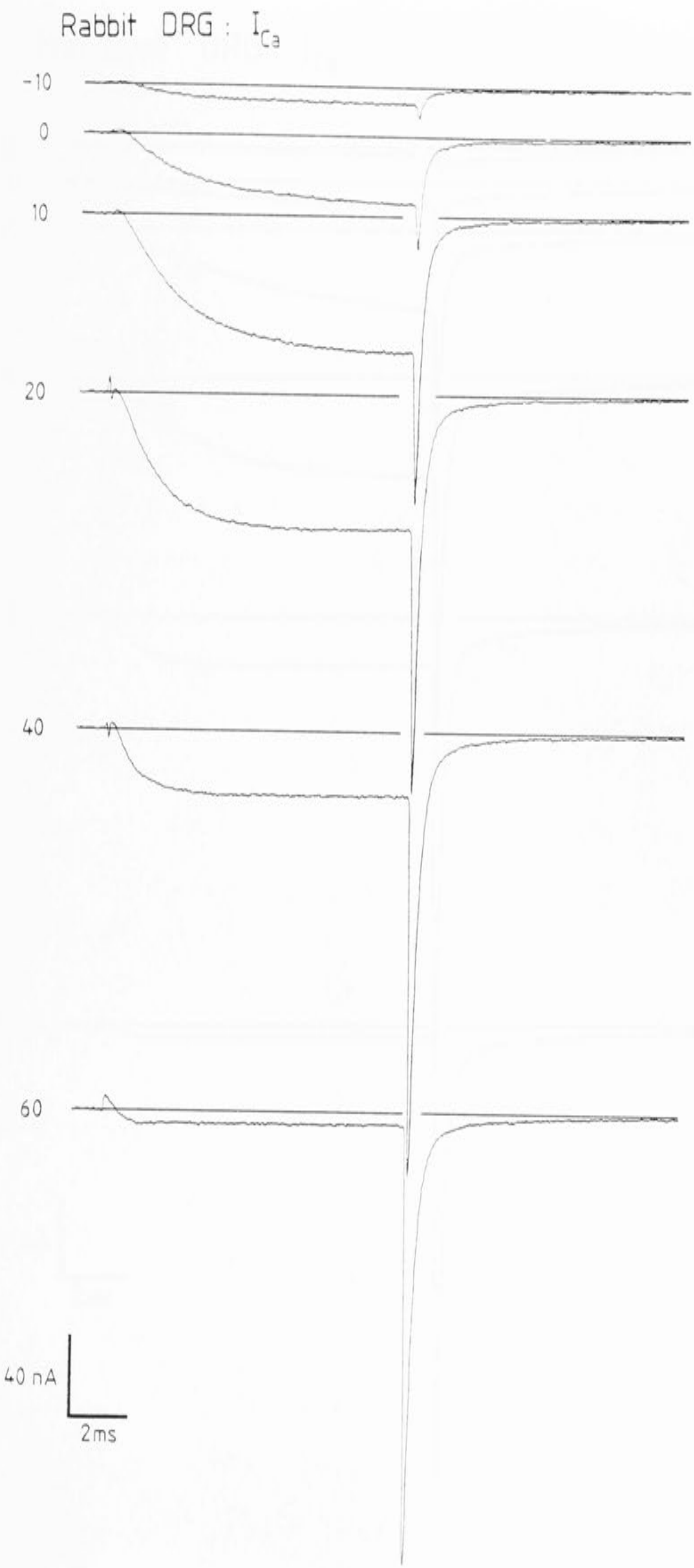
Rabbit DRG : I_{Ca}
-10
0
10
20
40
60
40 nA
2ms

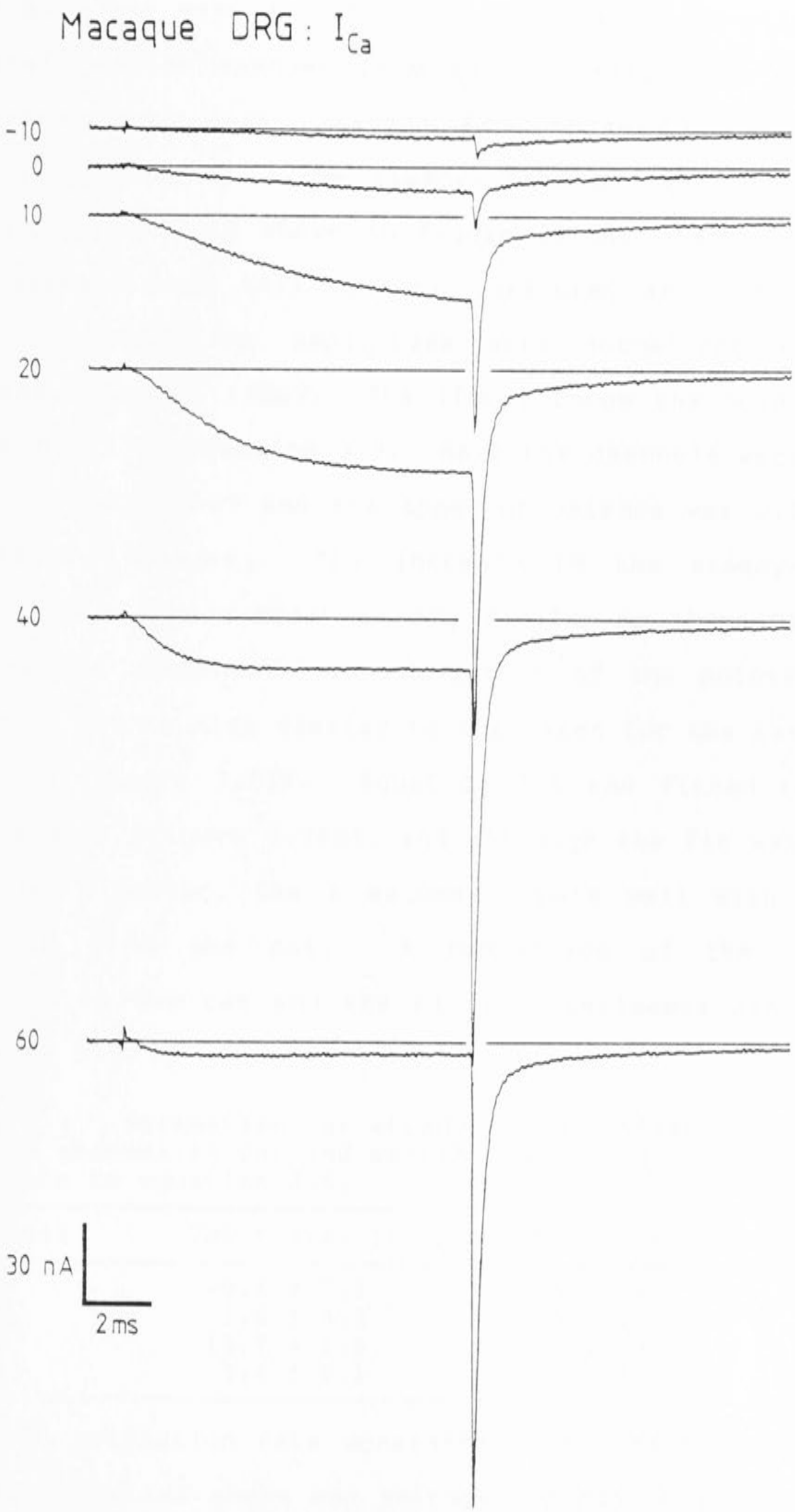
Macaque DRG : I_{Ca}
-10
0
10
20
40
60
30 nA
2 ms

thesis. They were sacrificed by cervical dislocation and several ganglia removed from each animal. The results presented here were obtained from three cells, in two different ganglia. The steady-state activation of the calcium current is shown in figure 3.28A. Each point is the average peak tail current (measured at -50mV) from three cells. The amplitudes were normalized to the average value at +50mV. The line through the points was the LMM fit to equation 3.5. Half the channels were open at V_0 = 7.7±0.8 mV and the apparent valence was 3.2 ±0.3 electronic charges. The increase in the steady-state number of channels open is very similar to that observed in the cat neurones. The deviation of the points from equation 3.5 is also similar to that seen for the cat data shown in figure 3.11B. Equation 3.6 was fitted to the rabbit data (figure 3.28B), and although the fit was only marginally better, the z values compare well with those obtained from the cat. A comparison of the values obtained in the cat and the rabbit experiments are shown in table 3.2.

Table 3.2 Parameters for steady state activation of the calcium channel in cat and rabbit DRG neurones, obtained from fits to equation 3.6.

Parameter	Cat ± s.e. (n=11)	Rabbit ± s.e. (n=3)
V_1	-9.4 ± 7.1	-1.8 ± 16
z_1	1.0 ± 0.2	1.7 ± 1.0
V_2	13.7 ± 1.8	5.9 ± 13
z_2	3.4 ± 0.1	3.3 ± 1.0

The relaxation rate constants in the rabbit neurones showed a similar shape and voltage dependence as those in

Figure 3.28 (A) Peak tail currents recorded at -50mV in rabbit DRG. Each point is the normalized average from 3 cells. The lines through the point shows the fit to equation 3.5. (B) Same data as in A, the line shows the fit to equation 3.6.

A

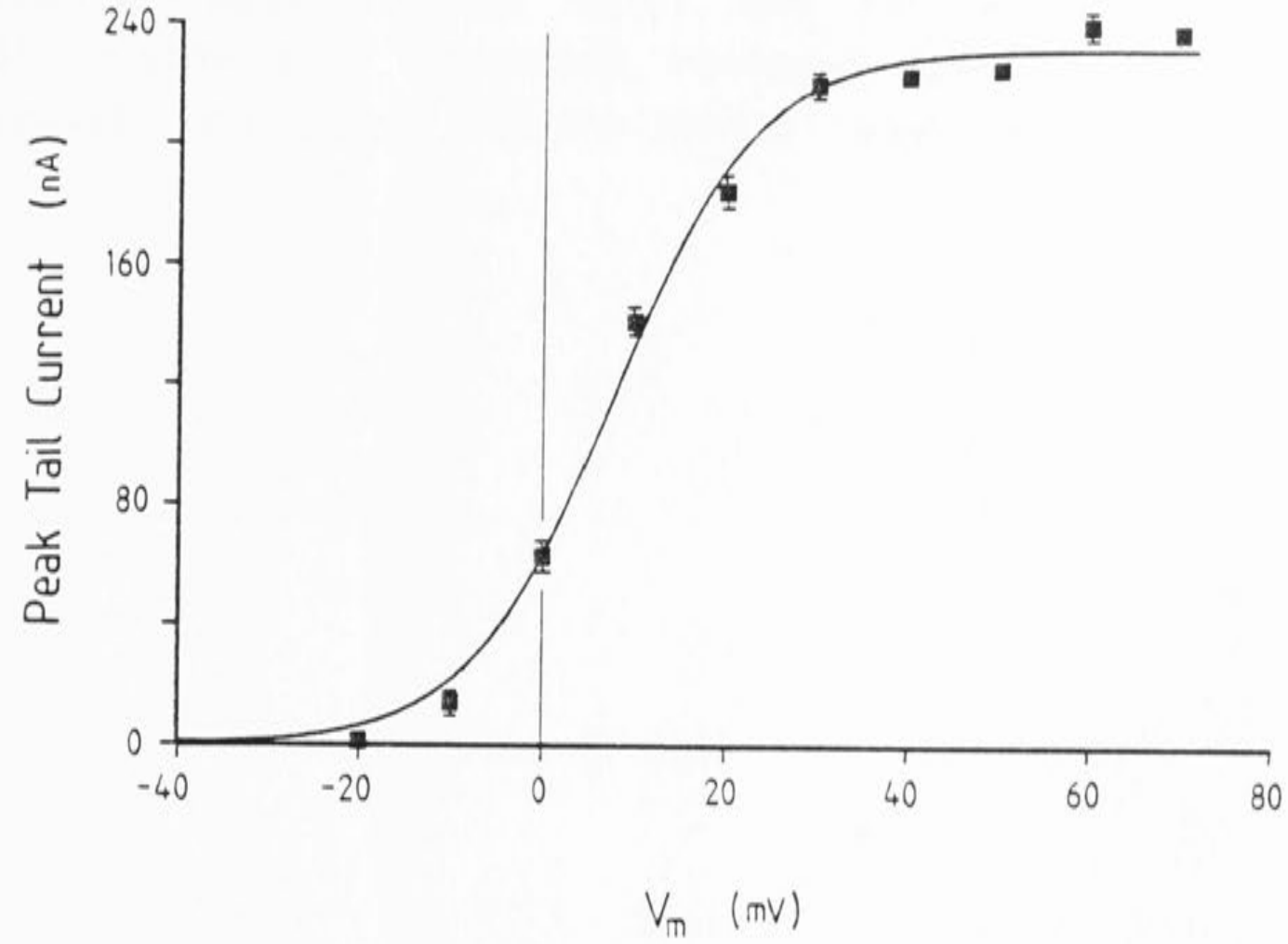
240
160
80
0
Peak Tail Current (nA)
-40
-20
0
20
40
60
80
V_m (mV)

B

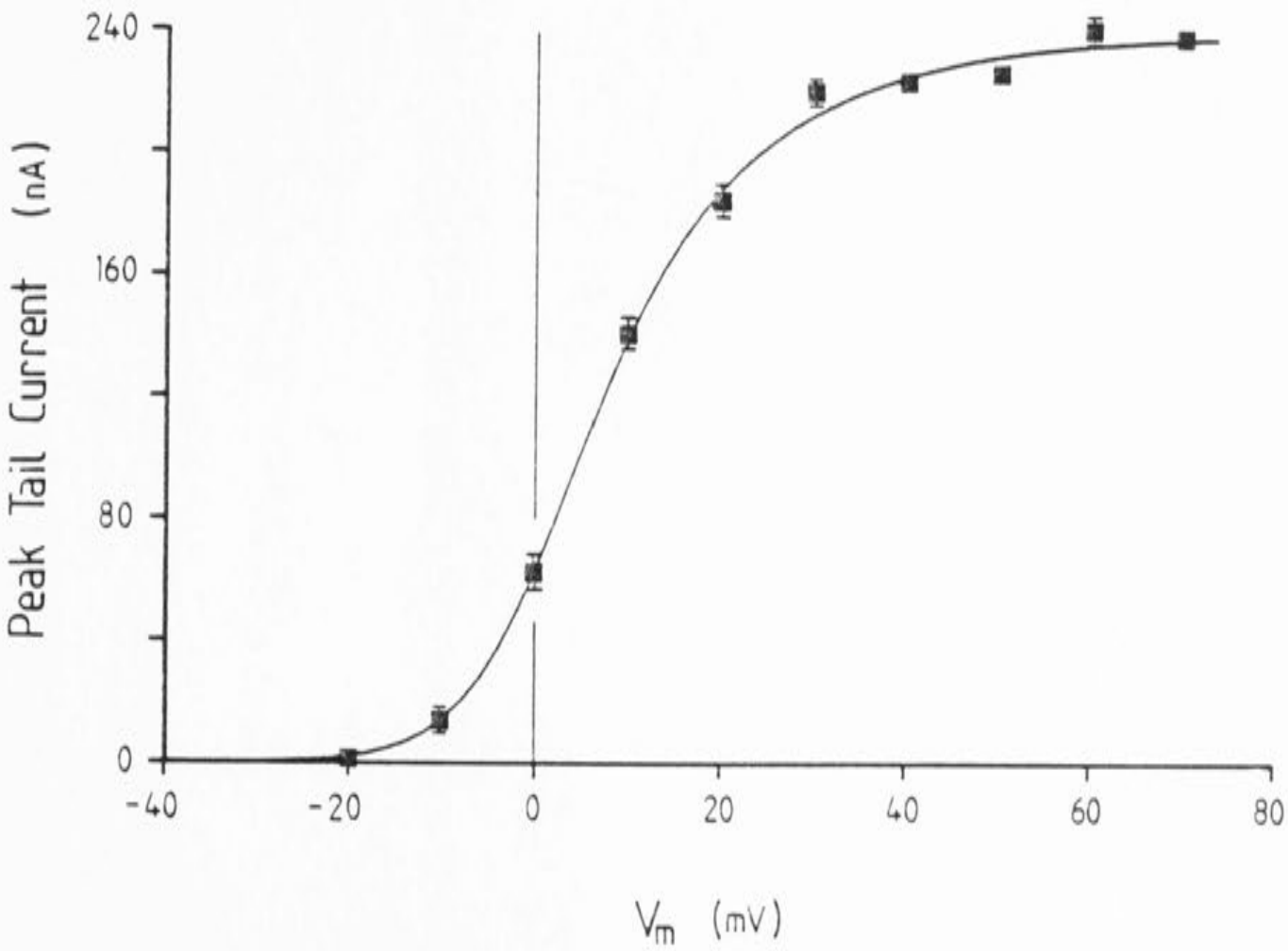
240
160
80
0
Peak Tail Current (nA)
-40
-20
0
20
40
60
80
V_m (mV)

Figure 3.29 Time constants reccorded in rabbit DRG neurones. (A) Fast time constants recorded from tail currents (squares, one cell) and activation (crosses, n=3). Slow time constants recorded from tail currents (circles, one cell), and activation (squares, n=3).

A

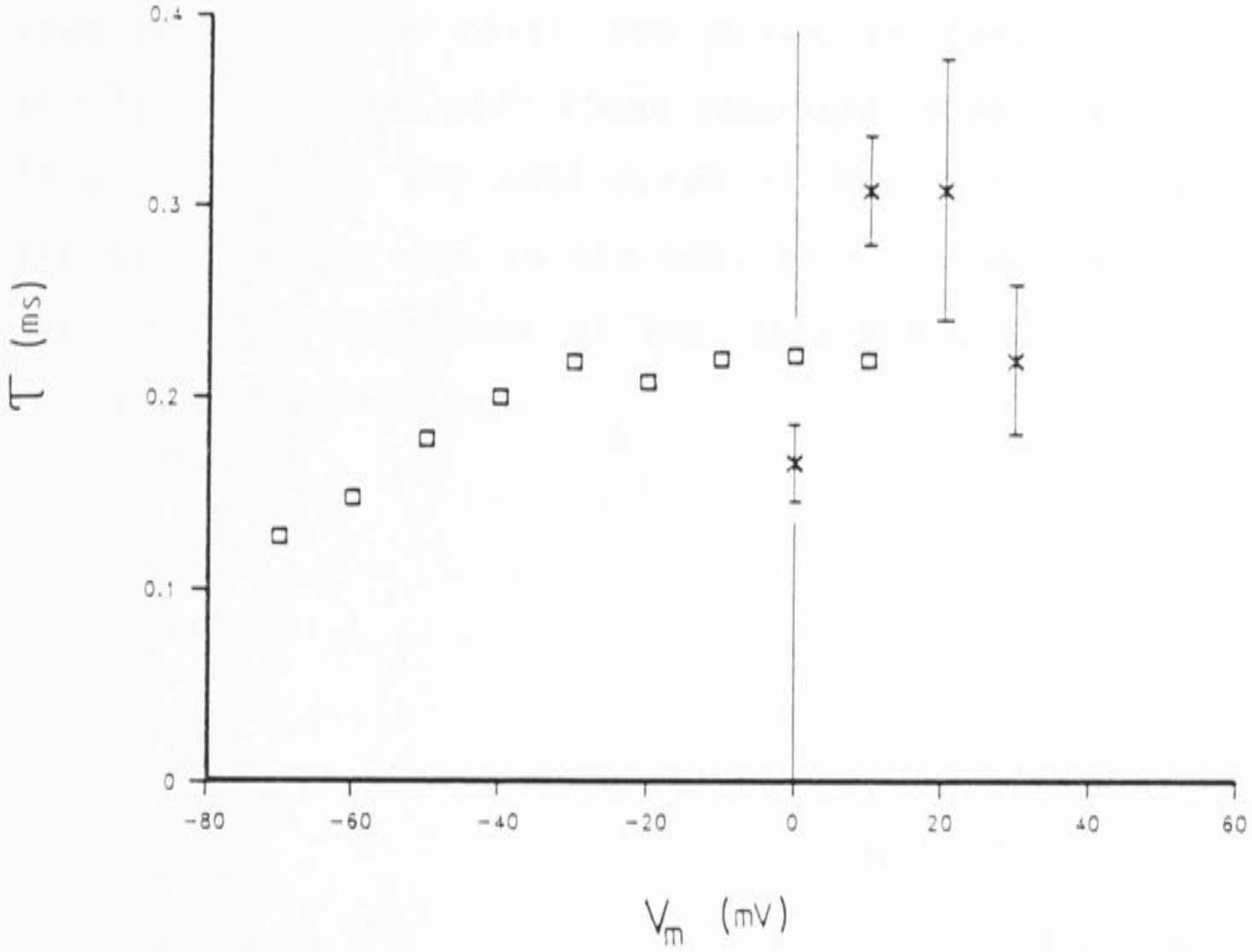
0.4
0.3
0.2
0.1
0
τ (ms)
-80
-60
-40
-20
0
20
40
60
V_m (mV)

B

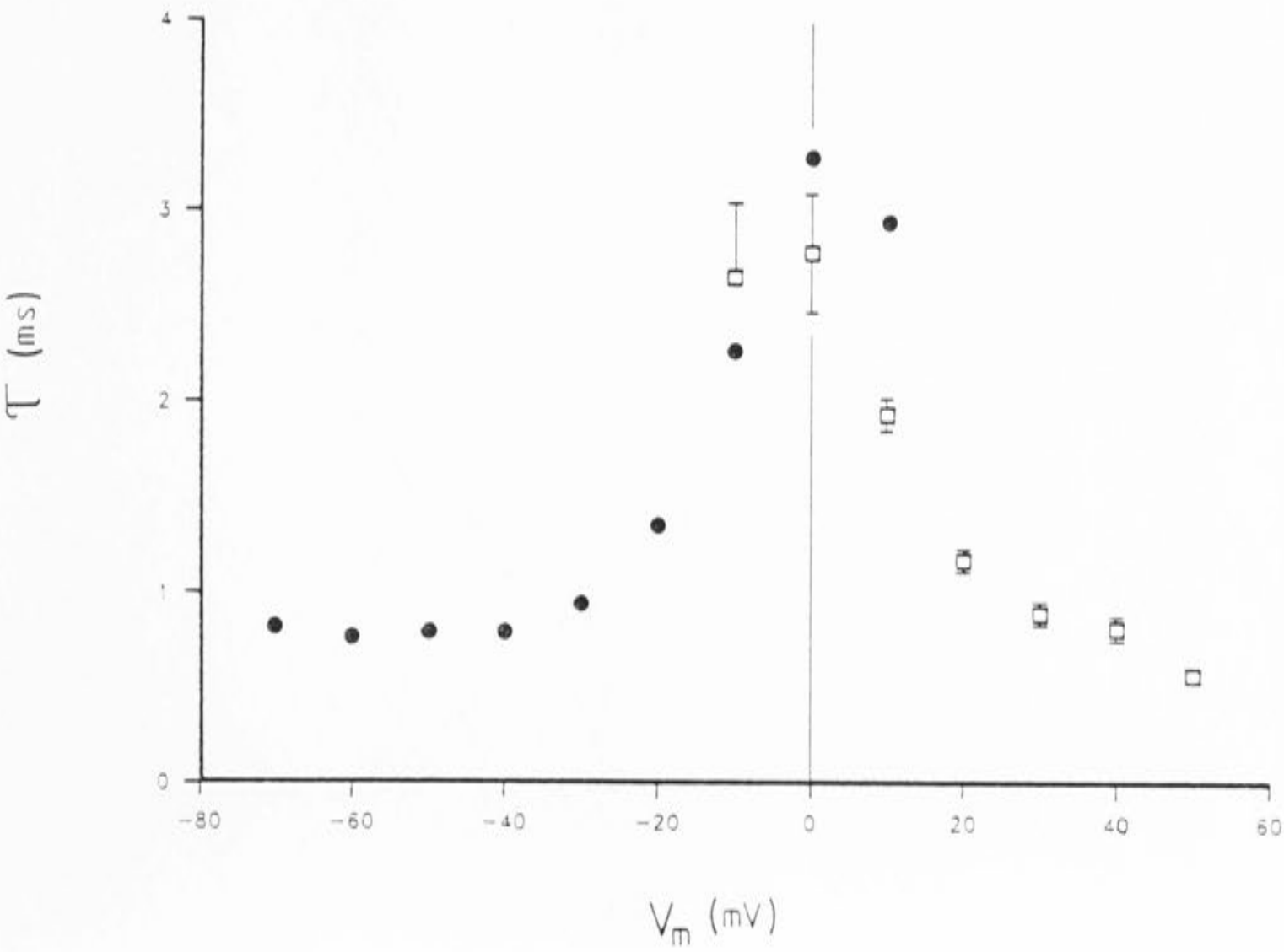
4
3
2
1
0
τ (ms)
-80
-60
-40
-20
0
20
40
60
V_m (mV)

the cat. The two time constants from tail current measurements (one cell) are shown in figure 3.29, and should be compared with those recorded in the cat neurones (figure 3.14). The activation of the currents was also similar to that seen in the cat, both in the voltage sensitivity and magnitude of the relaxation time constants (figure 3.29, 3 cells).

DISCUSSION

(i) Steady-state $P_o(V)$

It was shown that the $P_o(V)$ function was more accurately described by assuming there was more than one voltage sensitive reaction during activation. A similar shape for the $P_o(V)$ curve is evident in the work of Fenwick, Marty & Neher (1982, Fig 6B), obtained using similar measurement techniques. Kinetic schemes which involve the movement of 2 or more independent identical subunits (Hodgkin & Huxley 1952) will produce a similar shaped $P_o(V)$ curve.

Although a 3-state model was adequate to describe the steady-state activation (not unexpected since there were 5 free parameters), it may turn out that there are more voltage dependent steps during activation. The $P_o(V)$ measurements from whole cell records give the fraction of the maximum number of activatable channels which are active in the membrane. The actual probability that a single channel is open can only be obtained from single channel records, but one would predict that the two estimates would be identical, if there were no voltage independent reactions leading away from the open state. At present, the largest P_o value reported from single channel analysis is around 0.7 (Reuter et al. 1982, Reuter et al. 1986), although convincing data on the voltage dependence of this parameter showing clear saturation at positive potentials has yet to be obtained. In the next

few paragraphs follows a brief discussion of the interpretation of the parameters used to fit the steady-state data.

As a first approximation, the internal energy of the molecule is divided into two components, corresponding to two free parameters (Ehrenstien & Lecar 1977, Stevens 1978). The first component is the electrical energy (z_i), which is proportional to a dipole moment normal to the electric field across the membrane. This is quoted as an equivalent (and therefore not necessarily integral) number of positive charges moving across the entire membrane electric field. The estimate for the calcium channel of 3.4 e^+ for the first, and 1.0 e^+ for the second reaction are reasonable for a voltage activated channel. Previous estimates assumed a single voltage sensitive step. Brown and co-workers (1983) obtained a value of 1.7 e^+ in snail neurones and Rorsman & Trube (1986) obtained a value of 1.8 e^+ in clonal pituitary tumour cells. Calculations using the data shown in figure 6B of Fenwick, Marty & Neher (1982) suggest that $z = 3$ e^+ for bovine chromaffin cells, consistent with the present study.

The second energy component is the voltage independent energy of the channel, and includes all the other contributions to the internal energy. These can be termed comformational energies, since the major energy change during the activation of the channel is presumed to involve conformational changes of the protein molecule. The constants V_0, V_1 & V_2 in equations 3.5 & 3.6 are simply the membrane potentials at which the conformational

energy exactly balances the electrical energy, and the net free energy change across the reaction step is zero. Thus, the conformational energy determines the distribution of the channel between the two states of a given reaction step when the electric field across the critical dipole is zero (ie. the dipole energy = 0). This apparent conformational energy ($\Delta\omega$) is given by,

$$\Delta\omega_i = V_i / K_i \quad kJ/mol,$$

where V_i and K_i are defined in equations 3.5 & 3.6. Thus V_1 and V_2 obtained from the fit of equation 3.6 to the steady-state data are equivalent to conformational energies of 4.5 and -0.9 kJ/mol respectively. These energy values can be calculated if the dipole energy is defined to be zero at the measured zero membrane potential (see Appendix 1).

The magnitude of the conformational energies measured in these experiments depends on the environment of the channel. In biological membranes there is good evidence for the presence of a negative surface potential on the outside of the membrane (Frankenheuser 1957, Hille 1968). In the present study, changing the external divalent ion caused a shift of the $P_o(V)$ curve along the voltage axis. It was suggested that this was due to a change in the external surface charge. Such a shift will change the calculated $\Delta\omega$ values, although one may argue that the effect does not represent a change in the channel, but a change in its immediate environment. These effects can be allowed for by shifting the reference zero potential by an

appropriate amount (see Appendix 1).

One might expect the other major enviromental determinant of the conformational free energy to be lipid-protein interactions (Sakman & Bohiem 1979). Thus, the $\Delta\omega$ value for the potassium channel from the skeletal muscle sarcoplasmic reticulum appears to depend on the composition of the artificial lipid bilayer in which it is inserted (Labarca et al. 1980). This group found that the dipole moment of the potassium channel was unchanged by the type of lipid in the membrane. Their system is ideal for such analysis, since the channel conductance is large (120pS, 100mM K^+), and the kinetics simple (one open, one closed state). The situation is much more complicated for the calcium channel, which has at least 2 closed states and possibly more, and it is not possible to assign specific energy values to the reaction steps.

The uncertainty about the number of closed states, leads to uncertainty about the total dipole moment of the calcium channel protein. If the steady-state data is fitted with a 2-state scheme, the apparent dipole moment is 3.1 e^+ (figure 3.11A). If a 3-state scheme is assumed, then the data suggests that a total of 4.4 e^+ move across the membrane during activation (figure 3.11B). Increasing the number of closed states, will fit the data with increasing amounts of charge. This may explain in part the discrepency between the charge movement attributed to calcium channels, and the measured voltage sensitivity of the steady-state activation (see Chapter 4). In any case, the predicted charge movement associated with channel

activation may in general be larger than predicted from a the fit of equation 3.5 to the steady-state activation data.

(ii) The relative amplitudes of tail current components

It is interesting to note that the relative amplitude of the two exponential components of the tail currents at -50mV seems to be qualitatively consistent with the steady-state data. At 0mV the slow phase was a larger proportion of the tail current, than at more positive potentials. The calcium current in molluscan neurones shows a similar property. The slow phase of the tail current at the holding potential had a lower threshold than the fast phase (Fig. 5 Brown et al., 1983).

The voltage sensitivity of the relative amplitude of the slow phase was very consistent from cell to cell. This is potentially useful data, in that any kinetic scheme proposed to describe the calcium channel kinetics must also accurately predict this curve. The relative amplitudes of the exponential components can be calculated if the initial conditions of the system are known (see Appendix 2), and this data was used in a later section to fit a 4-state model to the data.

(iii) Kinetic measurements

This study shows the first accurate records of

calcium tail currents from a mammalian neurone. Two exponentials were resolved from tail current measurements, in agreement with previous studies (Fenwick et al. 1982, Brown et al. 1983, Dubinsky & Oxford 1984). The magnitude and voltage dependence of τ_f is very similar to that observed by Fenwick and co-workers (1982), who found that τ_f varied from 0.1ms at -70mV to 0.2ms at 0mV. In contrast, τ_f in molluscan (0.2ms, Brown et al. 1983, 0.3ms, Byerly et al. 1984) and clonal pituitary tumour cells (0.5ms, Dubinsky & Oxford 1984) was constant over a similar voltage range.

τ_s was 4-10 times slower than τ_s (Fenwick et al. 1982, Brown et al. 1983, Byerly et al. 1984, Dubinsky & Oxford 1984). In three of these studies, τ_s increased markedly between -70 and 0mV, in good qualitative agreement with the present study.

An attempt was made to relate the kinetic and steady-state measurements to a 3-state model. This was done by calculating the four rate constants, $k_1..k_4$, from the four measured parameters, r_f, r_s, E_1 & E_2. Although this approach produced reasonable values for the rate constants at any given potential, the voltage sensitivity of these rate constants was not exponential over the full voltage range tested. The values obtained are compared with those obtained from single channel recording techniques in table 3.3. The two single channel studies suggested that the second reaction step ($C_2 \leftrightarrow O$) was the fastest, which provided a reasonable rationale for using the solution (to equations 3.7-3.10) shown. The first two rate constants

agree reasonably well with the other analyses. The second two rate constants are faster than previously suggested, which may reflect the high time resolution of the present study.

Table 3.3 : Comparison of the calculated microscopic rate constants (s^{-1}) with values obtained in previous studies.

V_m	k_1	k_2	k_3	k_4	Reference
-5mV	61	606	345	1230	Fenwick,1982
-30mV	-	450	1130	530	Cavalie,1983
0mV	130	350	400	700	Brown, 1984b
0mV	130	820	2500	1700	This study

The general conclusion to be drawn from the results is that although a 3-state scheme will describe the current wave-form at any given potential (given arbitary amplitudes for the exponential components), it cannot be extended over the full potential range. A number of previous studies have also suggested that a 3-state scheme is not sufficient (Brown et al. 1983, Hagiwara & Ohmori, 1983, Hagiwara & Byerly 1983, Brown et al. 1984b).

(iv) Effects of temperature

The temperature experiments indicated that there was a difference in the temperature sensitivity of the slow time constants measured from turn-on and tail currents. The effect of temperature on the rate of reactions may be approximated by the Arrenhius equation, where entropy terms are included in k_0,

$$A \xrightarrow{k} B$$

$$k = k_0 \exp(-E_a/RT),$$

$$\ln\tau = \ln\tau_0 + E_a/RT , \quad \tau = 1/k. \qquad .. (3.11).$$

The equation suggests that the rate constants for reactions with a high activation enthalpy, will have a steep temperature dependence. Similarly, factors which change E_a, should also change the temperature dependence of the reaction. For example, measurement of the temperature dependence of the time constants at two different voltages will generally produce different results (Tsien & Noble, 1969). This is expected since the membrane potential represents an energy input to the system, which will lower the energy barriers and tend to "dilute" the temperature dependence of the time constants.

For this reason, a difference in the E_a of time constants measured at different potentials does not necessarily imply a difference in the underlying process. A simple example will illustrate the point. Suppose the reaction illustrated above has an E_a at +20mV of 85 kJ/mol (Q_{10}~3.4), and a voltage sensitivity equal to a minimum valence of 4 e^+ (from the present results). At -50mv, voltage will have lowered E_a by 27 kJ/mol ($z.\Delta V.F$), reducing the Q_{10} to ~2.3. Thus it is important to take into account other energy contributions when making comparisons of measured Q_{10}s or E_as. Such effects will not explain the very large difference in the Q_{10} of the slow time constant measured at positive and negative potentials in molluscan neurones (Q_{10}>6.5 at +25mV and Q_{10}≈1.9 at -50mV, Brown et al. 1983).

As would be expected from the above arguments, the apparent E_a is lower at -50mV than at +20mV for both the fast and the slow time constants (see Table 3.1). The difference in the apparent E_a values for the slow time constants, $\tau_l(+20mV)-\tau_s(-50mV)$, was 56kJ/mol. The voltage dependence of the activation could have contributed a maximum of 27kJ/mol to this reduction. The "extra" 29kJ/mol reduction may be due to the predominance of another reaction during activation at +20mV. Essentially the same conclusion was reached by Brown and co-workers (1983). Until more information is available on the activation reactions it is very difficult to provide a more detailed interpretation of the effects of temperature on the kinetics of channel activity.

The high E_a observed for the peak current at +20mV deserves some consideration. Similar results have been obtained for voltage activated calcium channels (Brown et al. 1983, Byerly et al. 1984) and sodium channels (Chui et al. 1979). If the heat capacity of the system is constant, then the temperature dependence of the peak current will be given by,

$$\ln(C_i/C_j) = \text{constant} - \Delta H/RT \qquad ..(3.12),$$

where C_i, C_j are the steady-state concentrations of the conformations of the temperature dependent step and ΔH is the enthalpy change for the reaction step (Edsall & Gutfreund, 1983). The decrease in the peak current is not wholly attributable to a decrease in the single channel current, assuming the Q_{10} of ~1.2 from snail neurones (Lux

& Brown, 1984) is applicable to the present data. If the peak current is corrected for the reduction in the single channel current the peak current Q_{10} is reduced to 2.2 (apparent E_a of 54kJ/mol). The high apparent E_a of the peak current implies that at least one step in the activation of the channel involves a large net energy change. This reaction step need not be part of the rapid activation time course observed during the present experiments. It could, for example, mediate a reduction in the number of immediately activatable channels in the membrane. There is some basis for such a suggestion, since previous single channel studies have shown that during repetitive depolarizations, many null sweeps (with no observed channel opening) are recorded (Reuter et al. 1982, Fenwick et al. 1982, Hess et al. 1984b, Brown et al. 1984, Reuter et al. 1985). The channel appears to be unactivatable during these sweeps, presumably because it is in some other state which is reached through a relatively slow transition. The effect of temperature on the peak calcium current might be explained by saying that the equilibrium between the dormant state and the activatable state has a high ΔH. If the transition were a spontaneous (reversible) reaction, the high enthalpy implies that the ratio of the dormant to activatable channels is very large ($\sim 10^{10}$), which would require a massive number of channels to be present in the membrane, to produce the observed calcium current. This objection can be answered if it is assumed that the transition between the dormant and activatable states is linked to

another process with a high E_a. Possible candidates are protein phosphorylation, which seems to be required to maintain active calcium channels in neurones (Chad & Eckert 1984b, Doroshenko et al. 1984) and interaction of the calcium channel with an intracellular component (Haga et al. 1984). There is no direct evidence that the calcium channel itself is phosphorylated, and it is possible that phosphorylation of another protein helps maintain the low intracellular calcium levels, essential for calcium channel function (Byerly & Yazejian 1986).

The Q_{10} of the peak current, and the loss of calcium current during internal perfusion could reflect aspects of a common process. The run-down of the calcium current could be explained if the rate of formation of active channels is coupled to a reaction dependent on some intracellular constituents, and the reversion of the channels to the dormant state occured spontaneously and essentially irreversibly as these intracellular components were lost during perfusion. These ideas could be tested further by first looking at the temperature dependence of the occurrence of null sweeps during single channel recording.

(v) Effects of Bay K 8644

Application of 10μM Bay K 8644 shifted the $P_o(V)$ curve slightly to the left and there appeared to be a significant change in the slope of the curve. Qualitatively, the Bay K favoured the open state. It was hoped that these experiments might give some clues as to

the mode of action of Bay K. Does the drug work by effects on the dipole energy, or by changing $\Delta\omega$? The fit of equation 3.6 to the $P_o(V)$ curve suggests that the drug produced a change in both the dipole and the $\Delta\omega$ energies of the reaction steps. However, the control data indicates that a 3-state model is inadequate, and so it is not possible to draw any firm conclusions about the mode of action of Bay K from the fit of equation 3.6 to the data.

Bay K produced complex changes in the measured time constants. In particular, there was a break in the τ_s-V curve in 10μM Bay K, at around the threshold potential for the calcium current. This observation could be explained if it is assumed that the rate constants are not accurate measurements of the eigenvalues (see Appendix 2) of the underlying kinetic scheme, but represent some complex mixture of the real eigenvalues. Thus, at threshold, τ_s changes suddenly perhaps because the relaxation rate is dominated by a different eigenvalue which is not greatly affected by Bay K.

Interpretation of the Bay K data is complicated by the suggestion that the calcium channel has different modes of activity (Hess et al. 1984b). On the basis of single channel records, these authors suggest that the 1,4-dihydropyridines (DHPs) act by stabilizing different modes of activity of the calcium channel. Nitrendipine was proposed to stabilize mode 0 activity, characterized by the absence of channel openings during a depolarizing step. Bay K was proposed to stabilize mode 2 activity,

characterized by an excess of long duration openings during the depolarizing step. Mode 1 is the normal mode of operation.

Their data was obtained using the racemate of both nitrendipine and Bay K. It has been shown that the two enantiomers of Bay K have agonist and antagonist effects on calcium dependent action potentials in guinea-pig heart cells. (-)Bay K (the agonist) had a much higher affinity for the channel than (+)Bay K since the effect of the racemic compound was much the same as that with (-)Bay K (Franckowiak et al. 1985). Sanguinetti & Kass (1984a,b) showed that Bay K had mixed effects on calcium channels in heart cells. At depolarized holding potentials Bay K blocked the calcium current, and at holding potentials more negative than -50mV Bay K had facilitatory effects. Patch clamp experiments have shown that (∓)nitrendipine also has mixed agonist/antagonist effects in rat heart (Hess et al. 1984b, Reuter et al. 1985). The DHP, 202-791, may also have steriospecific effects on calcium channels (Hof et al. 1985, Perney et al. 1986). It has been shown that the affinities for the DHP binding site(s) of the enantiomers of 202-791 are different, the isomer that stimulated the calcium current having the higher affinity (Williams et al. 1985).

The modal model accounts for the observation that both mode 2 (Bay K induced) and mode 1 (control) activity could be observed in the same patch in the presence of Bay K, during different pulses. The mechanisms for these effects are unknown. One possibility is that binding of

Bay K is slow, and that the behaviour of the channel is determined by the enantiomer of Bay K which occupies the site on the calcium channel at the time of the depolarization. The contingency tables and cluster analysis produced by Nowycky and co-workers (1985b), for the neuronal calcium channel, may reflect slow binding and unbinding of the drug. Thus the mode 1 activity observed in the presence of Bay K, may be due either to binding of the (+)enantiomer or to the Bay K site being unoccupied. Even if the binding reaction were relatively fast, this idea could be supported if one assumed that depolarization locked the Bay K molecule into, or excluded it from the binding site. It has been suggested that there are two DHP binding sites on cardiac calcium channels (Brown et al. 1986), but it is possible that these results are due to differences in the binding reactions of the enantiomers to a single site.

The change in the effect of nitrendipine with time (Reuter et al. 1985) could also be explained by slow binding reactions to a single site, given appropriate values for the K_ds and binding rates of the enantiomers. Although mode 0 events are commonly observed during single channel recording of calcium currents, there is no evidence to suggest that the extra mode 0 events recorded in the presence of nitrendipine reflect the same condition of the channel. It seems just as probable that the DHP antagonists induce a another mode of channel activity, mode 3 (nitrendipine induced). This question remains to be resolved.

How do these results relate to the present findings ? Firstly, the observation that there is a finite probability of the calcium channel entering the Bay K induced state in the absence of the drug will not complicate the interpretation of the control data unduly. The probability was low (<1%, Hess et al. 1984b), and so these events can safely be ignored. The Bay K data is more complex. Since the racemic compound was used, the channel could be in any one of three conditions at the time of the depolarization, corresponding to the Bay K site being unoccupied, or being occupied by the (+) or (-)enantiomer. Therefore, the Bay K will produce a mixed population of channels, and interpretation of the data in terms of a single kinetic scheme is no longer valid. At this stage, information is required on the electrophysiological effects, the binding rates and the K_ds of the optically pure isomers of the various DHPs, before a detailed explanation of the mechanism of action of these compounds can be advanced.

The results presented indicate that neuronal calcium channels may be relatively insensitive to nifedipine. It is interesting to note that nitrendipine and nimodipine block calcium channels in cardiac muscle more effectively at depolarized potentials (Sanguinetti & Kass 1984, Bean 1984), and it was suggested that these compounds stabilised the inactivated state of the channel. In this study, the calcium channels did not inactivate until the holding potential exceeded threshold. There seems to be very little potential dependent inactivation of calcium

channels in most preparations (Eckert & Chad 1984). The low sensitivity of the calcium current to DHP antagonists, and the lack of significant inactivation at the holding potential used, correlates well with the models of Sanguietti & Kass (1984) and Bean (1984).

(vi) Effects of external barium ions

External barium ions produced pronounced changes in the recorded time constants, and it was suggested that these effects could be explained in large part by changes in the external surface charge. There appeared to residual effects under conditions where the external surface charge effects should have been approximately equal to the control value. These residual effects could have been due to direct interaction of the ions with the channel.

The nature of the permeant ion has potent effects on channel kinetics in other systems (Hagiwara et al. 1977, van Helden et al. 1977, Chesnoy-Marchais 1985). The effect on calcium channels has been observed previously. Saimi & Kung (1982) found that the rise time of calcium currents in paramecium was slowed when the external calcium was replaced by barium. The activation time constant of calcium currents in bovine chromaffin cells was prolonged when the 5mM external calcium was replaced by isotonic barium (Fenwick et al. 1982). On the other hand, Hagiwara & Ohmori (1982) found that most of the kinetic effects of barium could be explained by changes in

the external surface charge, although there did appear to be a slight excess increase in the activation time constant with increasing external barium concentrations. Byerly & Hagiwara (1982) found no evidence for a direct effect of barium on calcium channel kinetics in snail neurones.

The present results indicate that the activation and deactivation kinetics may be altered by external barium. Two previous works have attempted to provide a theoretical basis for the interpretation of such effects observed in other systems (Ciani et al. 1978, Marchais & Marty 1979). One must assume that there is a fairly specific interaction of the ion with the channel, however the exact location of the specfic site is not obvious. Both of the theoretical treatments allowed for the ion binding site within the permeation pathway of the channel. The general idea is that occupation of the channel by a permeant ion prevents it from closing. If this were the case then one would expect that the time constants would become slower as the concentration of the specific permeant ion is increased. One problem with this type of explanation is that the single channel current is higher in barium solutions than calcium solutions (Hess et al. 1986). This suggests that each barium ion pauses in the channel for a shorter period of time during permeation, than calcium. One might then predict that the time constants would be faster in the presence of barium ions than calcium ions, contrary to observation. The other alternative is that the ions bind to a site external to the permeation

pathway. The data available on the calcium channel does not allow a firm conclusion on this point.

(vii) Consideration of a 4-state scheme

One simple modification to the 3-state model presented is to include another closed state in the reaction scheme (Hagiwara & Ohmori 1982, Fenwick et al. 1982, Byerly et al. 1984, Brown et al. 1983, Brown et al. 1984). The aim of this section is to explore the characteristics of a 4-state model, to see whether it is possible to reproduce the steady-state and kinetic data quantitatively. An immediate objection to such an endeavour is that a 4-state scheme will predict that the membrane current should relax with a three exponential time course. With the appropriate choice of rate constants, the 4-state scheme predicted an essentially two exponential time course for the current relaxations, the third component being very fast and of negligible amplitude.

The model was required to account for a number of observations: 1) The magnitude and voltage sensitivity of the time constants measured between -70 and +50mV (figures 3.14). 2) It should accurately predict the $P_o(V)$ curve (figure 3.11B). 3) It should also account for the $A_s/(A_s+A_f)$ curve between -70 and +10mV (figure 3.15). A single open state was assumed, since the single channel open time distributions appear to be described by a single exponential (Fenwick et al. 1982, Hagiwara &

Ohmori 1983, Lux & Brown 1984, Hess et al. 1984, Reuter et al. 1986). Only two closed states were resolved from the single channel data, and the model should be consistent with this observation.

It seems obvious that the time constants of any proposed 4-state scheme must be at least as fast as the slowest observed time constant, since slow time constants will be rate limiting, and therefore have significant amplitudes either during activation or deactivation. Therefore, in order for the 4-state scheme to fit the data, it is proposed that one of the time constants is much faster than the other two, and cannot be resolved. This being the case, the time constants recorded from the kinetic experiments can be taken as accurate measures of the two smaller eigenvalues of a 4-state sequential reaction scheme. This assumption is crucial for fitting the data.

It was found, by trial and error, that a 4-state sequential model will follow double exponential kinetics if the second closed state is very short-lived compared with the other channel states. This requires that the rate constants leading away from this state are much greater than the other rate constants in the scheme.

The direct search algorithm described by Hooke & Jeeves (1960) was used to fit the model to the data. The details of the calculations and fitting procedure used are set out in Appendix 2. A comparison of the fits of the 3-state and 4-state models are shown in figures 3.30, and the parameters used are shown below. The broken lines in

Figure 3.30 A comparison of the fits of the 3-state and the 4-state models to the kinetic and steady-state data. The data points shown in the figure are those that were used to fit the models. The data is replotted from figures 3.14A, 3.14B, 3.15 & 3.11B for A, B, C & D respectively. The points at -10, 0 & 10mV in B were simply the average values of the points shown in figure 3.14B. The prediction of the 3-state model are shown by the broken lines. The model was not consistent with the voltage sensitivity of the slow time constant, or the relative amplitude of the slow phase. The 4-state model accounted for the data reasonably accurately over the potential range investigated.

A

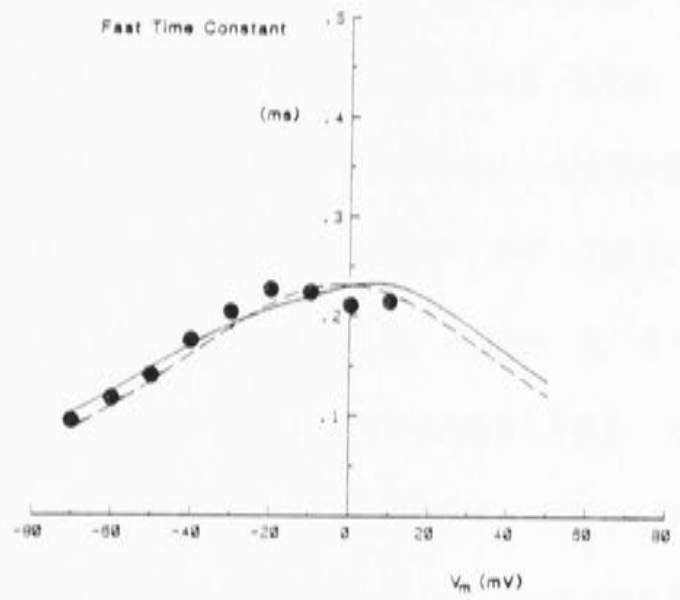
Fast Time Constant
(ms)
.5
.4
.3
.2
.1
-80
-60
-40
-20
0
20
40
60
80
V_m (mV)

B

Slow Time Constant
(ms)
4
3
2
1
-80
-60
-40
-20
0
20
40
60
80
V_m (mV)

C

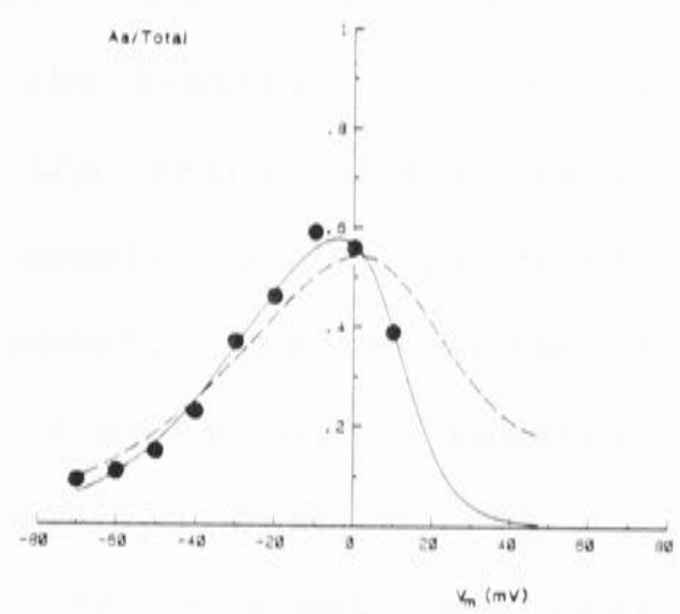
As/Total
1
.8
.6
.4
.2
-80
-60
-40
-20
0
20
40
60
80
V_m (mV)

D

P_0(V)
1
.8
.6
.4
.2
-40
-20
0
20
40
60
80
V_m (mV)

figure 3.30 show that the 3-state model was unable to account for the data accurately, particularly the voltage dependence of the slow time constant and the relative amplitude of A_s. This result confirms that already obtained in the results section. The solid lines in figure 3.30 show that the fit of the 4-state model to the data was reasonably close, and the result demonstrates that the activity of calcium channels can be predicted quite accurately from a 4-state model. The amplitude of the fastest exponential of the 4-state model remained negligible (<0.01%) at test potentials between -70 and +50mV from holding potentials of -50 or +50mV, and thus the model predicted that the time course of the calcium currents should be described by the sum of two exponentials, in agreement with observation.

Four-state model

Parameters obtained from the fit of the four state model to the data. The rate constants are in units of ms^{-1}.

$$C_1 \underset{k_2 = 12.7}{\overset{k_1 = 0.27}{\rightleftharpoons}} C_2 \underset{k_4 = 1.25}{\overset{k_3 = 12.0}{\rightleftharpoons}} C_3 \underset{k_6 = 1.97}{\overset{k_5 = 2.08}{\rightleftharpoons}} O$$

Fraction of the total valence for the forward rate constants

$\delta_1 = 0.49$ $\delta_3 = 0.95$ $\delta_5 = 0.51$

Total valence for the reaction step (e^+)

$z_{12} = 1.91$ $z_{23} = 2.59$ $z_{34} = 1.15$

Without confidence limits being placed on the parameters, it was not possible to say how well the values

were defined by the data. One point that was established, was that the data required the $C_3 \leftrightarrow O$ transition to be voltage sensitive (cf Hagiwara & Ohmori 1983). If the valence of this reaction was constrained to be zero ($z_{34} = 0$), then the fast time constant at negative potentials became essentially voltage insensitive, and adequate fits to the data could not be obtained. A similar problem was encountered when the fractional dipole moment of k_6 was constrained to be zero during the fit ($\delta_5 = 1$). Thus the fits to the data suggest the open time of the channel should be voltage sensitive, consistent with previous single channel studies (Fenwick et al. 1982, Lux & Brown 1984, Reuter et al. 1986). The predicted mean open time ($t_o = 1/k_6$) at 0mV of 0.5ms was also in good agreement with these studies.

The 4-state model was qualitatively consistent with the double exponential closed time distributions measured from single channel records. The second closed state (C_2) will have a very short mean life-time of $1/(k_2+k_3)$ = 42μs at 0mV, and it is unlikely to be resolved due to the band-width limitations of single channel recording. Thus only two closed states will be resolved and a double exponential closed time distribution predicted.

The short lived conformation, C_2, will have significant effects on the kinetic response of the system, and may provide a reasonable explanation for the latency-to-first-opening data of Brown & co-workers (1984b). They found that their waiting time distributions were not consistent with the fits of the open and closed time

distributions to a 3-state model. The channels did not open soon enough after the depolarization. The present model would account for this observation as follows; upon depolarization from a negative holding potential most of the channels will be in C_1. The delay before the first observed opening is determined by how quickly the channel can move through the various closed conformations and reach the open state. This time will be increased by the presence of C_2, since upon reaching this state there is an equal probability ($k_2 \approx k_3$ at 0mV) that the channel will return to C_1 or move to C_3. Thus the presence of a very short-lived intermediate closed state will cause an additional delay before activation. It is interesting to note that at more positive potentials the discrepency between the 3-state model and the waiting time became smaller (Brown et al. 1984b, fig. 6A). This is expected from the model since at positive potentials $k_3 > k_2$ and the additional delay introduced by C_2 will become much less.

When stepping from a holding potential of -50mV to +10mV the model predicts that $A_1/A_2 = 10$, while the measured value was 8.4. This will mean that the model will predict a slightly smaller delay before activation than was observed, however the difference is not large. A simulated voltage step from -50mV to +10mV was performed to illustrate the point and is shown in figure 3.31. The delay before activation of the current is only slightly less than that observed in figures 3.4, 3.7A & 3.16. The discrepancy is consistent with the presence of outward asymmetric capacitive currents at the start of records,

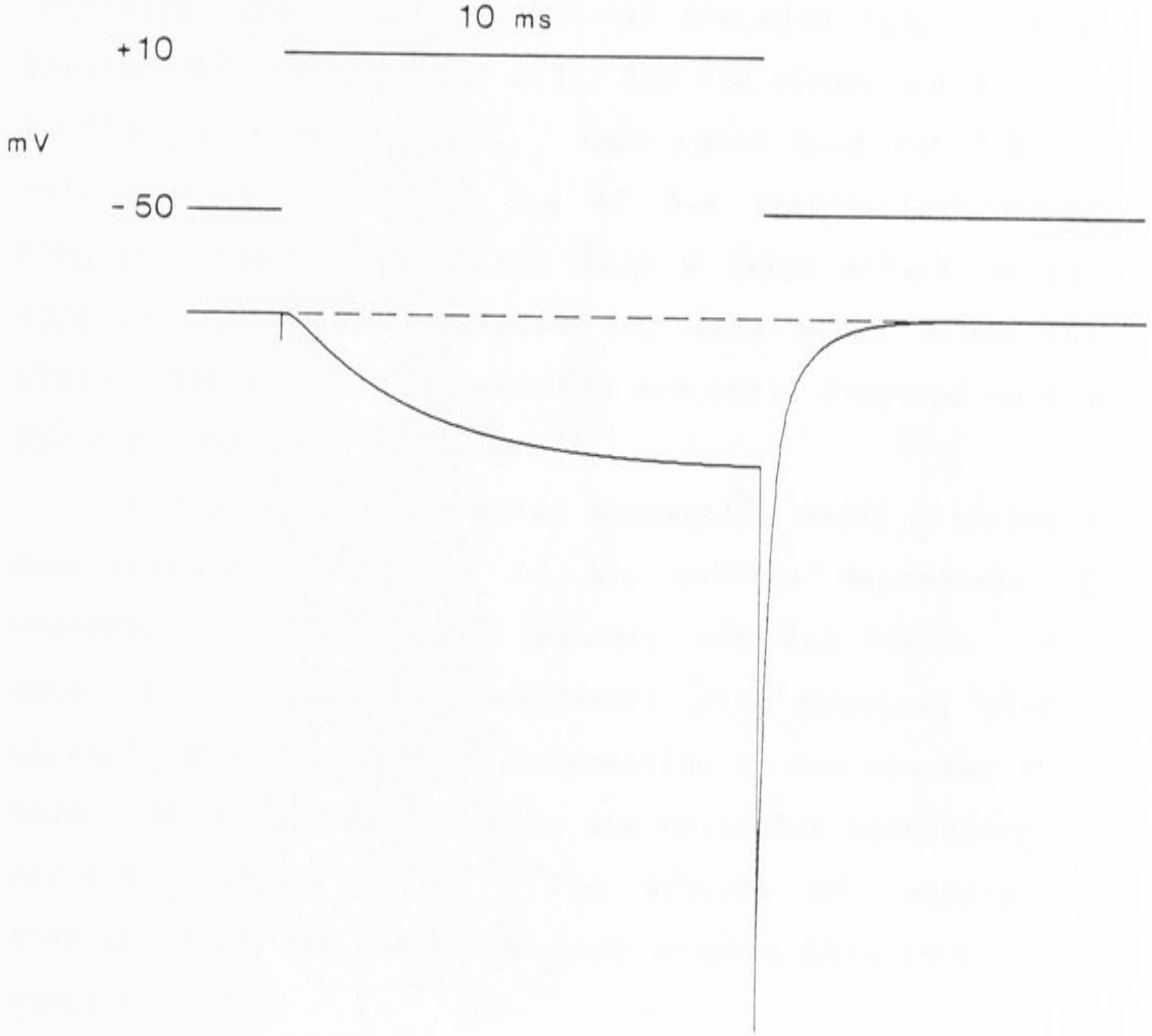

Figure 3.31 Simulation of the calcium current produced using the 4-state model fitted to the data in figure 3.30. The activation and deactivation curves were produced using equation 3.4, with N.i(V) taken from the fit in figure 5.19, and $P_o(V,t)$ set equal to equation A2.11. β_i were calculated at the appropriate starting potential according to equation A2.10. The small downward deflection marks the start of the simulation.

which would tend to increase the observed delay before the activation of the calcium current (see Chapter 4).

The model does not predict the temperature sensitivity of the time constants very well. Simulations indicated that the Q_{10}(+10mV) of the slow time constant between 283 and 293 K was 2.27, and was almost insensitive to the membrane potential. This value does not compare well with the measured Q_{10} of 3.4 (Table 3.1). The membrane potential will not have a large effect on the apparent activation energies for this model since the dipole energies of the reactions are small compared to the 0mV comformational energies.

In conclusion; a 4-state sequential model provides a quantitative description of the voltage dependence of neuronal calcium channels between -70 and +50mV. The model is qualitatively consistent with previous single channel data. It will be interesting to see whether this model has any similarities to the molecular mechanisms of calcium channel gating. The effects of temperature indicate that the gating is more complex than this model suggests.

Chapter 4

Asymmetric charge movement

Introduction

The asymmetric charge movement associated with sodium channel activation has been recorded in squid axonal membrane (Armstrong & Bezanilla 1974, Keynes & Rojas 1974), node of Ranvier from amphibia (Nonner et al. 1975, Neumke et al. 1976) and mammals (Chui 1980) and from skeletal muscle fibres (Collins et al. 1982). Charge movement associated with potassium channel activation has recently been recorded in squid axon (White & Bezanilla 1985). Charge movement attributed to calcium channel activation has been recorded in two invertebrate preparations (Adams & Gage 1976, Kostyuk et al. 1977, Kostyuk et al. 1981a) and in scorpion muscle (Scheuer & Gilly 1986). This chapter describes preliminary experiments aimed at measuring the charge movement associated with the activation of calcium channels in cat DRG neurones.

Initially experiments were performed to see whether a signal that resembled asymmetric charge movement could be recorded in the cell bodies of cat DRG neurones. Asymmetric capacitive currents which are linked to the activation of voltage dependent channels might be expected to have the following properties :

1) The current flow should be outward on

depolarization and inward upon repolarization.

2) The nonlinearity of capacitive current should appear in the same potential range, or negative to the potential range over which the voltage activated channels turn on.

3) The cumulative asymmetric charge should saturate.

4) The integral of the capacitive surge on depolarization must equal that on repolarization. This stems simply from the idea that the gating charges must be tethered to the channel protein, but ignores complications such as charge immobilization (as is seen in the sodium channel).

5) The time constants recorded from the charge movement transients should be the same as those recorded from the ionic current relaxations (French & Horn 1983). It would be expected that the relative amplitudes of the various exponential components would be different. The results in chapter 3 indicate that for the calcium channel, the time course of the ON charge movement should become faster at potentials more positive than +10mV.

6) In a given cell, the magnitude of the charge movement should correlate very closely with the amplitude of the current it is associated with. Thus cells with small calcium currents should have small calcium channel charge movements.

Each of these points will be addressed in the results section.

Methods

All the non-linear ionic currents must be blocked before capacitive currents can be measured. This was a relatively straight forward matter. Using the calcium-current-solutions (section 2.3) all other currents except the calcium currents and calcium-activated chloride current were eliminated. Calcium currents were blocked and calcium-activated chloride currents eliminated by replacing the external calcium chloride with cobalt chloride. This method was found to be ineffective at blocking outward currents in some cases, due to a TTX-insensitive sodium current (see chapter 6). A residual nonspecific outward current was also present in some cells. Cells with a large nonspecific outward current were not used.

Co^{2+} was the preferred calcium channel blocker for a number of reasons. 1) Unlike cadmium ions, the block by cobalt was voltage insensitive (Byerly et al. 1984 and figure 3.2). 2) The surface charge potential seemed to be approximately the same with 10mM calcium or 10mM cobalt. The evidence for this comes from the sodium current experiments, where the peak I-V seemed to be unaffected by the method of blocking calcium currents (see chapter 6). 3) Neurones appeared to survive longer in cobalt solutions than cadmium solutions.

The major problem in measuring charge movement is that the signal is very small. A few calculations illustrate this point. If one takes the single channel current for mammalian calcium channels to be 0.1pA at

+10mV in 10mM calcium (Fenwick et al. 1982, Hess & Tsien 1984) and the probability that the channel is open as 0.5 (figure 3.11B), then a typical inward current recorded in cat DRG neurones at +10mV, of -50nA, must be due to the activation of 10^6 channels. The $P_o(V)$ data suggests that the minimum number of electronic charges moving during activation is 4.4 per channel (fit of equation 3.6 to the steady-state data in figure 3.11B). Therefore, during the activation of the channels a maximum of about 0.70pC of charge will be displaced. If the charge movement followed a single exponential time course with a time constant of 0.5 ms, then 0.70 pC of charge would cause a peak current of 1.40nA. These calculations suggest that the peak charge movement associated with calcium channel activation should range between 0-1.4 nA. It was hoped that it would be possible to accurately measure such small currents by reducing the recording bandwidth and averaging a number of pulses.

Results

Results will be presented which relate to each of the points in the introduction. A total of 41 cells were used from 13 different ganglia during this section of the project. In the majority of the cells, a clear indication of asymmetric capacitive current could not be seen, mainly due to unfavourable noise levels. In a few cells it was possible to record currents which fulfilled, in part, a number of the criteria set out above. Figure 4.1 shows

Figure 4.1 (A) The traces illustrate the linearity of the membrane current between -40 & -20mV when stepping from a holding potential of -70mV. Nonlinear ionic currents have been blocked. The voltage pulse protocol used for the experiments is shown opposite. The initial control pulse was negative in some experiments. (B) Difference currents produced at the step potentials indicated next to each trace. At each potential the pulse train was averaged 9 times. The filter cut-off frequency set to 2 or 4 kHz. The external calcium was replaced by either Mn^{2+} or Co^{2+}.

A

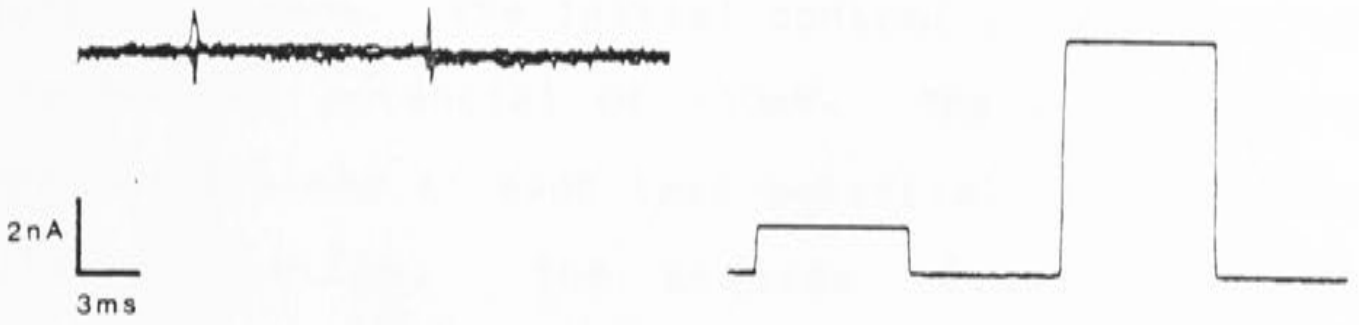

B

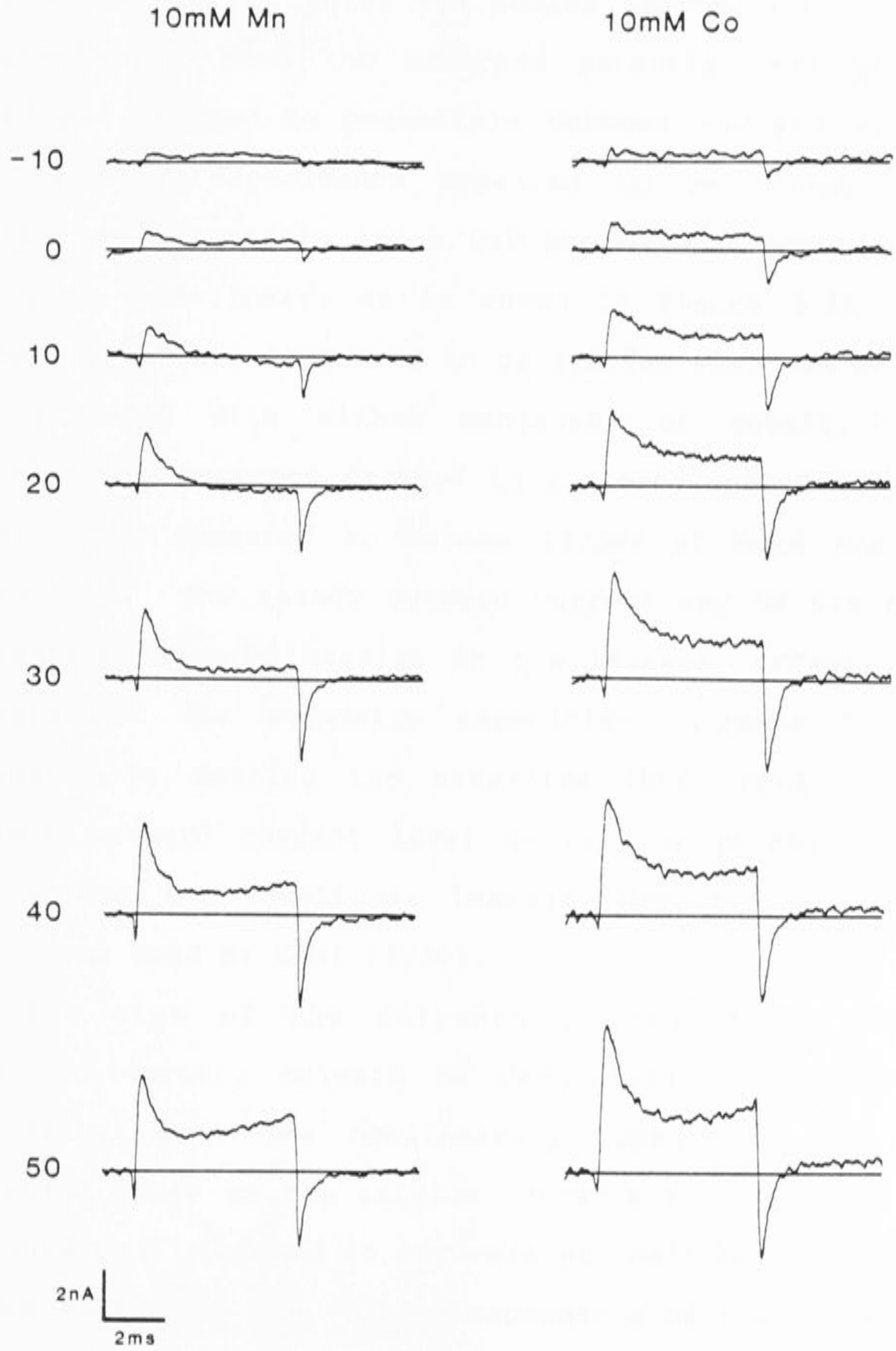

two examples. The voltage pulse profile is shown in the top right of figure. The initial control pulse was ±10mV from the holding potential of -50mV. The pulse profile was repeated 9 times at each test potential, and the data accumulated on-line. The records illustrated were obtained by subtracting the control pulse from the test pulse. The control pulse was scaled appropriately before subtraction. When the membrane potential was held at -70mV and stepped to potentials between -40 and -20 mV, the membrane capacitance appeared to be linear (Fig. 4.1A). At potentials above 0mV the capacitance appeared to become non-linear, as is shown in figure 4.1B. The asymmetry currents appeared to be similar when the calcium was replaced with either manganese or cobalt. The transient ON currents decayed to a steady outward current level which appeared to become larger at more positive potentials. The steady outward current may be due to an instantaneous non-linearity in the leakage current. The integral of the asymmetry capacitive currents (Q) was evaluated by setting the base-line level equal to the minimum outward current level during the pulse, thereby subtracting the non-linear leakage current. A similar method was used by Chui (1980).

The sign of the currents is consistent with a capacity current, outward on depolarization, inward on repolarization. The nonlinearity appears in the same potential range as the calcium currents recorded in these neurones, and appeared to saturate at positive potentials. Figure 4.2A shows the voltage dependence of the normalized

cumulative ON charge movement (Q_{on}), and figure 4.2B shows the normalized cumulative OFF charge movement (Q_{off}) in the same four cells. The curves through the points in these figures were drawn using equation 3.5, with V_0 = 10mV, and an effective valence of 3.1 e^+. The charge movement seems to have a similar potential dependence as the steady-state activation curve for the calcium current. The fit of equation 3.5 to the $P_o(V)$ curve in figure 3.11A produced values of V_0 = 11.5mV and an equivalent valence of 3.1.

The data in figures 4.2A and 4.2B were averaged to produce the points shown in figure 4.2C. The cumulative charge movement was fitted with equation 3.5, with V_0 = 10mV and an equivalent valence of the gating dipole moment of 2.6 e^+. The broken line in figure 4.2C shows the $P_o(V)$ curve for the calcium current taken from figure 3.11B. The results indicate that the charge movement is not inconsistent with the activation of calcium channels. The proportion of the total charge moved at any potential was greater than the proportion of the calcium channels activated at that potential. This is an essential feature of charge movement associated with activation of voltage sensitive channels that have more than one closed state in the activation scheme (Armstrong 1981).

Although the Q_{on} and Q_{off} appeared to show a similar voltage dependence to the calcium current, the integral of the charge moved was not equal. In 6 cells the maximum Q_{on} was 2.0±0.6 pC and the maximum Q_{off} was 1.3±0.4pC. The reasons for this difference were unknown. The average

Figure 4.2 Voltage sensitivity of the integral of the asymmetric capacitive currents (Q). Q was normalized by dividing each value by the maximum amount of charge moved (Q_{max}). Q_{max} was estimated by eye. This normalized integral of the ON (A) and the OFF (B) charge movement in 4 cells, is plotted against test potential. (C) The points in A and B were averaged and fitted with equation 3.5. The squares show the average ON charge movement, and the crosses show the average OFF charge movement. The broken line is the fitted line taken from figure 3.11B and shows the steady-state fraction of calcium channels activated as a function of potential.

A

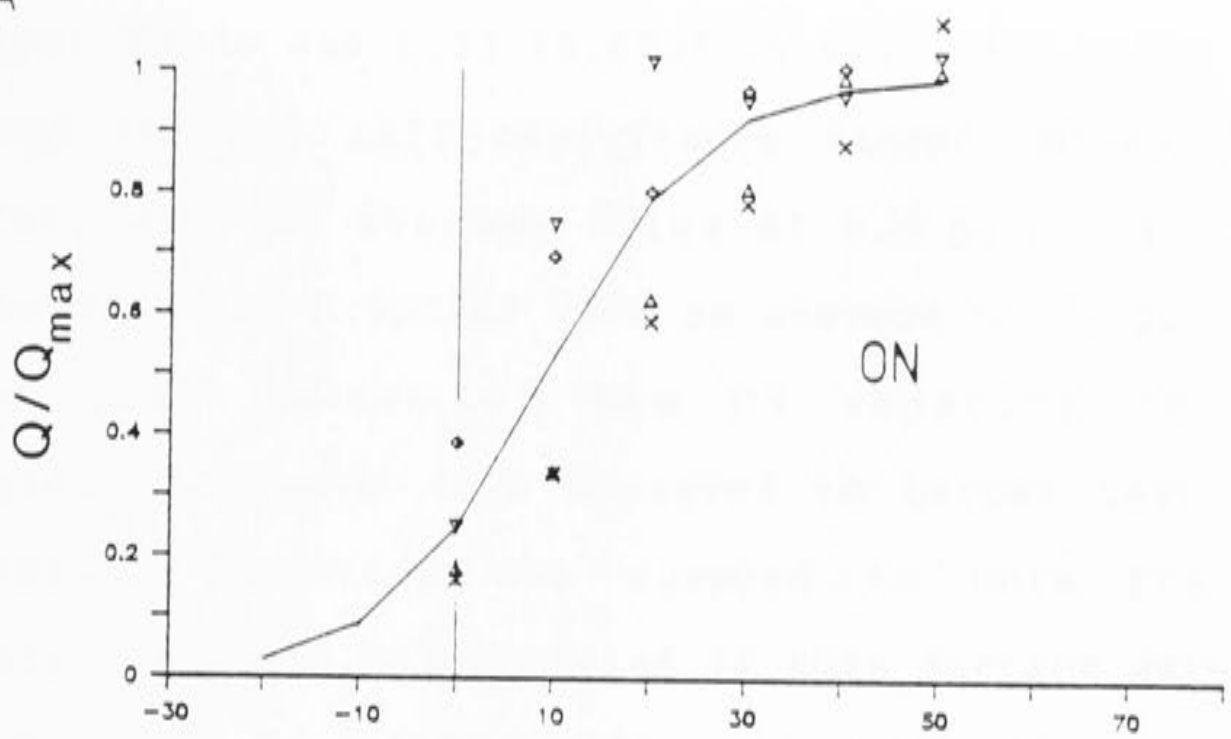
Q/Q max
1
0.8
0.6
0.4
0.2
0
-30
-10
10
30
50
70
ON

B

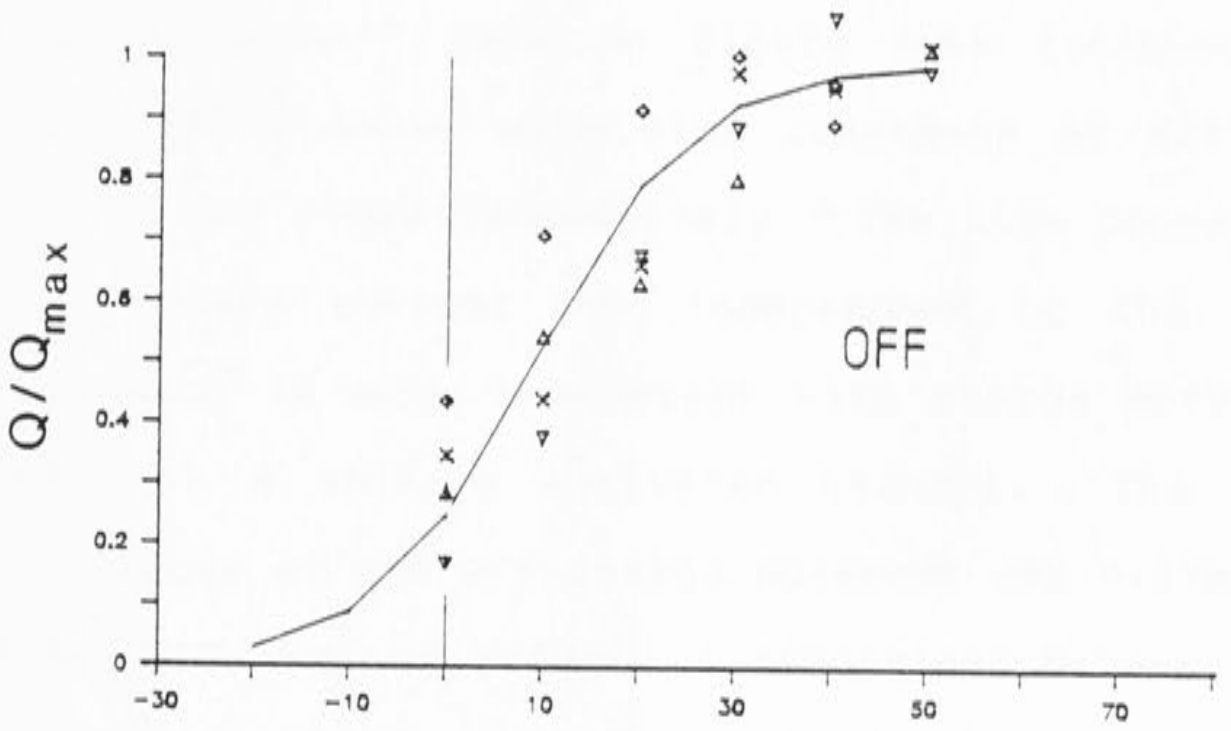
Q/Q max
1
0.8
0.6
0.4
0.2
0
-30
-10
10
30
50
70
OFF

C

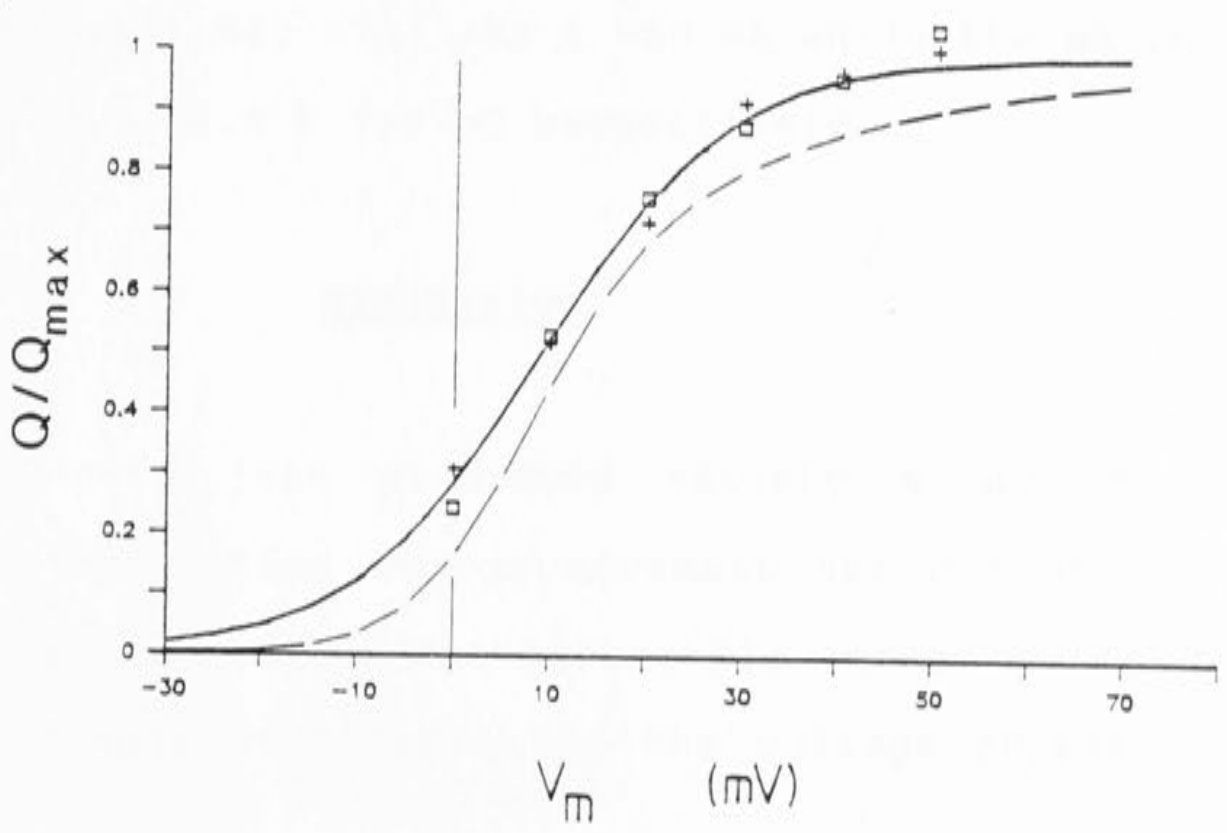
Q/Q max
1
0.8
0.6
0.4
0.2
0
-30
-10
10
30
50
70
Vm (mV)

cell capacitance was 0.33 ±0.02nF (n=6). In 5 cells Q_{on}, normalized for the cell capacitance ranged between 3.2-10.0pC/nF, with an average value of 6.3 pC/nF, and Q_{off} ranged between 2.0-6.9pC/nF with an average of 3.8pC/nF.

The time course of the ON capacity current illustrated in figure 4.1B appeared to become faster as the membrane potential was stepped to more positive potentials, as would be predicted if this current were the charge movement associated with activation of a voltage dependent channel. The decay of the transient ON charge movement for the Mn^{2+} data in figure 4.1B followed an exponential time course, with time constants of 0.85 to 0.40ms at +10 and +40mV respectively. The time course of the OFF asymmetry current was independent of the step potential, which is also consistent with charge movement associated with a voltage activated channel. The time constant of decay of the OFF charge movement was 0.17ms at the holding potential of -50mV. A comparison between the size of the asymmetry currents and the calcium ionic current was obtained in 4 cells. The peak calcium current at +15mV was -88, -73, -56 & -50 nA while the maximum Q_{on} was 2.7, 1.7, 2.8 & 2.9 pC respectively.

Discussion

The data just presented satisfy a number of the criteria for gating charge movement set out above. The best evidence linking the asymmetric charge movement with calcium channel activation is the voltage sensitivity of

the steady-state activation curve and the cumulative charge movement curve (figure 4.2C). Both curves predicted a similar valence for the protein dipole. The result indicates that the charge movement is not inconsistent with calcium channel activation, but does not unambiguously identify the source of the charge movement. Part of the charge movement observed could well be associated with the sodium or potassium currents present in these cells.

The time constant measured from the ON charge movement was faster than the slow time constant measured from the activation of the calcium current in the previous chapter. Since the activation charge movement must precede channel opening it is not unreasonable to assume that some of the charge movement may be associated with calcium channel activation. The time course of the OFF charge movement is also consistent with the calcium channel kinetics in that it decays at rougly the same rate as the fast phase of the calcium tail currents recorded in chapter 3.

The asymmetry currents do not appear to be purely capacitive. The integral of the ON asymmetry current did not equal the OFF asymmetry current in any of the cells where the currents were observed. Q_{on} was invariably larger than Q_{off}. A possible reason for this disparity is that there is some charge immobilization during the voltage pulse, which may occur for example if sodium channel gating currents made a significant contribution to Q_{on} (Armstrong 1981). It is also possible that the

asymmetry currents were capacitive but that part of OFF asymmetry current was too rapid to be adequately resolved, particularly if it decayed with a time course similar to the fast phase of the calcium tail currents.

The correlation between the size of the charge movement and the size of the calcium currents also indicates that there may be significant charge movement from other voltage activated channels, or contamination from unsuppressed ionic currents.

The techniques used are promising but need some refinement before more accurate records of calcium gating currents can be obtained. The ion sensitivity of the ON and OFF asymmetry currents must be tested, to see whether there is some contribution from unblocked ionic currents. This is a particularly important point, since the equality of the charge displaced at the onset and offset of the voltage pulse is a critical feature of capacitive currents. The viability of the calcium current in the neurone must be improved, since the calcium current ran-down quite rapidly in the present experiments, and this limited the amount of time available to obtain records. This factor is particularly crucial for the charge movement experiments since it took considerably longer to obtain each run, as several pulses were averaged at each potential. The data of Byerly & Yazejian (1986) suggest some possible strategies for maintaining functional channels for long periods of time in perfused neurones. For example, inclusion of adenosine-triphosphate and 1-2mM Mg^{2+} in the internal perfusion solution,

and a high sealing resistance between the suction electrode and the membrane helped maintain calcium currents in their experiments.

When normalized for the cell capacitance, the magnitude of Q_{on} was similar to that observed in molluscan neurones by Adams and Gage (Q_{on}= 4.6pC/nF, 1979b). The magnitude of the observed charge movement was about 3 times larger than expected from the calculations done in the introduction, which suggests a maximum of about 13 electronic charges per calcium channel. Lux & Brown (1984) calculated the electronic charge per calcium channel in molluscan neurones to be 350, and argued that most of the charge movement in molluscan neurones (Adams & Gage 1979b, Kostyuk et al. 1981a, Brown et al. 1983) is probably not associated with calcium channel actvation. This large excess of charge does not seem to be present in mammalian neurones.

The asymmetry currents observed when most of the ionic currents were blocked were very small, and do not contribute significantly to the tail current relaxations of the calcium currents in the previous chapter. There may have been a slight prolongation of the observed delay before activation of the calcium current due to the initial outward asymmetry current, however such an effect will not affect the conclusions from the results in Chapter 3 since neither the amplitude nor time course of this exponential component were used in the subsequent analysis.

Chapter 5

Some aspects of the permeation properties of calcium channels

Introduction

The mechanism of permeation of ions through calcium channels is unclear at present. The channel appears to be highly selective for calcium ions in the face of the relatively high concentrations of sodium and potassium ions in the physiological environment. A 2-site 3-barrier rate theory model has been proposed to model calcium channel permeation in skeletal muscle (Almers & McCleskey 1984) and in heart muscle (Hess & Tsien 1984). The model was proposed to account for three major observations. 1) When all the external calcium is removed ($<10^{-7}$M), the calcium channels become permeant to monovalent cations. Subsequent inclusion of micromolar quantities of calcium in the external solution causes a dramatic reduction (~50%) in the current through the calcium channels (Kostyuk & Krishtal 1977, Almers, McCleskey & Palade 1984, Hess & Tsien 1984). 2) In spite of the very tight binding of calcium ions to the channel that the previous observation implies, the single channel conductance of 7-10pS in 40-50mM Ca (Lux & Brown 1984, Cavalie et al. 1983) is comparable to that of other high selectivity channels. For example, the sodium channel has a conductance of 15-18 pS (Sigworth & Neher 1980, Horn, Patlak & Stevens 1981).

3) The channel displays anomalous mole fraction effects (of which point 1 is an extreme example) with various concentrations of calcium and barium ions (Almers & McCleskey 1984, Hess and Tsien 1984, Byerly, Chase & Stimers 1985).

The 2-site 3-barrier model proposed accounts for these observations fairly simply by assuming three basic properties of the calcium channel. Firstly the two energy wells (binding sites) are deep compared to the aqueous solution. The energy wells are deeper for calcium than for monovalent cations and barium ions. This can account for the block of the monovalent permeation by very low concentrations of calcium and partially explains the anomalous mole fraction effects with barium ions. Secondly, the channel is not restricted to single occupancy. Finally, there is significant repulsion between two ions occupying the two sites in the channel. The last assumption reduces the occupancy level of the calcium channel at a given concentration by greatly increasing the exit rate from the channel. Repulsion between ions in the channel produces a large increase in the apparent binding constant for calcium ions. Thus the conductance concentration relation does not saturate until the external calcium is raised to millimolar concentrations (Akaike, Lee & Brown 1978, Kostyuk, Mironov & Doroshenko 1982), despite the very tight binding of calcium to the channel sites. The instantaneous I-V of the calcium channel was obtained, and this compared with that predicted by the 2-site models proposed for the calcium channel.

Reversal of current flow through calcium channels is apparent in cardiac cells (Lee & Tsien 1984) and bovine chromaffin cells (Fenwick et al. 1982), where monovalents carry outward current at positive potentials. There has only been one report of reversal of calcium currents in nerve cells (Byerly, Chase & Stimers 1985). This thesis is the first study to examine the reversal of divalent ion (Ba^{2+}) flow through calcium channels in native membranes.

Cadmium is known to be potent blocker of the calcium channels in neuronal and cardiac cells. The block produced by cadmium ions is relieved as the membrane potential becomes more negative, as if Cd^{2+} were able to pass through the channels at very negative potentials (Byerly et al. 1984, Lansman, Hess & Tsien 1986). A number of ionic blockers, (eg. Co^{2+}, Cd^{2+}, Mg^{2+} and Mn^{2+}) compete with calcium for the blocking site, and it is thought that these ions lodge within the permeation pathway and prevent transfer of permeant ions. The sites of action of these ions may be very different, for example the voltage dependence of the block of calcium channels is very different for Cd^{2+} and Co^{2+} (Byerly et al. 1984). It is obvious that the mechanism of block for Co^{2+} and Cd^{2+} is quite different. This section sets out to investigate the voltage sensitivity of Cd^{2+} blockade, and presents a simple model which may account for the observations.

Recent single channel studies have shown that the rates of association and dissociation of cadmium ions may be relatively slow as suggested by the occurence of chattering of the channel in the presence of cadmium ions

(Hess, Lansman & Tsien 1984a, Lansman et al. 1986). This would be expected, for an ion that binds very strongly to the channel. This effect could complicate the analysis presented below, which relies on the assumption that the system is in the steady state at the time of the measurements. The kinetic effects of cadmium on the calcium currents will be examined.

Results

5.1 Instantaneous current-voltage relation

Instantaneous current-voltage relations (I-Vs) were obtained by measuring the peak of the tail currents at various return potentials, after activating a constant number of channels at +50mV. The extrapolated peak tail current, that is the amplitude of the fitted exponential at the time of the repolarization, was used. The extrapolation procedure effectively compensates for the limited time resolution of the voltage clamp (see section 2.9). The currents at negative potentials were more severely underestimated than those at positive potentials. Some examples of the measurements are shown in figure 5.1. The dotted lines show the extrapolation and illustrate the importance of employing this procedure. Figure 5.2A shows a comparison of the raw and corrected data. The shapes of the two I-Vs differ markedly.

A second source of error which may distort the shape of the instanteous I-V is series resistance. The series

Figure 5.1 Measurement of tail current amplitudes for the instantaneous I-V. The calcium-current-solutions were used internally and externally (section 2.3). The membrane potential was stepped to +50mV for 3ms from a holding potential of -50mV and then to the return potentials indicated. The broken lines are the double exponential fits to the current relaxations extrapolated back to the step time. The peak of the tail currents occurred about 60-80μs after the voltage step. The fits were calculated for the points >100μs after the step. The lower calibration bar applies to the bottom four traces.

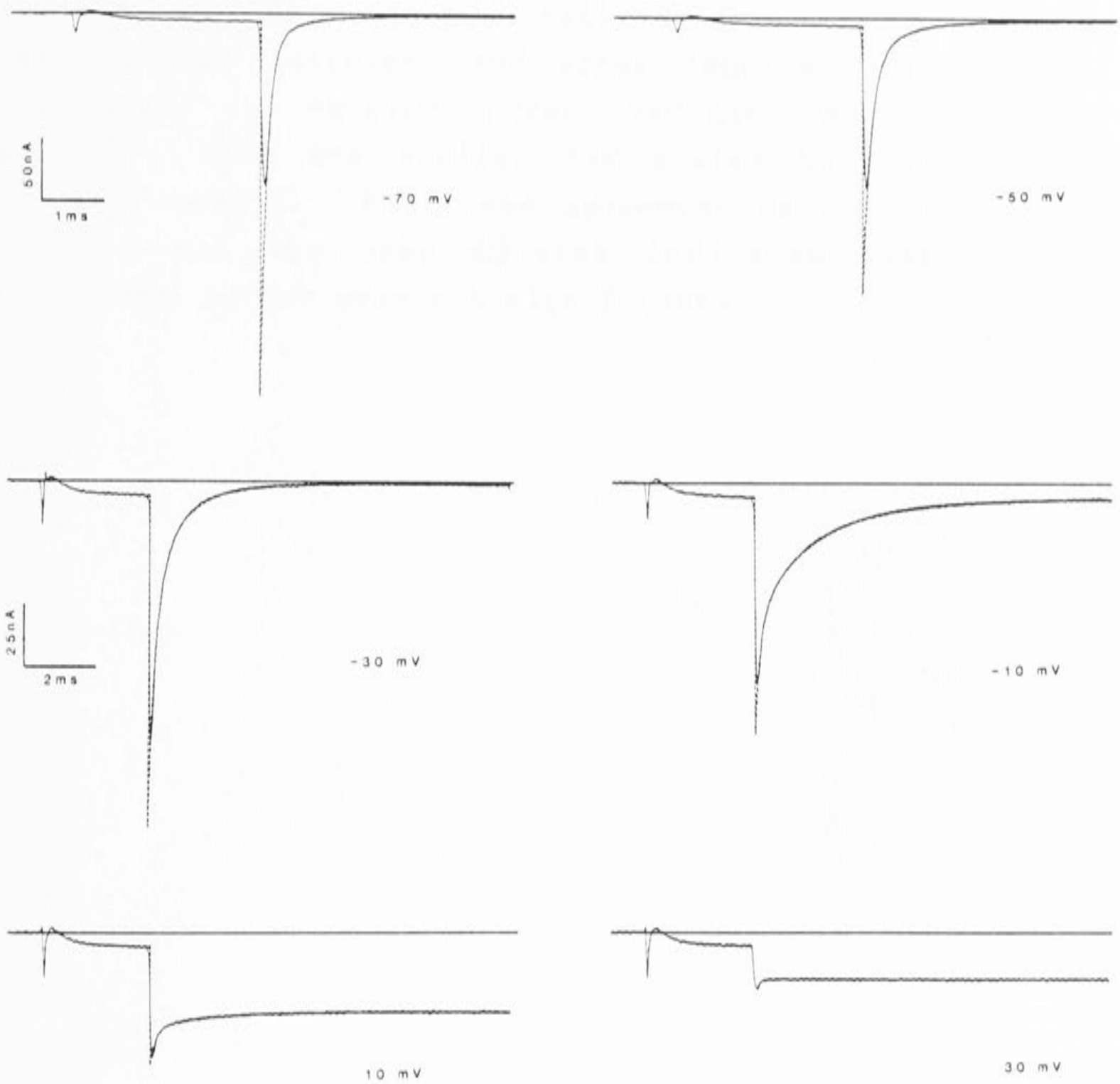
50nA
1ms
-70 mV
-50 mV
25nA
2ms
-30 mV
-10 mV
10 mV
30 mV

Figure 5.2 (A) Open squares show the uncorrected peak tail current. Solid squares show the extrapolated peak tail currents measured in the same cell. (B,C) The solid symbols show the peak tail currents recorded in two cells before (circles) and after (squares) significant rundown of the calcium current had occurred. The open squares show the smaller I-V scaled to overlie the initial control. The close agreement between the solid circles and the open squares indicates that series resistance errors were not significant.

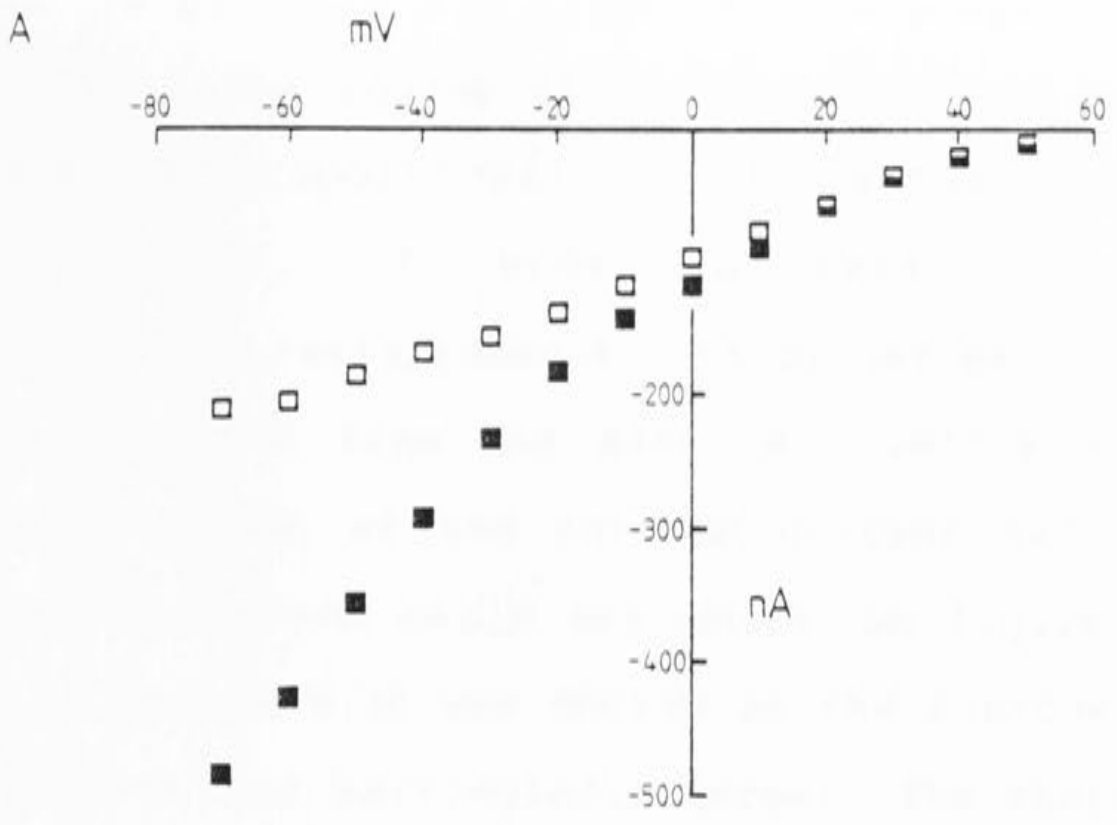
A
mV
-80
-60
-40
-20
0
20
40
60
-200
-300
-400
-500
nA

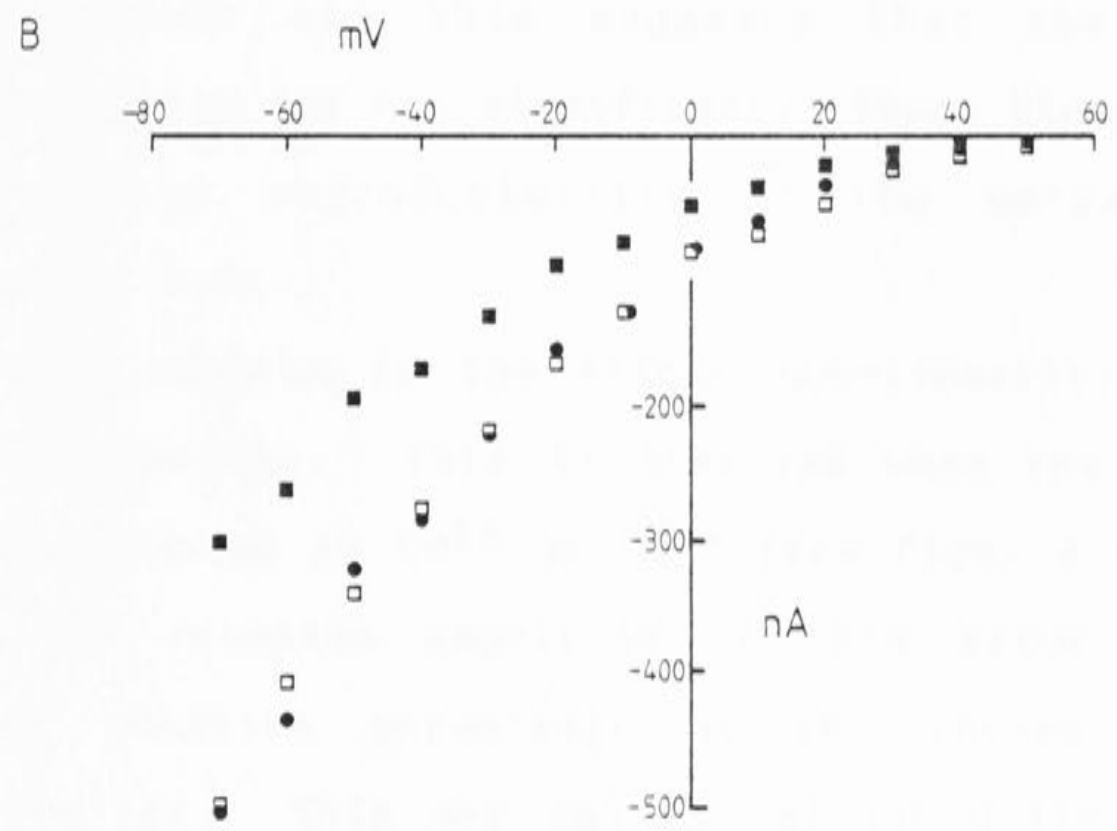
B
mV
-80
-60
-40
-20
0
20
40
60
-200
-300
-400
-500
nA

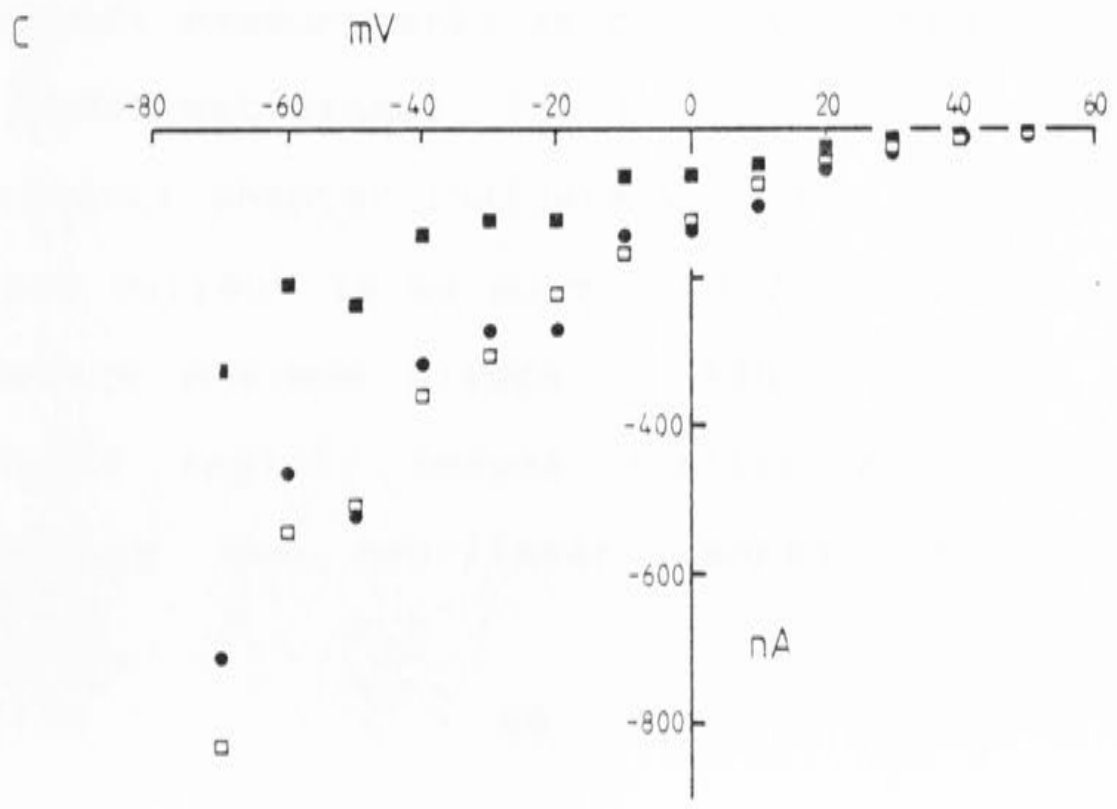
C
mV
-80
-60
-40
-20
0
20
40
60
-400
-600
-800
nA

resistance is probably not large in this preparation (see section 2.5). The amount of error introduced by series resistance is proportional to the amplitude of the membrane current. In order to check for possible distortion of the instantaneous I-Vs by series resistance, I-Vs were obtained from the same cell before and after significant rundown of the calcium current had occured. The results from two cells are shown in figure 5.2B,C. The cell in figure 5.2C was chosen as the run-down of the calcium current was particularly large. The shape of the I-V appears to be independent of the magnitude of the calcium current and this suggests that the series resistance errors are not significant. These figures also illustrate the reproducibility of the extrapolated instantaneous I-Vs.

Another problem is the slight non-linearity of the leakage conductance. This is observed when the calcium current is blocked by Cd^{2+} or Co^{2+} (see figs. 4.1, 5.15, 5.17). The relative magnitude of this error becomes larger at positive potentials as the inward current becomes smaller. This may cause a slight distortion of the instantaneous I-V at positive potentials, since the inward current measurements at positive potentials will be slightly under-estimated. The gating current measurements in the previous chapter indicate that the non-linearity in the leakage current is no more than 2-3nA at +50mV, which would produce maximum errors of ≈20-30%. The relative errors would rapidly become smaller at more negative potentials as the non-linear leakage current became

smaller, and the calcium tail current became larger.

Outward current flow through calcium channels was not observed at potentials up to +70mV. Figure 5.3 shows the current in response to voltage steps to +50, +60 and +70mV. At these potentials the current reaches a peak in less than 1 ms, and at +70mV there is no significant outward or inward current for the first millisecond. A similar result is observed in figure 3.9. In other cells where the potential was stepped to potentials greater than +70mV, the nonlinearity in the leakage current was too large to decide whether there was true reversal of the calcium current.

The average instantaneous I-V obtained from 9 cells is shown in figure 5.4. Each I-V was normalized to the average value of the tail current at -40mV. The solid line through the points was produced using the GHK constant field equation (Goldman 1943, Hodgkin & Katz 1949) for a single permeant ion,

$$I_m = P_{Ca}\frac{z^2VF^2}{RT}\,\frac{a_i - a_o\exp(-zVF/RT)}{1 - \exp(-zVF/RT)} \qquad ..(5.1),$$

where a_o,a_i are the activities of calcium outside and inside the cell, P_{Ca} is the permeability of calcium, z the valence and V the voltage applied to the membrane. The permeation parameter was varied to fit the data at 0mV; in this case P_{Ca} = 0.07 cm/s.

The GHK equation predicts a steeper voltage dependence for the current than is observed. The voltage dependence of current in equation 5.1 is equal to the

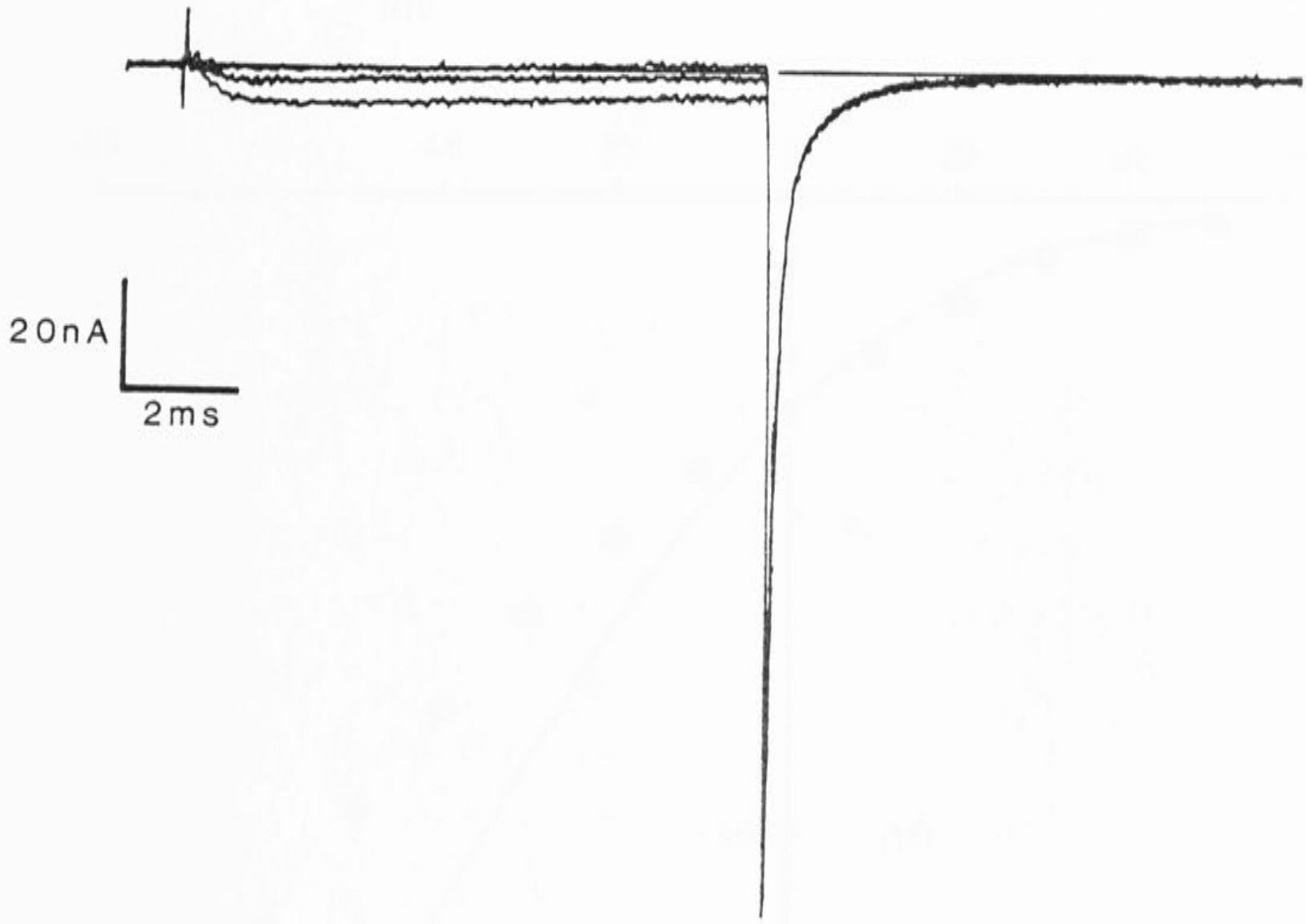

Figure 5.3 Response to voltage steps to +50, +60 and +70mV. Holding potential -50mV, pulse duration 10ms. There is no significant inward or outward current during the step to +70mV.

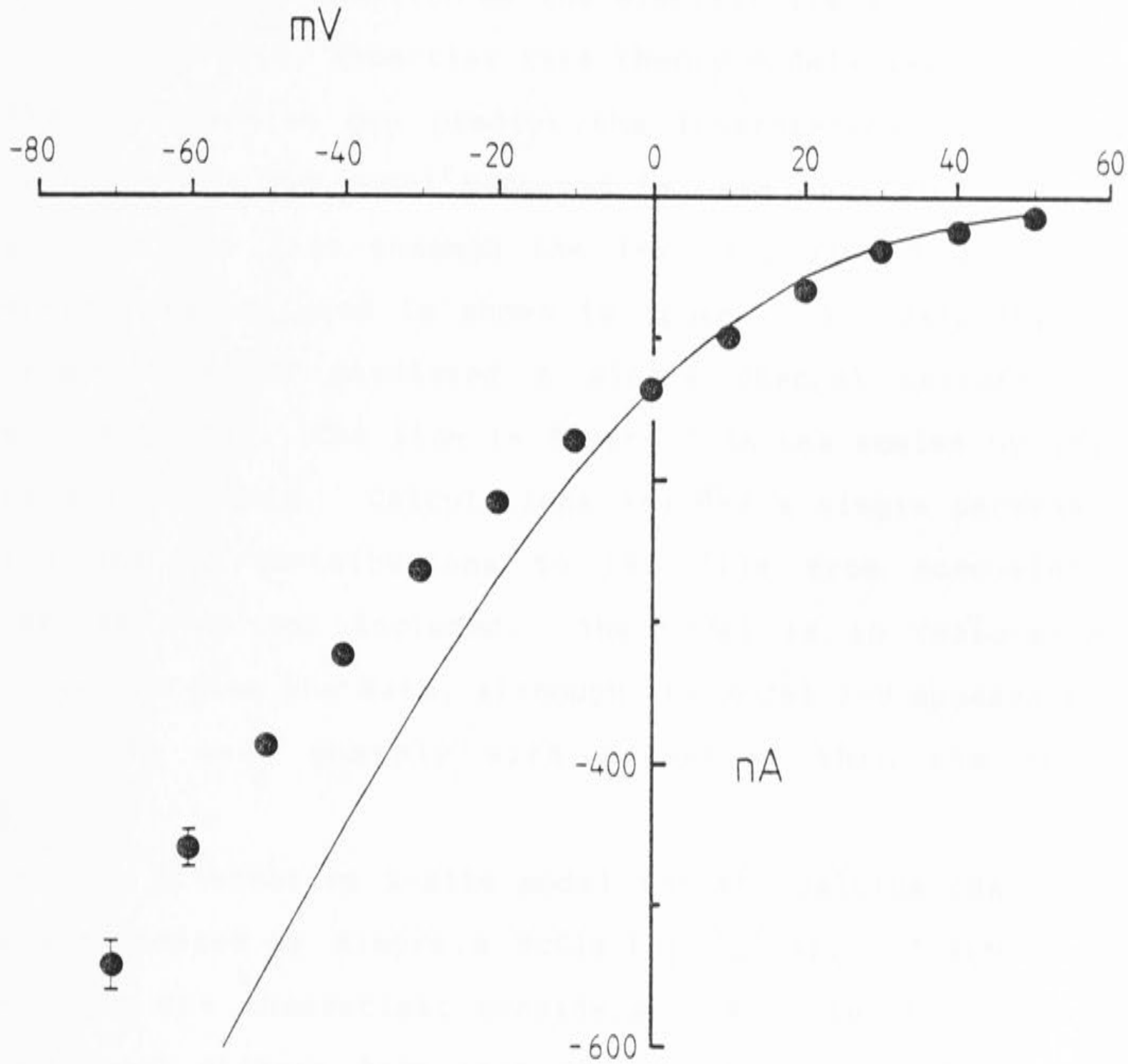

Figure 5.4 The data points show the normalized average instantaneous I-V from 9 cells. The standard errors were smaller than the symbols for all but two of the points. The solid line was produced using equation 5.1, constrained to pass through the point at 0mV.

energy change as the divalent ion falls through the electric field across the membrane. The lower voltage dependence shown by the data suggests that, in crossing the membrane, the rate limiting step involves the ion traversing some fraction of the electric field.

The 2-site, 3-barrier rate theory models described in the introduction can predict the instantaneous I-V more accurately. The model proposed by Hess and Tsien (1984) produced the line through the I-V in figure 5.5A. The energy profile used is shown in Appendix 3. Calulations from the model predicted a single channel current of 0.16pA at 0mV. The line in figure 5.5A was scaled by eye to fit the data. Calculations assumed a single permeant ion and so contributions to the flux from monovalent cations were not included. The model is in reasonable agreement with the data, although the model I-V appears to increase more sharply with potential than the data points.

An alternative 2-site model for the calcium channel, was suggested by Almers & McCleskey (1984), and embodies some of the theoretical considerations of Levitt (1978). The model differs from that proposed by Hess & Tsien in two respects: 1) the fraction of the membrane electric field sensed by permeant ions entering the channel is small (d1,d6 in Appendix 3), 2) the entry rate of permeant ions into the channel is unaffected by occupancy of the other site ($R_{in} = 1$). The effects of these assumptions is discussed further below.

The energy profile for the Almers and McCleskey model

Figure 5.5 The data points are replotted from figure 5.4. The lines through the points were produced using the 2-site 3-barrier models proposed by Hess & Tsien (A) and Almers & McCleskey (B). The energy profiles and other parameters for the models are outlined in Appendix 3.

A

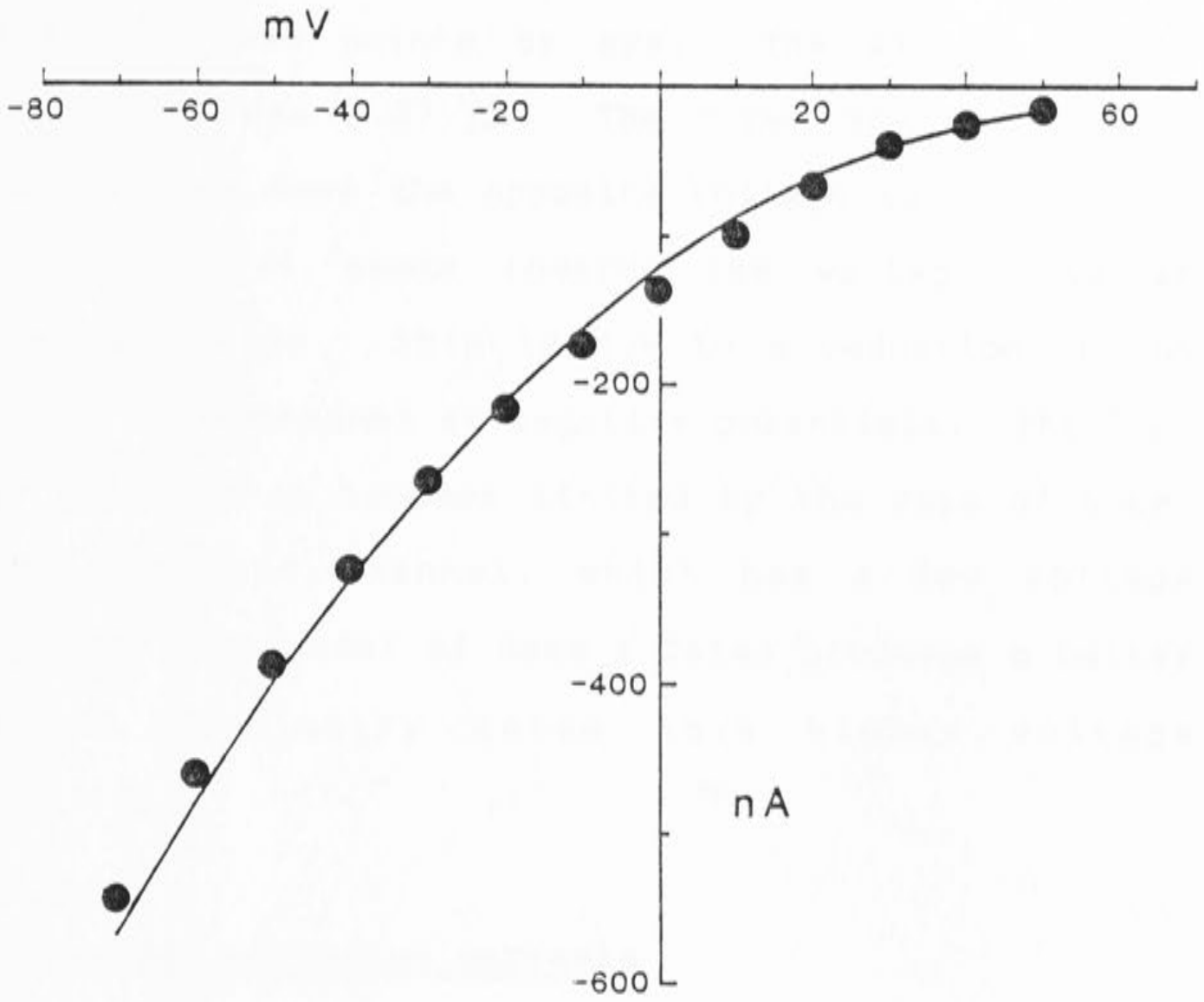
mV
-80
-60
-40
-20
20
60
-200
-400
nA
-600

B

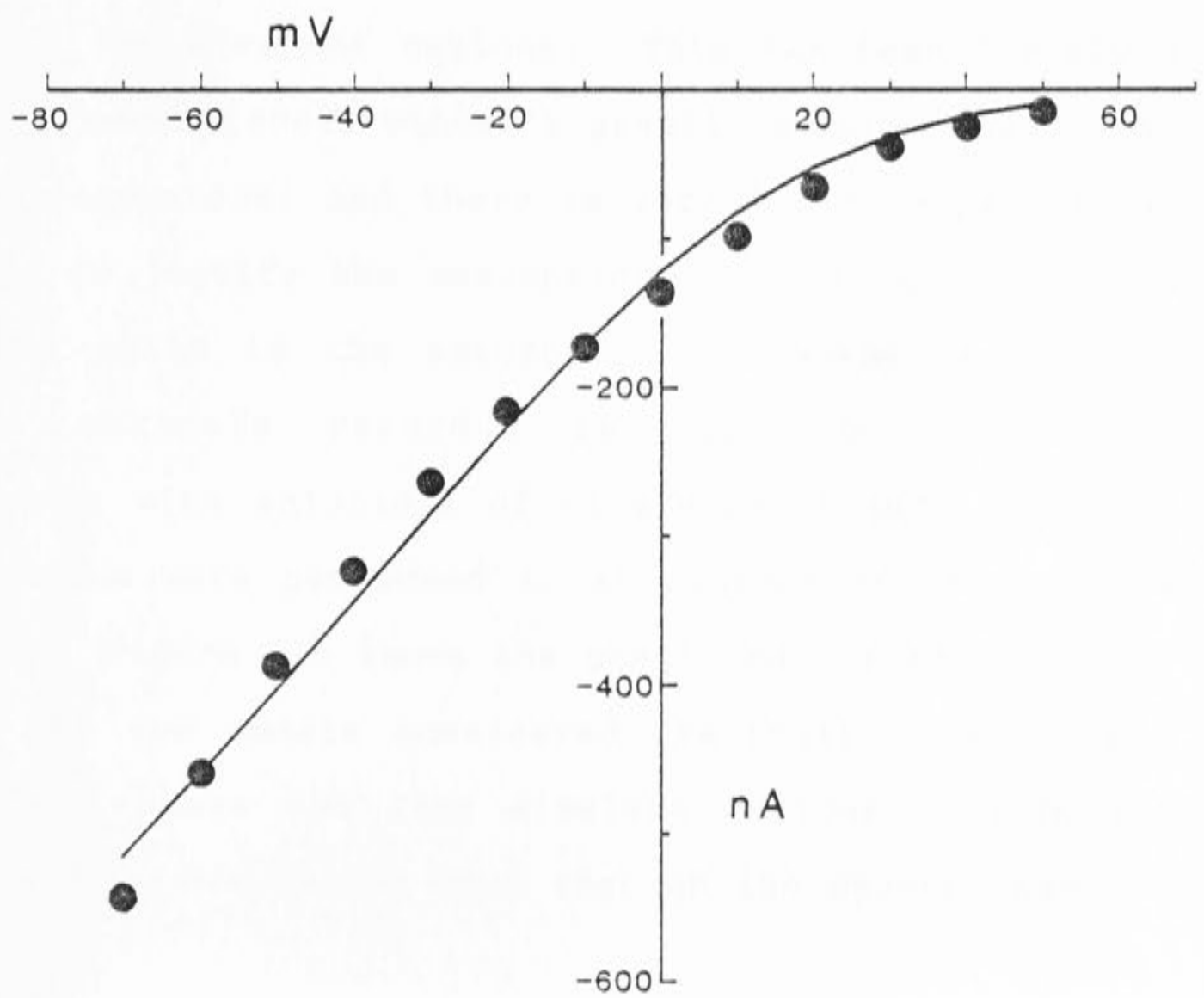
mV
-80
-60
-40
-20
20
60
-200
-400
nA
-600

is shown in Appendix 3, and the fit to the instantaneous I-V is shown in figure 5.5B. The theoretical curve was scaled to fit the points by eye. The single channel current at 0mV was 0.07 pA. The curve produced by the model appears to have the opposite voltage sensitivity to that observed; it bends towards the voltage axis at negative potentials. This is due to a reduction in the occupancy of the channel at negative potentials. The flux through the channel becomes limited by the rate of entry of ions into the channel, which has a low voltage sensitivity. The model of Hess & Tsien produces a better fit since the entry rates have higher voltage sensitivities.

5.2 Reversal of barium currents

The models presented have assumed that the channel is symmetric for divalent cations. This has been largely a matter of convenience, since it greatly reduces the number of free parameters, and there is very little experimental evidence to justify the assumption. An obvious question is : How valid is the assumption of symmmetry for the calcium channels recorded in cat DRG neurones ? Experiments with solutions of divalents on both sides of the membrane were performed in an attempt to answer this question. Figure 5.6 shows the predicted instantaneous I-V from the two models considered previously. For these simulations there was 20mM divalent cations outside and 10mM inside. Monovalent flux through the channel was not

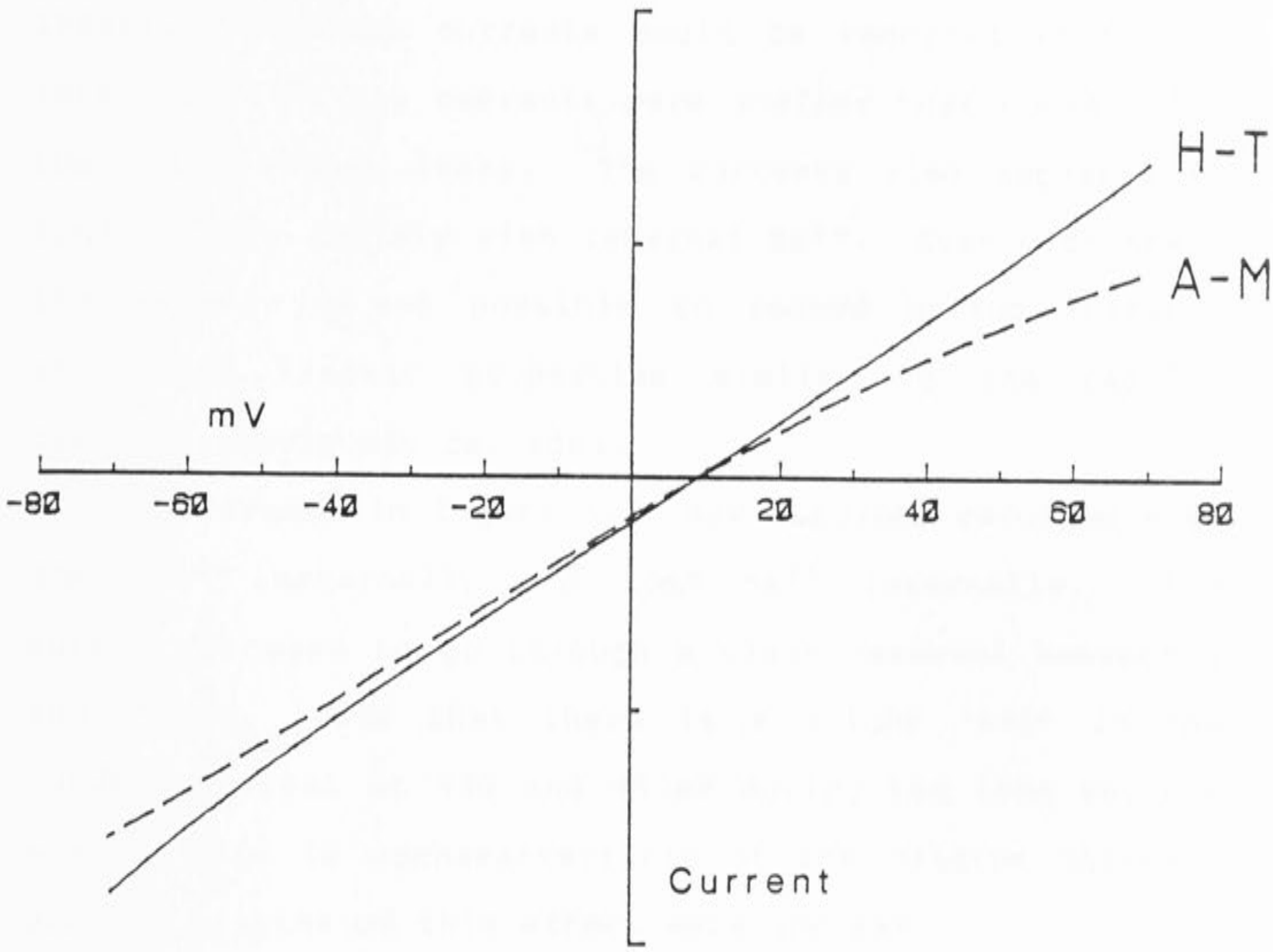

Figure 5.6 Predicted instantaneous I-V for the two models, Hess & Tsien (H-T) and Almers & McCleskey (A-M). The curves were calculated for a single permeant divalent ion; 20mM externally and 10mM internally. The current units are arbitary.

included.

Barium ions were used as the divalent in these experiments, since relatively low concentrations of internal calcium render the channels unactivatable (Hagiwara & Nakajima 1966, Kostyuk & Krishtal 1977, Chad & Eckert 1984b). Although currents could be recorded with 10mM internal Ba^{2+}, the currents were smaller than normal, and the cells rather leaky. The currents also appeared to rundown more rapidly with internal Ba^{2+}. Even with these limitations it was possible to record barium currents which had kinetic properties similar to the calcium currents previously recorded.

The traces in figure 5.7 show currents recorded with 10mM Ba^{2+} externally and 10mM Ba^{2+} internally. The current is seen to go through a clear reversal between 0 and +10mV. Note that there is a slight 'sag' in the outward current at +30 and +50mV during the 10ms voltage step. This is uncharacteristic of the calcium channel, and the origins of this effect were unclear.

The peak barium current is plotted against the step potential in figure 5.7A. The barium currents recorded with symmetric barium reversed at +5mV, slightly more positive than the Nernst equilibrium potential of 0mV. An interesting feature of this data is the decline of the peak outward current at potentials greater than +40mV. This effect is not due to a decrease in the number of channels activated at positive potentials. Figure 5.8B shows a plot of the peak tail currents (when returning to -50mV) recorded in the same cell. The number of open

Figure 5.7 Reversal of the barium current flow through calcium channels. Currents were activated by stepping to the potentials indicated next to each trace. Clear reversal of the current was seen between 0 and +10mV. The holding potential was -50mV.

Barium Currents

10 mM External Ba

10 mM Internal Ba

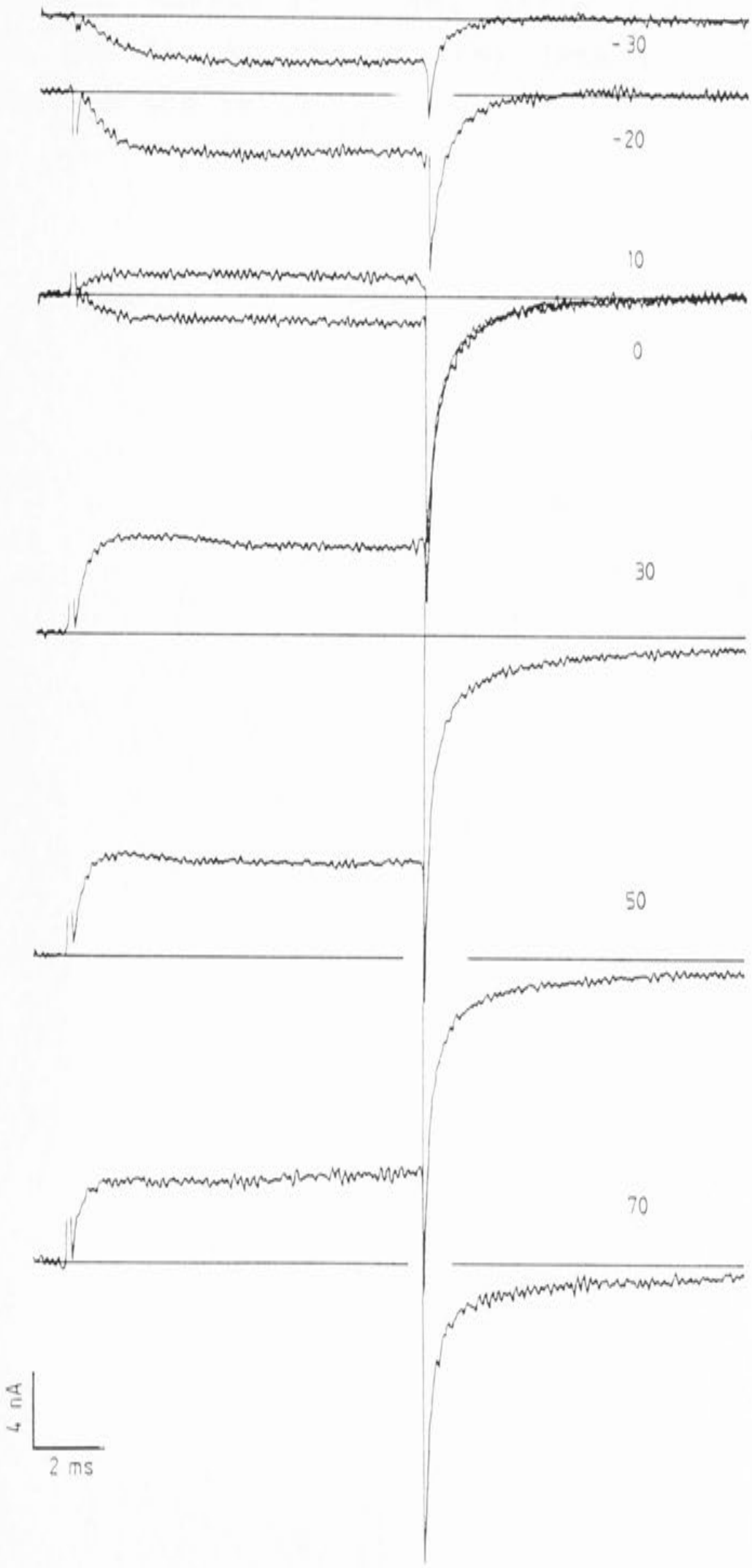

Figure 5.8 (A) Peak barium current I-V. The cell was the same as that shown in figure 5.7. The interpolated reversal potential was +5mV. (B) $P_o(V)$ curve for the barium current. The points show the amplitude of the tail currents at -50mV, plotted against the activation potential. The solid line through the points was the fit to the control data in figure 3.11B, shifted 30mV to the left.

A

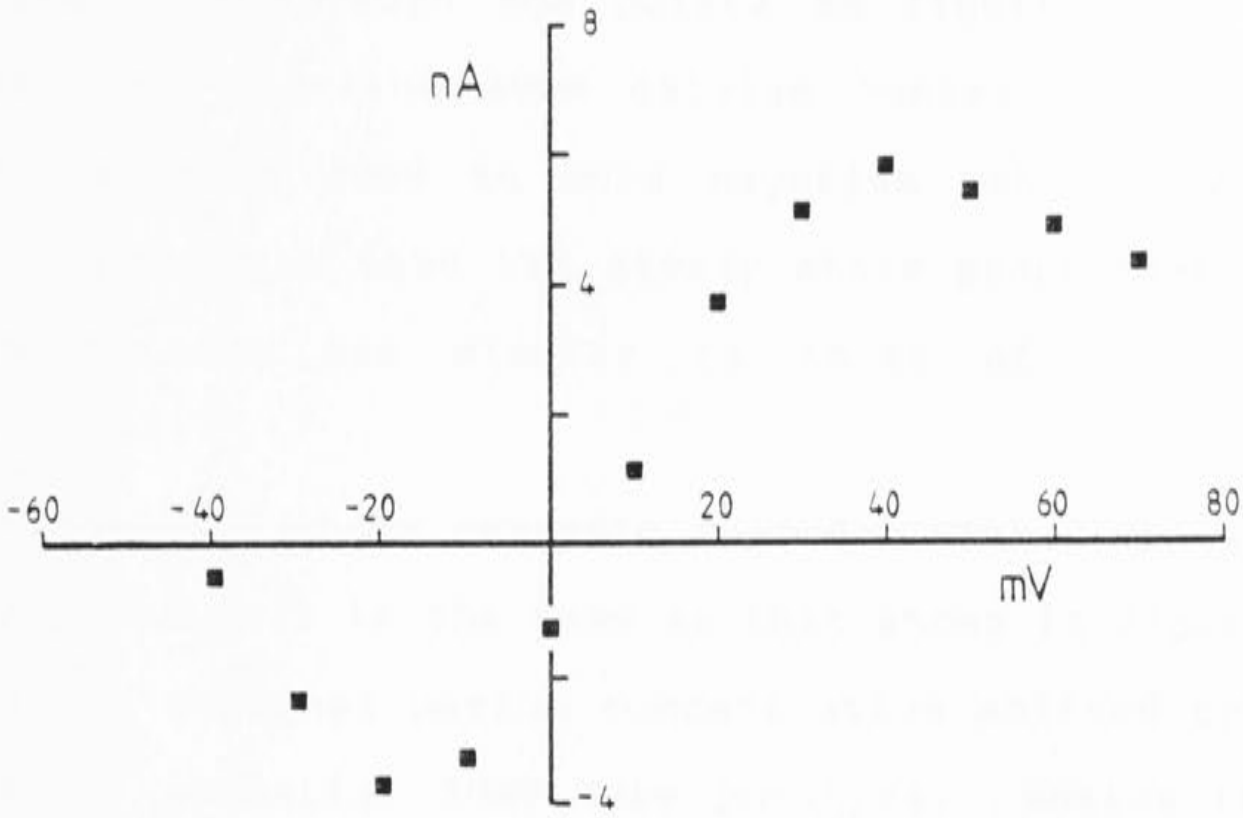

B

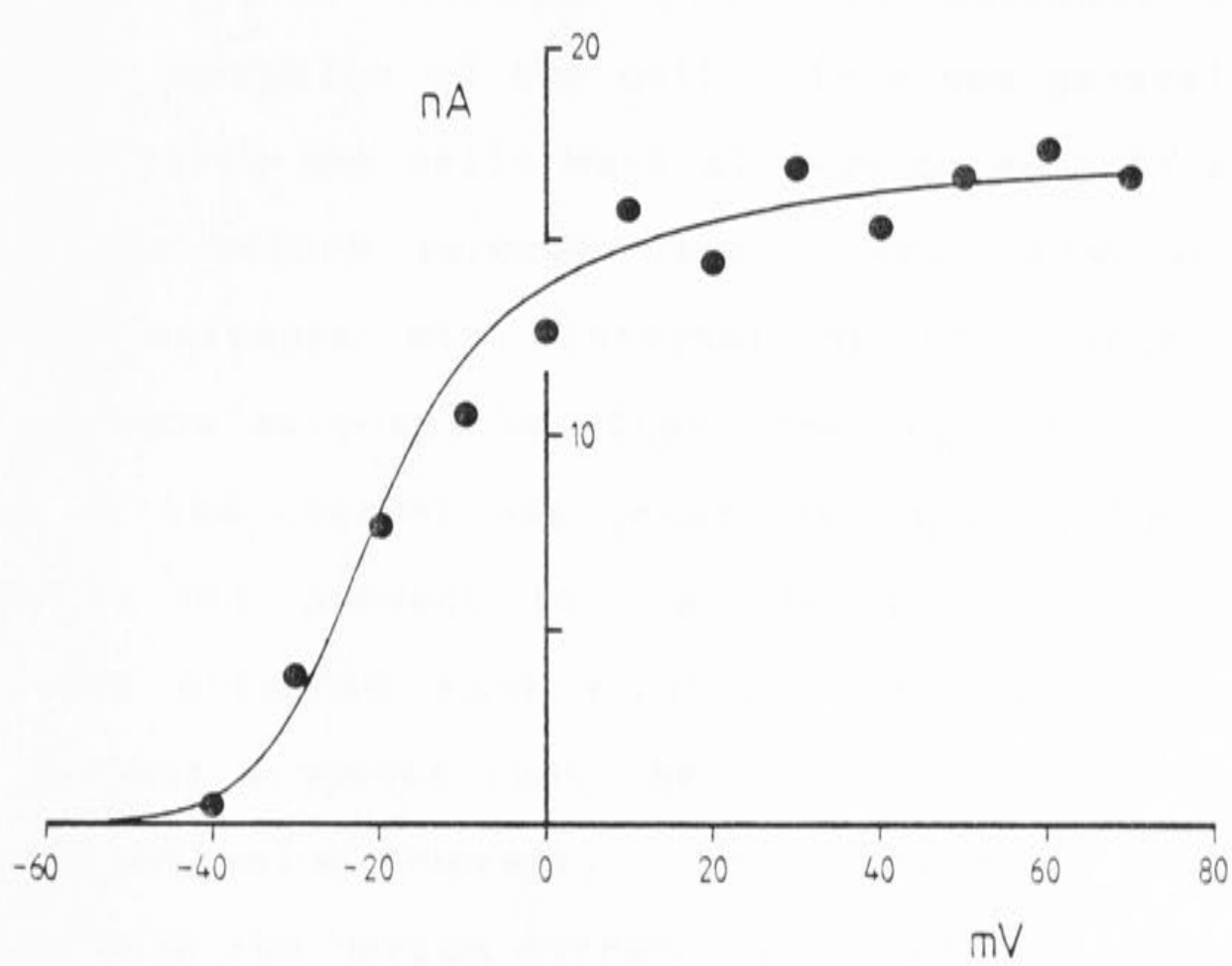

channels plateaus at around +10mV, and so the saturation in outward Ba^{2+} current cannot be explained by a decrease in the number of active channels.

The line through the points in figure 5.8B is the fitted line from the 10mM calcium control data (figure 3.11B), shifted 30mV to more negative potentials. The graph illustrates that the steady state properties of the barium current are similar to those of the calcium current.

Figure 5.9 shows currents recorded with 20mM external barium. The cell is the same as that shown in figure 5.8. The higher external barium concentration shifted the null (reversal) potential 20mV more positive. Notice that in this cell, there is a slowly developing outward current at positive potentials, which first appears at +20mV. This may have been a residual potassium current, due to incomplete perfusion of the cell. This was generally not a problem since the cells were allowed to equilibrate for two minutes before records were taken. However, when recording currents with internal barium, records were taken as soon as possible after clamping the cell, since rundown of the current was generally rapid. The outward current is not present in the currents in figure 5.8, which were obtained some minutes later, an observation which further suggests that the outward current may be a residual potassium current. The current is slower to activate than the barium current, and does not introduce a large error to the measurements. At positive potentials the peak current was measured close to the beginning of

Figure 5.9 Reversal of barium currents. The currents were elicited by stepping to the potentials indicated. The voltage pulse protocol used is shown at the bottom of the figure. Note the presence of a slowly activating outward current at potentials of +20mV and greater. Holding potential -50mV.

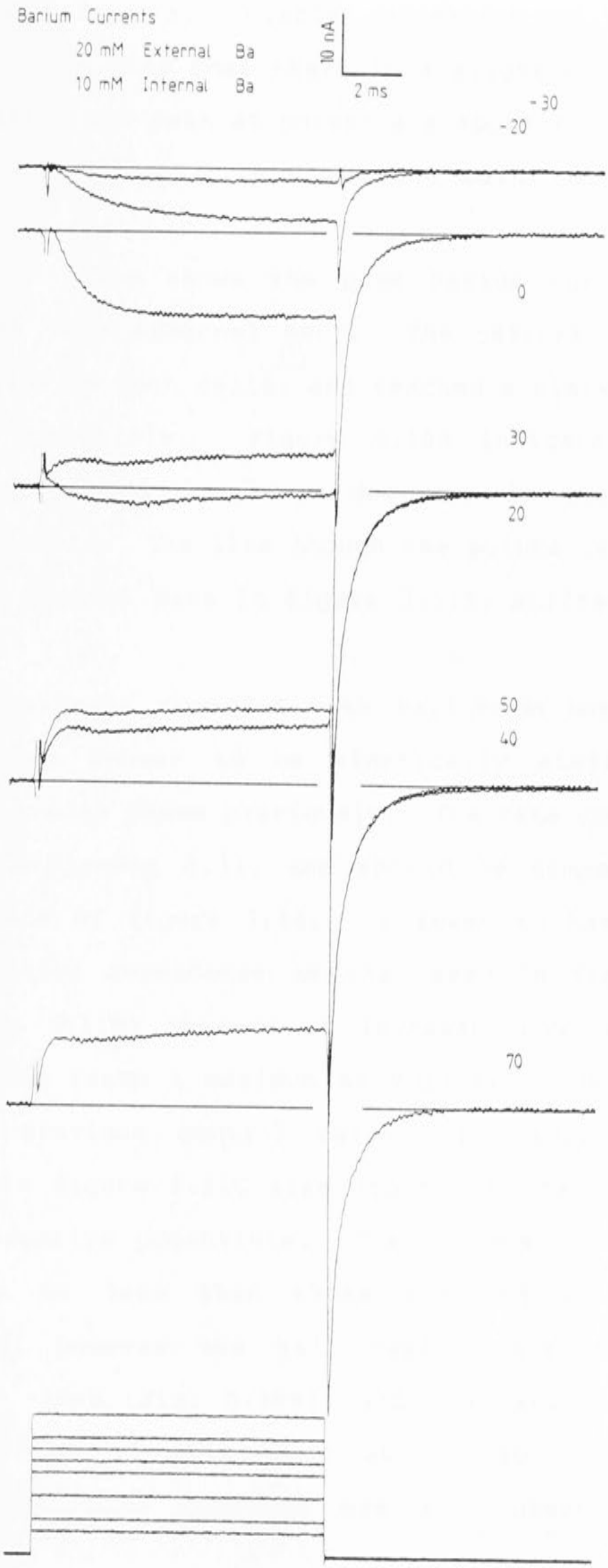
Barium Currents
20 mM External Ba
10 mM Internal Ba
10 nA
2 ms
-30
-20
0
30
20
50
40
70

the trace before appreciable activation of the outward current. Note also that there is a slight decline of the current after the peak at potentials above +30mV. This is similar to the sag in the current seen in 10mM barium (figure 5.8).

Figure 5.10A shows the peak barium current in two cells with 20mM external Ba^{2+}. The current reversed at around +24mV in both cells, and reached a plateau level at positive potentials. Figure 5.10B indicates that the saturation is not due to a decrease in the number of active channels. The line though the points is the fitted line from control data in figure 3.11B, shifted 20mV more negative.

The currents recorded with barium on both sides of the membrane appear to be kinetically similar to the calcium currents shown previously. The rate constants are plotted in figures 5.11, and should be compared to the control data of figure 3.14. τ_f seems to have much the same potential dependence as that seen in figure 3.14A. τ_s (figure 5.11B) appears to increase more slowly with voltage, and reach a maximum at more negative potentials than the previous control data. The activation time constant in figure 5.11C also appears to reach a maximum at more negative potentials. The maximum time constants seemed to be less than those recorded with 10mM Ca externally, however the half maximal activation point occurs at -10mV (Fig. 5.10B), and the maximum slow time constants were also observed at -20 to -10mV. The maximum slow time constant was also observed at the

Figure 5.10 (A) Peak barium current I-V obtained in two cells. In both cases the reversal potential was close to +24mV. (B) $P_o(V)$ curve for one of the cells shown in A. The line through the points was the fit to the control data in figure 3.11B.

A

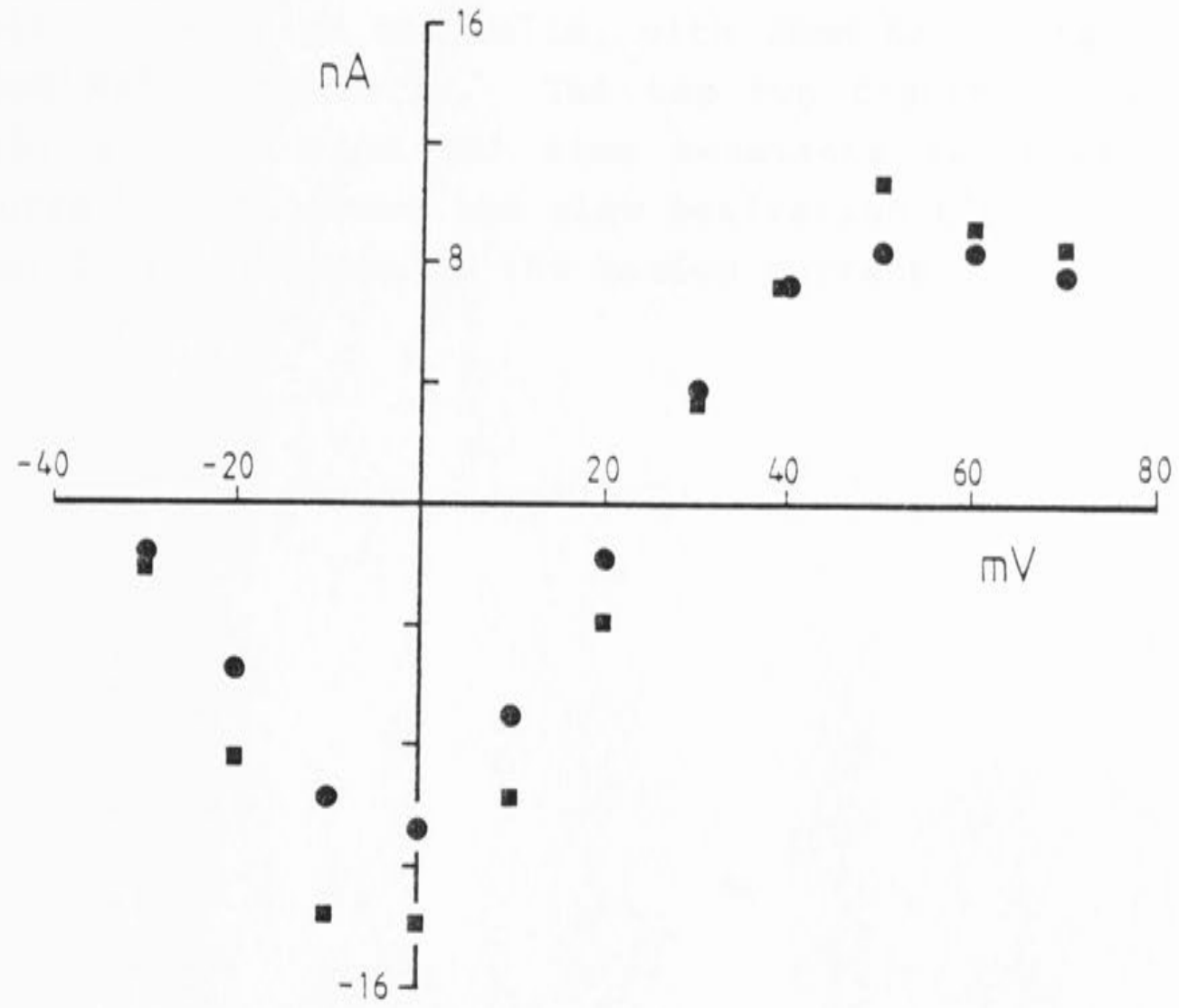

B

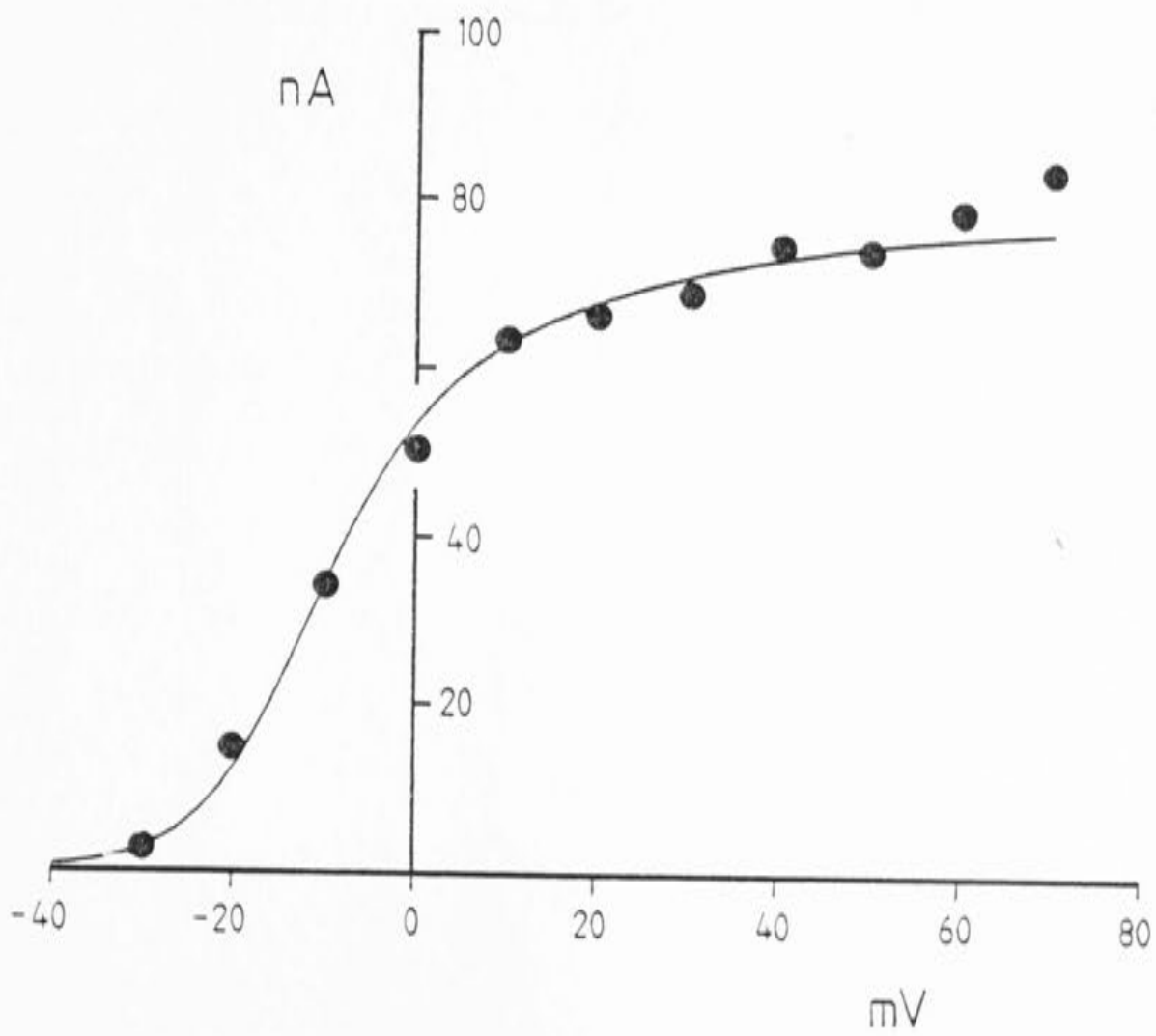

Figure 5.11 Time constants measured from activation and tail currents in two cells, with 20mM Ba^{2+} externally and 10mM Ba^{2+} internally. The top two figures show the fast (A) and the slow (B) time constants recorded from tail currents. C, shows the slow activation time constant recorded during turn-on of the barium current.

A

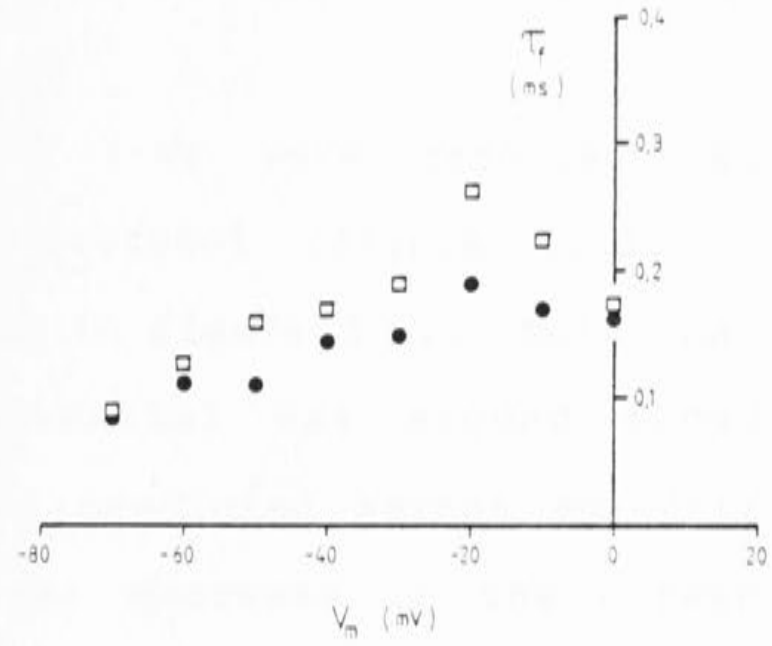
τ_f
(ms)
0,4
0,3
0,2
0,1
-80
-60
-40
-20
0
20
V_m (mV)

B

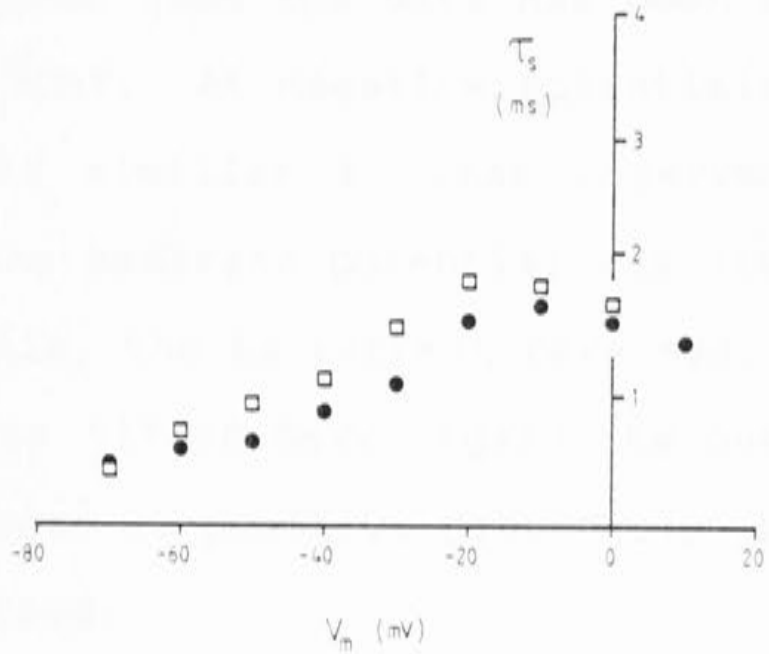
τ_s
(ms)
4
3
2
1
-80
-60
-40
-20
0
20
V_m (mV)

C

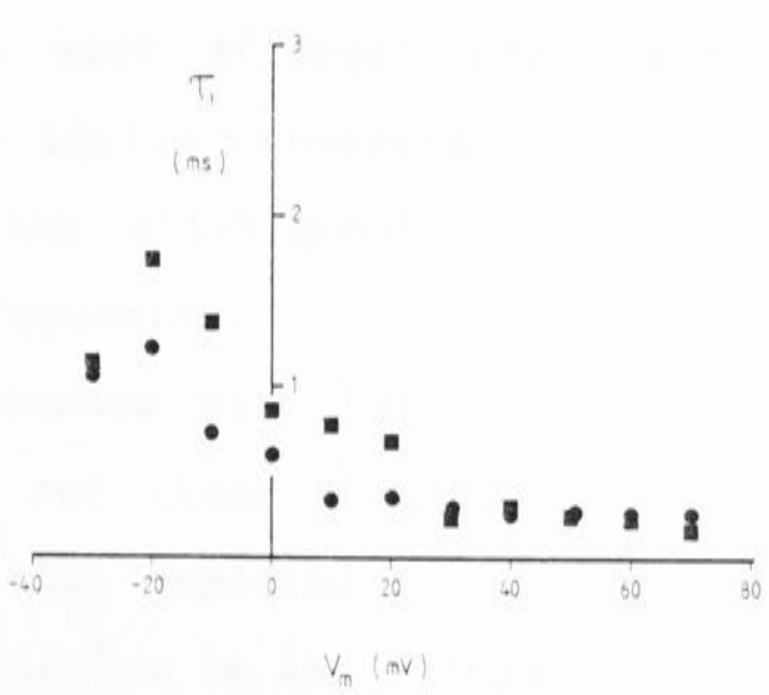
τ_i
(ms)
3
2
1
-40
-20
0
20
40
60
80
V_m (mV)

potential were approximately half the channels were activated when 10mM Ca was the charge carrier (figure 3.11B & 3.14B).

Instantaneous I-Vs were recorded using the tail current voltage protocol (figure 5.12). Some sample currents are shown in figure 5.12. Note that in this cell the reversal potential was around +20mV, 11mV more positive then the predicted Nernst potential of +8.8mV. There was a slight decrease in the outward current at +50mV during the recording period.

The instantaneous I-Vs from 3 cells are plotted in figure 5.13. In each case the data has been normalized to the average at -30mV. At negative potentials, the barium current I-V looks similiar to that observed in calcium solutions. As the membrane potential was stepped to more positive potentials, the Ba current reversed. The average null potential was +17 ±0.8mV. Again the outward current was seen to saturate at positive potentials in each of the three cells examined.

The shape of the I-V in figure 5.13 deviates sharply from that predicted by the 2-site model (fig. 5.6). The rectification is much stronger than expected from the asymmetry of the barium concentration. Consideration of possible mechanisms which produce such a non-linearity is left to the discussion.

These experiments with barium have complicated the picture. It is not clear whether the deviation of the barium I-V from that expected from the symmetrical model is present when calcium is the charge carrier.

Figure 5.12 Barium tail currents recorded at the return potentials indicated with 20mM Ba^{2+} externally and 10mM Ba^{2+} internally. The recorded voltage traces are shown at the bottom of the figure. Note that the peak outward current recorded at +50mV is slightly less in the top set of traces than the bottom set, due to run-down of the current during the voltage run. The run-down was usually rapid with 10mM internal Ba^{2+}.

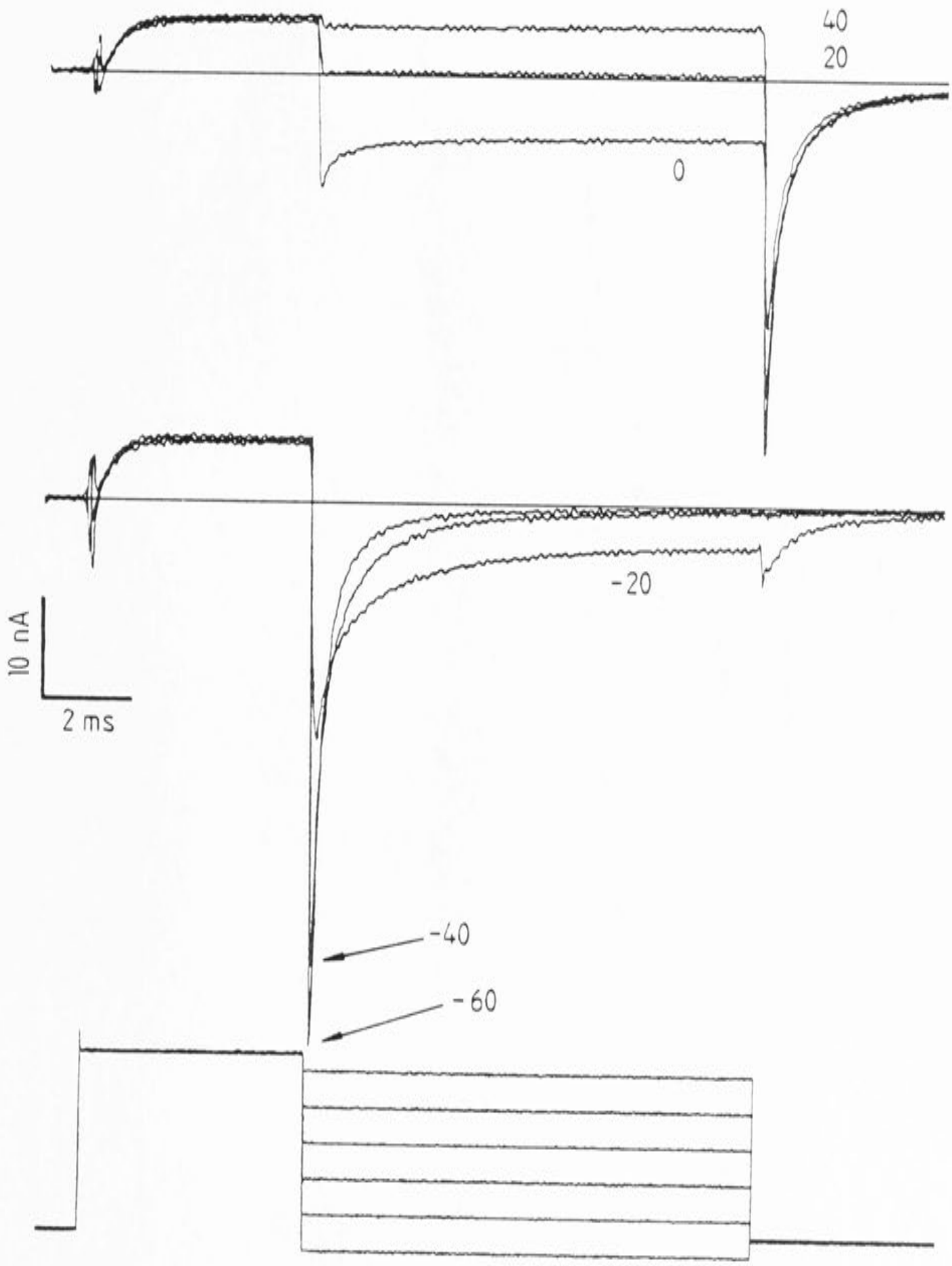
40
20
0
-20
10 nA
2 ms
-40
-60

Figure 5.13 Instantaneous I-V recorded in three cells with 10mM Ba^{2+} internally and 20mM Ba^{2+} externally. The cells were normalized to the average value at -30mV. The outward current is seen to saturate at positive potentials, and is smaller than that expected from figure 5.6.

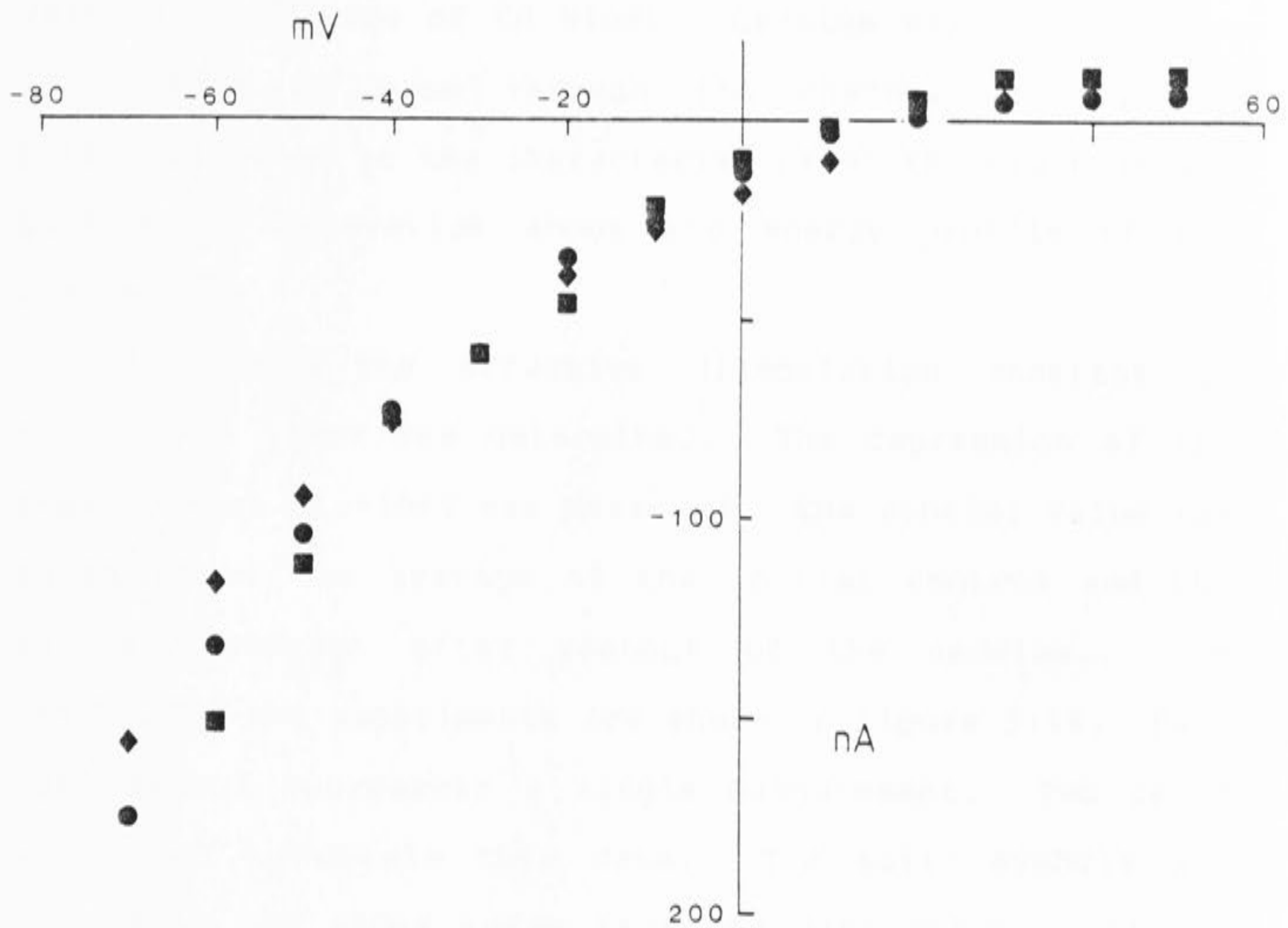
mV
-80
-60
-40
-20
60
-100
nA
200

5.3 Cadmium Block of the Calcium Channel

To investigate further the suitability of the 2-site model presented, experiments were performed to examine the voltage dependence of Cd block. Cadmium was chosen since it appears to pass through the channel at negative potentials, and so the characteristics of the block should give some information about the energy profile of the channel.

Initially the effective dissociation constant of cadmium at +10mV was determined. The depression of the peak current at +10mV was measured. The control value was taken to be the average of the initial control and the recovery current after washout of the cadmium. The results of the experiments are shown in figure 5.14. Each open symbol represents a single measurement. Two cells were used to obtain this data. The solid symbols are the values at +10mV taken from the data shown in figure 5.16A. The value for 150µM cadmium in figure 5.14 was that predicted by the smooth curve at +10mV in figure 5.16A. The fraction of channels not blocked (F) is well approximated by the equation,

$$F = \frac{1}{1 + \frac{[Cd]}{K_d}} \qquad ..(5.2),$$

with K_d, the dissociation constant at +10mV, equal to 10µM. Equation 5.2 assumes one-to-one binding of the cadmium with the channel, and the data is consistent with

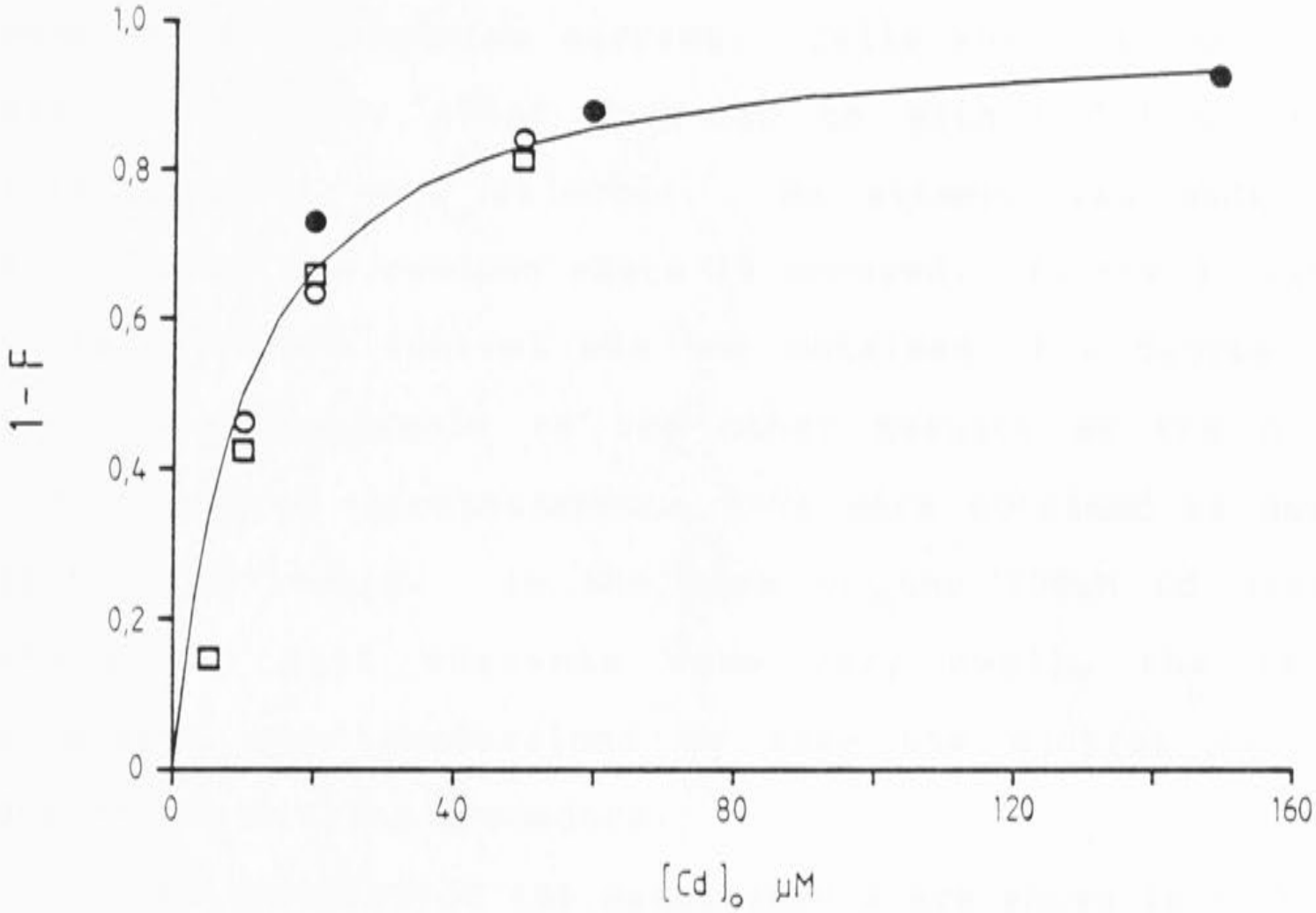

Figure 5.14 Block of the calcium channel at +10mV. One corresponds to complete block. The line through the points was fitted by eye using equation 5.2, with K_d = 10µM. Run-down of the calcium current was allowed for by taking the average of the pulses before application of cadmium and after washing it out. The open symbols show the results from two cells. The solid symbols for 20 and 60µM cadmium were calculated from the values at +10mV in figure 5.16A. The 150µM point was calculated from the value predicted by the solid line at +10mV in figure 5.16A.

a single cadmium ion blocking the channel.

The voltage sensitivity of cadmium block was examined in some detail. Instantaneous I-Vs were recorded before and after perfusion of Cd at 4 concentrations: 20, 60, 150 and 500μM. These experiments were complicated by the rundown of the calcium current. Cells where the current did not recover after wash-out to within 75% of the initial level were rejected. No attempt was made to correct for the rundown where it occured. In the 3 cases where a second control was not obtained, the degree of block was comparable to the other results at the same concentration. Instantaneous I-Vs were obtained as described previously. In the case of the 500μM Cd data, where the tail currents were very small, the rate constants were constrained to take the control values during the fitting procedure.

Some examples of the measurements are shown in figure 5.15. The broken line through each trace is the double exponential fit produced by the LMM algorithm. The fit was extrapolated back to the time of the repolarization. The peak of the cadmium currents is indicted by the arrows. Using the extrapolated peak current tended to be more reliable than direct measurement as the observed peak current was often not accurately resolved for the small currents in the presence of cadmium due to incomplete subtraction of the capacity transient.

The data points shown in figure 5.16A are the average results from 4 measurements in different cells at each concentration. The error bars are standard errors.

Figure 5.15 The effects of cadmium on calcium tail currents in two cells. The calcium current was activated by stepping to +50mV for 3ms, before returning to the test potential indicated next to each trace. The inward current during the activation pulse and the larger tail currents are the control records. The broken lines are double exponential fits to the tail currents extrapolated back to the step time. The arrows indicate the amplitudes of the fits to the tail currents in the presence of cadmium. Note that the tail current at 0mV in the presence of 60μM Cd^{2+} has a much slower time course than the control current, possibly due to slow unbinding of cadmium at this potential. In the presence of both concentrations of cadmium the calcium current was completely blocked at +50mV, and an outward non-linear leakage current is evident in these records.

Cd 60 µM

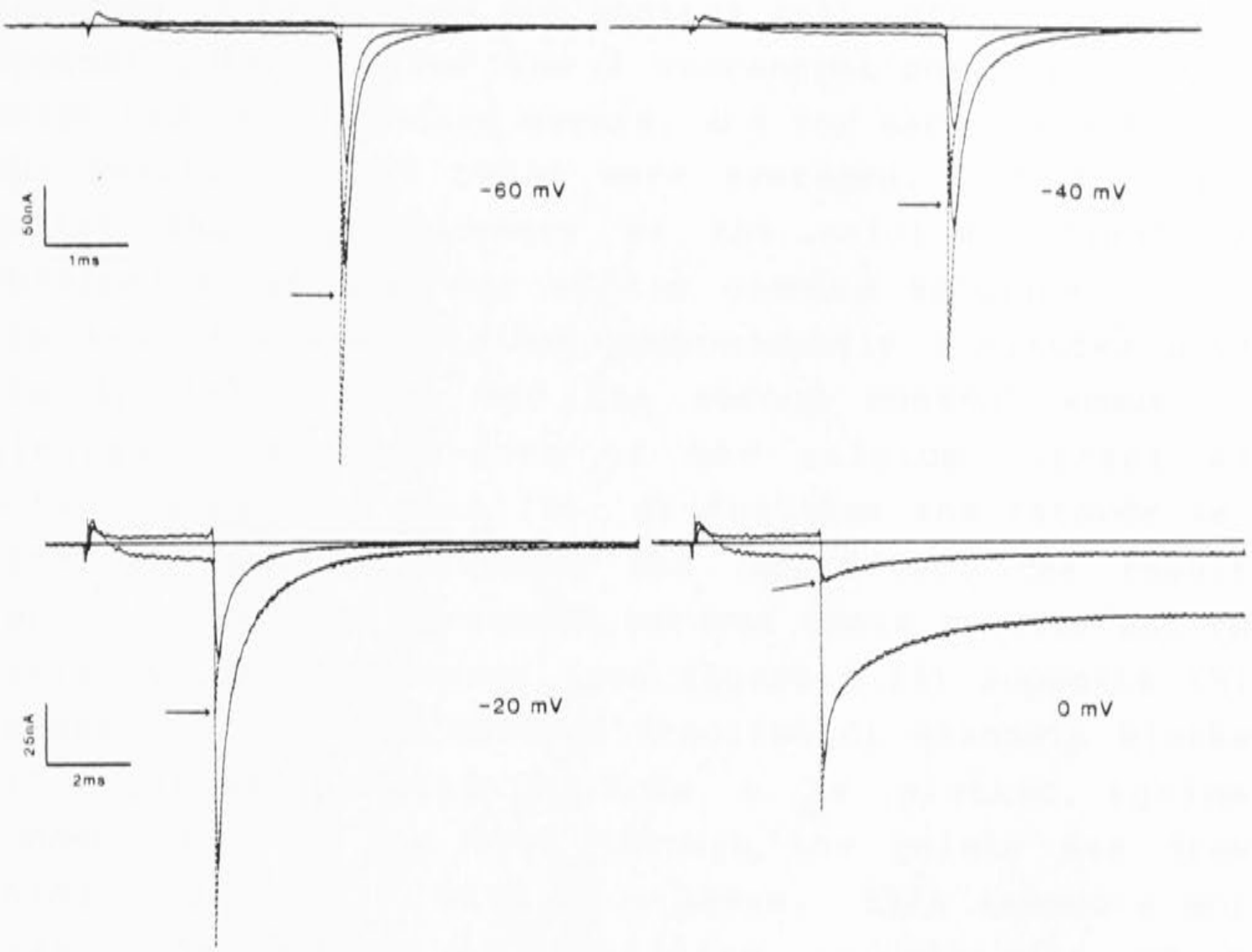

Cd 500 µM

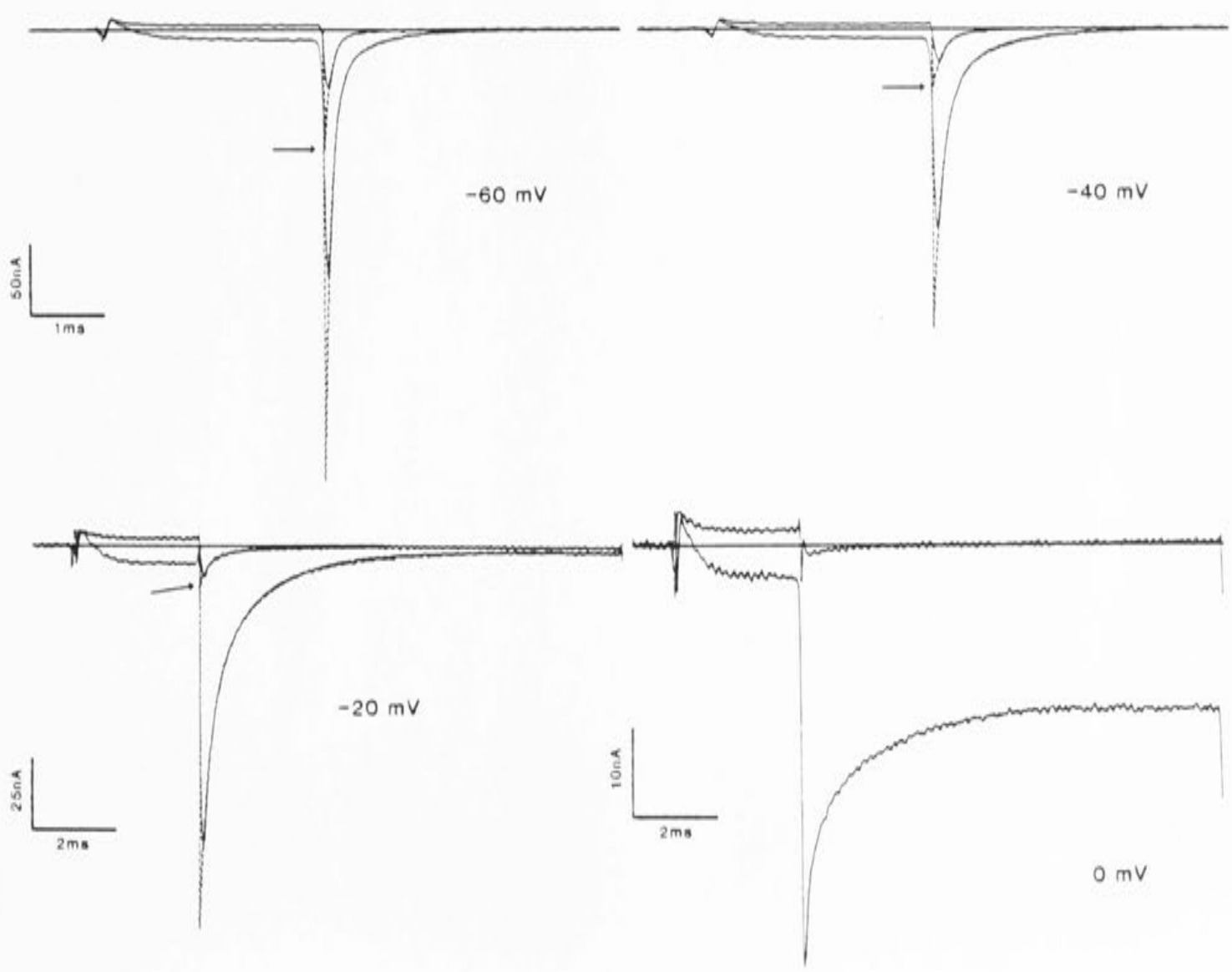

Figure 5.16 (A) The ratio of the tail current in the presence of cadmium to the control tail current is plotted against potential for the 4 concentrations tested. The error bars are standard errors, and for each concentration the results from 4 cells were averaged. In all cases better than 75% recovery of the calcium current was obtained after wash-out of the cadmium solution. Since the test I-V was obtained approximately 3 minutes after the initial control and the second control about 3-4 minutes later, run-down of the calcium current was considerably less than 75% at the time the records were obtained, and so probably did not affect the results unduly. The good agreement between these results and the single pulse experiments (see figure 5.14) supports this assertion. (B) The maximum fraction of channels blocked at negative potentials from A is plotted against concentration. The line through the points was drawn using equation 5.2, with K_d = 106μM. This seemed a more reasonable method of obtaining an estimate of K_e (equation 5.4) than simply averaging the values in table 5.1.

A

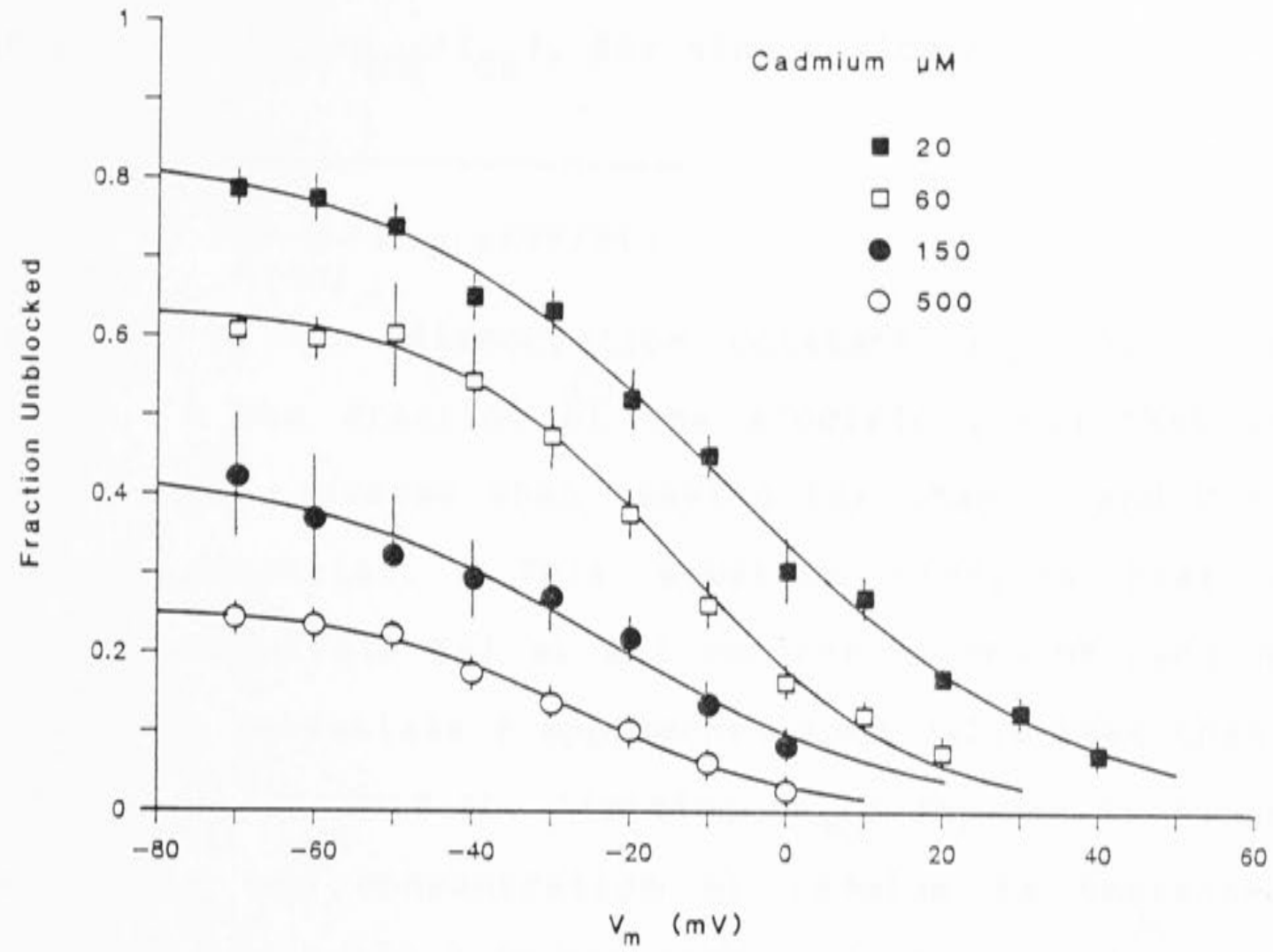
Cadmium µM
20
60
150
500
Fraction Unblocked
1
0.8
0.6
0.4
0.2
0
−80
−60
−40
−20
0
20
40
60
V_m (mV)

B

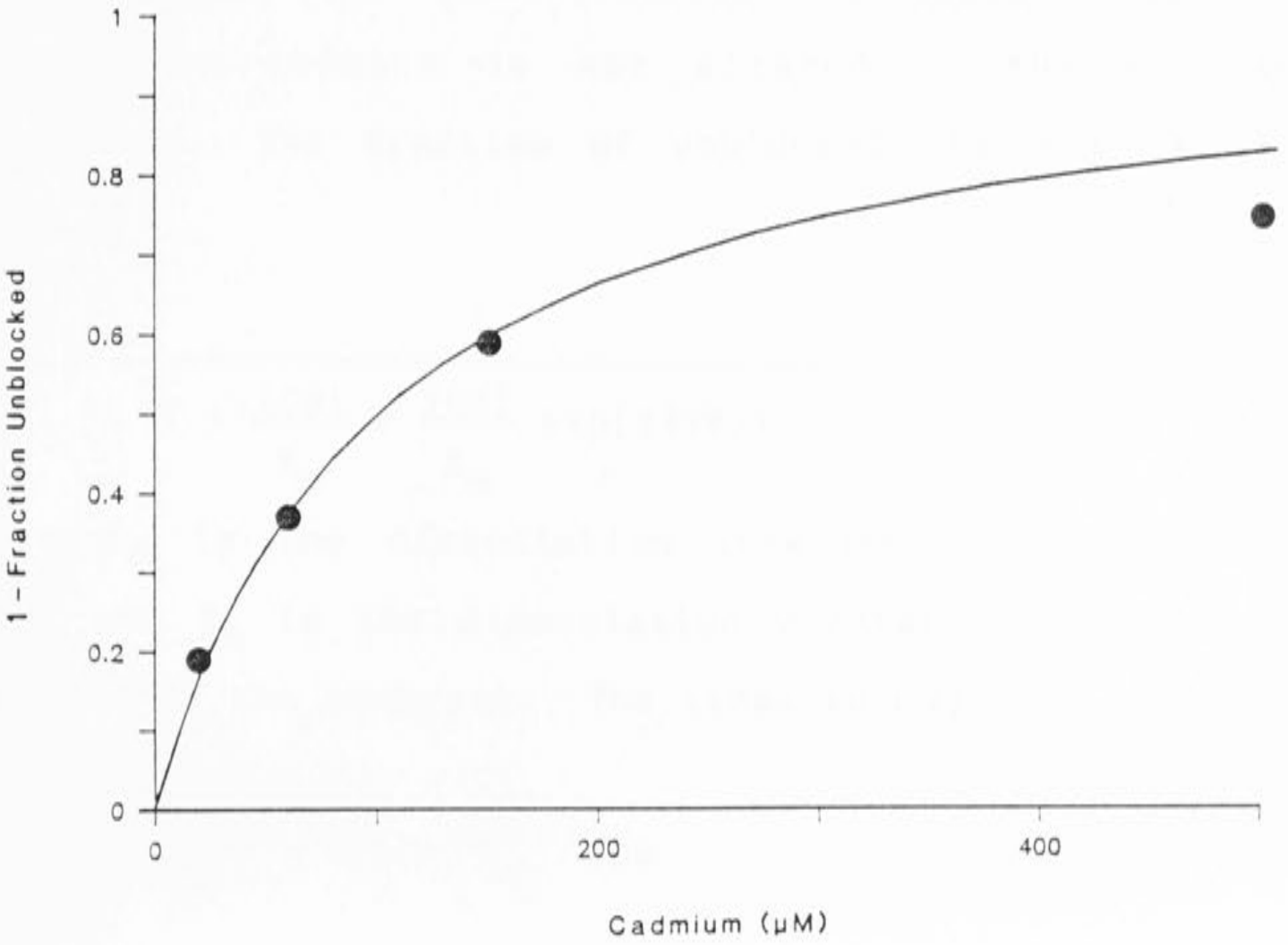
1 - Fraction Unblocked
1
0.8
0.6
0.4
0.2
0
0
200
400
Cadmium (µM)

The cadmium data cannot be described by assuming voltage dependent binding to a single site. The fraction not blocked ($F = I_{Cd}/I_{Ca}$), for single site models is,

$$F = \frac{1}{1 + \frac{K_d}{[Cd]} \exp(z\delta VF/RT)} \qquad ..(5.3),$$

where K_d is the dissociation constant at 0mV, z the valence, δ the fraction of the electric field that the cadmium ions traverse when leaving the channel and V the membrane potential. This equation predicts that at negative potentials F→1 at all concentrations of cadmium. At negative potentials F approaches some value less than 1 in figure 5.16A, and the limiting ratio appears to become smaller as the concentration of cadmium is increased. Therefore equation 5.3 is not applicable to this data.

The simplest alternative model is to assume that cadmium blocks the calcium channel by binding to two independent sites, one within the electric field of the membrane, and the other outside the field, where the binding of cadmium is not altered by the membrane potential. The fraction of unblocked channels is then given by,

$$F = \frac{1}{1 + \frac{[Cd]}{K_e} + \frac{[Cd]}{K_m} \exp(z\delta VF/RT)} \qquad ..(5.4),$$

where K_e is the dissociation constant of the external site, and K_m is the dissociation constant at 0mV of the site within the membrane. The lines through the points in

figure 5.16A were obtained by fitting equation 5.4 to the data using the LMM algorithm. If this two site model is reasonable then the parameters K_e, K_m and δ should be the same at each concentration. The values obtained are shown in table 5.1.

At very negative potentials equation 5.4 reduces to equation 5.2 with K_d replaced by K_e, and so plotting the maximum F values in figure 5.16A versus concentration is approximated by equation 5.2. This is shown in figure 5.16B, with K_e = 106µM, and gives some idea of of the error involved in the K_e measurement. The point at 500µM is lower than expected possibly due to the errors involved in measuring the small currents at this concentration.

Table 5.1
Parameters in equation 5.4 estimated from the data in figure 5.16A. The dissociation constants are given in micromolar. Approximate standard errors produced by the fitting routine are included.

[Cd] µM	K_e ± SE	K_m ± SE	δ ± SE
20	100 ± 16	12 ± 1	0.60 ± 0.04
60	106 ± 7	15 ± 1	0.87 ± 0.06
150	114 ± 18	19 ± 4	0.67 ± 0.14
500	172 ± 5	18 ± 2	0.92 ± 0.06

The cadmium block seems to be well described by assuming two independent binding sites, one with a K_d of around 106µM, and the other with a K_d of 16µM at 0mV and voltage sensitive binding equivalent to a divalent charge moving across approximately 75% of the electric field of the membrane.

5.4 Cadmium affects the kinetics of calcium channels

The final observation to be made in this section concerns changes in the kinetics of the calcium currents produced by cadmium at potentials positive to 0mV. Three examples recorded at the potentials indicated are shown in figure 5.17. The bottom trace in each example is the control record. The top traces show the currents recorded in 20 micromolar cadmium. The broken lines are the relaxations expected if the cadmium had no effect on the kinetics of the current flow, and were produced by scaling down the control traces. At 0mV the effect is not great although there is a slight slowing of the decay rate. At 10mV the rapid closure of channels has disappeared in the presence of cadmium, and the trace is almost flat. The records at +20mV indicate that there is a slight outward relaxation in the presence of 20μM Cd^{2+}. Similar changes in the kinetics were seen in 60μM Cd^{2+} at 0 mV (see figure 5.15).

The most obvious explanation for the effect is that the rate of unblocking of the channels is comparable to the relaxation time constants at these potentials. Further evidence consistent with this interpretation is given below. The +10mV trace is particularly useful. In this case the trace in the presence of cadmium is almost flat. This suggests that the rate of unblocking of the channels is equal to the rate of closure of the channels at +10mV, and that these two exponential relaxations

Figure 5.17 Tail currents recorded in the presence of 20μM Cd^{2+}. The calcium current was activated by stepping to +50mV for 3ms, and returning to the test potentials indicated. The broken lines show the control relaxations scaled down to overlie the current recorded in cadmium solution. In each case the time course of the current relaxation is slowed and the initial fast relaxation is reduced, an effect that is most obvious at +10mV.

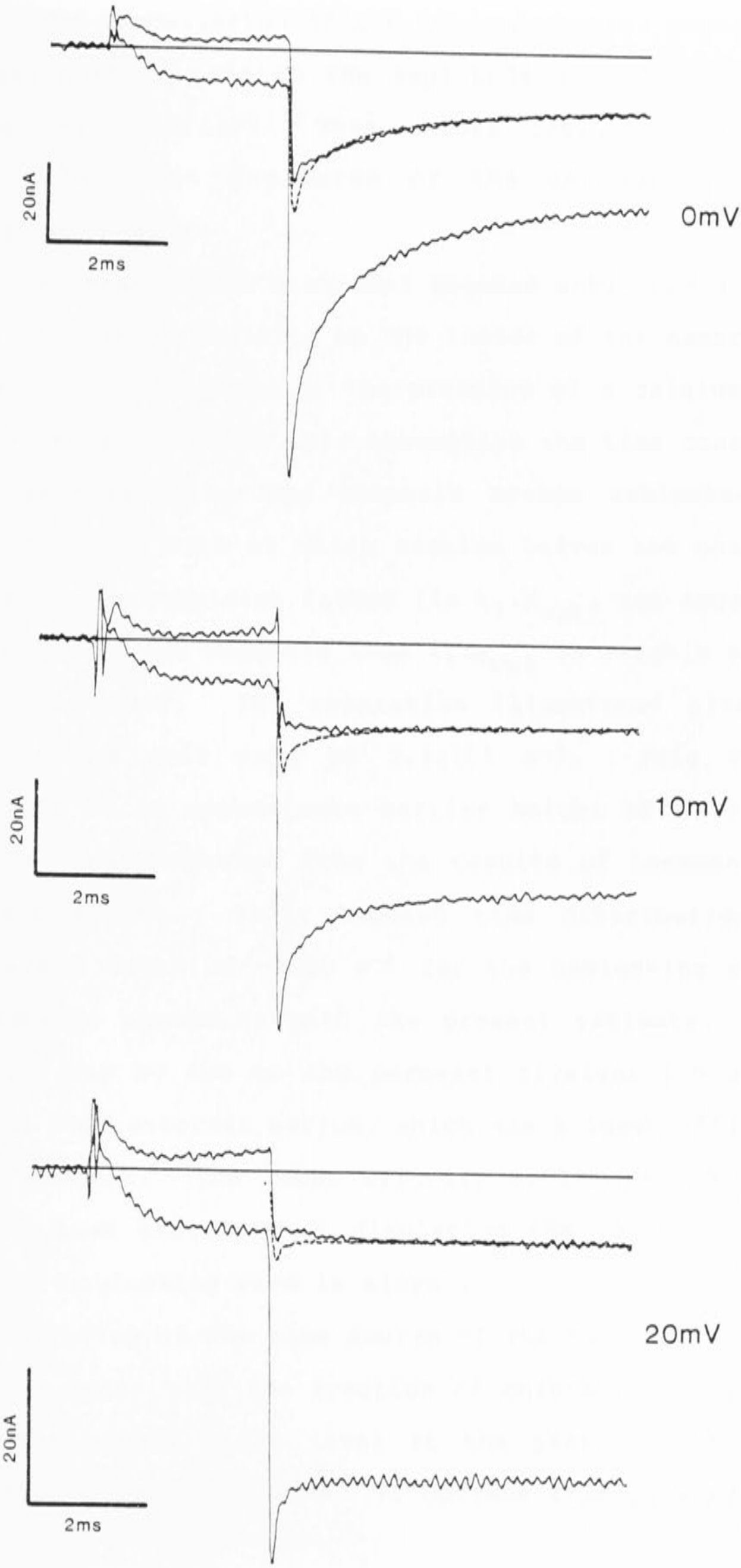
20nA
2ms
0mV
20nA
2ms
10mV
20nA
2ms
20mV

cancel. The cancellation of the two exponential processes is almost perfect, and so the amplitude and time courses must be very similar. This rather fortuitous result allows some rough estimates of the unblocking rate constant to be made.

It is assumed that a channel becomes unblocked when a cadmium ion leaves the site on the inside of the membrane, and that it is displaced by the presence of a calcium ion in the outer site. With this assumption the time constant of the relaxation as the channels become unblocked is dominated by the rate at which cadmium leaves the channel multiplied by a repulsion factor (ie $k_5 . R_{out}$, see Appendix 3). The above data suggests that $k_5 . R_{out}$ is roughly equal to $1/\tau_f$ at +10mV. The relaxation illustrated gives a value for the exit rate of 3.3×10^3 s^{-1}. This value corresponds to an approximate barrier height of 21.3 RT, lower than that expected from the results of Lansman and co-workers (1986). Their blocked time distribution at -20mV gave a value of ~2000 s^{-1} for the unblocking rate, in reasonable agreement with the present estimate. The difference may be due to the permeant divalent ion used. They used 50mM external barium, which has a lower affinity for the channel. The lower affinity will mean that the barium is less efficient at displacing the cadmium ions, and so the unblocking rate is slower.

The slowing of the time course of the calcium current by cadmium means that the fraction of channels blocked is not at the steady state level at the peak of the tail currents at potentials >0mV. To obviate this problem the

measurements of the proportionate block at 0mV and above presented in figure 5.16A were obtained from measurements of the steady state inward current. The rate constants of the tail currents at the negative potentials were unaffected by cadmium ions, as would be expected for the steep potential dependence of the relief of block. Figure 5.18 shows a plot of the fast rate constant versus potential in 60μM cadmium. Only the values at -20mV & -10mV appear to differ from the control values. Thus the estimates of proportionate block by extrapolation should be reliable.

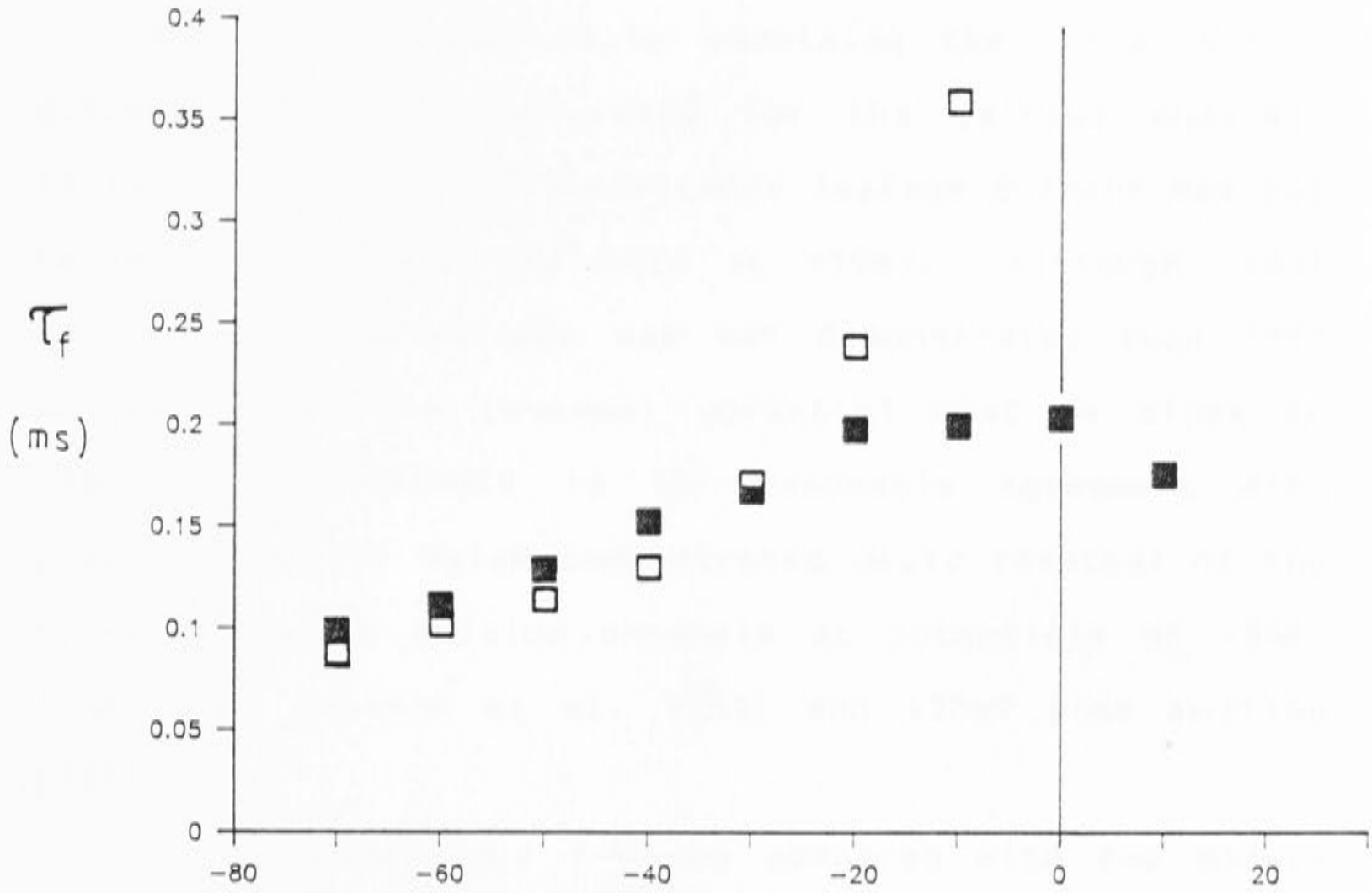

Figure 5.18 The solid symbols show the fast tail current time constant recorded in control. The open squares are the fast time constant recorded in the presence of 20μM Cd^{2+}. For most of the potential range the fast time constant is unaffected by cadmium, but there is some divergence at -20 and -10mV. There may have been a significant contribution to the tail current relaxations by slow unblocking events at these potentials.

Discussion

(i) Voltage sensitivity of the instantaneous I-V

The chapter started by examining the instantaneous current voltage relationship for the calcium channel. In two cells where the non-linear leakage current was not large, the current was zero at +70mV. Although clear reversal of the current was not demonstrated such data suggests that the reversal potential must be close to +70mV. This result is in reasonable agreement with previous results which demonstrated clear reversal of the current through calcium channels at potentials of +56mV (1mM Ca^{2+}, Fenwick et al. 1982) and +70mV (Lee & Tsien 1984).

The instantaneous I-V was compared with two models for calcium channel permeation. The only question that can be addressed directly is whether the voltage sensitivity of the I-V is accounted for by these models. The voltage sensitivity of the single channel I-V was described more accurately by the Hess & Tsien model. The energy profiles proposed for the calcium channel differ quite considerably. On one point they agree quite closely, and this is the proposed well depth for calcium ions (-15 and -14.5 RT). These values were assigned because the sodium flux through the calcium channel was half blocked by <1μM external calcium ($\Delta G = -RT\ln(K_d)$).

In assigning these values both studies ignored the

possible effects of negative fixed surface charges on the neuronal membrane. The surface potential produced by these charges is neutralized by screening as well as direct binding by monovalent and divalent ions (Eisenberg, Gresalfi, Riccio & McLaughlin 1979, McLaughlin, Mulrine, Gresalfi, Vaio & McLaughlin 1981). At physiological concentrations, divalent ions are mainly responsible for screening surface charge (McLaughlin et al. 1971), and for this reason, surface charge effects become particularly large at low divalent concentrations. The surface charge potential (ψ_s) will increase the concentration of divalent ions near the surface more effectively than monovalent ions, according to the equation,

$$c_m = c_b \exp(-z\psi_s F/RT) \qquad \ldots (5.5)$$

where z is the valence of the ion, c_b is the bulk concentration and c_m is the concentration near the surface of the membrane. This equation suggests that ψ_s will preferentially increase the surface concentration of calcium ions over the monovalent ions present, and increase the apparent affinity of the channel for calcium ions. A few calculations will put this into perspective.

Wilson, Morimoto, Tsuda & Brown (1983) proposed a maximum surface charge density, σ_s, of 1 $e^-/80Å^2$ and a limiting ψ_s = -116mV for the surface membrane of molluscan neurones (Helix Aspersa). The σ_s estimate compares favourably with measurements in other neural preparations (see Ohmori & Yoshii, 1977 for references). ψ_s will approach the limiting value (-116mV) at

micromolar external divalent ion concentrations (Wilson et al. 1983, figure 1) and such a surface potential will increase the calcium concentration at the surface of the membrane by 255 fold (using equation 5.5). The effect may not be as large as this. If one assumes that the mouth of the channel lies in the centre of an uncharged disc with a radius of 1 Debye, then the approximate reduced ψ_s at the centre of the disc will be given by equation 6 of Apell, Bamberg & Lauger (1979). In this case the calcium concentration at the mouth of the channel will be increased 30 fold. These calculations suggest that the calcium concentration at the mouth of the channel may be one or two orders of magnitude higher than the bulk concentration and indicate that the actual affinity of the calcium channel for calcium may be much lower than previously supposed.

The two models proposed rather different values for the external barrier height. On the one hand Almers & McCleskey suggested a value of 10.8 RT while Hess & Tsien suggested a value of 4.5 RT (estimated from the diagram in figure 4, Hess & Tsien 1984). The minimum height of the outside barrier must be set by the rate at which ions can diffuse into a hypothetical hemisphere (reaction target) at the channel mouth. It is assumed that any ion which enters this reaction target also enters the channel. The equation is,

$$k_{in} = 2\pi rcND_{Ca} \quad \text{ions/s},$$

where r is the capture radius (radius of the hemisphere),

D_{Ca} is the diffusion coefficient for calcium (D_{Ca} = $8x10^{-6}$ cm^2/s, Wang 1953) c is the concentration of calcium and N is Avogadros constant. Almers & McCleskey assumed a value of r = 3Å, giving a minimum equivalent external barrier height of 7.6 RT for c = 3.4mM (υ = kT/h). The capture radius of 3Å is about 3 crystal radii (Pauling 1948), and seems a reasonable value for a single file channel. The external barrier height suggested by Hess & Tsien is perhaps lower than expected for diffusion limited access to the channel. An external barrier of 4.5 RT (with c = 3.4mM) implies a capture radius of 66Å, which seems a little implausible.

The final point is the choice of electrical distances used. The basic difference between the models was the assignment of voltage sensitivity to the entry of ions to the channel. The Almers & McCleskey model had a low voltage sensitivity for the entry rates, similar to previous work on the gramicidin channel (Levitt 1978, Urban, Hladky & Haydon 1978). The present data would appear to imply that the entry of calcium has a high voltage sensitivity. The I-V predicted by the Almers & McCleskey model does not fit the data as well, due to a drop in the channel occupancy at negative potentials as the rate of entry becomes diffusion limited. However, the data does not necessarily imply that the entry of ions into the channel must have a high voltage sensitivity. A modified model with low voltage dependence of ion entry fits the data reasonably well (figure 5.19). For this fit the two energy wells are shallower than the previous

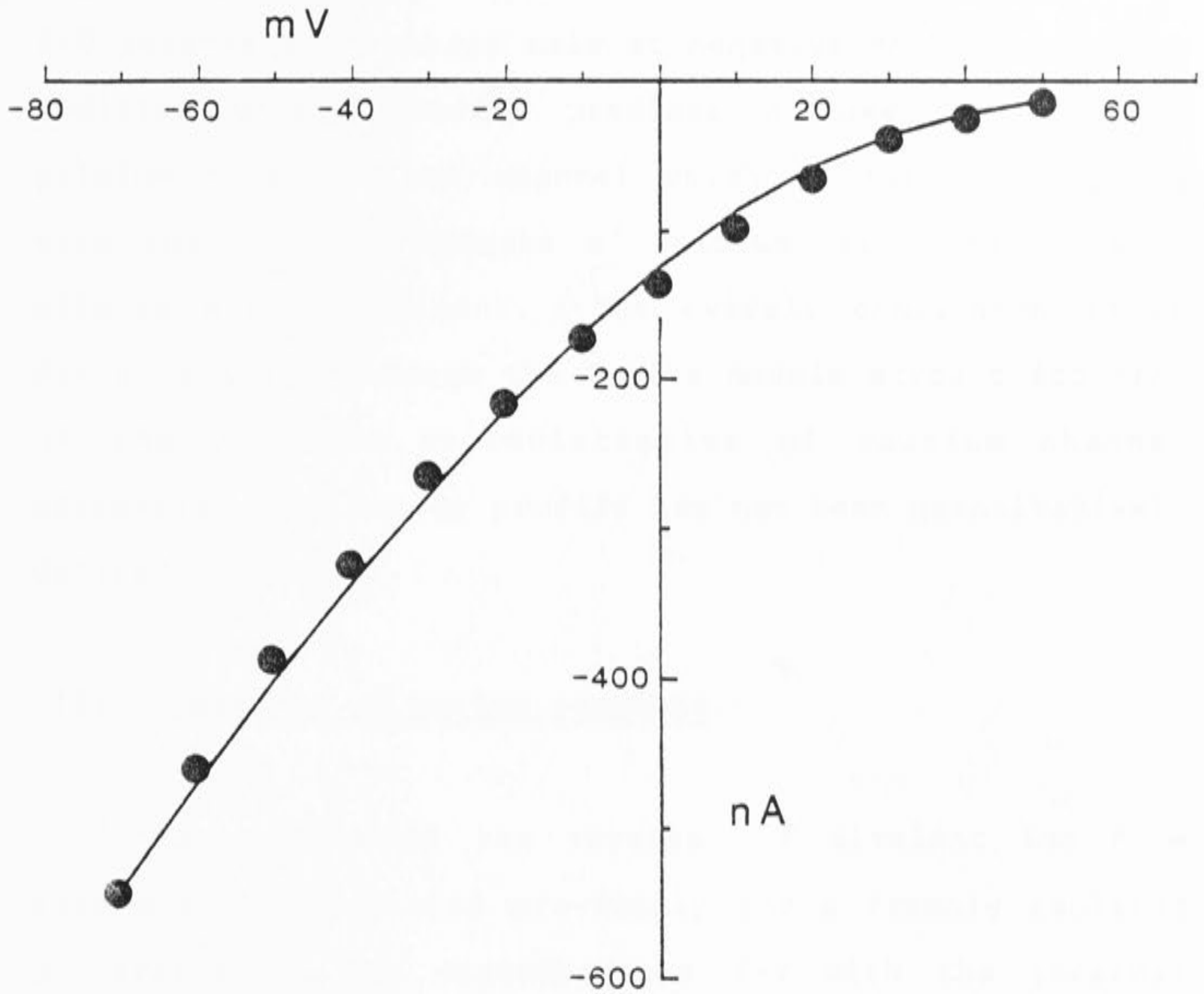

Figure 5.19 This figure shows the fit to the data of a two site model with low voltage sensitivity of the entry rate constants. The energy profile used to produce the fitted line is shown in figure A3.3.

models and the repulsion factor is reduced. These two modifications increased the occupancy of the channel at negative potentials, and thus reduced the curvature of the I-V towards the voltage axis at negative potentials. The modified energy profile predicts a lower affinity of calcium ions for the channel which is not inconsistent with the blocking effects of calcium, if surface charge effects are significant. The overall conclusion to be drawn is that although the 2-site models account for many of the observed characteristics of calcium channel permeation, the energy profile has not been quantitatively defined.

(ii) Reversal of barium currents

Measurements of the reversal of divalent ion flow have not been reported previously for a freshly isolated preparation. The instantaneous I-V with the internal barium showed a sharp rectification. The outward current appeared to saturate at positive potentials, but this did not appear to be due to a reduction in the number of active channels. Mechanisms which produce such effects can be divided broadly into three groups.

1) Voltage dependent changes in the kinetics of the channel activity. This includes any proposed event which reduces the amount of time the channel spends open, by the formation of an additional kinetic state. Such events would be evident as rapid flickering in single channel records. For example there may be voltage dependent block

of the channel by an internal molecule.

2) Voltage dependent reduction in the ion flux through the channel. In this case the single channel current would be reduced, with no changes in the kinetics of the channel activity. The curvature of the I-V may then be due to the asymmetry of a static permeation energy profile, or to voltage dependent fluctuations in the energy barriers or wells (see Lauger 1984,1985) of the permeation energy profile.

3) Depletion of permeant cations around the internal mouth of the channel. This is probably not a factor since the single channel conductance is small and the whole cell current in this case is small.

The results presented are preliminary and it is not possible to decide which of these alternatives is applicable to the data. Single channel recording might answer the question, although it is doubtful whether the time resoluton of this technique would be sufficient to decide whether rapid flickering of the channel was present. Further experiments must be done to establish the cause of the strong rectification.

An obvious possibility is that an internal cation blocks the channel in a voltage dependent manner. There is some indication that the outward current passes through a maximum in figures 5.8 & 5.10, and one might expect such an effect if there were voltage dependent block by an internal cation. It would be useful to record the barium I-V with different internal solutions, to test this hypothesis. It seems unlikely that Cs^+ ions could block

the channel by competing with barium for channel binding sites. Firstly if the general form of the two site model is correct, the monovalents would be rapidly expelled from the channel by the barium ions. Secondly, Cs^+ ions are permeable through calcium channels in other preparations.

Another possibility is that the saturation of the outward barium current is due to a direct action of the internal barium on the calcium channel. The normal steady state activation curve in figures 5.8B & 5.10B suggest that the reduction in the current produced by barium must involve a closed state that is not part of the normal activation reaction. The apparently normal tail currents also suggest the internal barium ions may be in rapid voltage dependent equilibrium with a site on the calcium channel. Occupation of this site shuts the channel. This idea could be tested by looking at the effect of changing the internal barium concentration on the barium I-V. Suggestion of such a site is not entirely arbitary. There is ample evidence that increasing the internal calcium concentration causes inactivation of the channel (Eckert & Chad 1984). The voltage dependent blocking site suggested for internal barium, could be a short lived precursor of the main inactivated state.

The two possible explanations just mentioned are included in group 1 above. They both involve the formation of another kinetic state separate from the normal activation scheme, and are useful in that they are easily tested. It seems pointless at this stage to speculate on group 2 mechanisms, until more detailed

knowledge is available on the permeation mechanism.

Reversal of the current flow through calcium channels in planar lipid bilayers has been observed previously (Ehrlich et al. 1986, Rosenberg et al. 1986). The single channel I-Vs were found to be linear over a wide potential range in symmetrical solutions of 100mM $BaCl_2$ (Rosenberg et al. 1986) indicating that cardiac sarcolemma calcium channels in lipid bilayers are symmetric with respect to current flow. Calcium channels have also been isolated from rat brain and incorporated into planar lipid bilayers (Nelson et al. 1984). The outward current flow through these channels increased linearly with potential between +20 and +100mV (Nelson et al. 1984). Thus it would appear that the rectification of the calcium channel I-V observed in this study is not a feature of the single channel I-Vs recorded in lipid bilayers. The calcium channels isolated from rat brain synaptosomes were different in some respects to those recorded in cat DRG neurones. The kinetics were much slower, and they did not appear to be as labile as the calcium channels in freshly isolated, perfused cells. Much higher concentrations of cadmium were required to block these calcium channels (K_d = 9.3mM, Nelson 1986). Therefore it seems that the calcium channels isolated from rat brain synaptosomes are not comparable to those recorded in cat DRG neurones.

(iii) Cadmium block

The observed dissociation constants of cadmium from the calcium channel agree well with previous observations

in molluscan neurones (Byerly et al. 1985). The present results produced strong evidence for the existence of two binding sites for cadmium, one within the electric field of the membrane, and one external to this field. In the discussion that follows, the results are related to permeation models for the calcium channel which include two binding sites for divalents.

The model, suggested by Kostyuk and co-workers (1983), may be applicable the present results. Their model was proposed to explain the block of the sodium flux through calcium channels in molluscan neurones at low concentrations of external calcium. They proposed two cation binding sites on the calcium channel. One within the channel, the permeation site, and one on the external face of the channel, the selectivity controlling site. The external site was supposed to bind micromolar concentrations of calcium, and through a conformational change, block the sodium flux through the channel.

In terms of this model the cadmium block might be explained if the cadmium competed with calcium for the 2-sites. The voltage sensitive block would be produced as cadmium bound to the site within the membrane, but passed through the channel at negative potentials. The voltage independent block would result from cadmium binding to the external site and, through a conformational change, blocking the flux of calcium through the channel. The anomalous mole fraction effects observed with mixtures of calcium and barium would presumably have a similar explanation.

Single channel data does not appear to be consistent with this type of model (Lansman et al. 1986), and these authors have argued in favour of a 2-site 3-barrier model. The calculations of Levitt (1978) would suggest that a 2-site model is a minimal model for a channel where the dielectric constant within the channel is lower than the external bulk solution. They also indicate that the potential drop down the length of the pore is very close to linear, when the radius of the pore is much less than the length. If these two conditions hold for the calcium channel, the membrane potential will decrease linearly from the mouth of the channel and the two binding sites will be within the electric field of the membrane. The two binding sites proposed for calcium result in two apparent binding constants. One with high affinity for calcium (K_d~μM) when the channel is occupied by a single ion, and the other with much lower affinity (K_d~mM) due to binding of two ions within the channel, with significant repulsion between the ions. The voltage independent component of block produced by cadmium seems to be inconsistent with such a model, since it suggests that one of the cadmium binding sites is external to the membrane electric field.

(iv) Is cadmium block consistent with a 2-site model ?

Equation 5.4 seemed to describe the data fairly accurately, and suggests that cadmium interacts with two independent binding sites on the calcium channel. In this

section a possible physical interpretation of the two binding sites is presented. In essence, the two internal sites of the 2-site 3-barrier models are approximated by a single voltage dependent binding site and an additional voltage independent binding site is proposed to exist at the mouth of the channel.

Assuming that the two sites are independent, then it is suggested that the voltage sensitive term in equation 5.4 reflects interaction of cadmium ions with the binding sites of a 2-site model. Can the voltage dependence of cadmium block be explained by a 2-site model ? To answer this question, qualitatively at least, simulations were performed to see whether the 2-site model could reproduce the steep voltage dependent relief of block observed. The energy profiles used for calcium and cadmium are shown in figure A3.3. Cadmium block was modelled by assuming that the energy barriers were same for the two ions, but that cadmium had a much higher affinity for the external site than did calcium. The depth of this well was set so that the proportionate block at 0mV was the same as that observed (figure 5.16A). Asymmetry of the two binding sites for cadmium was essential to produce steep voltage dependence. The voltage sensitivity of the entry rate for cadmium also had a significant effect on the voltage sensitivity, and d1 for cadmium (see figure A3.3) was reduced slightly to produce the desired slope. The simulation for the model with 20µM cadmium and 10mM calcium is shown in figure 5.20A. The solid curve shows the simulation and the broken line was produced using

Figure 5.20 The fraction of channels unblocked (F) plotted against the test potential. (A) The solid curve was produced using the cadmium blocking model illustrated in Appendix 3, figure A3.3. The broken line was the best fit of equation 5.3 to the simulation, and demonstrates that the voltage dependent component of cadmium block, predicted by a 2-site model, can be approximated by a single voltage sensitive binding site. (B) The solid lines show the predicted fraction of channels unblocked at the four concentrations used. The data is replotted from figure 5.16A. The agreement between the data and the model is fairly good, considering the values for the energy profile in figure A3.3 were assigned in order to fit the 20μM Cd^{2+} data by eye.

A

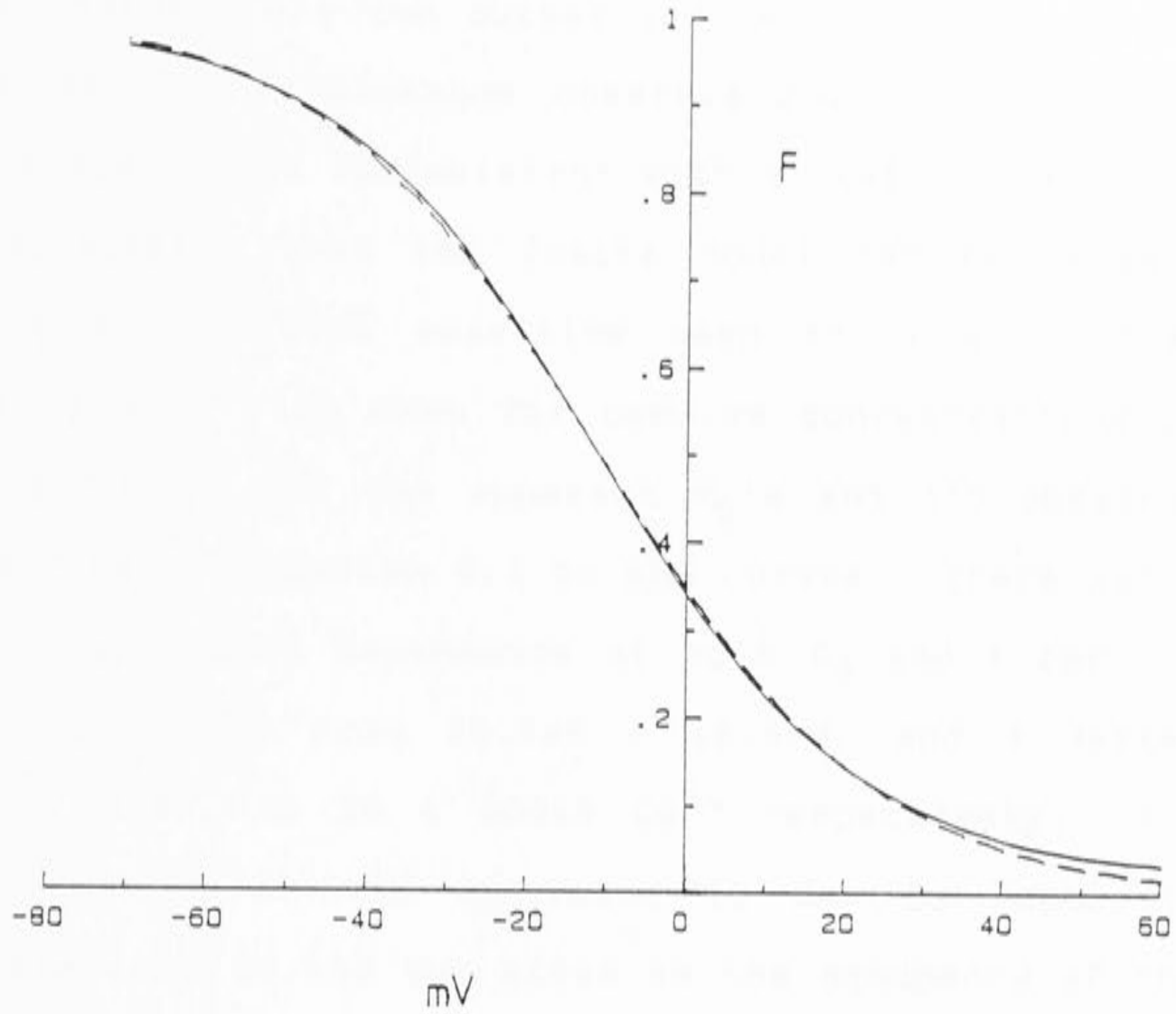

B

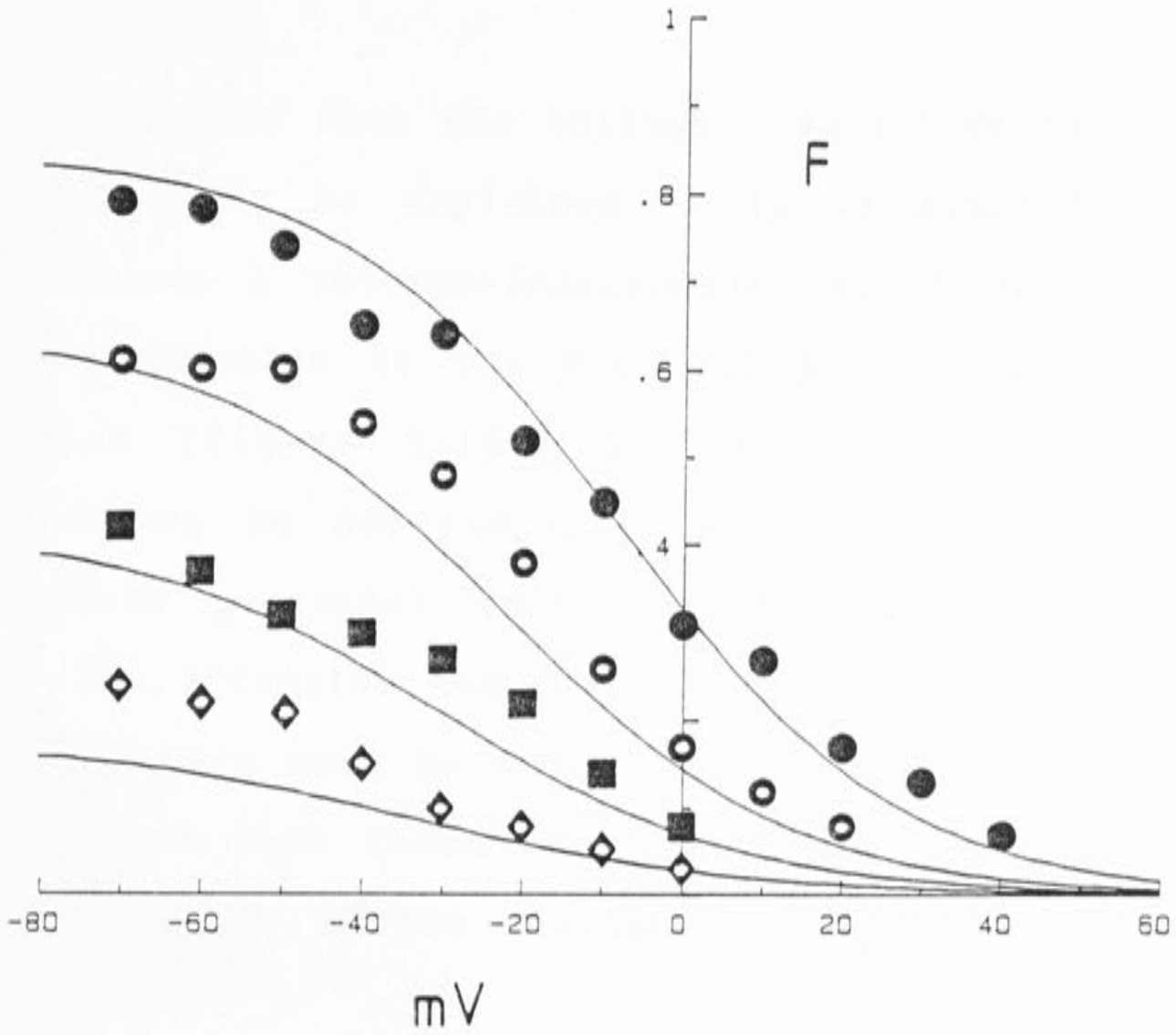

equation 5.3, with K_d = 11μM and δ = 0.72. The good agreement between the two curves indicates that the large apparent electrical distance observed for the relief of cadmium block is not inconsistent with a 2-site model. It also demonstrates that the 2-site model can be approximated by the voltage sensitive term in equation 5.4. Simulations were also done for cadmium concentrations of 60, 150 & 500μM, and the apparent K_d's and δ's obtained from LMM fits of equation 5.3 to the curves. There was a slight concentration dependence of both K_d and δ for the model; K_d varied from 10.8μM - 16.9μM, and δ varied from 0.72 -0.62, in 20 & 500μM Cd^{2+} respectively. The slight reduction in the K_d value is due to repulsion between the ions in the two sites as the occupancy of the channel is raised at higher cadmium concentrations. The higher occupancy also causes an apparent increase in δ, as the channel is less likely to be cleared of cadmium at negative potentials.

It is proposed that the voltage insensitive term in equation 5.4 might be explained if it is assumed that cadmium produces a voltage-independent reduction of the calcium concentration at the mouth of the pore, with a K_d of 106μM (figure 5.16B) in 10mM calcium. The reduction cannot be due simply to screening of the external surface potential (Muller & Finkelstein 1974), since the low effective concentrations of cadmium would suggest that there must be some binding to the membrane. It is suggested that there are divalent cation binding sites at the mouth of the calcium channel, outside the

electric field of the membrane, which effectively raise the local concentration of permeant ions.

External cadmium would be expected to reduce the single channel current, since a reduction in the external calcium concentration is equivalent to increasing the external barrier height. Lansman et al. (1986) recorded the effects of 20μM cadmium on the single channel current in heart cells. The results presented here suggest that they should have observed a 20% reduction in the amplitude of the single channel currents. This effect was not reported, but might easily have been missed due to the numerous rapid blocking and unblocking events. In the same study, magnesium reduced the single channel current and this was attributed to very rapid blocking events. The present results suggest that the effect may have been partially due to a reduction in the external permeant ion concentration.

To answer the question posed in this section; a 2-site model can describe the data at least qualitatively, when an external binding site is included. The solid curves in figure 5.20B were produced using equation 5.4, K_e was set to 106μM. K_m and δ were set from the fits of equation 5.3 to the 2-site simulations at each concentration. The lines are qualitatively consistent with the data, although they deviate considerably from the data points at higher concentrations. A closer fit might have been obtained by varying the energy profiles in figure A3.3, however this point does not seem worth pursuing until more definite information is available on the energy

profile for the calcium channel.

Previous results are consistent with the presence of low affinity cation binding sites at the mouth of the calcium channel. The observation of Almers & McCleskey (1984), that cobalt and cadmium were no more effective at blocking the sodium current through the calcium channel than the calcium current may be consistent with the model, assuming that the external sites are weakly selective for cations in skeletal muscle. Magnesium and cobalt block calcium channels with low voltage sensitivity (Byerly et al. 1984, Lansman et al. 1986), and both these ions also bind water very tightly, and have long dipole relaxation times (Hille 1984). The major blocking effects of these ions may be at the external binding site which would explain the weak blocking effects of these ions, and the lack of significant voltage dependence of the block.

Permeation through the calcium channel may involve a 2-step dehydration process similar to that proposed for the gramicidin channel (Eisenman, Sandblohm & Neher 1978). The outer sites may contain partially hydrated permeant ions, which must exchange most of their water molecules with polar groups at the high affinity binding sites within the channel before they can pass through the channel. This would account for the very high affinity of the calcium channel for permeant divalent ions, and the low permeability of divalent ions with long (Mg^{2+} & Co^{2+}) and intermediate (Mn^{2+}, Akaike, Nishi & Oyama 1983, & Zn^{2+}, Kawa 1979) dipole relaxation times.

Chapter 6.

Two sodium currents

Introduction

TTX-insensitive, sodium-dependent action potentials have been observed in cultured mouse (Matsuda et al. 1978, Heyer & Macdonald 1982) and rat (Baccaglini & Cooper 1982) sensory neurones and in freshly isolated mouse (Yoshida et al. 1978) and cat (Gallego 1983) sensory neurones. A TTX-insensitive sodium current which may underlie these action potentials has also been recorded in sensory neurones (Kostyuk, Veselovsky & Tsyndrenko 1981, Bossu & Feltz 1984, Ikeda et al. 1986). The TTX-insensitive sodium current differs from the more common TTX-sensitive sodium current in three respects : 1) The time course of activation and inactivation is slower for the TTX-insensitive sodium current (slow sodium current), than for the TTX-sensitive current (fast sodium current). 2) The slow sodium current has a higher threshold than the fast sodium current, and the peak I-V is shifted to more positive potentials. The steady-state inactivation also occurs over more positive potentials for the slow sodium current (Kostyuk et al. 1981b). 3) It is also apparent that the slow sodium current is blocked by external Cd, Co & Mn ions. Bossu and Feltz (1984) found that 100µM Cd^{2+} was enough to block the current, Ikeda and coworkers found

that 500μM produced a 50% block. Kostyuk and co-workers (1981b) found that 5mM Co^{2+} & Mn^{2+} reduced the current to less than 50% of the control level.

This section demonstrates the existence of a transient inward current in cat DRG neurones, which appears to be similar to the TTX-resistant current recorded previously. Gallego (1983) found evidence for a TTX-insensitive sodium action potential potential in cat DRG, which suggests that the current should be present in these neurones. The present results also indicate that there are marked differences in the selectivity of the fast and slow sodium currents for monovalent cations, and suggest that the sensitivity of the slow sodium current to cadmium ions is lower in this preparation, than has been observed previously.

Results

Sodium currents were recorded using 115mM NaCl externally, and 20mM NaCl internally. The calcium currents were blocked using either 1mM$CdCl_2$ or by replacing the external $CaCl_2$ with $CoCl_2$. The lower trace in figure 6.1A shows the currents recorded in one cell with 10mM $CaCl_2$ externally. The membrane potential was stepped from -50 to +10 mV for 10ms. There is an initial rapidly activating sodium current superimposed on the more slowly activating sustained calcium current. The large fast calcium tail current is observed on repolarization. The calcium current was blocked by perfusing 1mM $CdCl_2$.

The middle trace (b), shows the fast, rapidly inactivating sodium current observed during a similar voltage jump. Finally, 0.3 µM TTX was perfused, and this sodium current disappeared (c). The small residual tail current was probably due to the voltage sensitivity of the cadmium block.

Figure 6.1B shows the isolation of the slow sodium current in the presence of 0.3µM TTX. The lower trace (a), shows the calcium current recorded when the membrane potential was stepped to +10mV. This current appears to inactivate slightly during the 10ms pulse, which is uncharacteristic of this current. When the 10mM external calcium was replaced by $CoCl_2$, the upper trace (b) was recorded using an identical voltage step. This residual, transient current is the slow (TTX-insensitive) sodium current.

The slow sodium current has properties similar to other voltage activated currents. In particular, there is an initial delay before the activation of the current after a voltage step. This is shown in figure 6.2. The currents were elicited by stepping from -50mV to the potentials indicated. Notice that the trace is initially flat for about 200µs after the capacitive artifact at 0mV, and that this delay becomes shorter as the membrane potential is stepped to more positive potentials. This delay is generally interpreted as evidence for more than one closed state preceding the open state(s) (Armstrong 1981).

The voltage sensitivity of the two sodium currents is

Figure 6.1 (A) Separation of the calcium and sodium currents. The control pulse to +10mV (a) shows the rapid activation and inactivation of the sodium current, followed by the slower calcium current. The large rapidly decaying calcium tail current is seen upon repolarization. 1mM $CdCl_2$ blocks the calcium current and leaves the transient sodium current (b). This sodium current is completely suppressed by 0.3µM TTX (c). The slow sodium current is not present in this cell. (B) Currents recorded in another cell. The fast sodium current is suppressed by 0.3µM TTX. The inward current during the control pulse is dominated by the calcium current which appears to inactivate during the 10ms pulse. Replacing the external calcium with cobalt reveals the presence of a slow transient current. This is tentatively identified as the slow sodium current.

A

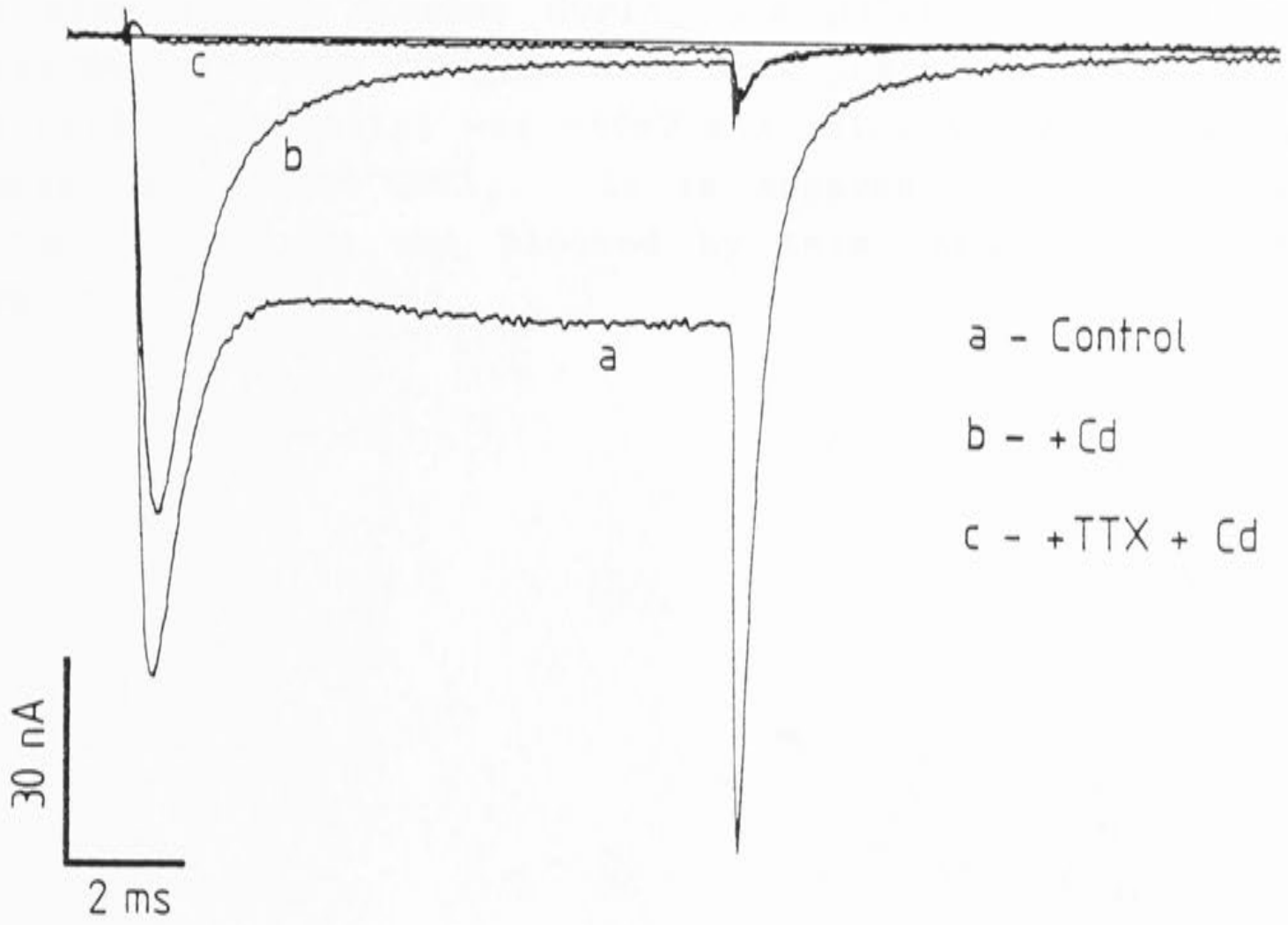
c
b
a
a - Control
b - + Cd
c - + TTX + Cd
30 nA
2 ms

B

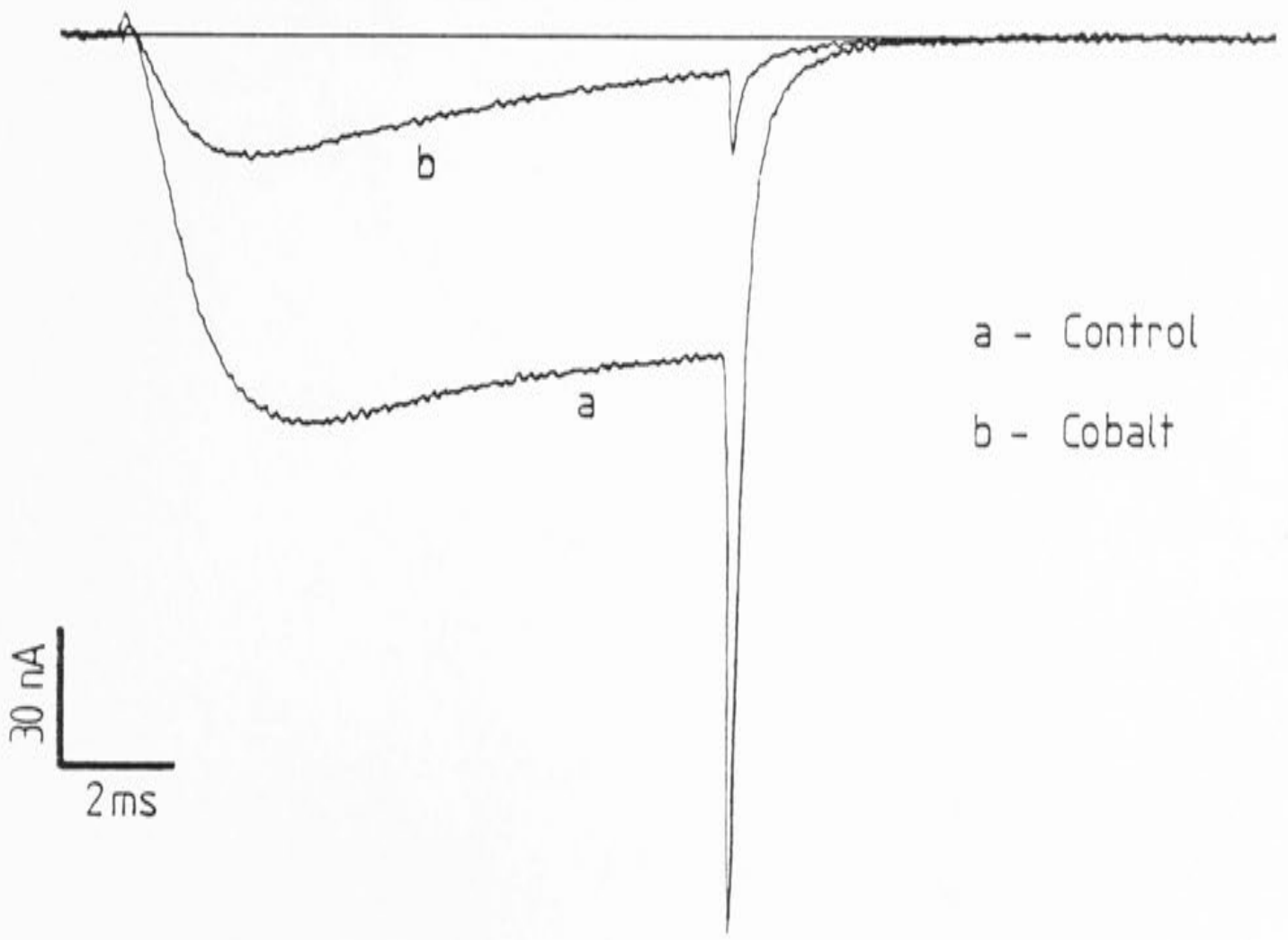
b
a
a - Control
b - Cobalt
30 nA
2 ms

Figure 6.2 The artifacts at the beginning of the traces are due to incomplete subtraction of the capacitive transients. There is a clear delay before activation of the slow sodium current during the pulse to 0mV. The delay becomes less pronounced at more positive potentials. The holding potential was -50mV and calcium currents were blocked using 1mM $CdCl_2$. It is apparent that the slow sodium current is not blocked by this concentration of cadmium.

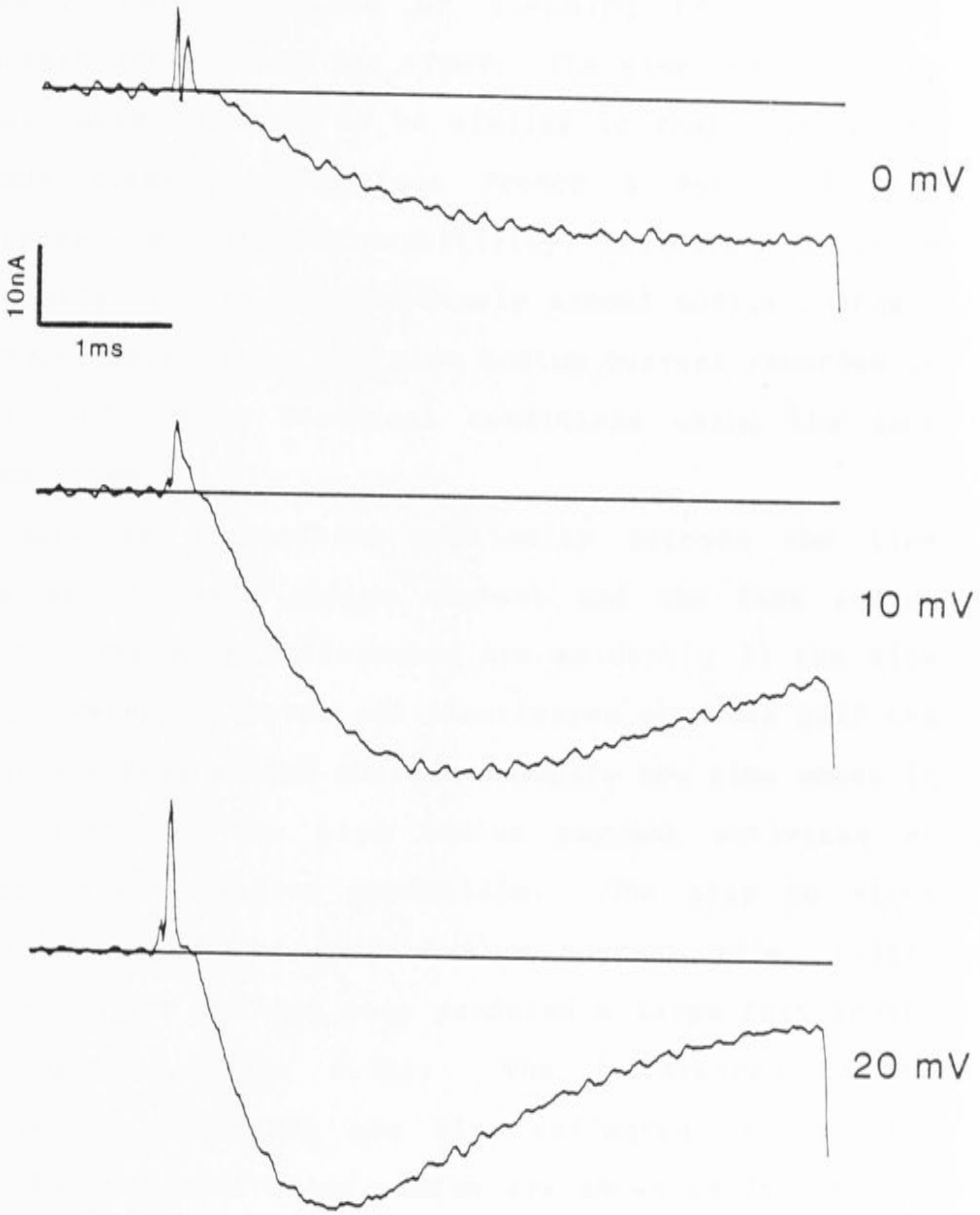
0 mV
10nA
1ms
10 mV
20 mV

illustrated in figure 6.3. The top figure shows the fast sodium current recorded on stepping from -50mV to potentials between -10 and +70mV. The time course of the current, which appears to be similar to that observed in numerous other studies (see French & Horn 1983 for references), and its TTX-sensitivity, indicate that it is very similar to the Hodgkin-Huxely axonal sodium channel. The lower figure shows the slow sodium current recorded in another cell under identical conditions using the same voltage steps.

There is a striking similarity between the time course of the slow sodium current and the fast sodium current. Two main differences are evident ; 1) the slow sodium current activates and inactivates at about half the rate of the fast sodium current (compare the time bases in figure 6.3), 2) The slow sodium current activates at slightly more positive potentials. The step to -10mV barely activated the slow sodium current (fig. 6.3B), while a similar voltage step produced a large fast inward sodium current (fig. 6.3A). The differences in the kinetics of activation are also reflected in the time constants of inactivation, which are shown in figure 6.4. The potential dependence and magnitude of the time constant is lower for the fast sodium (fig. 6.4A) current than the slow sodium current (fig. 6.4B). These observations are in agreement with the previous studies.

The steady state inactivation curve for the slow sodium current is plotted in figure 6.5, and a Boltzmann type function (equation 3.5) was drawn through the points.

Figure 6.3 The top set of traces show the fast sodium current recorded during 5ms pulses to -10, 0, 10, 20, 40, 50 & 70 mV. The bottom set of traces show the slow sodium current recorded in another cell during 10ms pulses to the same potentials. The holding potential was -50mV for both cells. The "sodium-current-solutions" listed in section 2.3 were used internally and externally. 1mM $CdCl_2$ was included in the external solutions for both cells. The slow sodium current was recorded in the presence of 0.3µM TTX.

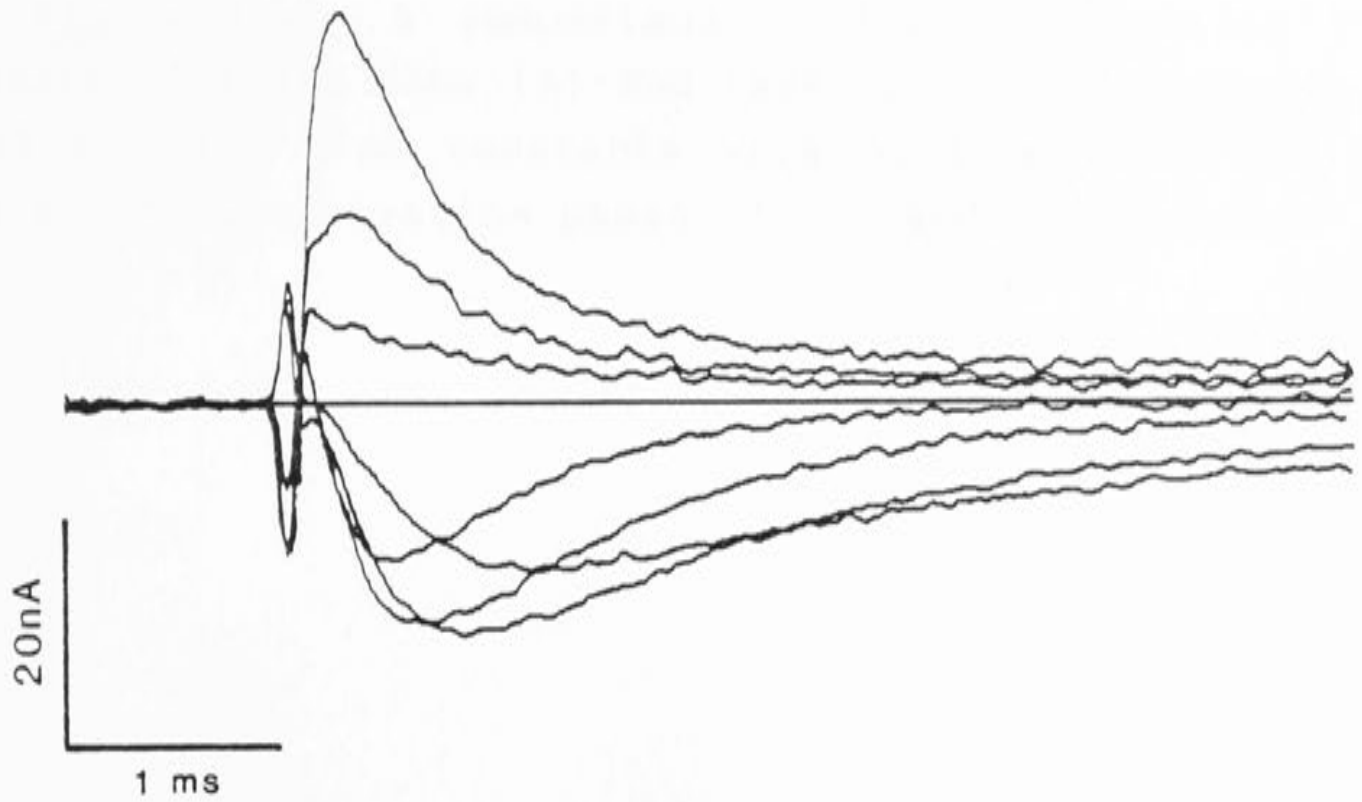
20nA
1 ms

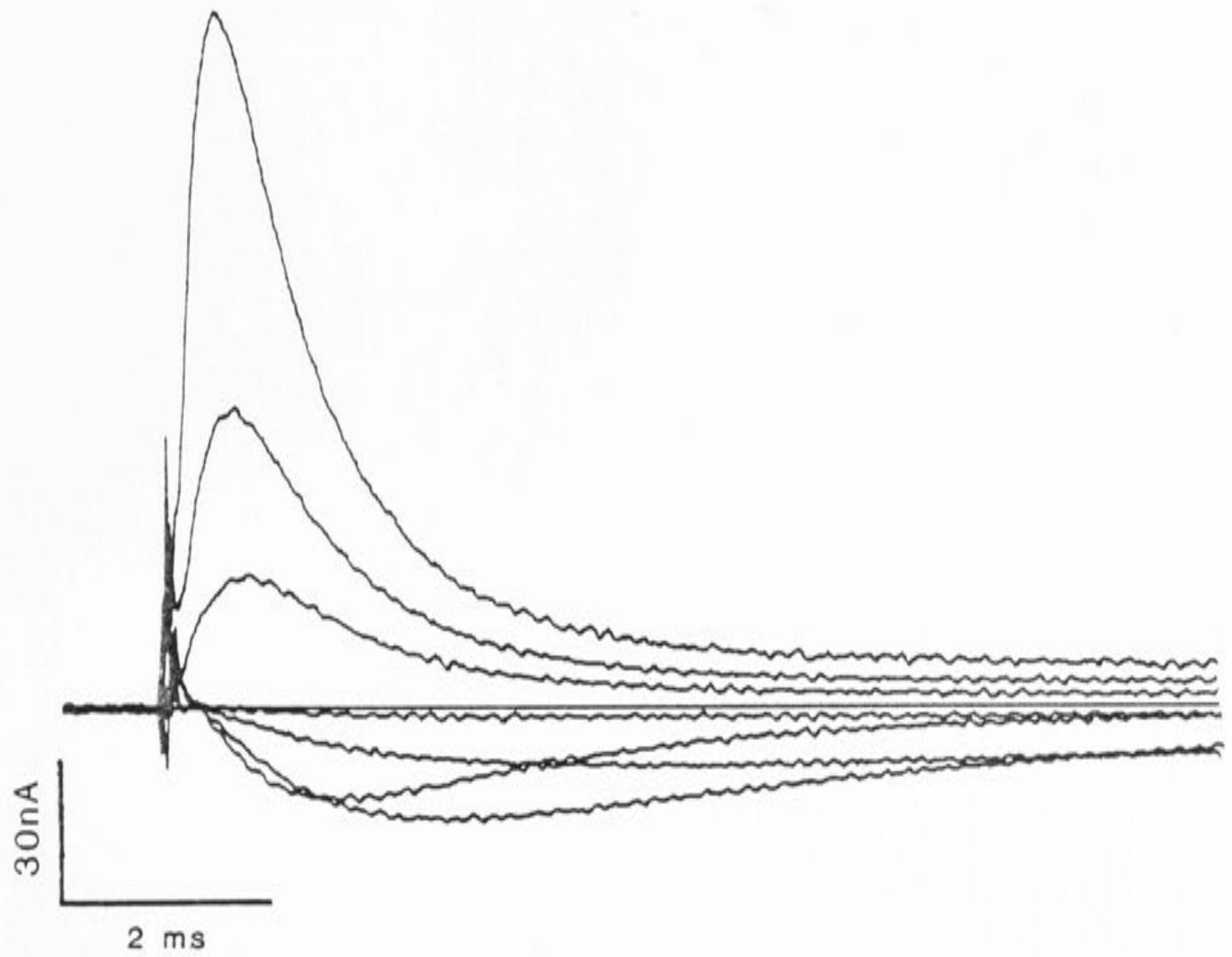
30nA
2 ms

Figure 6.4 A comparison of the inactivation time constants for the slow (A) and fast (B) sodium currents in 6 cells. The time constants were obtained from the LMM fits to the inactivation phase of the sodium currents.

A

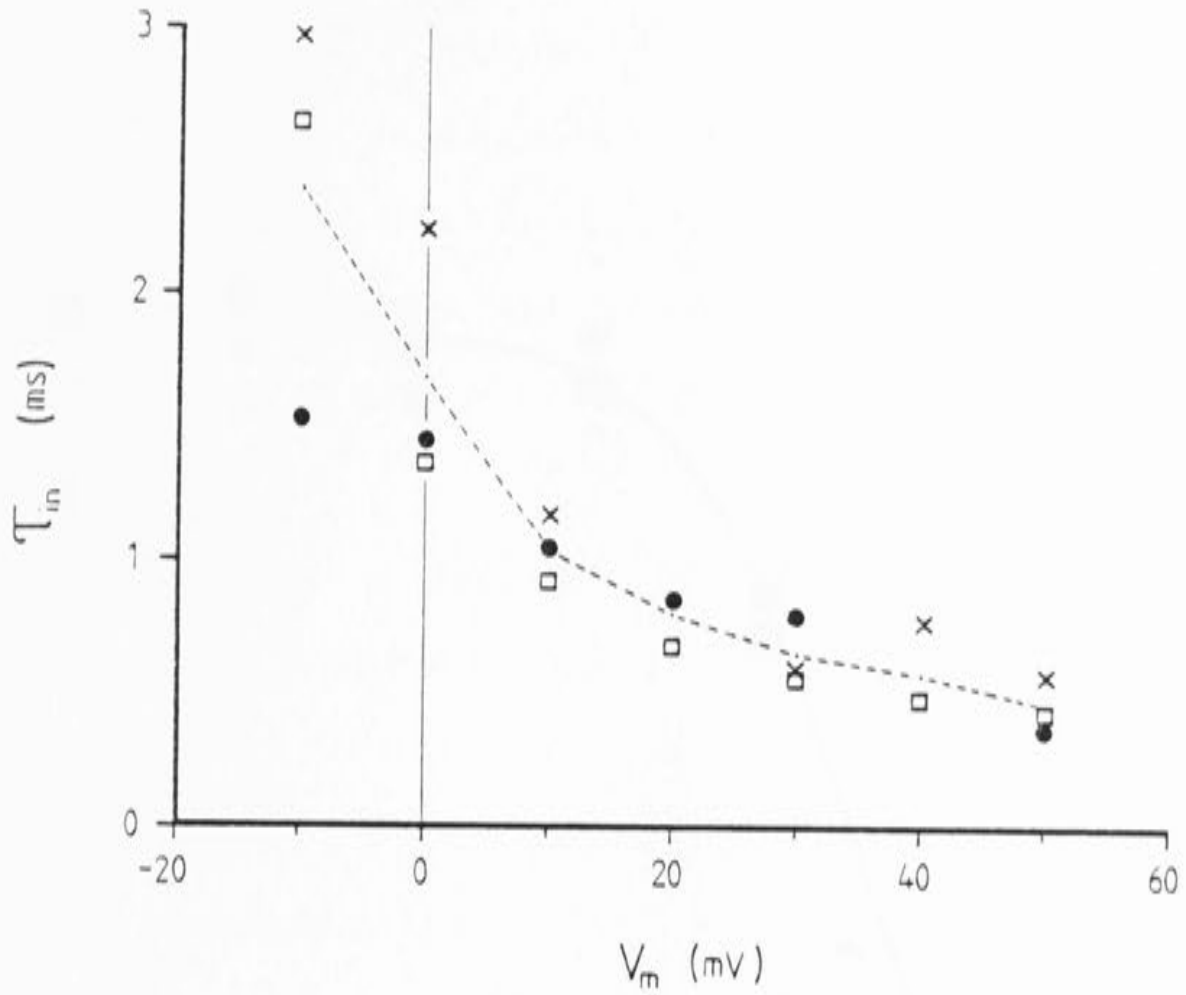

B

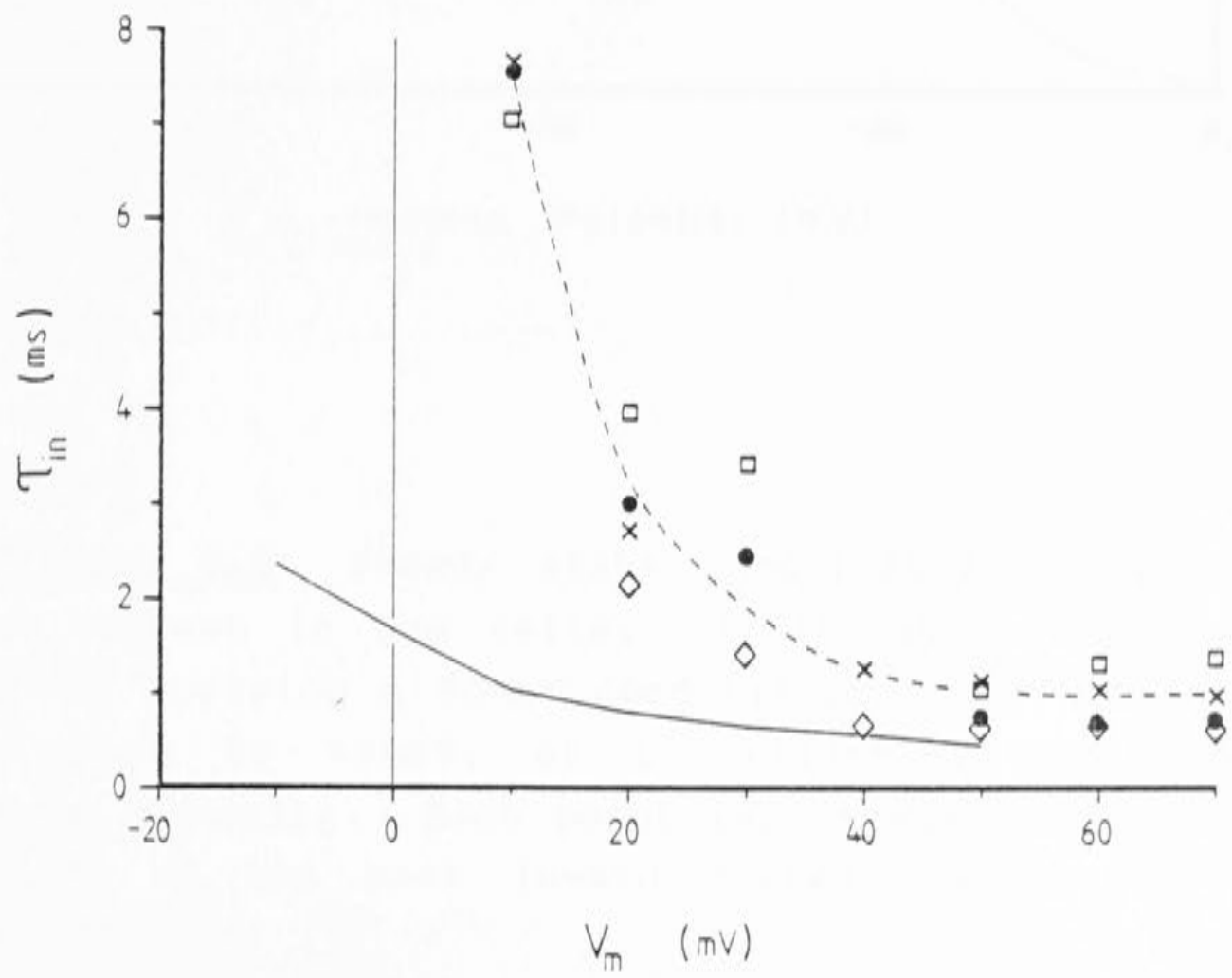

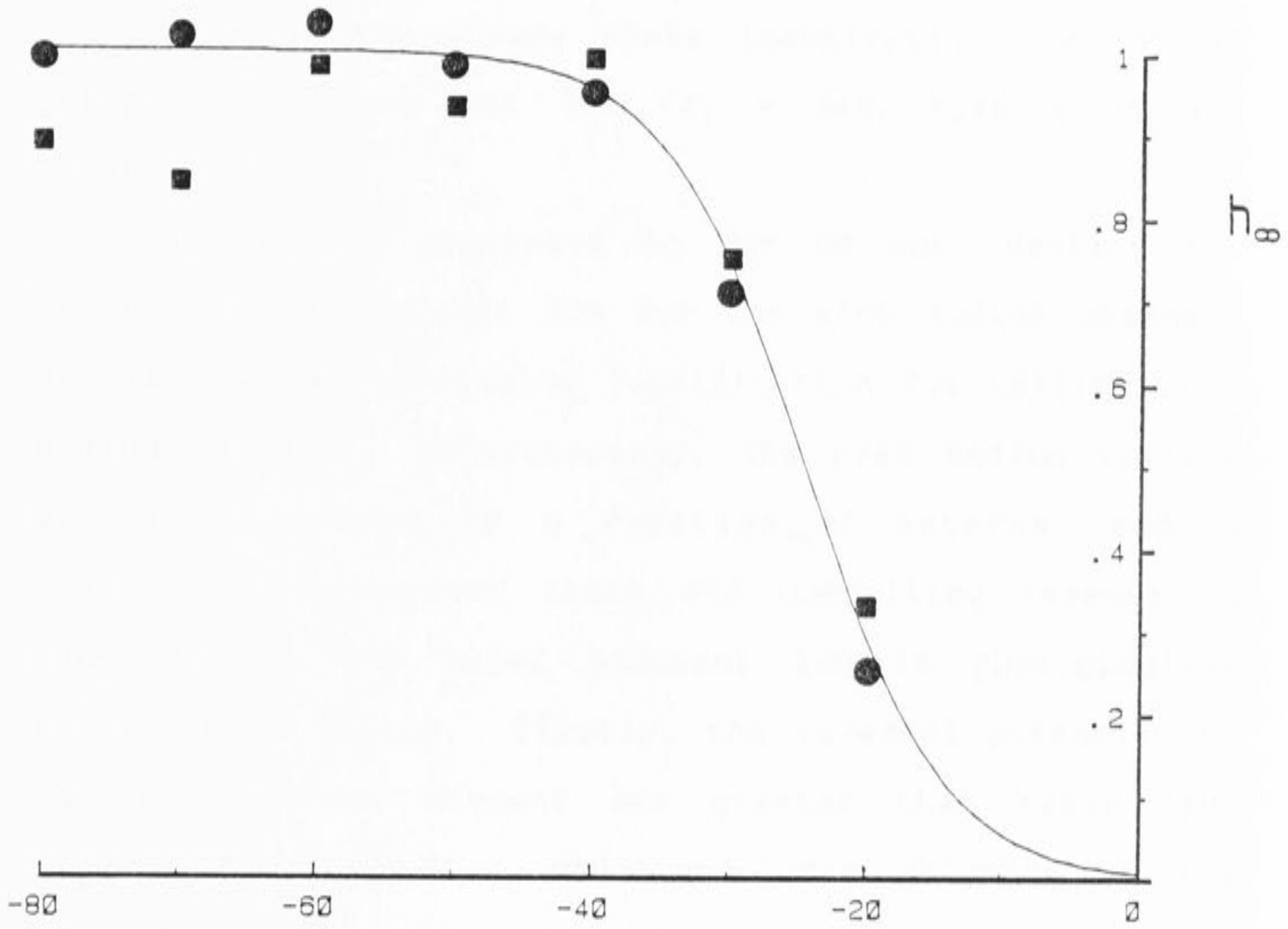

Figure 6.5 Steady state inactivation of the slow sodium current in two cells. Inactivation was induced either by applying a 500ms conditioning pulse before the test pulse to +20mV, or by adjusting the holding potential manually. Each point represents the normalized amplitude of the peak inward current during the test pulse.

The parameters used were V_0 = -26 ±0.4mV and K_0 = 4.9 ±0.3mV. Bossu & Feltz (1984) found that the slow sodium current was half inactivated at around -20 to -25mV and the inactivation range was -40 to -10mV. The data in figure 6.5 agrees well with their findings. The voltage dependence of the steady state inactivation was not as steep in new-born rat DRG (K_0 = 9mV, Kostyuk et al. 1981b).

The results presented so far do not identify the nature of the permeant ion for the slow sodium channel, and so give no convincing justification for calling it a sodium current. Unfortunately, the peak sodium current was not measured as a function of external sodium concentration, however there are compelling reasons to suppose that the major permeant ion in physiological solutions is sodium. Firstly, the reversal potential of the slow sodium current was greater than +25mV (see figures 6.6 & 6.7). This precludes chloride as the current carrier, since the chloride reversal potential is predicted to be around 0mV. Secondly, it is probably not a calcium selective channel, since the current can be recorded in the presence of the inorganic calcium channel blockers Co^{2+} and Cd^{2+}. Finally it is unlikely to be a potassium selective channel, since it appears to be able to support outward caesium currents. This finding is illustrated in figure 6.6. The top set of traces show the fast sodium current recorded at step potentials between -10 and +70mV. The major external cation was 115mM Na^+, and the internal cation was 140mM Cs^+. The current

Figure 6.6 The top traces show the fast sodium current during 10ms pusles to -10, 0, 10, 20, 40, 50 & 70 mV from a holding potential of -50mV. The lower traces show the slow sodium current recorded during a similar pulse run in another cell. The internal calcium-current-solution and external sodium-current-solutions were used (section 2.3). Calcium currents were blocked by 1mM $CdCl_2$ for the fast sodium current and 10mM $CoCl_2$ for the slow sodium current.

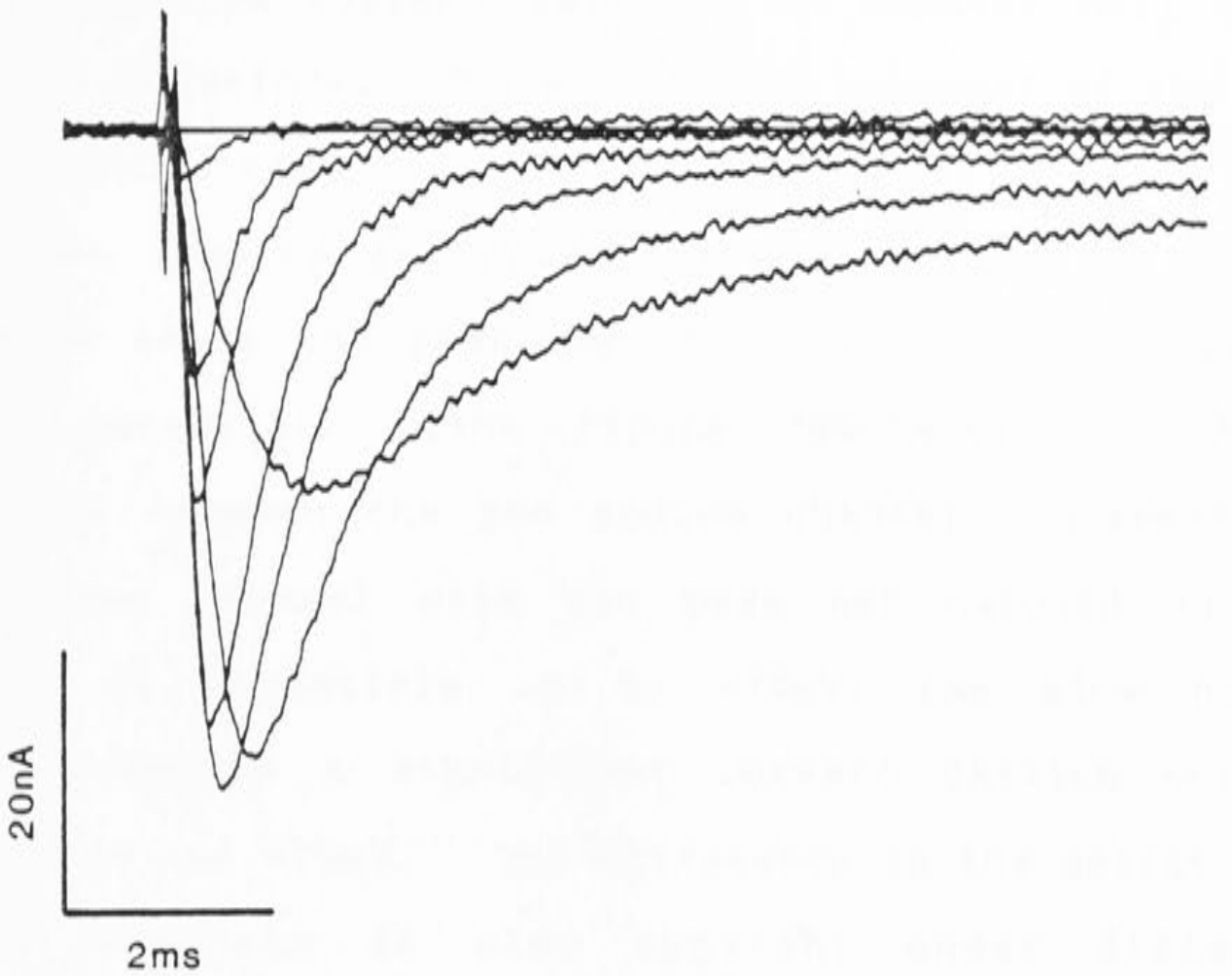
20nA
2ms

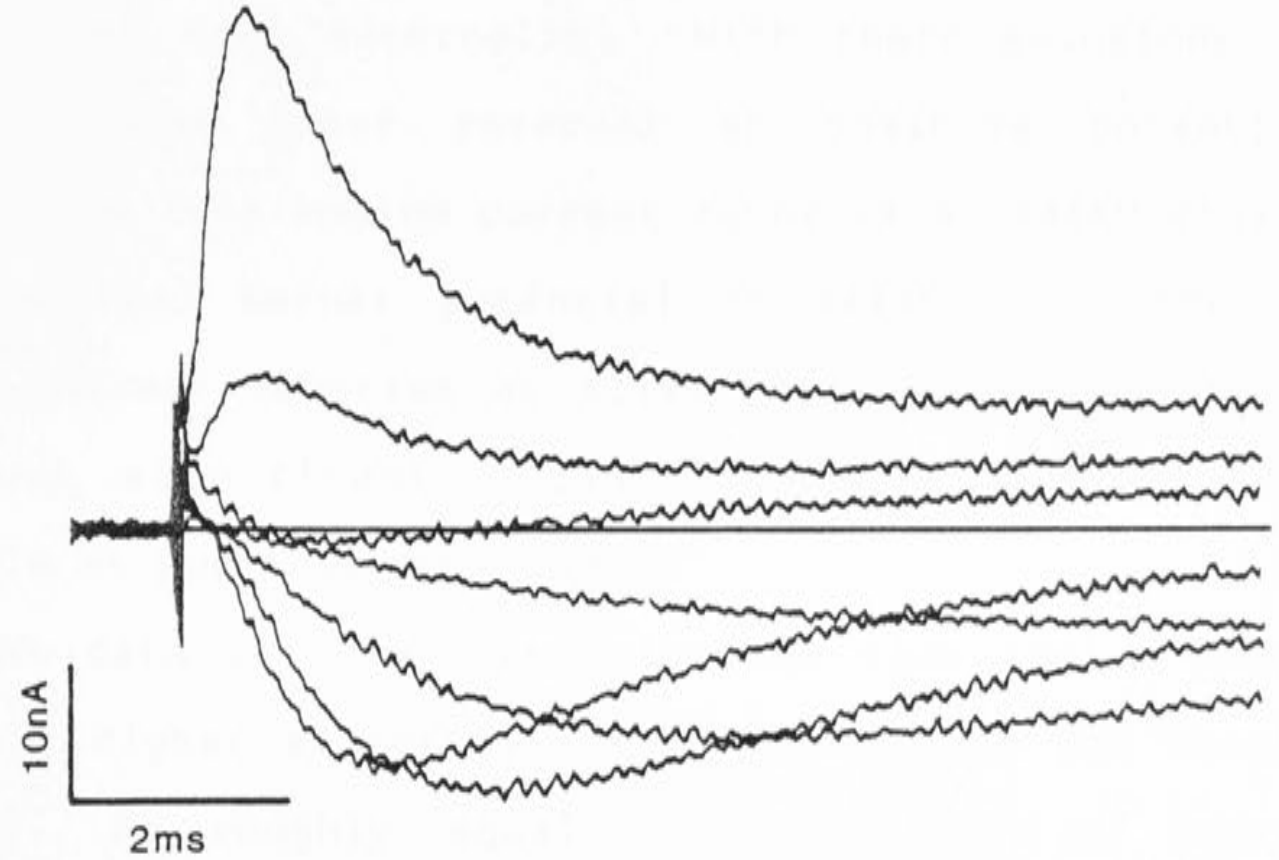
10nA
2ms

remains inward up to +70mV. The lower set of traces shows the slow sodium current recorded in another cell using identical solutions. There is clear reversal of the current around +40mV.

These results are presented more clearly in figure 6.7 which shows the peak sodium current plotted against holding potential. The figure demonstrates a basic difference between the two sodium channels; whereas the fast sodium channel will not pass net outward caesium currents at potentials up to +70mV, the slow sodium channel supports a significant outward caesium current between +40 and +70mV. The difference in the selectivity of the channels is also apparent under different conditions. Figure 6.8 shows a comparison of the two currents recorded with 115mM NaCl externally and 20mM NaCl, 110mM CsCl internally. With these solutions both currents show clear reversal at positive potentials, however the fast sodium current reverses at +46mV close to the predicted Nernst potential of +44mV while the slow sodium current reverses at +31mV, consistent with caesium carrying significant outward current through these channels at positive potentials.

The data is consistent with the slow sodium channel having a higher selectivity for sodium than for caesium. Firstly, in roughly equal concentrations of internal caesium and external sodium, the current reverses at +40mV (fig. 6.8). This suggests that the channel will pass inward sodium currents in preference to outward caesium currents. This point is supported by comparison of

Figure 6.7 Peak inward current-voltage relations for the fast and slow sodium currents. The sodium-current-solution in section 2.3 was used externally, and the calcium-current-solution used in the electrodes. TTX (0.3μM) was included in the solutions when recording the slow sodium current. Calcium currents were blocked using 1mM $CdCl_2$ for the fast sodium current and 10mM $CoCl_2$ for the slow sodium current. The lines through the points were drawn by eye.

Peak sodium current

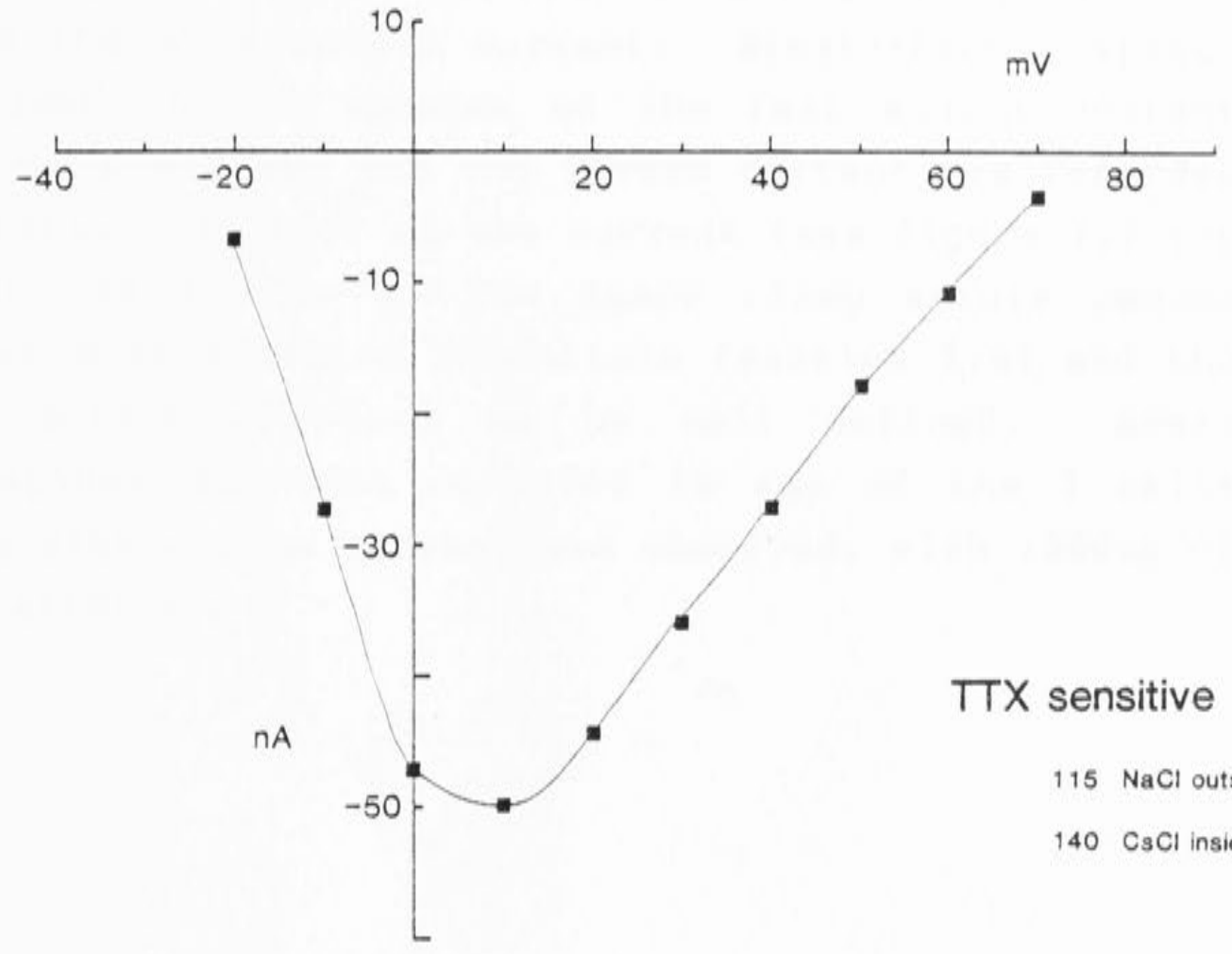

TTX insensitive

115 NaCl outside

140 CsCl inside

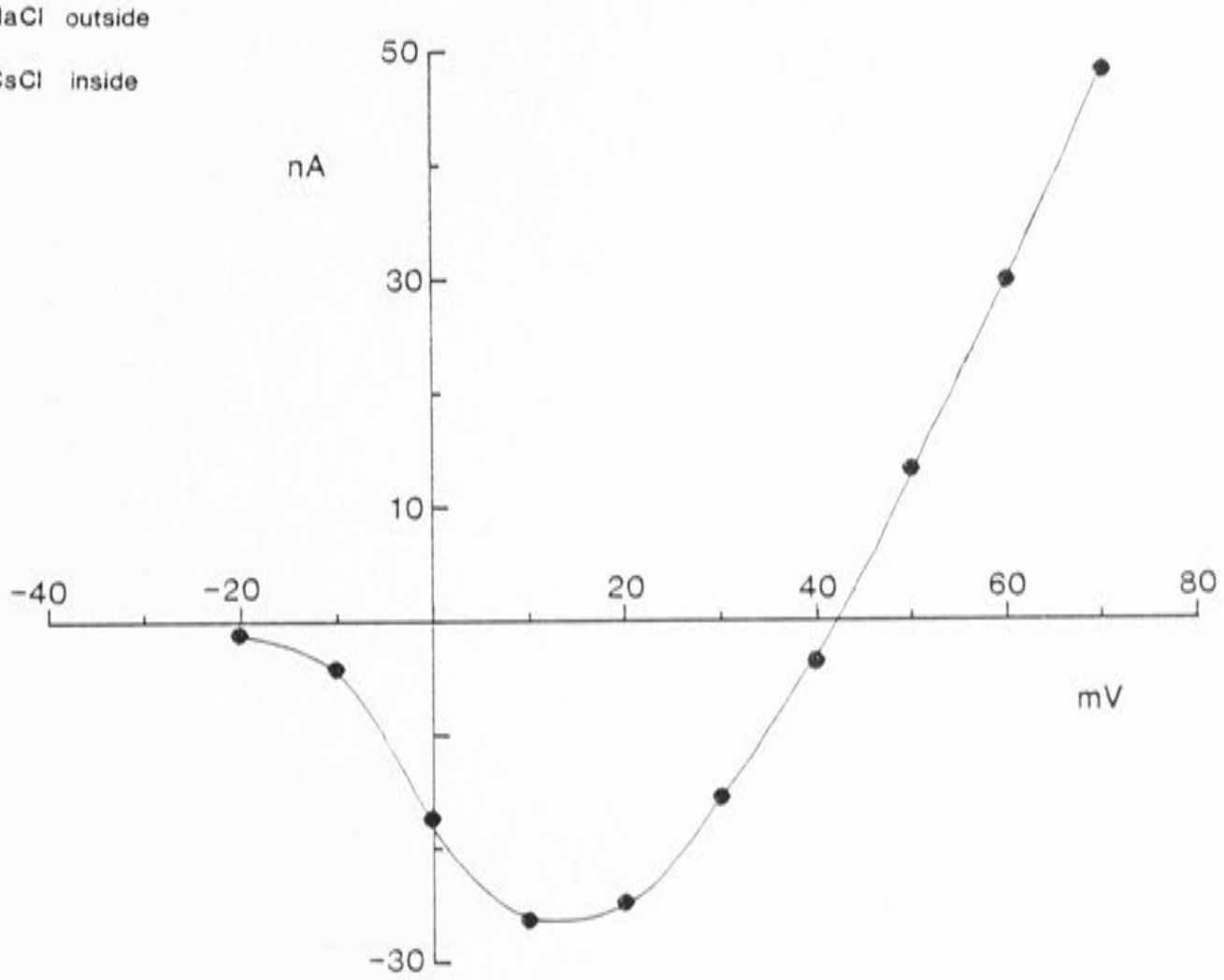

Figure 6.8 Peak inward current-voltage relation for the fast and slow sodium currents with sodium-current-solutions on both sides of the membrane. $CdCl_2$ (1mM) was included in the external solutions for both cells. TTX (0.3µM) was included in the external solution for recording the slow sodium current. Break-through spikes were evident in the records of the fast sodium current between -30 & -10 mV, and the inward current was recorded at the initial shoulder of the current (see figure 2.2 top trace) at -30 & -20mV. The space clamp errors become smaller at more positive potentials (section 2.6) and the reversal potential seems to be well defined. Break through spikes were not observed in any of the 3 cells where the slow sodium current was observed, with >200µm of the axon attached.

TTX sensitive

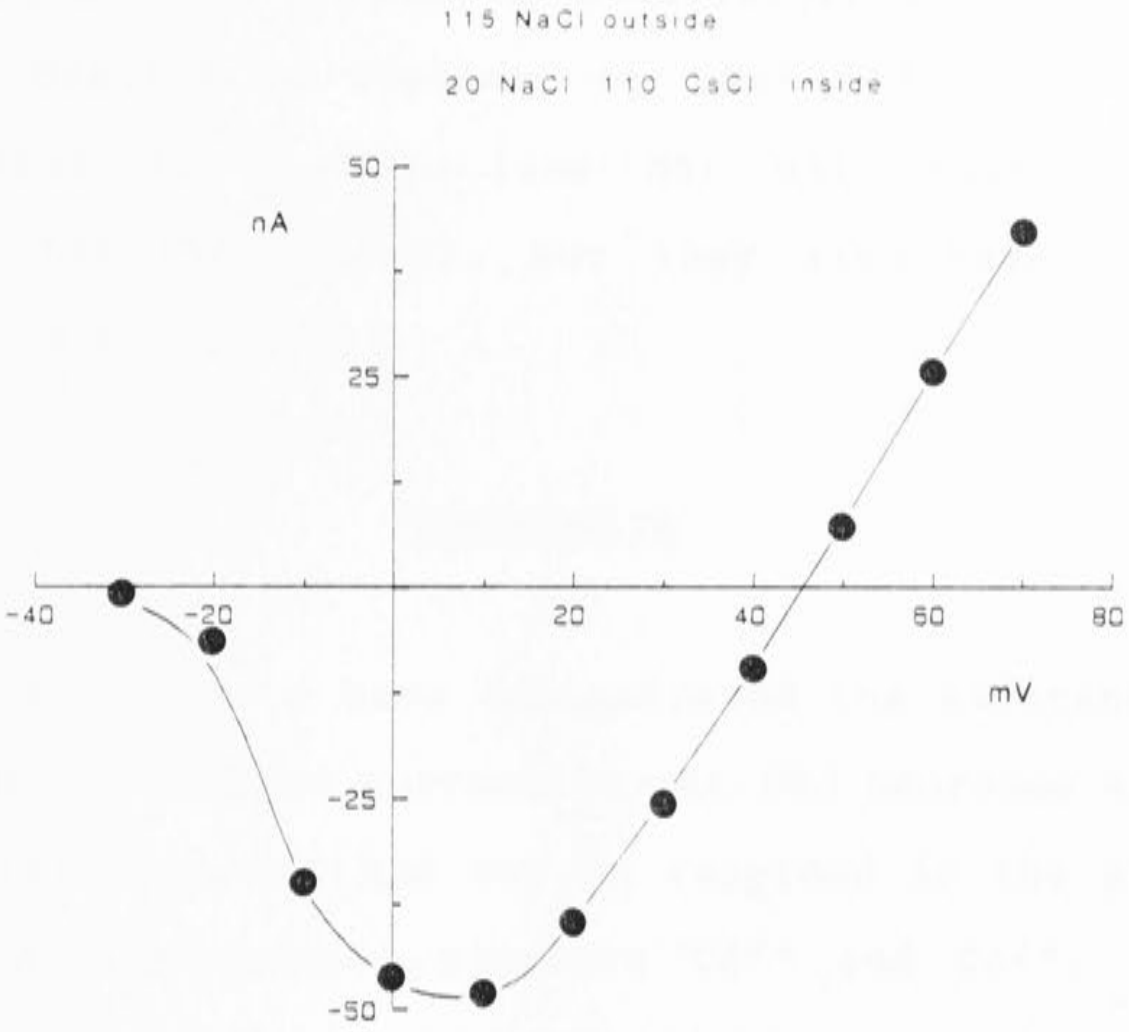

TTX insensitive

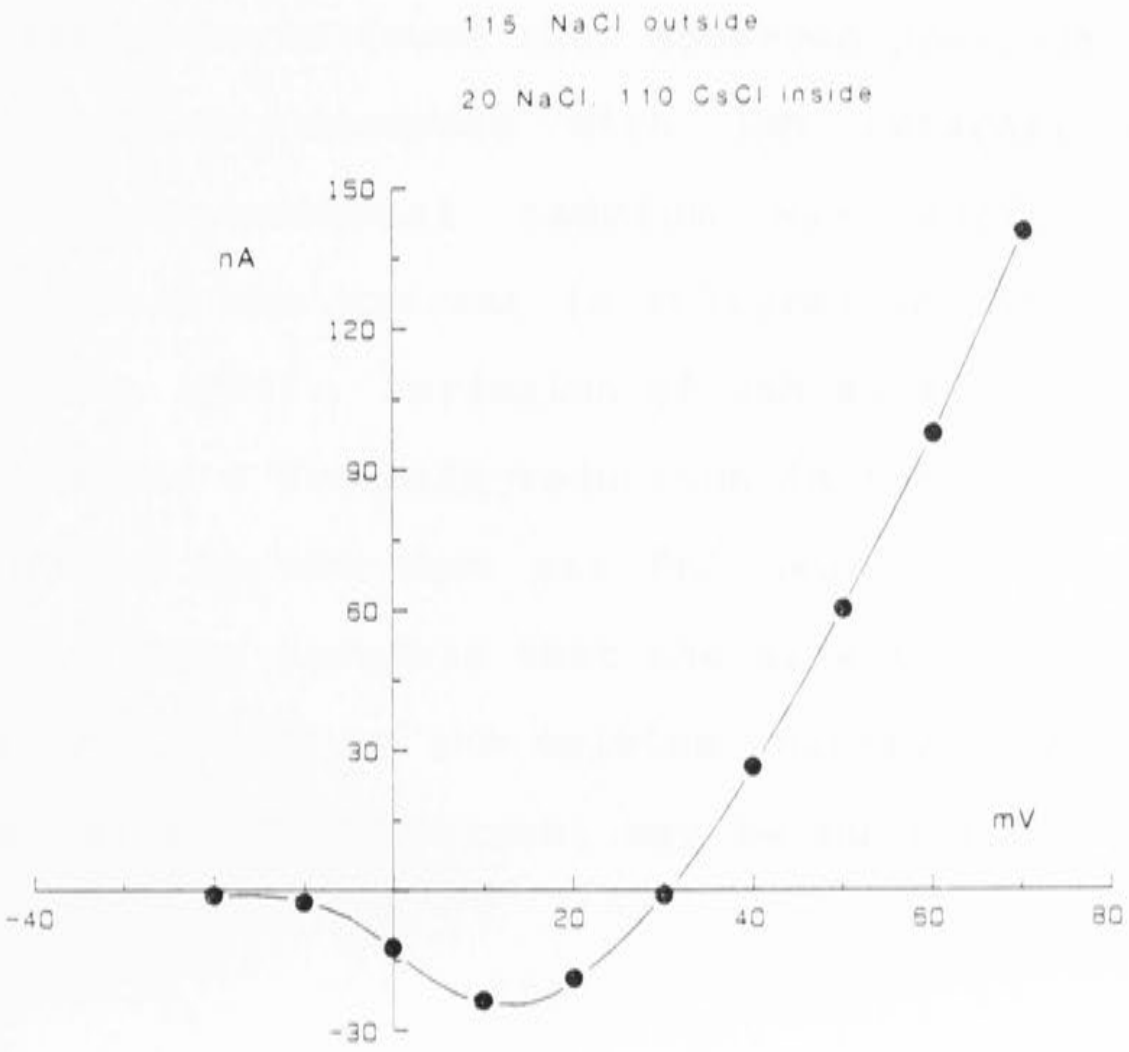

the lower graphs in figures 6.7 and 6.8. Although the maximum inward currents are roughly equal in these two cells, the outward current is much larger when 20mM of the internal caesium is replaced by 20mM sodium. It would appear that the sodium ions not only have a higher affinity for the channel, but they also have a higher mobility in the channel.

Discussion

The experiments have demonstrated the existence of a slow transient inward current in cat DRG neurones which is not sensitive to TTX and can be recorded in the presence of the calcium channel blockers Cd^{2+} and Co^{2+}. It is suggested that the current underlies the broad TTX-insensitive, sodium-dependent action potentials seen in peripheral nerve cell bodies. The current appeared to be similar to TTX-resistant sodium currents recorded in other preparations, however the sensitivity to calcium channel blockers seemed to be lower than observed previously. The current could be recorded with 1mM external cadmium whereas 100µM external cadmium was sufficient to completely block the current in cultured sensory neurones (Bossu & Feltz 1984). Perfusion of 5mM external manganese or cobalt caused a dramatic reduction in the TTX-resistant sodium current in new-born rat DRG neurones (Kostyuk et al. 1981b). It is possible that the slow sodium current is partially blocked by the calcium channel blockers used and so the slow sodium current may be much larger in cat

DRG neurones than the present results indicate. The major new observation in this section is that the slow sodium channel appears to be permeable to both sodium and caesium ions which suggests that the channel may discriminate poorly between monovalent cations. Previous reversal potential measurements also indicate that the TTX-resistant sodium channel in new-born rat DRG may be less selective for monovalent cations than the TTX-sensitive channel (Kostyuk et al. 1981b). The permeability of this channel for the alkali cations should be tested in more detail.

The slow sodium channel was seen only rarely during the present experiments, and was only recorded when the main external cation was sodium (3 out 19 cells). The slow sodium current was not observed in any of the 145 neurones in which calcium currents were recorded using the calcium-current-recording solutions, and yet Yoshida and co-workers (1978) found TTX-resistant sodium spikes in 27% of the mouse sensory neurones. The infrequency of the slow sodium current in cat DRG neurones may be a genuine deficit of the channel type, or could be due to the recording conditions used. For example, it is possible that external choline-Cl actively blocks the slow sodium channel.

The physiological significance of the slow sodium current is not immediately obvious. In every preparation in which the current has been reported the neurones were obtained from peripheral ganglia. It is interesting to note that cat preganglionic spinal neurones (Yoshimura et

al. 1983) and cultured spinal neurones (Heyer & Macdonald 1982) do not appear to support TTX-insensitive sodium spikes. The slow sodium channel may be restricted to the soma of peripheral neurones, since axonal break through spikes (eg figure 2.2) were not observed in any of the three cells where the slow sodium current was recorded. In contrast, cells in which the fast sodium channel was recorded would invariably produce an axonal spike when a sufficient length of the axon remained intact. If the slow sodium channels are restricted to the cell bodies of DRG neurones, as these limited results suggest, the physiological significance of the channel seems even more obscure.

References

Adams, D.J. & Gage, P.W. (1976). Gating currents associated with sodium and calcium currents in an Aplysia neurone. Science 192, 783-784.

Adams, D.J. & Gage, P.W. (1979a). Characteristics of sodium and calcium conductance changes produced by membrane depolarization in an Aplysia neurone. J. Physiol. 289, 143-161.

Adams, D.J. & Gage, P.W. (1979b). Sodium and calcium gating currents in an Aplysia neurone. J. Physiol. 291, 467-481.

Akaike, N., Lee, K.S. & Brown, A.M. (1978). The calcium current in Helix neurones. J. Gen. Physiol. 71, 509-531.

Akaike, N., Nishi, K. & Oyama, Y. (1983). Characteristics of manganese current and it's comparison with currents carried by other divalent cations in snail soma membranes. J. Memb. Biol. 76, 289-297.

Almers, W., McCleskey, E.W. & Palade, P.T. (1984). A non-selective cation conductance in frog muscle blocked by micromolar external calcium ions. J. Physiol. 353, 565-583.

Almers, W., & McCleskey, E.W. (1984). Non-selective conductance in calcium channels of frog muscle : calcium selectivity in a single file pore. J. Physiol. 353, 585-608.

Apell, H.-J., Bamberg, E., & Lauger, P. (1979). Effects of surface charge on the conductance of the gramicidin channel. Biochim. Biophys. Acta 552, 369-378.

Armstrong, C.M. (1981). Sodium channels and gating currents. Physiol. Rev. 61, 644-683.

Armstrong, C.M. & Bezanilla, F. (1974). Charge movement associated with the opening and the closing of the activation gates of the Na channels. J. Gen. Physiol. 63, 533-552.

Armstrong, C.M. & Matteson, D.R. (1985). Two distinct populations of calcium channels in a clonal line of pituitary cells. Science 227, 65-67.

Attwell, D. & Eisener, D. (1978). Discrete membrane surface charge distribution. Biophys. J. 24, 869-875.

Baumann, G. & Easton, G.S. (1981). Markov process characteristization of a single membrane gating site. J. Theor. Biol. 93, 785-804.

Baccaglini, P.I. & Cooper, E. (1982). Electrophysiological studies of new-born rat nodose neurones in cell culture. J. Physiol. 324, 429.

Bean, B.P. (1984). Nitrendipine block of cardiac calcium channels : High-affinity binding to the activated state. Proc. Natl. Acad. Sci. U.S.A. 81, 6388-6392.

Bean, B.P. (1985). Two kinds of calcium channels in canine atrial cells. J. Gen. Physiol. 86, 1-30.

Beauchamp, K., & Yuen, C. (1979). Digital Methods for Signal Analysis. George, Allen & Unwin, London.

Begenisich, T.B. & Cahalan, M.D. (1980a). Sodium channel permeation in squid axons I : reversal potential experiments. J. Physiol. 307, 217-242.

Begenisich, T.B. & Cahalan, M.D. (1980b). Sodium channel permeation in squid axons II : Non-independence and current-voltage relations. J. Physiol. 307, 243-257.

Bossu, J.-L. & Feltz, A. (1984). Patch-clamp study of the tetrodotoxin-resistant sodium current in group C sensory neurones. Neuroscience Letters 51, 241-246.

Bossu, J.-L., Feltz, A. & Thomann, J.M. (1985). Depolarization elicits two distinct Ca currents in vertebrate sensory neurones. Pflugers Arch. 403, 360-368.

Brauer, F., Nohel, J.A. & Schnieder, H. (1970). Linear Mathematics. An introduction to linear algebra and linear differential equations. W.A. Benjamin Inc. N.Y.

Brodwick, M.S. & Eaton, D.C. (1982). Chemical modification of excitable membranes. In, Proteins in the nervous system : Structure and function. Alan R. Liss Inc. N.Y. pp 51-72.

Brown, A.M., Kunze, D.L. & Yatani, A. (1984a). The agonist effect of dihydropyridines on Ca channels. Nature 311, 570-572.

Brown, A.M., Kunze, D.L. & Yatani, A. (1986). Dual effects of dihydropyridines on whole cell and unitary calcium current in single ventricular cells of guinea-pig. J. Physiol. 379, 495-514.

Brown, A.M., Lux, H.D. & Wilson, D.L. (1984b) Activation and inactivation of single calcium channels in snail neurons. J. Gen. Physiol. 83, 751-769.

Brown, A.M., Tsuda, Y., & Wilson, D.L. (1983) A description of activation and conduction in calcium channels based on tail and turn-on current measurements in the snail. J. Physiol. 344, 549-583.

Byerly, L., Chase, P.B. & Stimers, J.R. (1984) Calcium current activation kinetics in neurones of the snail Lymnea stagnalis. J. Physiol. 348, 187-207.

Byerly, L., Chase, P.B. & Stimers, J.R. (1985) Permeation and interaction of divalent cations in calcium channels of snail neurones. J. Gen. Physiol. 85, 491.

Byerly, L. & Hagiwara, S. (1982) Calcium currents in internally perfused nerve cell bodies of Lymnea stagnalis. J. Physiol. 322, 503-528.

Byerly, L. & Yazejian, B. (1986). Intracellular factors for the maintainence of calcium currents in perfused neurones from the snail, Lymnaea stagnalis. J. Physiol. 370, 631-650.

Carbone, E. & Lux, H.D. (1984). A low voltage-activated Ca conductance in embryonic chick sensory neurones. Biophys. J. 46, 413-418.

Catterall, W.A. (1986). Voltage-dependent gating of sodium channels : correlating structure and function. TINS 9, 7-10.

Cavalie, A., Ochi, R., Pelzer, D. & Trautwien, W. (1983). Elementary currents through Ca channels in guinea pig myocytes. Pflugers Arch. 398, 284-297.

Chad, J.E. & Eckert, R. (1984a). Kinetics of calcium dependent inactivation of calcium current in voltage-clamped neurones of Aplysia californica. J. Physiol. 347, 279-306.

Chad, J.E. & Eckert, R. (1984b). Stimulation of cAMP-dependent protein phosphorylation retards both inactivation and 'wash-out' of Ca current in dialysed Helix neurones. Neurosci. Abstr. 10, 866.

Chesnoy-Marchais, D. (1985) Kinetic properites and selectivity of calcium-permeable channels in Aplysia neurones. J. Physiol. 367, 457.

Chou, P.Y. & Fasman, G.D. (1978). Empirical predictions of protein conformation. Ann. Rev. Biochem. 47, 251-276.

Chothia, C. (1984). Principles that determine the structure of proteins. Ann. Rev. Biochem. 53, 537-572.

Chui, S.Y., Mrose, H.E. & Ritchie, J.M. (1979) Anomalous temperature dependence of sodium conductance in rat nerve compared with frog nerve. Nature 279, 327.

Chui, S.Y. (1980). Asymmetry currents in the mammalian myelinated nerve. J. Physiol. 309, 499-519.

Ciani, S., Krasne, S., Miyazaki, S. & Hagiwara, S. (1978) A model for anomalous rectification : electrochemical-potential-dependent gating of membrane channels. J. Memb. Biol. 44, 103.

Cognard, C., Lazdunski, M. & Romey, G. (1986). Different types of calcium channels in mammalian skeletal muscle cells in culture. Proc. Natl. Acad. Sci. U.S.A. 83, 517-521.

Collins, C.A., Rojas, E. & Suarez-Isla, B.A. (1982). Fast charge movements in skeletal muscle fibres from Rana temporaria. J. Physiol. 324, 319-345.

Colquhoun, D.C. & Hawkes, A.G. (1977). Relaxation and fluctuations of membrane currents that flow through drug-operated channels. Proc. R. Soc. B 199, 231-262.

Connor, J.A. (1979). Calcium current in molluscan neurones : measurement under conditions which maximise its visibility. J. Physiol. 286, 41-60.

Conti, F., Fioravanti, R., Segal, J.R. & Stuhmer, W. (1982). Pressure dependence of sodium currents of squid giant axon. J. Memb. Biol. 69, 23-34.

Conti, F. & Wanke E. (1975). Channel noise in nerve membranes and lipid bilayers. Q. Rev. Biophys. 8, 451-506.

Coronado, R., Rosenberg, R.L. & Miller, C. (1978). Ionic selectivity, saturation and block in a K-selective channel from sarcoplasmic reticulum. J. Gen. Physiol. 76, 425.

Dichter, M.A. & Fischbach, G.D. (1977). The action potential of chick dorsal root ganglion neurones maintained in cell culture. J. Physiol. 276, 281-298.

Doroshenko, P.A., Kostyuk, P.G., Martynyuk, A.E., Kursky, M.D. & Vorobetz, Z.D. (1984). Intracellular protein kinase and calcium inward currents in perfused neurones of the snail helix pomatia. Neurosci. 11, 263-267.

Dreyer, F., Peper, K. & Sterz, R. (1978). Determination of dose-response curves by quantitative ionophoresis at the frog neuromuscular junction. J. Physiol. 281, 395-419.

Droogmans, G. & Callewaert, D. (1986). Ca^{2+}-channel current and its modification by the dihydropyridine agonist Bay K 8644 in isolated smooth muscle. Pflugers Arch. 406, 259-265.

Dubinsky, J.M. & Oxford, G.S. (1984) Ionic currents in two strains of rat anterior pituitary tumour cells. J. Gen. Physiol. 83, 309-339.

Eckert, R. & Chad, J.E. (1984). Inactivation of calcium channels. Prog. Biophys. Molec. Biol. 44, 215-267.

Edsall, J.T. & Gutfreund, H. (1983). Biothermodynamics. The study of biochemical processes at equilibrium. John Wiley & Sons Ltd.

Ehrenstein, G. & Lecar, H. (1977). Electrically gated ionic channels in lipid bilayers. Q. Rev. Biophys. 10, 1-34.

Ehrlich, B.E., Schen, C.R., Garcia M.L. & Kaczorowski, G.J. (1986). Incorporation of calcium channels from cardiac sarcolemmal membrane vesicles into planar lipid bilayers. Proc. Natl. Acad. Sci. U.S.A. 83, 193-197.

Eisenberg, D. (1984). Three dimensional structure of membrane and surface proteins. Ann. Rev. Biochem. 53, 595-623.

Eisenberg, M., Gresalfi, T., Riccio, T. & McLaughlin, S. (1979) Adsorption of monovalent cations to bilayer membrane containing negative phospholipids. Biochemistry 18, 5213-5223.

Eisenman, G., Sandblom, J. & Neher, E. (1978) Interactions in cation permeation through the gramicidin channel : Cs, Rb, K, Na, Li, H, and effects of anion binding. Biophys. J. 22, 307-340.

Fedulova, S.A., Kostyuk, P.G. & Veselovsky, N.S. (1985). Two types of calcium channels in the somatic membrane of newborn rat dorsal root ganglion neurones. J. Physiol. 359, 431-446.

Fenwick, E.M., Marty, A. & Neher, E. (1982). Sodium and calcium channels in bovine chromaffin cells. J.Physiol. 331, 599-635.

Fertuck, H.C. & Salpeter, M.M. (1974). Localization of acetylcholine receptor by ^{125}I-labeled α-bungarotoxin binding at mouse motor end-plate. Proc. Natl. Acad. Sci. U.S.A. 71, 1376.

Finkel, A. (1985). Useful Circuits for Voltage Clamping with microelectrodes. In, Voltage and Patch Clamping with Microelectrodes. Smith T.G., Lecar H., Redman S.J. & Gage P.W. eds. Am. Phys. Soc.

Finkel, A., & Gage, P.W. (1985). Conventional Voltage Clamping with Two Intracellular microelectrodes. In, Voltage and Patch Clamping with Microelectrodes. Smith T.G., Lecar H., Redman S.J. & Gage P.W. eds. Am. Phys. Soc.

Franckowiak, G., Bechem, M., Schramm, M. & Thomas, G. (1985). The optical isomers of the 1,4-dihydropyridine Bay K 8644 show opposite effects on Ca channels. Eur. J. Pharm. 114, 223-226.

Frankenhaeuser, B. & Hodgkin, A.L. (1957). The action of calcium on the electrical properties of squid axon. J. Physiol. 137, 218-244.

French, R.J. & Adelman Jr., W.J. (1976). Competition, saturation and inhibition ; ionic interactions shown by membrane ionic currents in nerve, muscle and bilayer systems. Curr. Top. Membranes Transp. 8, 161-207.

French R.J. & Horn R. (1983). Sodium channel gating : models, mimics, and modifiers. Ann. Rev. Biophys. Bioeng. 12, 319.

Fukushima, Y. & Hagiwara, S. (1985). Currents carried by monovalent cations through calcium channels in mouse neoplastic B lymphocytes. J. Physiol. 358, 255-284.

Gage, P.W. & Armstrong, C.M. (1968). Miniature end-plate currents in voltage-clamped muscle fibres. Nature 218, 363-365.

Gallego, R. (1983). The ionic basis of action potentials in petrosal ganglion cells of the cat. J.Physiol. 342, 591.

Geduldig, D. & Greuner, R. (1970). Voltage clamp of the Aplysia giant neurone : early sodium and calcium currents. J. Physiol. 211, 217-244.

Gilly, WM. F. & Armstrong, C.M. (1982). Divalent cations and the activation kinetics of potassium channels in squid giant axons. J. Gen. Physiol. 79, 965-996.

Glasstone, S., Laidler, K.J. & Eyring, H. (1941). The Theory of Rate Processes. McGraw-Hill Book Company Inc. N.Y.

Goldman, L. (1943). Potential, impedence and rectification in membranes. J. Gen. Physiol. 27, 37-60.

Goult, R.J., Hoskins, R.F., Milner, J.A. & Pratt, M.J. (1974). Computational Methods in Linear Algebra. Stanley Thornes Pub. London.

Greenblatt, R.E., Blatt, Y. & Montal, M. (1985). The structure of the voltage-sensitive sodium channel. FEBS 193, 125-134.

Guy, H.R. & Seetharamulu, P. (1986). Molecular model of the action potential sodium channel. Proc. Natl. Acad. Sci. U.S.A. 83, 508-512.

Haga, N., Forte, M., Ramanathan, R., Saimi, Y., Takahashi, M. & Kung, C. (1984). Purification of a soluble protein controlling Ca^{2+} channel activity in paramecium. Biophys. J. 45, 130-132.

Hagiwara, S. & Byerly, L. (1981). Calcium channel. Ann Rev. Neurosci. 4, 69-125.

Hagiwara, S. & Byerly, L. (1983). The calcium channel. TINS 6, 189-193.

Hagiwara, S. & Nakajima, S. (1966). Effects of intracellular Ca ion concentration upon the excitability of the muscle fiber membrane of a barnacle. J. Gen. Physiol. 49, 807-818.

Hagiwara, S. & Ohmori, H. (1982). Studies of calcium channels in rat clonal pituitary cells patch electrode voltage clamp. J. Physiol. 331, 231-252.

Hagiwara, S. & Ohmori, H. (1983). Studies of single channel currents in rat clonal pituitary cells. J. Physiol. 336, 649-661.

Halliwell, J.V. (1983). Caesium-loading reveals two distinct Ca-currents in voltage-clamped guinea-pig hippocampal neurones *in vitro*. *Proc. Physiol. Soc.* March 1983, 11P.

Hamill, O.P., Marty, A., Neher, E., Sakmann, B. & Sigworth, F.J. (1981). Improved patch-clamp techniques for high-resolution current recording from cells and cell free membrane patches. *Pflugers Arch.* 391, 85-100.

Harper, A.A. & Lawson, S.N. (1985). Electrical properties of rat dorsal root ganglion neurones with different peripheral conduction velocities. *J. Physiol.* 359, 47-63.

Hess, P. & Tsien, R.W. (1984). Mechanism of ion permeation through calcium channels. *Nature* 309, 453-456.

Hess, P., Lansman, J.B. & Tsien, R.W. (1984). Blockade of single cardiac calcium channels by Mg^{2+}, Cd^{2+} and Ca^{2+} in guinea-pig ventricular cells. *Proc. R. Soc.* Sept. 77P.

Hess, P., Lansman, J.B. & Tsien, R.W. (1984). Different modes of Ca channel gating behaviour favoured by dihydropyridine Ca agonists and antagonists. *Nature* 311, 538-544.

Hess, P., Lansman, J.B. & Tsien, R.W. (1986). Calcium channel selectivity for divalent and monovalent cations. Voltage and concentration dependence of single channel current in ventricular heart cells. *J. Gen. Physiol.* 88, 293-319.

Heyer, E.J. & Macdonald, R.L. (1982). Ca and Na dependent action potentials of mouse spinal cord and dorsal root ganglion neurones in cell culture. *J. Neurophysiol.* 47, 641.

Hille, B. (1968). Charges and potentials at the nerve surface : Divalent ions and pH. *J. Gen. Physiol.* 51, 221-236.

Hille, B. (1984). Ionic channels of excitable membranes. Sinauer Associates Inc., Sunderland, Massachusetts.

Hille, B. & Schwarz, W. (1978). Potassium channels as multi-ion single file pores. J. Gen. Physiol. 72, 409-442.

Hodgkin, A.L. & Huxley, A.F. (1952). A quantitative description of membrane current and its application to conduction and excitation in nerve. J. Physiol. 117, 500-544.

Hodgkin, A.L. & Katz, B. (1949). The effect of sodium ions on the electrical activity of the giant axon of the squid. J. Physiol. 108, 37-77.

Hodgkin, A.L. & Keynes, R.D. (1955). The potassium permeability of a giant nerve fibre. J. Physiol. 128, 61.

Hof, R.P., Puegg, U.T., Hof, A. & Vogel, A. (1985). Stereoselectivity at the calcium channel : opposite action of enantiomers of 1,4-dihydropyridine. J. Cardiovasc. Pharmac. 7, 689-693.

Hooke, R. & Jeeves, T.A. (1960). "Direct search" solution of numerical and statistical problems. Am. Stat. 163, 212-229.

Horn, R. & Lange, K. (1983). Estimating kinetic constants from single channel data. Biophys. J. 43, 207-223.

Horn, R., Patlak, J. & Stevens, C. (1981). The effect of tetramethylammonium on single sodium channel currents. Biophys. J. 36, 321-327.

Ikeda, S.R., Schofield, G.G. & Weight, F.F. (1986). Na^+ and Ca^+ currents of acutely isolated adult rat nodose ganglion cells. J. Neurophysiol. 55, 527-539.

Junge, D. & Miller, J. (1977). Different spike mechanisms in axon and soma of molluscan neurone. Nature 252, 155-156.

Kawa, K. (1979). Zinc-dependent action potentials in giant neurones of the snail Euhadra quaestia. J. Memb. Biol. 49, 325.

Keynes, R.D. & Rojas, E. (1974). Kinetics and steady state properties of the charged system controlling sodium conductance in the squid giant axon. J. Physiol. 239, 393-434.

Kokubun, S. & Reuter, H. (1984). Dihydropyridine derivatives prolong the open state of Ca channels in cultured cardiac cells. Proc. Natl. Acad. Sci. U.S.A. 81, 4824-4827.

Kootsey, J.M. & Johnson, E.A. (1973). Buffer amplifier with femptofarad input capacity using operational amplifiers. Trans. Biomed. Eng. 20, 389-391.

Kostyuk, P.G. & Krishtal, O.A. (1977). Effects of calcium and calcium-chelating agents on the inward and outward current in the membrane of mollusc neurones. J. Physiol. 270, 569-580.

Kostyuk, P.G., Krishtal, O.A. & Pidoplichko, V.I. (1975). Effect of internal flouride and phosphate on membrane currents during intracellular dialysis of nerve cells. Nature 257, 691.

Kostyuk, P.G., Krishtal, O.A. & Pidoplichko, V.I. (1977). Asymmetrical displacement currents in nerve cell membrane and effect of internal flouride. Nature 267, 70-72.

Kostyuk, P.G., Krishtal, O.A. & Pidoplichko, V.I. (1981a). Calcium inward current and related charge movements in the membrane of snail neurones. J. Physiol. 310, 403-421.

Kostyuk, P.G., Krishtal, O.A. & Doroshenko, P.A. (1974). Calcium currents in snail neurones. I. Identification of calcium currents. Pflugers Arch. 348, 83-93.

Kostyuk, P.G., Mironov, S.L. & Doroshenko, P.A. (1982). Energy profile of the calcium channel in the membrane of mollusc neurones. J. Memb. Biol. 70, 181-189.

Kostyuk, P.G., Mironov, S.L. & Shuba, Ya.M. (1983). Two ion-selecting filters in the calcium channel of the somatic membrane of mollusc neurones. J. Memb. Biol. 76, 83-93.

Kostyuk, P.G., Veselovsky, N.S. & Tsyndrenko, A.Y. (1981b). Ionic currents in the somatic membrane of rat dorsal root ganglion neurons. I. Sodium currents. Neuroscience 6, 2423-2430.

Kostyuk, P.G., Veselovsky, N.S. & Tsyndrenko, A.Y. (1981c). Ionic currents in the somatic membrane of rat dorsal root ganglion neurons. II. Calcium currents. Neuroscience 6, 2431-2437.

Krishtal, O.A. & Pidoplichko, V.I. (1976). Intracellular perfusion of Helix giant neurones. Neurophysiol. 7, 258-259.

Labarca, P., Coronardo, R. & Miller, C. (1980). Thermodynamic and kinetic studies of the gating behaviour of a K^+-selective channel from the sarcoplasmic reticulum membrane. J. Gen. Physiol. 76, 397-424.

Lamb, G.D. (1985). Components of charge movement in rabbit skeletal muscle: the effect of tetracaine and nifedipine. J. Physiol. 376, 85-100.

Lansman, J.B., Hess, P. & Tsien, R.W. (1985). Direct measurement of entry and exit rates for calcium ions in single calcium channels. Biophys. J. 47, 67a.

Lansman, J.B., Hess, P. & Tsien, R.W. (1986). Blockade of current through single calcium channels by Cd^{2+}, Mg^{2+} & Ca^{2+}. Voltage dependence of calcium entry into the pore. J. Gen. Physiol. 88, 321-347.

Lauger, P. (1984). Channels with multiple conformational states : interrelations with carriers and pumps. In Current Topics in Membranes and Transport. Vol. 21, pp 309-326.

Lauger, P. (1985). Ionic channels with conformational substates. Biophys. J. 47, 581-591.

Lauger, P. & Apell, H.-J. (1982). Jumping frequencies in membrane channels. Comparison between stochastic molecular dynamics simulation and rate theory. Biophys. Chem. 16, 209-221.

Lee, K.S., Akaike, N. & Brown, A.M. (1978). Properties of internally perfused, voltage-clamped, isolated nerve cell bodies. J. Gen. Physiol. 71, 489-507.

Lee, K.S. & Tsein, R.W. (1984). High selectivity of calcium channels in single dialysed heart cells of the guinea-pig. J. Physiol. 354, 253-272.

Levitt, D.G. (1978). Electrostatic calculations for an ion channel : I. Energy and potential profiles and interactions between ions. Biophys. J. 22, 209-219.

Llinas, R., Steinberg, I.Z. & Walton, K. (1981). Presynaptic calcium currents in squid giant synapse. Biophys. J. 33, 289-322.

Lux, H.D. & Brown, A.M. (1984). Patch and whole cell calcium currents recorded simultaneously in snail neurons. J. Gen. Physiol. 83, 727-750.

Magelby, K.L. & Stevens, C.F. (1973). A quantitative description of end-plate currents. J. Physiol. 223, 173-197.

Marchais, D. & Marty, A. (1979). Interaction of permeant ions with channels activated by acetylcholine in Aplysia neurones. J. Physiol. 297, 9-45.

Matsuda, Y., Yoshida, S. & Yonezawa, T. (1978). Tetrodotoxin sensitive and calcium component of action potentials of mouse dorsal root ganglion cells cultured in vitro. Brain Res. 154, 69-82.

Matthews, B.W. & Bernhardt, S.A. (1973). Structure and symmetry of oligomeric enzymes. Ann. Rev. Biophys. Bioeng. 2, 257-317.

Matteson, D.R. & Armstrong, C.M. (1986). Properties of two types of calcium channels in clonal pituitary tumour cells. J. Gen. Physiol. 87, 161-182.

Mayer, M.L. (1985). A calcium-activated chloride current generates the after-depolarization of rat sensory neurones in culture. J. Physiol. 364, 217-239.

McLaughlin, S., Mulrine, N., Gresalfi, T., Vaio, G. & McLaughlin, A. (1981). Adsorption of divalent cations to bilayer membranes containing phosphatidylserine. J. Gen. Physiol. 77, 445-473.

McLaughlin, S.G.A., Szabo, G. & Eisenman, G. (1971). Divalent ions and the surface potential of charged phospholipid membranes. J. Gen. Physiol. 58, 667-687.

Meves, H. & Vogel, W. (1973). Calcium inward currents in internally perfused giant axons. J. Physiol. 235, 225-265.

Miledi, R. & Parker, I. (1982). Chloride current induced by injection of calcium into Xenopus oocytes. J. Physiol. 357, 173-188.

Miller, A.J. (1981). LMM - A subroutine for unconstrained non-linear least-squares fitting. CSIRO Division of Mathematics & Statistics, Consulting Report No. VT 81/23.

Miller, R.J. & Freedman, S.B. (1984). Minireview : Are dihydropyridine binding sites voltage sensitive calcium channels ? Life Sci. 34, 1205-1221.

Muller, R.U. & Finkelstein, A. (1974). The electrostatic basis of Mg^{++} inhibition of transmitter release. Proc. Natl. Acad. Sci. U.S.A. 71, 923-926.

Nelson, M.T. (1986). Interactions of divalent cations with single calcium channels from rat brain synaptosomes. J. Gen. Physiol. 87, 201-222.

Nelson, M.T., French, R.J. & Kreuger, K. (1984). Voltage-dependent Ca channels from rat brain incorporated into planar lipid bilayers. Nature 308, 77.

Neumke, B., Nonner, N. & Stampfli, R. (1976). Asymmetric displacement current and its relation with the activation of sodium current in the membrane of frog myelinated nerve. Pflugers Arch. 363, 193-203.

Nilius, B., Lansman, J.B. & Tsein, R.W. (1985). A novel type of cardiac calcium channel in ventricular cells. Nature 316, 443.

Noda, M., Takahashi, H., Tanabe, T., Toyasato, M., Kikyotani, S., Furutani Y., Hirose, T., Takashima, H., Inayama S., Miyata, T. & Numa, S. (1983). Structural homology of Torpedo californica acetyl-choline receptor subunits. Nature 302, 528-532.

Noda, M., Shimizu, S., Tanabe, T., Takai, T., Kayano, T., Ikeda, T., Takahashi, H., Nakayama, H., Kanoaka, Y., Minamino, N., Kangawa, K., Matsuo, H., Raftery, M.A., Hirose, T., Inayama, S., Hayashida, H., Miyata, T. & Numa, S. (1984). Primary structure of Electrophorus electricus sodium channel deduced from cDNA sequence. Nature 312, 121-127.

Nonner, W., Rojas, E. & Stampfli, R. (1975). Displacement currents in the node of Ranvier. Voltage and time dependence. Pflugers Arch. 354, 1-18.

Nowycky, M.C., Fox, A.P. & Tsein, R.W. (1985). Three types of neuronal Ca channels with different Ca agonist sensitivity. Nature 316, 440.

Nowycky, M.C., Fox, A.P. & Tsien, R.W. (1985). Long-opening mode of gating of neuronal calcium channels and its promotion by the dihydropyridine calcium channel agonist Bay K 8644. Proc. Natl. Acad. Sci. 82, 2178-2182.

Ohmori, H. & Yoshii, M. (1977). Surface potential reflected in both gating and permeation mechanisms of sodium and calcium channels of the tunicate egg cell membrane. J. Physiol. 267, 429-463.

Osborne, M.R. (1976). Non-linear least squares - the Levenberg algorithm revisited. J. Austral. Math. Soc. B 19,343-357.

Owen, D.A., Segal, M. & Barker, J.L. (1984). A Ca-dependent Cl^- conductance in cultured spinal cord neurones. Nature 311, 567-570.

Pannese, E., Gioia M., Carandente, O. & Ventura, R. (1983). A quantitative electron microscopic study of the perikaryal projections of sensory ganglion neurons. I. Cat and Rabbit. J. Comp. Neurobiol. 214, 239-250.

Pauling, L. (1948). The nature of the chemical bond and the structure of molecules and crystals. Cornell University Press 2nd edition.

Perney, T.M., Hirning, L.D., Leeman, S.E. & Miller, R.J. (1986). Multiple calcium channels mediate neurotransmitter release from peripheral neurones. Proc. Natl. Acad. Sci. U.S.A. 83, 6656-6659.

Polymeropolous, E.E. & Brickmann, J. (1985). Molecular dynamics of ion transport through transmembrane model channels. Ann. Rev. Biophys. Biophys. Chem. 14, 315-330.

Reuter, H., Stevens, C.F., Tsien, R.W. & Yellen, G. (1982). Properties of single calcium channels in cardiac cell culture. Nature 297, 501-504.

Reuter, H., Porzig, H., Kokubun, S. & Prod'hom B. (1985). 1,4-Dihydropyridines as tools in the study of Ca^{2+} channels. TINS 8, 396-400.

Reuter, H., Kokubun, S. & Prod'hom, B. (1986). Properties and modulation of cardiac calcium channels. J. Exp. Biol. 124, 191-201.

Rorsman, P. & Trube, G. (1986). Ca and delayed K currents in mouse pancreatic ß-cells under voltage-clamp conditions. J. Physiol. 374, 531-550.

Rosenberg, R., Hess, P., Reeves, J., Smilowitz, H. & Tsein, R.W. (1985). Calcium channels in planar lipid bilayers : Insights into mechanims if ion permeation and gating. Science 231, 1564-1566.

Saimi, Y. & Kung, C. (1982). Are ions involved in the gating of calcium channels ? Science 218, 153-156.

Sakman, B. & Bohiem, G. (1979). Alamethicin-induced single channel conductance fluctuations in biological membranes. Nature 282, 336-339.

Sanguinetti, M.C. & Kass, R.S. (1984a). Voltage-dependent block of calcium channel current in the calf cardiac purkinje fiber by dihydropyridine calcium channel antagonists. Circ. Res. 55, 336-348.

Sanguinetti, M.C. & Kass, R.S. (1984b). Regulation of cardiac calcium channel current and contractile activity by the dihydropyridine Bay K 8644 is voltage dependent. J. Mol. Cell. Cardiol. 16, 667-670.

Scheuer, T. & Gilly, W.M. (1986). Charge movement and depolarization-contraction coupling in arthropod vs. vertebrate skeletal muscle. Proc. Natl. Acad. Sci. U.S.A. 83, 8799-8803.

Schramm, M., Thomas, G., Towart, R. & Franckowiak, G. (1983) Novel dihydropyridines with positive ionotropic action through activation of Ca^{2+} channels. Nature 303, 535-537.

Sine, S. & Steinbach, J.H. (1986). Acetylcholine receptor activation by a site selective ligand; nature of brief open and closed states in BC3H-1 cells. J. Physiol. 370, 357-379.

Sigworth, F.J. & Neher, E. (1980). Single Na^{+} channel currents observed in cultured rat muscle cells. Nature 287, 447-449.

Standen, N.B. (1974). Properties of a Ca channel in snail neurones. Nature 250, 340.

Stein, D.L. (1985). A model of protein conformational substates. Proc. Natl. Acad. Sci. U.S.A 82, 3670.

Stevens, C.F. (1978). Interactions between intrinsic membrane protein and electric field. Biohys. J. 22, 295-306.

Tsien, R.W. & Noble, D. (1969). A transition state theory approach to the kinetics of conductance changes in excitable membranes. J. Memb. Biol. 1, 248-273.

Urban, B.W., Hladky, S.B. & Haydon, D.A. (1978). The kinetics of ion movements in the gramicidin channel. Fed. Proc. 37, 2628-2632.

van Helden, D.F., Hamill, O.P. & Gage, P.W. (1977). Permeant cations alter end-plate channel characteristics. Nature 269, 711-712.

Wang, J.H. (1953). Tracer diffusion in liquids. IV. Self-diffusion of calcium ion and chloride ion in aqueous calcium chloride solutions. J. Am. chem. Soc. 75, 1769-1770.

White, M.M. & Bezanilla, F. (1985). Activation of squid axon K^{+} channels. Ionic and gating current studies. J. Gen. Physiol. 85, 539-555.

Williams, J.S., Grupp, I.L., Gunter, G., Vaghy, P.L., Yatani, A., Hamilton, S. & Brown, A.M. (1985). Profile of the oppositely acting enantiomers of the dihydropyridine 202-791 in cardiac preparations : receptor binding, electrophysiological and pharmacological studies. Biochem. Biophys. Res. Comm. 131, 13-21.

Willis, W.D. & Coggeshall, R.E. (1978). Sensory mechanisms of the spinal cord. Plenum Press N.Y.

Wilson, D.L., Morimoto, K., Tsuda, Y. & Brown, A.M. (1983). Interaction between calcium ions and surface charge as it relates to calcium currents. J. Memb. Biol. 72, 117-130.

Yoshida, S. & Matsuda, Y. (1979). Studies on sensory neurones of the mouse with intracellular recording and horseradish peroxidase techniques. J. Neurophysiol. 42, 1134-1146.

Yoshida, S., Matsuda, Y. & Samejima, A. (1978). Tetrodotoxin-resistant sodium and calcium components of action potentials in dorsal root ganglion cells of adult mouse. J. Neurophysiol. 41, 1096-1106.

Yoshimura, M., Polosa, C. & Nishi, S. (1986). Electrophysiological properties of symathetic preganglionic neurones in the cat spinal cord in vitro. Pflugers Arch. 406, 91-98.

Zimmerberg, J. & Parsegian, V.A. (1986). Polymer inaccessible volume changes during opening and closing of a voltage-dependent ionic channel. Nature 323, 36-39.

Appendix 1

Equations describing the voltage dependence of the transition rate constants of a voltage activated channel are presented, in order to define various quantities that are referred to in the text. These equations were derived in detail by Stevens (1978) and assume that there is no distortion of the protein dipoles by the electric field of the membrane.

The n'th step in an activation scheme may be represented by a two state transition (Figure A1.1). For the purposes of this discussion, k_i is increased by positive voltages, and k_j is decreased. Conventional rate theory (Glasstone et al. 1949), requires that the two rate constants are related to the barrier height by,

$$k_{i,j} = \nu.\exp(-\Delta G^*_{i,j}) \qquad \ldots (A1.1),$$

where $\nu = kT/h$, and,

$$\Delta G^*_{i,j} = w_m - w_{i,j} \mp z_{i,j}\mu_n F/RT \ ,$$

where w_m is the energy of the transition state, $w_{i,j}$ are the predominant energy levels of the two conformations and μ_n is the electric field across the dipole moment of the channel. $z_{i,j}$ are the dipole moments of $k_{i,j}$ normal to the membrane electric field, and represent some fraction of the total dipole moment of the reaction step. Steady-state measurements give an estimate of the ratios of the rate constants,

$$E_n = \frac{k_i}{k_j} = \exp[-(\Delta w_n - z\mu_n F/RT)] \qquad \ldots (A1.2),$$

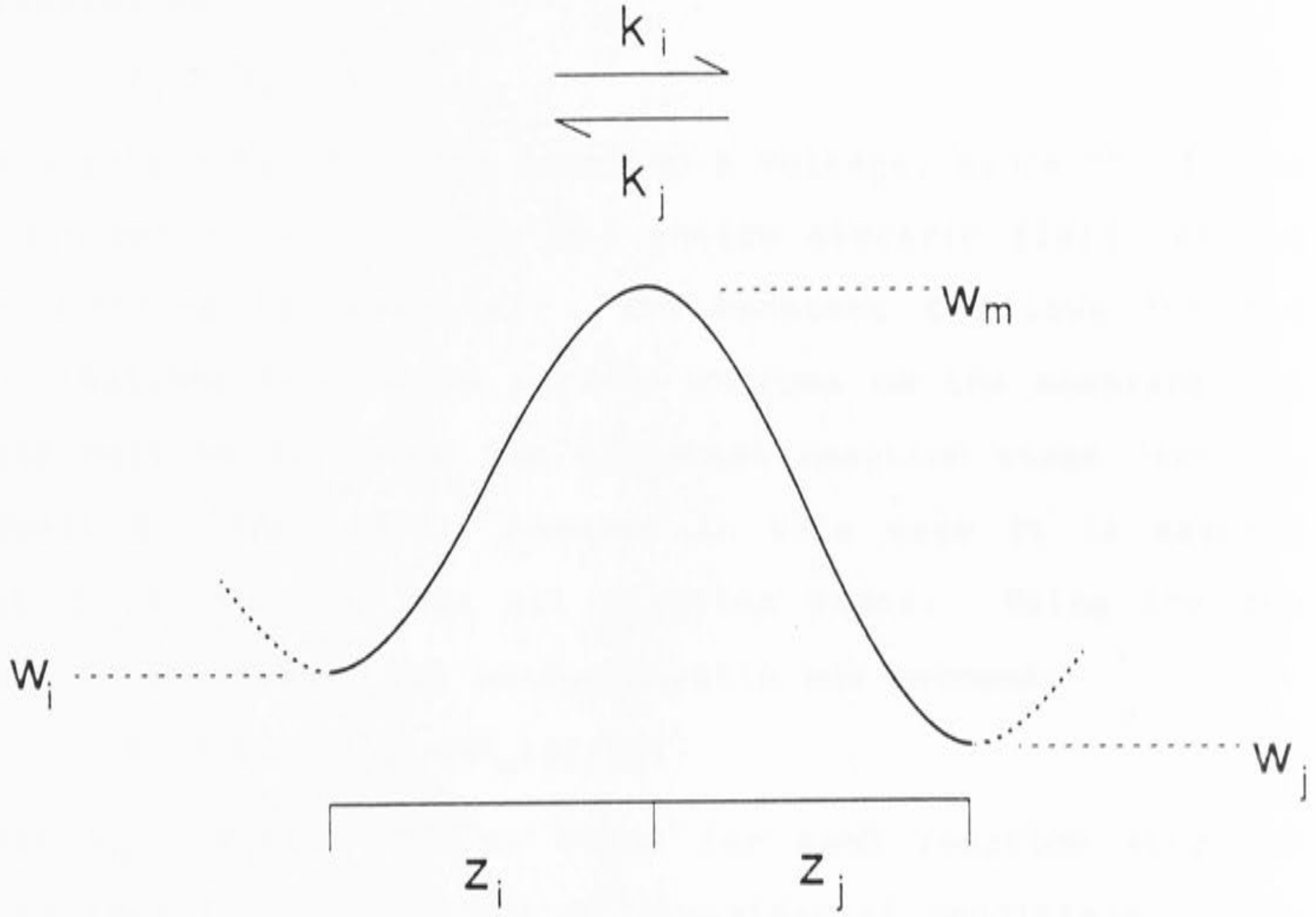
k i
k j
w m
w i
w j
z i
z j

where $\Delta w_n = w_j - w_i$ & $z = z_i + z_j$. If Δw_n is expressed as the equivalent voltage, $V_w = \Delta w_n RT/zF$, equation 2 becomes,

$$E_n = \exp[-(V_w - \mu_n)zF/RT],$$

Now assume that μ_n is related to the measured membrane potential by,

$$\mu_n = V_m + \xi.$$

The electric field is set equal to a voltage, since the dipole is assumed to move across the entire electric field, and so the distance terms cancel. The constant ξ allows for the contributions from fixed surface charges on the membrane. ξ could well be different for different reaction steps (see eg. Attwell & Eisner 1978), however in this case it is assumed that ξ is the same for all reaction steps. Using the two previous equations, the measured ratio now becomes,

$$E_n = \exp[-(V_n - V_m)zF/RT],$$

where $V_n = V_w + \xi$. The Δw value for each reaction step can be defined for a given set of experimental conditions. This is done by arbitarily setting ξ equal to the measured zero membrane potential. The apparent conformational energy for the reaction step is then,

$$w_n = V_n zF/RT.$$

Changes in the surface charge potential can then be allowed for by changing ξ by an amount equal to the shift in the $P_o(V)$ curve, and the calculated w_n values are then independent of the changes in the surface charge potential.

Appendix 2

Solution of Differential Equations for the Models Used

A standard result for the solution of linear first order differential equations with constant coefficient matrices is used. The reader can consult any text on linear differential equations for more detail on the methods used (eg. Brauer et al. 1970).

The main aims of this section were firstly, to derive equations which could be used to relate the model rate constants to the rate constants of the observed relaxations, and secondly to find unique solutions for the amplitudes of the various exponential components as a function of the model rate constants and the initial conditions. Although the expressions for these various relations become rather involved, even for the simplest models, the results can be used if one has access to reasonable computing facilities.

The solution for the 3-state model is first shown in some detail, and the main results for the 4-state model are outlined subsequently.

3-State Model

Reaction scheme : $C_1 \underset{k_2}{\overset{k_1}{\rightleftharpoons}} C_2 \underset{k_4}{\overset{k_3}{\rightleftharpoons}} C_3$

where C_i (i = 1..3) are the channel protein conformations, and $k_i > 0$ (i = 1..4) are the transition probabilities. The differential equations describing the behaviour of this system

can be written in the form,

$$f'(t) = A_{33}f(t), \qquad ..(A2.1)$$

where,

$$f'(t) = \begin{vmatrix} C_1'(t) \\ C_2'(t) \\ C_3'(t) \end{vmatrix}, \quad A_{33} = \begin{vmatrix} -k_1 & k_2 & 0 \\ k_1 & -(k_2+k_3) & k_4 \\ 0 & k_3 & -k_4 \end{vmatrix}, \quad f(t) = \begin{vmatrix} C_1(t) \\ C_2(t) \\ C_3(t) \end{vmatrix}.$$

The solution matrix to this system $\Phi(t)$ must satisfy equation 1 above, that is $\Phi'(t) = A_{33}\Phi(t)$. This fundamental matrix has the form,

$$\Phi(t) = \bar{v}_i \exp(\lambda_i t),$$

where λ_i and $\bar{v}_i$ $(i = 0..2)$ are the eigenvalues and eigenvectors of A_{33} respectively. Calculation of $\Phi(t)$ involves finding the eigenvalues and eigenvectors such that,

$$(\lambda_i I - A_{33})\bar{v}_i = \bar{0} \qquad ..(A2.2),$$

where I is the unit matrix. Equation 2 has a nontrivial solution for values of λ_i such that,

$$\det(\lambda_i I - A_{33}) = 0.$$

Now,

$$\det(\lambda I - A_{33}) = \det\begin{vmatrix} (\lambda+k_1) & -k_2 & 0 \\ -k_1 & (\lambda+k_2+k_3) & -k_4 \\ 0 & -k_3 & (\lambda+k_4) \end{vmatrix}$$

$$= \lambda^3 + (k_1+k_2+k_3+k_4)\lambda^2 + (k_1k_3+k_1k_4+k_2k_4)\lambda \qquad ..(A2.3)$$

Equation 3 is called the characteristic polynomial for this system of equations, and the solutions to this equation give the eigenvalues of the system. That is,

$$\lambda(\lambda^2 + b\lambda + c) = 0, \qquad \text{where } b = (k_1+k_2+k_3+k_4),$$
$$\text{and } c = (k_1k_3+k_1k_4+k_2k_4).$$

There are 3, not necessarily distinct, eigenvaules,

$$\lambda_0 = 0, \qquad \lambda_{1,2} = \frac{-b \pm \sqrt{(b^2-4c)}}{2} \qquad ..(A2.4).$$

Note that $\lambda_{1,2} < 0$. This is apparent if one notes that $k_i > 0$ $(i = 1..4)$ and therefore $c > 0$.

The corresponding eigenvectors for λ_i are found by solving the homogeneous linear system of equations,

$$(\lambda_i I - A_{33})\bar{v}_i = \bar{0}.$$

To find the solution vectors $\bar{v}_i$, the matrix

$$(\lambda_i I - A_{33}) = \begin{vmatrix} (\lambda_i+k_1) & -k_2 & 0 \\ -k_1 & (\lambda_i+k_2+k_3) & -k_4 \\ 0 & -k_3 & (\lambda_i+k_4) \end{vmatrix},$$

is reduced to row echelon form, and becomes,

$$A_{RO} = \begin{vmatrix} 1 & 0 & \dfrac{-k_2(\lambda_i+k_4)}{k_3(\lambda_i+k_1)} \\ 0 & 1 & \dfrac{-(\lambda_i+k_4)}{k_3} \\ 0 & 0 & Z \end{vmatrix},$$

where $Z = 0$. This must be the case, since the rank of $A_{RO} < 3$. If the rank of $A_{RO} = 3$ then the system of equations would have only the trivial solution, contrary to the fact that $\det(\lambda_i I - A_{33}) = 0$. The required eigenvectors have the form,

$$\bar{v}_i = \alpha_i \begin{vmatrix} \dfrac{k_2(\lambda_i+k_4)}{k_3(\lambda_i+k_1)} \\ \dfrac{(\lambda_i+k_4)}{k_3} \\ 1 \end{vmatrix} = \alpha_0 \begin{vmatrix} \dfrac{k_2 k_4}{k_1 k_3} \\ \dfrac{k_4}{k_3} \\ 1 \end{vmatrix} \quad \text{for } i = 0,$$

where α_i is an arbitary constant. The fundamental matrix can now be written as,

$$\Phi_{33}(t) = \alpha_i \bar{v}_i \exp(\lambda_i t), \quad i = 0..2. \qquad ..(A2.5).$$

Application of this result to the electrophysiological data is now straightforward. If C_3 is taken to be the active conducting conformation, then the current flow is described by the sum of the terms in the bottom row of $\Phi_{33}(t)$. Thus,

$$I_m(t) = C_3(t)$$

$$= \alpha_0 v_{03} + \alpha_1 v_{13} \exp(\lambda_1 t) + \alpha_2 v_{23} \exp(\lambda_2 t) \qquad ..(A2.6);$$

where α_i are chosen to give the appropriate units. The last two terms of equation 6 give the transient response of the system. Note that the amplitudes of the two exponential components are arbitary, and in fact depend on the initial conditions of the system. A useful result that can be obtained from equation 6 is the steady state probability that the channel is open at $t >> 0$. This is given by the first term in equation 6, with the added constraint that the sum of the concentrations of all species is one. Therefore, it is convenient to choose α_0 such that,

$$\alpha_0 = \frac{1}{v_{01} + v_{02} + v_{03}} \qquad ..(A2.7),$$

and the steady state occupancy of C_3 becomes,

$$P_o(V) = \alpha_0 v_{03} = \frac{1}{\frac{k_2 k_4}{k_1 k_3} + \frac{k_4}{k_3} + 1} \qquad ..(A2.8)$$

There are simpler and more direct ways of obtaining equation 8. The general form of the eigenvectors was derived to obtain the unique solution (with the same form as equation 5) of equation 1 for given initial conditions of the system. The solution is found by evaluating the arbitary constants α_i for a given set of initial conditions. This requires a solution to the equation,

$$\Phi_{33}(0)\bar{\beta} = \bar{c} \ , \qquad ..(A2.9)$$

where $\bar{\beta}$ is a column vector with elements α_i (i = 0..2), and $\bar{c}$ is a column vector giving the initial values of C_1, C_2 and C_3. The vector $\bar{c}$ is set at the appropriate starting potential by $\bar{c} = \alpha_0 \bar{v}_0$, where α_0 is assigned with the constraint that mass is conserved (similar to equation A2.7). The solution, $\bar{\beta}$ is unique, since the eigenvectors are linearly independent (the rank of $\Phi_{33}(0)=3$). Substitution of the α_i values obtained from equation 9 into equation 5 gives a solution to equation 1 valid for all t, since it is a solution for an arbitary value $t_o = 0$. These results allow the relative amplitudes of the exponential components to be calculated from the kinetic scheme, which provides a further check of the validity of the proposed models.

4-State Model

Reaction scheme : $C_1 \underset{k_2}{\overset{k_1}{\rightleftharpoons}} C_2 \underset{k_4}{\overset{k_3}{\rightleftharpoons}} C_3 \underset{k_6}{\overset{k_5}{\rightleftharpoons}} C_4$

The system of equations is,

$$f'(t) = A_{4\,4} f(t)$$

The eigenvalues are calculated, from the characteristic polynomial,

$$\lambda(\lambda^3 + b\lambda^2 + c\lambda + d) = 0$$

where, $b = (k_1+k_2+k_3+k_4+k_5+k_6)$,

$c = k_1(k_3+k_4+k_5+k_6) + k_2(k_4+k_5+k_6) + k_3(k_5+k_6) + k_4k_6$,

and $d = k_1k_3(k_5+k_6) + k_4k_6(k_1+k_2)$.

Again note that $\lambda_i \leq 0$, and that $\lambda_0 = 0$. The other eigenvalues can be obtained by solution of the cubic $\lambda^3+b\lambda^2+c\lambda+d = 0$. The descriminant of this equation was obtained by setting $\lambda = x-b/3$, and proved to be a useful check during calculations. The equation becomes,

$$x^3 + px + q = 0, \quad \text{where } p = c-(b^2/3),$$
$$\text{and } q = d + 2b^3/27 - bc/3.$$

The discriminant of the cubic is,

$$D = 4p^3 + 27q^2.$$

If two of the roots are equal then $D = 0$.

If all the roots are real and distinct then $D < 0$.

If two of the roots are imaginary then $D > 0$.

The general form of the eigenvectors for the 4-state

model is,

$$\bar{v}_i = \alpha_i \begin{vmatrix} \dfrac{k_2(\lambda_i^2+(k_4+k_5+k_6)\lambda_i) + k_2k_4k_6}{k_3k_5\lambda_i + k_1k_3k_5} \\ \dfrac{\lambda_i^2+(k_4+k_5+k_6)\lambda_i + k_4k_6}{k_3k_5} \\ \dfrac{(\lambda_i + k_6)}{k_5} \\ 1 \end{vmatrix}, \quad i = 0..3.$$

In practice the eigenvalues were calculated using Newtons method. The eigenvectors were then calculated directly using the algebraic solutions shown above.

Once the eigenvalues and eigenvectors were known the relative amplitudes of the exponential components could be calculated from a given set of initial conditions. This involved finding a solution to the equation,

$$\Phi_{44}(0)\bar{\beta} = \bar{c} \ , \qquad ..(A2.10),$$

which is similar to equation 9 above. Similarly, the initial conditions used were,

$$\bar{c} = \alpha_0\bar{v}_0,$$

where α_0 was set with the constraint that mass is conserved (similar to equation A2.7), and $\bar{v}_0$ was calculated at the appropriate starting potential.

Taking C_4 to be the open conducting conformation of the channel, the membrane current is now given by,

$$I_m(t) = M(\beta_0 v_{04} + \beta_1 v_{14}\exp(\lambda_1 t) + \beta_2 v_{24}\exp(\lambda_2 t) + \beta_3 v_{34}\exp(\lambda_3 t)) \quad ..(A2.11)$$

where the constant M is chosen to give the appropriate units.

Curve fitting procedure

Equations 9 & 10 were solved using Gaussian elimination with partial pivoting, followed by back substitution (Goult et al. 1974). The results could be checked by substituting the solution vector into the original equation. The programs were written in 'C' using double precision floating point numbers for the calculations. The results were consistent to better than 13 significant figures, indicating that rounding errors were not a problem. During the fitting procedure the eigenvalues and eigenvectors had to be calculated at each membrane potential. The voltage dependence of the rate constants was set according to equation A1.1.

Both the 3-state and the 4-state models were fitted to the data to provide a comparison. These models had 8 & 12 free parameters respectively, four free parameters per reaction step corresponding to $w_{i,j}$ & $z_{i,j}$ in equation A1.2. None of the parameters were constrained during the fitting procedure mainly because there were no adequate estimates of the various values available. The data used to fit the models is shown in figure 3.30. The 'direct-search' algorithm described by Hooke & Jeeves (1960) was used to minimise the function,

$$S = \Sigma(x_i - s_i)^2,$$

where x_i were the data points shown in figure 3.30 and s_i were the values predicted from the models. The starting values for the 3-state model were taken from straight lines in figure 3.17, and the curve fitting algorithm converged to the

solution shown in figure 3.30. The fit was better than that produced by the analysis in Chapter 3 (figures 3.18), but the 3-state scheme did not provide an accurate description of the data.

Starting values for the 4-state model were obtained by trial and error, using the best fit from the 3-state model as initial estimates for some of the parameters. The 4-state model predicted a 3 exponential time course for the current relaxations according to equation 11. The starting values were chosen such that the fastest exponential (λ_1) was very fast and of negligible amplitude ($\beta_1 \sim 0$). This exponential component was ignored during the fitting procedure, and the data was fitted to the two slower exponential components. Under these conditions the 'direct-search' algorithm converged to a minimum, and the fastest exponential remained less than 0.01% of the total amplitude of the current relaxations during the search.

Appendix 3

Techniques and equations used to calculate I-Vs from 2-site

3-barrier permeation models

The methods used are essentially the same as those set out by Begenisich & Cahalan (1980a). The current-voltage relationship for the 2-site model with one or two ions was obtained by calculating the steady state flux for each ion (denoted by A & B) according to the state diagram shown in figure A3.1, where OO represents two empty sites, AO is formed when the left hand site (lower figure A3.1) is occupied by ion A and the other site is empty etc. Nine differential equations were obtained, one for each species shown in the diagram. These were set equal to zero, since it was assumed that the system reached a steady state much more rapidly than the recording equipment. The dOO/dt equation was replaced with the conservation equation, which simply sets the sum of all the species equal to unity. The resulting non-homogeneous set of linear equations was solved using Gaussian elimination with partial pivoting (Goult et al. 1974). Programs were written in 'C', and run on a Pyramid computer using double precision floating point numbers. Calculation of a 13 point I-V took less than a second.

The current was calculated from the net transfer of ions across the central energy barrier. Thus for the two ions A & B, the membrane current was given by,

Figure A3.1 The top figure shows the state diagram for a two site model, with two permeant ions, A & B. The ions bind to empty sites (O), and cannot pass each other in the channel. The bottom figure shows a hypothetical energy profile for a channel. The external solution is on the left of the profile, and the cytoplasm is on the right. This convention is followed for all the diagrams.

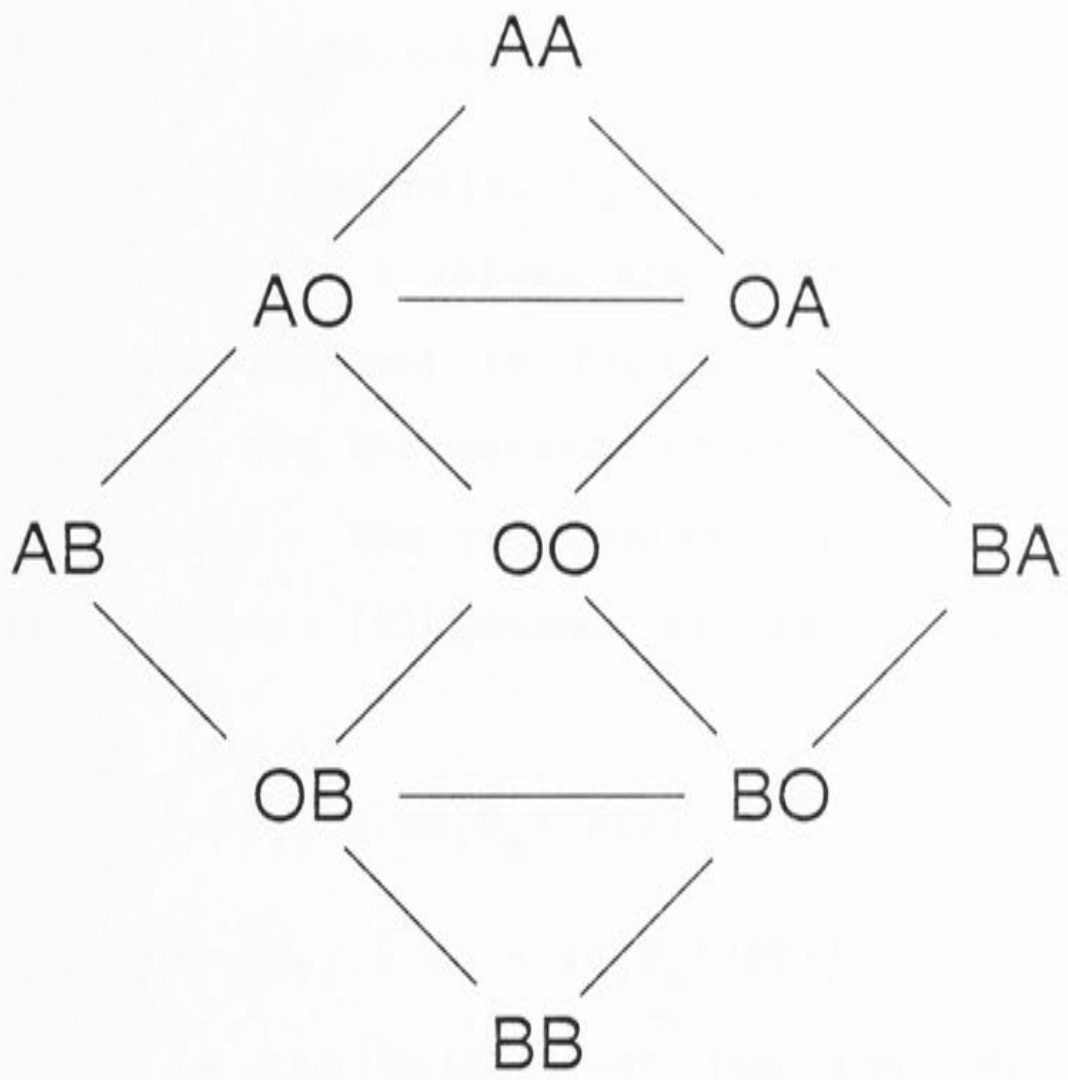
AA
AO
OA
AB
OO
BA
OB
BO
BB

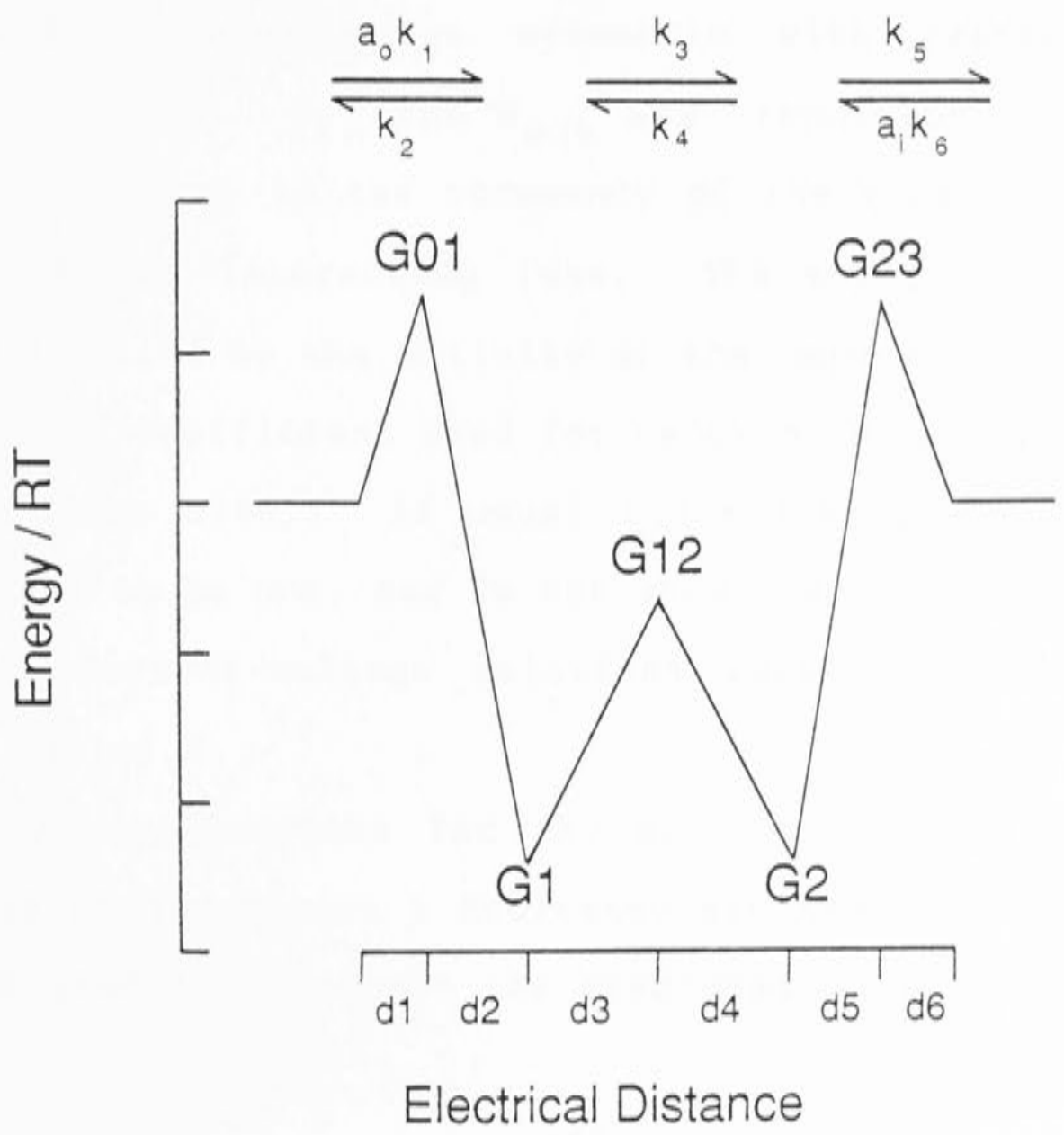
a0k1
k2
k3
k4
k5
a1k6
G01
G23
G12
G1
G2
Energy / RT
d1
d2
d3
d4
d5
d6
Electrical Distance

$$I_m = -\frac{N.F}{N_a}(k_3AO - k_4OA + k_3'BO - k_4'OB)$$

where N is the number of channels, N_a is Avogadros number, F is Faradays constant and the k values are transition rates for the two ions, and are defined in figure A3.1. G1 is the binding site closest to the the outside of the membrane and G2 is closest to the inside. The rate constants were set using conventional rate theory (Glasstone et al. 1941). For example,

$$k_1 = \nu.R_{in}.\exp(-(G_{01} + zd_1V_mF/RT)),$$

$$k_2 = \nu.R_{out}.\exp(-(G_{01} - G_1 - zd_2V_mF/RT)),$$

where $\nu = kT/h$, z is the valence of the ion, d_i is the electrical distance the ion moves in reaching the transition state and V_m is the membrane potential. In all cases the electrical distances were symmetric with respect to the central barrier. R_{in} and R_{out} are repulsion factors which are set according to the occupancy of the other site and the valence of the interacting ions. The entry rate constants were multiplied by the activity of the permeant ion (a_o, a_i). The activity coefficient used for calcium and barium was 0.341 (Hess & Tsien 1984). As usual the transmission coefficient was assumed to be one, and is not shown explicitly above. The predicted current-voltage relations were scaled to fit the data by varing N.

The energy profiles for the calcium channel proposed by Hess & Tsien and Almers & McCleskey are shown in figure A3.2, and were used to calculate the predicted I-Vs shown in figure

Figure A3.2 Energy profiles proposed previously for the calcium channel. The values for the repulsion factors and the electrical distances are shown on the right and were used to produce the solid lines in figure 5.5.

Hess & Tsien, 1984

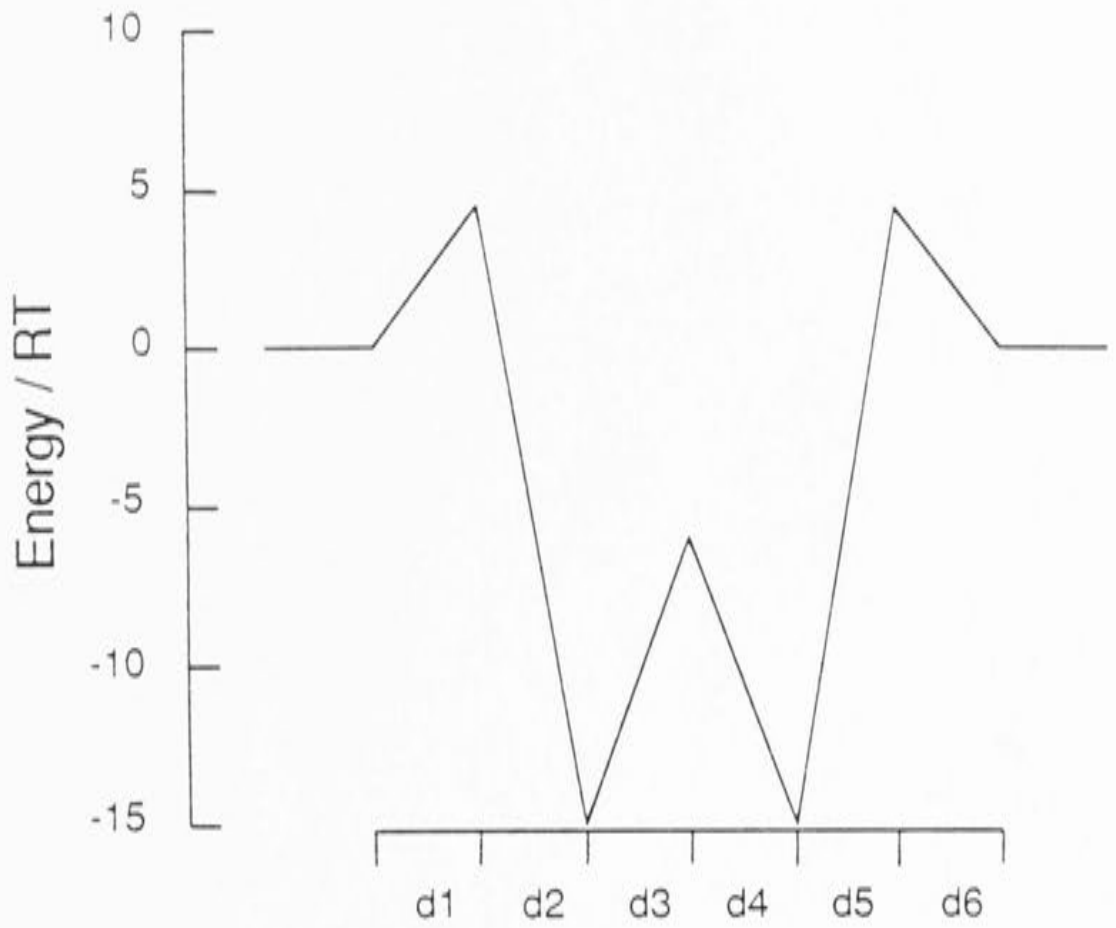

Rin = 81
Rout = 81

d1 = 1/6
d2 = 1/6
d3 = 1/6

Almers & McCleskey, 1984

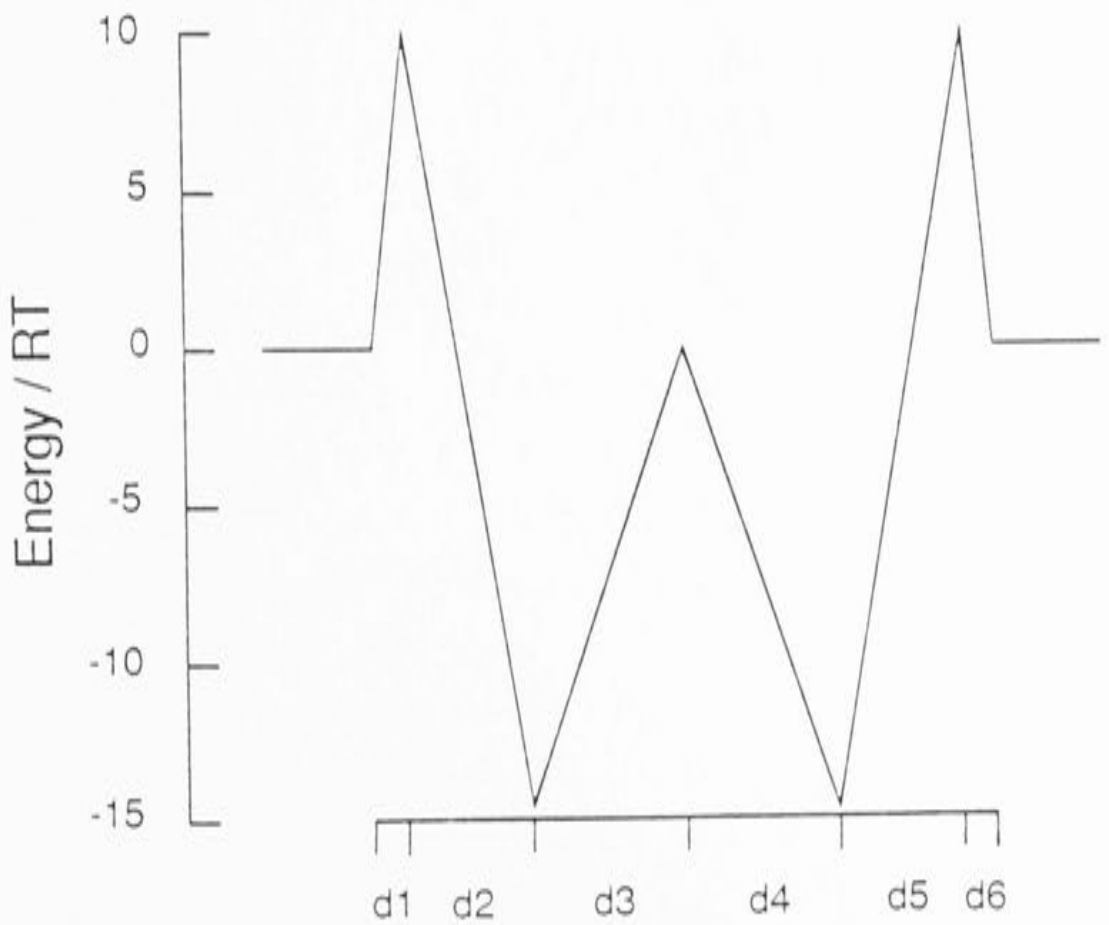

Rin = 1
Rout = 20,000

d1 = 0.05
d2 = 0.283
d3 = 0.167

5.5. Figure A3.3 shows the energy profile (dark line) for the instantaneous I-V shown in figure 5.19. The broken line shows the proposed energy profile for Cd^{2+}, qualitatively consistent with the blocking effects of this ion.

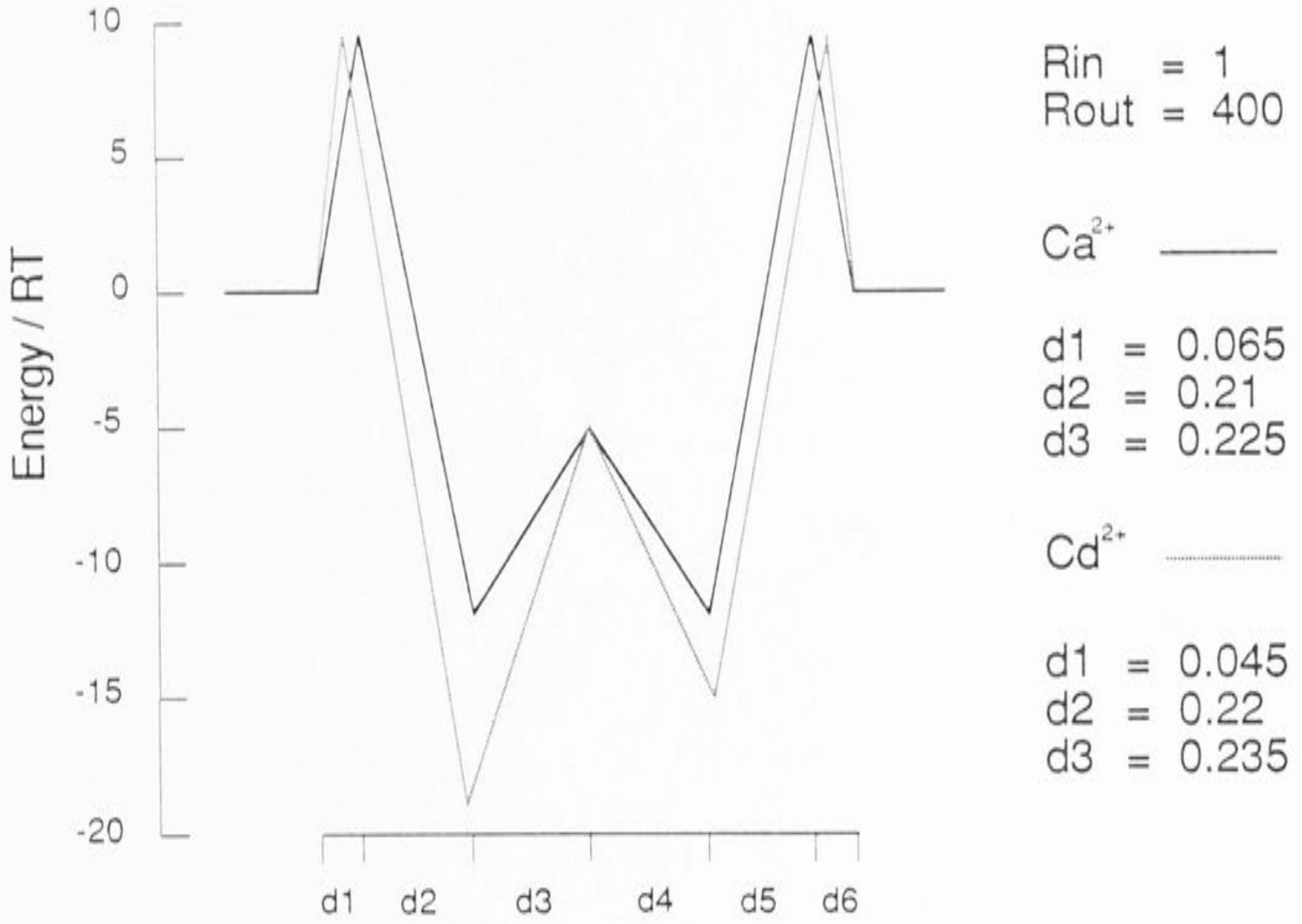

Figure A3.3 The solid line shows the energy profile used to fit the control instantaneous I-V (figure 5.19). The broken line shows the proposed energy profile for Cd^{2+} which was qualitatively consistent with the blocking effects of this ion. Important features of the model are the much deeper well for Cd^{2+} at the outside binding site of the channel, and the shorter electrical distance for the Cd^{2+} ions entering the channel. The repulsion factors and electrical distances for the two ions are shown on the right of the figure.